Spring 2017

Design and theoretical analysis of advanced power based positioning in RF system

Lei Wang

Department: Electrical and Computer Engineering

DESIGN AND THEORETICAL ANALYSIS OF ADVANCED POWER BASED POSITIONING IN RF SYSTEM

by

LEI WANG

A DISSERTATION

Presented to the Graduate Faculty of the

MISSOURI UNIVERSITY OF SCIENCE AND TECHNOLOGY

In Partial Fulfillment of the Requirements for the Degree

DOCTOR OF PHILOSOPHY

in

COMPUTER ENGINEERING

2017

Approved by

Dr. Maciej Zawodniok, Advisor
Dr. Jagannathan Sarangapani
Dr. Reza Zoughi
Dr. Kurt Kosbar
Dr. Akim Adekpedjou

PUBLICATION DISSERTATION OPTION

This dissertation has been prepared using the Publication Option. It consists of the following five papers.

Paper I, L. Wang and M. Zawodniok, "Ubiquitous Tracking Using Motion and Location Sensor With Application to Smartphone," under review by 2017 IEEE International Conference on Smart Computing (SMARTCOMP).

Paper II, L. Wang and M. Zawodniok, "Bias and CRB Analysis of LoS-based and RSS-based Ranging Methods," IEEE Transactions on Vehicular Technology, vol. 65, no. 11, pp. 9085-9097, Nov. 2016.

Paper III, L. Wang and M. Zawodniok, "New Theoretical Limit Analysis of LoS and RSS Based Positioning Methods for Ricean Fading Channel in RF Systems," under review by IEEE Transactions on Mobile Computing.

Paper IV, L. Wang and M. Zawodniok, "ARPAP: A Novel Antenna-Radiation-Pattern-Aware Power-Based Positioning in RF System," to be submitted," under review by IEEE Transactions on Vehicular Technology.

Paper V, L. Wang and M. Zawodniok, "ML ARPAP: the Maximum Likelihood based Antenna Radiation-Pattern-Aware Power-Based Positioning in RF System," under review by IEEE Transactions on Vehicular Technology.

ABSTRACT

Accurate locating and tracking of people and resources has become a fundamental requirement for many applications. The global navigation satellite systems (GNSS) is widely used. But its accuracy suffers from signal obstruction by buildings, multipath fading, and disruption due to jamming and spoof. Hence, it is required to supplement GPS with inertial sensors and indoor localization schemes that make use of WiFi APs or beacon nodes. In the GPS-challenging or fault scenario, radio-frequency (RF) infrastructure based localization schemes can be a fallback solution for robust navigation. For the indoor/outdoor transition scenario, we propose hypothesis test based fusion method to integrate multi-modal localization sensors. In the first paper, a ubiquitous tracking using motion and location sensor (UTMLS) is proposed. As a fallback approach, power-based schemes are cost-effective when compared with the existing ToA or AoA schemes. However, traditional power-based positioning methods suffer from low accuracy and are vulnerable to environmental fading. Also, the expected accuracy of power-based localization is not well understood but is needed to derive the hypothesis test for the fusion scheme. Hence, in paper 2-5, we focus on developing more accurate power-based localization schemes. The second paper improves the power-based range estimation accuracy by estimating the LoS component. The ranging error model in fading channel is derived. The third paper introduces the LoS-based positioning method with corresponding theoretical limits and error models. In the fourth and fifth paper, a novel antenna radiation-pattern-aware power-based positioning (ARPAP) system and power contour circle fitting (PCCF) algorithm are proposed to address antenna directivity effect on power-based localization. Overall, a complete LoS signal power based positioning system has been developed that can be included in the fusion scheme.

ACKNOWLEDGMENTS

I am immensely thankful to my advisor, Dr. Maciej Zawodniok for his constant guidance, intellectual support and moral inspiration. I am truly grateful to him for taking the time out of his busy schedule to guide me when I needed him, and for being an excellent advisor throughout.

I am also extremely grateful to Dr. Jagannathan Sarangapani, Dr. Reza Zoughi, Dr. Kurt Kosbar and Dr. Akim Adekpedjou for their invaluable support, academic guidance and for graciously consenting to be on my committee.

No words in the world can express my gratitude to my parents, Erlie Wang and Congli Li, for their invaluable love, sacrifices and support. I would also like to thank my parents-in-law, Dezhong Feng and Xiufang Zhang, for their unconditional love and help; my wife, Li Feng, for her limitless love, encouragement, and always believing in me; and my loving son, Ryan, for bring me happiness everyday. Without all of you, this would be meaningless. I love you all!

TABLE OF CONTENTS

Page

LIST OF ILLUSTRATIONS

LIST OF TABLES

SECTION

1. INTRODUCTION

Wireless localization has become a fundamental requirement in many areas of practical applications, including autonomous vehicular navigation, healthcare, security, geographic routing, cyber-physical system, etc. Many different technologies for localization and tracking exist. They have own strength and weaknesses. Hence, a fusion of such multimodal sensor would be desired to combine the best features of each technology.

Global navigation satellite systems (GNSS), which is the most widely-used positioning technology, can provide accurate position estimation. However, GNSS often provide insufficient accuracy and reliability, depending on the number of visible satellites, the relative position and radio electric coverage of the satellites [1]. Additionally, interference and malicious jamming or spoofing can lead to GNSS failure [2, 3]. Therefore, in the GPS-denied environment, the inertial sensors and indoor localization schemes that make use of the WiFi access point or beacon nodes are required. In the GPS-challenging/GPS-fault scenario, radio-frequency (RF) infrastructure based localization schemes can be a fallback solution for a robust navigation.

For the indoor/outdoor transition scenario, we propose the multi-modal localization sensor fusion scheme, ubiquitous tracking using motion and location sensor (UTMLS), which integrates different localization schemes with the consumer grade motion sensor. A hypothesis test scheme is proposed to evaluate the absolute position estimates with the analytical error models. Though the inertial sensors based dead reckoning is accurate in short period of time but will accumulate drift error over time. Thus, the supplementary absolute position estimation that is based on the wireless RF signal coming from, e.g., WiFi access point or beacon nodes, is necessary.

Besides, as the fallback approach for the GPS-denied or GPS-fault scenario, the ideal solution would use the existing communication systems and rely on an existing standard, for example, the cellular network, wireless local area network (WLAN), wireless sensor network (WSN). Furthermore, minimum modification to the existing device hardware and software is preferred. Therefore, power-based positioning is considered in this dissertation. Comparing to the time-of-arrival (ToA), time-difference-of-arrival (TDoA), or angle-of-arrival (AoA) based schemes, it is cost-effective.

However, traditional power-based positioning methods suffer from low accuracy and are vulnerable to environmental fading. Also, the theoretical accuracy limits are not well understood. Hence, our work focuses on developing LoS-based positioning scheme and, further, an antenna-radiation-pattern-aware power-based (ARPAP) positioning system to address the issues of multipath fading, nonlinearity, and antenna directivity injected localization error. In addition, corresponding error models are developed. These can be used to develop hypothesis test for the multi-modal sensor fusion algorithm.

1.1. CHALLENGES

The main challenge in RSS based positioning suffers from low accuracy due to the presence of multipath fading. In the multipath fading environment, the received signal consists of a direct LoS component superimposed with several copies of the signal from different NLoS paths. Besides, due to different lengths of NLoS paths, the signal transmitted at a particular time instance arrives at the receiver over a spread of time. This will result in intersymbol interference (ISI) in wireless communication system. Thus, the environment dependent NLoS signal component injects temporal and spatial variation to the total power measurement, and subsequently to the range and location estimation.

Widely accepted model of the signal amplitude received at mobile equipment (ME) over a local area is a composite distribution consisting of a fast fading (Rayleigh) and a slow fading (lognormal) [4, 5, 6]. The local average power (slow fading) is acquired by

smoothing out the fast fading [4, 7, 8, 5, 9, 6]. The RSSI is the local average power and is indicated in *dBm* unit [10]. The smoothing operation renders the lognormal property of the local average power.

The conventional model of the power (lognormal) is not able to distinguish the NLoS component in the fading signal. The received signal is the original signal sent from transmitter after path-loss (LoS component) superimposed with several different copies of itself (NLoS component) from different paths (/directions) due to reflection, diffraction, and scattering. The magnitude of NLoS component in the fading signal depends on the environment. The local average power converges to Normal distribution under the Central Limit Theorem (CLT). Thus, the RSSI (local average power) in the conventional method has a lognormal distribution. The power of code/symbols will raise the mean level proportionally. The average value of the received signal power contains an NLoS signal portion. It introduces bias to the range estimation. Both the RSSI-based range and position estimations have already been explored by Dr. Zanella and Bardella [8] and Dr. Li [9]. But NLoS effect has not been modeled.

Furthermore, the unrealistic assumption of the isotropic radiation pattern in conventional power-based localization schemes results in large localization error. The positioning algorithms [11, 12, 13, 14] are simplified to finding the intersection of several circular power contours whose radius are determined by range estimation. This allows reducing the computational complexity. Error model and the theoretical limit of ranging and range-based positioning in fading channel can be found in [15, 16]. However, in realistic RF system, some antennas are made directional to enhance the performance in terms of energy efficiency, security, and communication quality. For example, the sector antenna deployed in the cellular network. And some antennas are made omnidirectional to optimize the signal reception, for example, the antenna mounted on mobile phones and laptops. Antenna radiation pattern depends on antenna geometry configuration (shape and dimension), dielectric

material, combination (antenna array), and signal wavelength. Thus, the over-relaxed assumption of the isotropic antenna in conventional multilateration methods results in large positioning error.

1.2. ORGANIZATION OF THE DISSERTATION

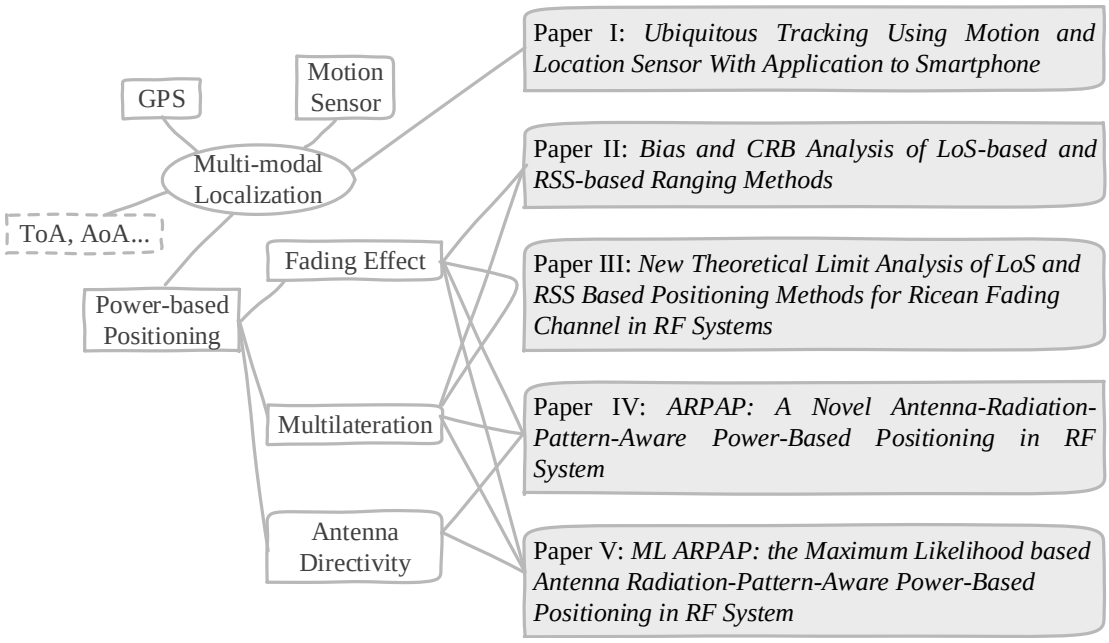

Figure 1.1. Dissertation Organization

This dissertation consists of five papers. The relationship to one another is illustrated in Fig. 1.1.

In the first paper, we develop a multi-modal localization sensor fusion algorithm based on the proposed hypothesis test and drift reduction methods. In general, it can be extended to any location sensing modality. However, it requires a model of localization error. It is easily obtained from GPS. However, in the case of cost-effective power-based localization schemes, such models and accuracy are not sufficient. Consequently, paper 2-5 focus on improving power-based localization and deriving error models. In the second paper, we propose Line-of-sight (LoS) based range estimation in the fading channel, corresponding theoretical analysis and error model are derived. The third paper introduces

LoS based positioning which addresses the fading caused localization error. The fourth paper addresses the antenna directivity introduced localization error. An antenna radiation pattern aware power based positioning system (ARPAP) is proposed. Theoretical limit analysis and numerical validation are provided. In the fifth paper, we introduce maximum likelihood based ARPAP positioning method and propose a power contour circle fitting (PCCF) algorithm for initial position guess.

Paper I focuses on multi-modal localization sensor fusion. A ubiquitous tracking using motion and location sensor (UTMLS) scheme is proposed. Inside the UTMLS, a hypothesis test based absolution positioning fault detection method is proposed. An accurate non-GPS tracking method that makes use of consumer-grade inertial sensors is developed. The performance of the system is evaluated on an Android smartphone platform.

Paper II looks into the multipath fading effect on range estimation in RF power based localization system. We propose LoS-based range estimation. Conventional received signal strength indicator (RSSI) provides measurements of the total power [10] present in a received signal. It contains the power of transmitted payload (codes/symbols), fading channel which includes LoS, Non-Line-of-Sight (NLoS) signal component, and noise. Among all these component, only the LoS power is a univariate function of the radial distance (range). The proposed LoS-based ranging scheme reduces the distance estimation error by distinguishing LoS and NLoS components in the fading signal. Corresponding bias and Cramer-Rao Lower Bound (CRB [17, 18]) of the proposed range estimator is derived.

Paper III deals with the multipath fading effect on power-based position estimation. Bias and CRB analysis for the proposed LoS- and conventional RSS-based positioning methods are derived. In contrast to the conventional lognormal based analysis, the derived error models take into account the environmental multipath fading effect. The proposed LoS-based scheme improves positioning accuracy by eliminating the effect of non-range dependent portion of powers from received signal.

Paper IV addresses the localization error introduced by antenna directivity. An ARPAP positioning system is proposed. It optimizes the position estimation by finding the intersection of several non-circular power contours, based on Taylor series expansion. Simulation results show that the proposed method suppressed the antenna directivity effect on localization error, and reduced the positioning error due to the power measurement noise. The proposed scheme is instantiated for the cellular network. The derived error models are validated by simulation result.

Paper V introduces a maximum likelihood (ML)-based ARPAP positioning system. Numerical results show that the ML ARPAP is accurate and is robust to environmental fading disturbance. Moreover, due to the nonlinear nature of the ARPAP system model, an initial position guess is required for accurate ARPAP positioning. Existing solutions are based on either projection onto convex (POC), semidefinite programming (SDP), or approximate maximum likelihood (AML); and assume circular power contours (second order polynomial). However, the antenna directivity employed ARPAP path-loss model is highly nonlinear which renders difficulty of using these existing solutions. Therefore, a PCCF algorithm is proposed to find the initial position guess for ARPAP positioning.

1.3. CONTRIBUTIONS

This dissertation provides contributions to the field of wireless device localization using signal strength measurements.

Paper I introduces the development of a proposed UTMLS tracking system. The algorithm is implemented on a smartphone platform. And the performance is evaluated by experiment. The conducted experiments show that the UTMLS system efficiently reduces the drift in the consumer-grade inertial sensor-based dead reckoning, and effectively detects the GPS-fault while maintaining an acceptable accuracy.

Paper II introduces a new, LoS-based ranging, which suppresses multipath fading effect on the range estimation. The derived LoS- and RSS-based ranging error models bring a new insight into how the multipath propagation affects range estimation. They enable the elimination of the bias and variance introduced by fading signal from the range estimation.

Paper III introduces LoS based positioning. The position estimation accuracy is improved comparing to the conventional RSS based methods. The derived error model is capable of predicting LoS- and RSS-based positioning error, which is not present in exist literature. Also these error models can aid in assessing expected performance and planning the deployment of reference points.

Paper IV proposes the novel ARPAP positioning method to address the antenna radiation pattern injected localization error. The method is instantiated for the cellular network. Analytic performance guarantees are included. In addition, simulation results show that the proposed scheme is accurate and robust to power measurements error.

Paper V presents a novel maximum likelihood based ARPAP positioning algorithm. Simulation results proved its accuracy. Moreover, a new power contour circle fitting (PCCF) algorithm is developed for finding the initial position guess for accurate ARPAP positioning. Furthermore, LoS ML ARPAP is shown to be robust to fading disturbance.

PAPER

I. UBIQUITOUS TRACKING USING MOTION AND LOCATION SENSOR WITH APPLICATION TO SMARTPHONE

L. Wang and M. J. Zawodniok

Department of Electronic & Computer Engineering

Missouri University of Science and Technology

Rolla, Missouri 65409–0050

Tel: (409) 692-9235, (573) 341-4361

Email: lw3r6@mst.edu, mjzx9c@mst.edu

ABSTRACT

In this paper, a cost efficient fusion scheme, Ubiquitous Tracking with Motion and Location Sensor (UTMLS), is proposed for the accurate localization and tracking in mixed GPS-friendly, GPS-challenging, and GPS-denied scenario. The proposed drift-reduction method in UTMLS addresses the cumulating error issue in the indoor tracking with the consumer grade motion sensor. The proposed hypothesis test method in UTMLS improves the tracking sensor fusion precision by detecting distorted GPS reports and intelligently switching between GPS and inertial sensor based schemes. The proposed scheme is instantiated and implemented on an Android smartphone platform. Experiments have been conducted to evaluate and validate the accuracy. Experimental results show that 1) the proposed drift-reduction method effectively suppresses the non-GPS tracking error accumulation due to the integration of acceleration noise with time 2) UTMLS realizes robust indoor/outdoor seamless tracking, preventing GPS fault estimates introduced tracking error in the conventional Kalman filtering process.

Keywords: Localization; GPS; IMU; Kalman Filter; Android; Smartphone; Sensors.

1. INTRODUCTION

Location-based services (LBS) has become a key part of smart systems, including healthcare, autonomous vehicle, security, building automation, robotics, etc. Accurate localization and tracking of a mobile unit are the essential for context awareness of the applications. The global navigation satellite systems (GNSS), e.g. GPS, has long been used in mobile unit localization. In the outdoor, unobstructed environment, it provides acceptable accuracy. However, its accuracy can degrade in many situations, for example, when buildings overshadow some satellite in line-of-sight (LoS) or cause reflection (multipath fading effect), or when there is interference from a nearby device. Such a scenario with increased localization error is considered a GPS-challenging environement[1, 2, 3]. Moreover, since the satellite signal can be easily blocked by the buildings and ground, it is not suitable for the indoor localization which is also known as the GPS-denied environment.

Extensive research on fusion algorithms exploiting the complementary error characteristics of GPS and inertial measurement unit (IMU) have been performed for several decades [4, 5, 6, 7, 8, 9]. However, the accurate tracking with seamless transition between GPS-friendly and GPS-challenging/fault/denied environment remains an unsolved problem. Moreover, the accuracy of an indoor (non-GPS) tracking with the low-cost motion sensor is still insufficient. Though existing step/stripe recognition and estimation methods had some success in tracking human walking, it is still challenging for robotic and wheelchair applications.

As indicated in our experimental results in Section 4.2, in the indoor and outdoor combined tracking scenario, GPS may provide erroneous position reports. This leads to undesired tracking errors. As the tracked object approaches the building, the building obstructs the signals from some satellites. Hence, the line-of-sight signals are blocked. The non-line-of-sight (NLoS) signals reflected from the surroundings distort GPS signal

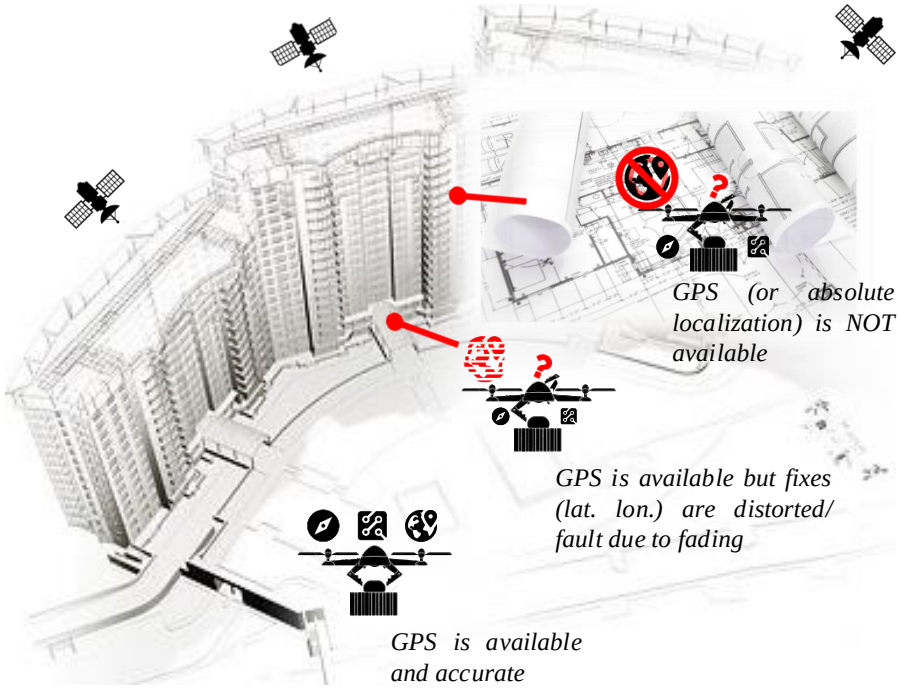

Figure 1. Motivation

lock, thus inject noises in GPS pseudo-range estimation. Hence, the GPS location reports are inaccurate. When the object is entering the building, LoS signals become completely blocked, while the NLoS signals may travel through the build via reflection. As the GPS receiver makes use of these fading signals, large localization errors may occur, *which is considered as GPS fault*.

Let us consider a smart robotic package delivery application as shown in Fig. 1. Suppose that the autonomous robots are assigned to deliver packages door to door. Tracking and navigating the robots from warehouse to the customer building's front door have been well addressed by existing solutions (e.g. GPS). However, when the robots approach the building, the GPS location reports may become erroneous/distorted *rather than become entirely absent*. Without extra sensors (e.g., camera, sonar, lidar), it is difficult to navigate the robot entering the building. On the other hand, tracking the robots with the low-cost inertial sensor in the indoor/non-GPS environment is still challenging due to the accumulated

error in displacement estimation with noise. Hence, a cost-efficient and smarter tracking and navigation approach, that can maintain sufficient indoor tracking accuracy, evaluate GPS reports, and smoothly switching between GPS and GPS-fault/denied navigation mode is desired.

In this paper, we propose a cost-effective Ubiquitous Tracking with Motion and Location Sensor (UTMLS) system which integrate the GPS and consumer grade IMU for indoor and outdoor seamless tracking. It achieves: 1) Seamless context-switching between indoor (GPS-challenging/denied) and outdoor (GPS-friendly) while maximizing the accuracy 2) the reduction of drift in the dead reckoning mode when using low-cost IMU. Moreover, the tracking accuracy is evaluated and validated by experiments with a prototype implemented on an Android smartphone platform.

For the GPS fault and challenging scenario, the proposed UTMLS detects the GPS fault through the proposed hypothesis test method which introduces the tracking robustness and improves the accuracy. The multivariate hypothesis test evaluates the GPS reading. When the reading is detected to be erroneous, the UTMLS will switch to indoor mode.

For the GPS-denied situation, existing solutions rely either on the pre-existing infrastructure, or human activity recognition (HAR) [10, 11, 12]. The pre-existing infrastructure augmented methods require the knowledge of the anchor nodes (e.g., WiFi access point, Bluetooth, ZigBee nodes, etc.) deployment in the building, which is difficult to obtain for security consideration in most of the scenarios. Or, it requires the time-consuming offline training (war-driving) phase to construct the radio map [13, 14, 15]. In contrast, in our proposed UTMLS system, infrastructure information or radio map are not required, which broadens applications and makes it more feasible for most indoor tracking scenarios.

The HAR based methods require step recognition and stride length estimation for dead reckoning. However, in the smart applications, the tracking object may be the package-delivering robots, or wheelchair, where human activities are absent in these scenarios.

The proposed UTMLS makes use of only the consumer grade IMU and estimates the displacement of the object in the heading direction. A high-pass filter is introduced in the UTMLS speed estimation to conquer the drift.

The proposed system is instantiated and evaluated on an Android phone. As an ideal platform for the low-cost smart LBS, the smartphone has become more and more popular[16] . The essential GPS receiver, motion sensor(accelerometer, gyroscope), and magnetometer have already been the standard modules equipped in the mainstream smartphone. In this paper, we introduced the prototype implementation and software design of the system.

2. METHODOLOGY

In this section, the methodology used for indoor and outdoor seamless tracking in the UTMLS system is presented.

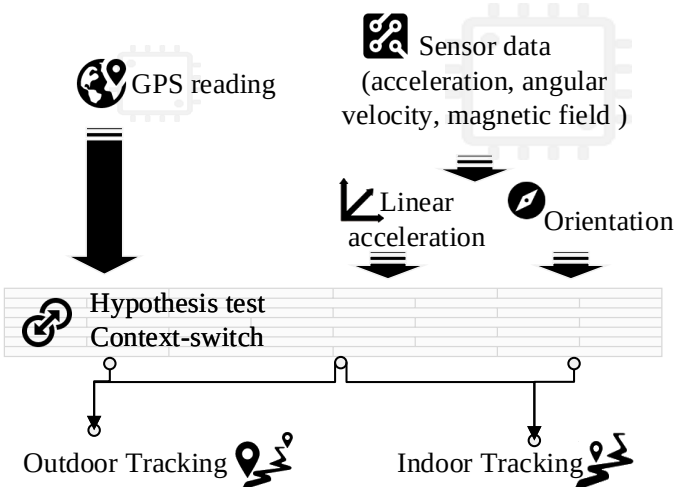

Figure 2. Overview

2.1. Overview. Fig. 2 depicts the overall systemic strategy of sensor fusion and indoor/outdoor tracking-mode switching in the proposed UTMLS. GPS estimation of the absolute position is fed into the system. At the same time, IMU readings are fed into the indoor tracking algorithm, to calculate the non-GPS based localization information. In the next step, the *Hypothesis-test Context-switcher*, which uses kinetic model and Kalman filter,

evaluates the data set. When the accuracy of GPS reports is acceptable, the system performs Kalman filtering in outdoor mode. In case that GPS fault (i.e. distorted GPS positioning) is detected, the system will switch to indoor mode. In the indoor mode, with the proposed drift-reduction method, accurate tracking (evaluated in Section 4) with the low-cost IMU is achieved.

In the following subsections, the dynamic system model and Kalman filter are briefly introduced in Section 2.2. Next, the proposed hypothesis test method is introduced in Section 2.3. Then, the indoor-mode tracking including the orientation and linear acceleration estimation, and velocity drift reduction is presented in Section 2.4.

2.2. Kinetic Model and Kalman Filter. For completeness, the dynamic model and Kalman filter update law are briefly introduced here. The state space continues time representation of the kinetics can be described as [17],

$$\begin{aligned} \dot{\boldsymbol{x}} &= \boldsymbol{A}\boldsymbol{x} + \boldsymbol{B}(\boldsymbol{u} + \tilde{\boldsymbol{\sigma}}) \\ \boldsymbol{y} &= \boldsymbol{C}\boldsymbol{x} + \boldsymbol{v}. \end{aligned} \tag{1}$$

where $\boldsymbol{A}$ is the state transition matrix, $\boldsymbol{B}$ is the control input matrix, $\boldsymbol{C}$ is the measurement matrix. $\boldsymbol{u}$ represents the control input which contains noise $\tilde{\boldsymbol{\sigma}}$. $\boldsymbol{y}$ is the measurement model with $\boldsymbol{v}$ representing the noise. $\boldsymbol{x}$ is the states in the system, and $\dot{\boldsymbol{x}}$ the derivative of it.

The kinetic model with the linear acceleration as the dynamic control input is given in Appendix 6.1.

By discretization,

$$\boldsymbol{x}_{k+1} = \boldsymbol{F}\boldsymbol{x}_k + \boldsymbol{G}\boldsymbol{u}_k + \boldsymbol{\sigma}_k. \tag{2}$$

$$\boldsymbol{y}_k = \boldsymbol{C}\boldsymbol{x}_k + \boldsymbol{v}_k. \tag{3}$$

where $\boldsymbol{F}$ is the Taylor expansion of $e^{\boldsymbol{A}\Delta t}$ and keep the lower order terms of Δt. And, $\boldsymbol{G} = \boldsymbol{F}\int_0^{\Delta t} e^{-\boldsymbol{A}\tau} d\tau \boldsymbol{B}$. $\boldsymbol{\sigma}_k$ and $\boldsymbol{v}_k$ are the noise in the state and observation, respectively.

Assuming $\boldsymbol{\sigma}_k$ and $\boldsymbol{v}_k$ are zero mean Gaussian, the process noise covariance matrix $\boldsymbol{Q}_k = E\left[\boldsymbol{\sigma}_k \boldsymbol{\sigma}_k^T\right]$, and the measurement noise covariance matrix $\boldsymbol{\Sigma}_k = E\left[\boldsymbol{v}_k \boldsymbol{v}_k^T\right]$.

Providing the state estimation $\boldsymbol{x}_{k-1}$, we can predict the state at k, $\boldsymbol{x}_k^-$, via (2). Thus, given observation at k, the estimation of the state at k is [18, 17],

$$\boldsymbol{x}_k^+ = \boldsymbol{x}_k^- + \boldsymbol{K}_k\left(\boldsymbol{y}_k - \boldsymbol{C}\boldsymbol{x}_k^-\right) \tag{4}$$

where,

$$\begin{aligned}
\boldsymbol{K}_k &= \boldsymbol{P}_k^- \boldsymbol{C}_k^T \left(\boldsymbol{C}_k \boldsymbol{P}_k^- \boldsymbol{C}_k^T + \boldsymbol{\Sigma}_k\right)^{-1} \\
\boldsymbol{P}_k^- &= \boldsymbol{F}_{k-1} \boldsymbol{P}_{k-1}^+ \boldsymbol{F}_{k-1}^T + \boldsymbol{Q}_{k-1} \\
\boldsymbol{P}_k^+ &= (\boldsymbol{I} - \boldsymbol{K}_k \boldsymbol{C}_k) \boldsymbol{P}_k^- (\boldsymbol{I} - \boldsymbol{K}_k \boldsymbol{C}_k)^T + \boldsymbol{K}_k \boldsymbol{\Sigma}_k \boldsymbol{K}_k^T .
\end{aligned} \tag{5}$$

2.3. Multivariate Hypothesis Test based GPS Fault Detection. In this section, Preposition 1 shows how we use covariance matrix to evaluate the accuracy of GPS location reports so as to decide whether its accuracy is sufficient or there is GPS fault. And in 2.3-2, we show how to obtain the observation covariance matrix from the dynamic.

1) The Multivariate Hypothesis Test:

Let $\boldsymbol{\Sigma}$ be the covariance matrix of the GPS observation $\boldsymbol{y} = [y_1, y_2]^T$. Assume that the noise of the GPS observation on the coordinate elements, i.e., y_1, y_2, is independent. Given the ideal performance of the GPS receiver, i.e., the covariance matrix $\boldsymbol{\Sigma_0}$, in the open outdoor environment. To detect the GPS-challenging context is equivalent to compare the generalized variance $|\boldsymbol{\Sigma}|$ with $|\boldsymbol{\Sigma_0}|$.

It has been proven in [19], $\sqrt{N-1}\left(\frac{|\boldsymbol{\Sigma}|}{|\boldsymbol{\Sigma_0}|} - 1\right)$ is asymptotically distributted as Normal, $\mathcal{N}(0, 2p)$. Where N is the number of sample, $p \times p$ is the dimension of the covariance matrix.

Preposition 1 provides the criterion for the hypothesis test.

Preposition 1. *The criterion for testing the hypothesis* $\boldsymbol{H}_0$*:* $|\boldsymbol{\Sigma}| \leq |\boldsymbol{\Sigma}_0|$*:*

$$Z = \sqrt{\frac{N-1}{2p}} \left(\frac{|\boldsymbol{\Sigma}|}{|\boldsymbol{\Sigma}_0|} - 1 \right). \tag{6}$$

The reject region (RR), $\boldsymbol{H}_1$*:* $|\boldsymbol{\Sigma}| > |\boldsymbol{\Sigma}_0|$*, given the significant level* α*:*

$$RR = \{ |\boldsymbol{\Sigma}| : Z(|\boldsymbol{\Sigma}|) \geq -Z_{1-\alpha} \}. \tag{7}$$

Remark 1 gives the power of the test. The power of a hypothesis test is the probability that the test correctly rejects $\boldsymbol{H}_0$ when $\boldsymbol{H}_1$ is true. A type II error occurs when $\boldsymbol{H}_0$ is false, but erroneously accepted. [20] Thus, the power of a test is found by calculate the probability of not committing a type II error. [21]

Remark 1. *The power of the test* $|\boldsymbol{\Sigma}| \leq |\boldsymbol{\Sigma}_0|$ *is,*

$$\pi(\sigma) = 1 - \boldsymbol{\phi} \left(\sqrt{\frac{(N-1)}{2p}} \left[\frac{|\boldsymbol{\Sigma}|}{\sigma} \left(1 - \sqrt{\frac{2p}{N-1}} Z_{1-\alpha} \right) - 1 \right] \right). \tag{8}$$

where $\boldsymbol{\phi}(\cdot)$ *is the cumulative distribution function (CDF) of the standard normal distribution.*

Proof. The type II error,

$$\begin{aligned} \boldsymbol{\beta}(\sigma) &= \mathbb{P}(fail\ to\ reject\ \boldsymbol{H}_0\ |\boldsymbol{H}_1\ is\ true) \\ &= \mathbb{P}(Z < -Z_{1-\alpha} |\, |\boldsymbol{\Sigma}_0| = \sigma) \\ &= \mathbb{P}\left(\sqrt{\frac{N-1}{2p}} \left(\frac{|\boldsymbol{\Sigma}|}{\sigma} - 1 \right) < \sqrt{\frac{N-1}{2p}} \left[\frac{|\boldsymbol{\Sigma}|}{\sigma} \left(1 - \sqrt{\frac{2p}{N-1}} Z_{1-\alpha} \right) - 1 \right] \right) \\ &= \boldsymbol{\phi} \left(\sqrt{\frac{N-1}{2p}} \left[\frac{|\boldsymbol{\Sigma}|}{\sigma} \left(1 - \sqrt{\frac{2p}{N-1}} Z_{1-\alpha} \right) - 1 \right] \right) \end{aligned}$$

Thus, the power of the test is $\pi(\sigma) = 1 - \beta(\sigma)$, which is (8). □

2) The Covariance Matrix in Observation:

The covariance matrix, $\mathbf{\Sigma}$, can be obtained from innovation vector,

$$\boldsymbol{i}_k = \boldsymbol{y}_k - \boldsymbol{y}_k^-. \tag{9}$$

where $\boldsymbol{y}_k^- = \boldsymbol{C}_k \boldsymbol{x}_k^-$. The covariance of the innovation is
$E\left[\boldsymbol{i}_k \boldsymbol{i}_k^T\right] = \boldsymbol{C}_k E\left[(\boldsymbol{x}_k - \boldsymbol{x}_k^-)(\boldsymbol{x}_k - \boldsymbol{x}_k^-)^T\right] \boldsymbol{C}_k^T + \mathbf{\Sigma}_k$.

The maximum likelihood estimator of the measurement noise is [22],

$$\mathbf{\Sigma}_k = \boldsymbol{V}_k - \boldsymbol{C}_k \boldsymbol{P}_k^- \boldsymbol{C}_k^T. \tag{10}$$

where $\boldsymbol{V}_k = \frac{1}{N} \sum_{j=j_0}^{k} \boldsymbol{i}_j \boldsymbol{i}_j^T$. And, N is the size of the moving estimation window, $j_0 = k - N + 1$.

2.4. Proposed Non-GPS Tracking Scheme. In the indoor mode, the non-GPS tracking of the mobile object is calculated based on the orientation estimation and drift-reduced velocity. The proposed drift-reduction method makes accurate indoor tracking with consumer grade IMU possible.

In this section, a gradient descent algorithm is first introduced for calculating the orientation quaternion in 2.4 1). Next, based on the orientation estimation, linear acceleration in the earth inertial frame is found in 2.4 2). Then, in 2.4 3), a drift-reduction method for the velocity estimation is presented.

1) Orientation:

The orientation of a mobile unit is the angle of the mobile body frame relative to the earth inertial frame. To determine the orientation, we integrate the gravity, angular velocity, and magnetic field measurements. They are measured by the accelerator, gyroscope, and magnetometer inside the smartphone IMU, respectively.

Let ${}_E^S\boldsymbol{q}$ be the quaternion that describes the orientation of the earth inertial frame relative to the sensor body frame.

The gyroscope measured angular velocity can be written in quaternion form as,

$$ {}^{S}\boldsymbol{\omega} = \left[0, \omega_x, \omega_y, \omega_z\right]. \tag{11} $$

The quaternion at time instance k can be calculated as [23],

$$ \begin{aligned} {}^{S}_{E}\dot{\boldsymbol{q}}_{\omega,k} &= \frac{1}{2}\, {}^{S}_{E}\hat{\boldsymbol{q}}_{k-1} \otimes {}^{S}\boldsymbol{\omega}_k \\ {}^{S}_{E}\boldsymbol{q}_{\omega,k} &= {}^{S}_{E}\hat{\boldsymbol{q}}_{k-1} + {}^{S}_{E}\dot{\boldsymbol{q}}_{\omega,k}\Delta t. \end{aligned} \tag{12} $$

where $\otimes$ represents the quaternion multiplication [23]. ${}^{S}_{E}\hat{\boldsymbol{q}}_{est,k-1}$ is the orientation quaternion estimation at $k-1$ epoch. And, $\hat{(\cdot)}$ represents the normalized quantity, i.e., $\|\hat{(\cdot)}\| == 1$.

Let ${}^{S}\boldsymbol{s}$ and ${}^{S}\boldsymbol{m}$ represents the acceleration and magnetic field measurement, respectively. And, the normalized reference gravity is ${}^{E}\hat{\boldsymbol{g}} = [0, 0, 0, 1]$, the earth magnetic field reference is ${}^{E}\hat{\boldsymbol{b}} = [0, b_x, 0, b_z]$. The orientation is the quaternion that minimize the function,

$$ \boldsymbol{f}({}^{S}_{E}\boldsymbol{q}) = \begin{bmatrix} {}^{S}_{E}\hat{\boldsymbol{q}}^{*} \otimes {}^{E}\hat{\boldsymbol{g}} \otimes {}^{S}_{E}\hat{\boldsymbol{q}} - {}^{S}\hat{\boldsymbol{s}} \\ {}^{S}_{E}\hat{\boldsymbol{q}}^{*} \otimes {}^{E}\hat{\boldsymbol{b}} \otimes {}^{S}_{E}\hat{\boldsymbol{q}} - {}^{S}\hat{\boldsymbol{m}} \end{bmatrix} \tag{13} $$

where $(\cdot)^{*}$ represents quaternion conjugate [23].

By gradient descent algorithm, the orientation quaternion,

$$ {}^{S}_{E}\hat{\boldsymbol{q}}_{\nabla,k} = {}^{S}_{E}\hat{\boldsymbol{q}}_{k-1} - \mu_k \frac{\nabla \boldsymbol{f}}{\|\nabla \boldsymbol{f}\|}. \tag{14} $$

where $\nabla \boldsymbol{f} = \left[\frac{\partial}{\partial({}^{S}_{E}\hat{\boldsymbol{q}})}\boldsymbol{f}\right]^{T} \boldsymbol{f}({}^{S}_{E}\hat{\boldsymbol{q}})$.

Thus, the orientation estimation is obtained by weighting the quaternion calculation from angular rate (12) and from gravity and magnetic field (14) [24],

$$ \begin{aligned} {}^{S}_{E}\boldsymbol{q}_k &= {}^{S}_{E}\hat{\boldsymbol{q}}_{k-1} + {}^{S}_{E}\dot{\boldsymbol{q}}_k\Delta t \\ {}^{S}_{E}\dot{\boldsymbol{q}}_k &= {}^{S}_{E}\dot{\boldsymbol{q}}_{\omega,k} - \beta\frac{\nabla \boldsymbol{f}}{\|\nabla \boldsymbol{f}\|} \end{aligned}. \tag{15} $$

2) Linear Acceleration:

The accelerometor readings are the measurements of the force along the coordinates of the sensor body frame. In ground mobile tracking application, due to the earth gravity, accelerometer reading will be nonzero even the sensor is static. The linear acceleration represents the force (without gravity) relative to the earth inertial frame, which can be estimated as,

$$\boldsymbol{u} = {}^{S}_{E}\boldsymbol{q}\ {}^{S}\boldsymbol{s}\ {}^{S}_{E}\boldsymbol{q}^{*} - \boldsymbol{g}. \tag{16}$$

where ${}^{S}\boldsymbol{s}$ is the accelerometor reading, ${}^{S}_{E}\boldsymbol{q}$ is the orientation estimated from (15), and $\boldsymbol{g} = [0, 0, 0, g]^{T}$ ($g = 9.807 m/s^{2}$).

Let ${}^{S}_{E}\boldsymbol{q} = [q_1, q_2, q_3, q_4]$, the heading (the azimuth angle of the orientation) is,

$$\psi = atan2(2q_3q_4 - 2q_1q_2,\ 2q_1^2 + 2q_4^2 - 1). \tag{17}$$

Thus, the acceleration in the heading direction can be found by the dot production of $\boldsymbol{u}$ and heading unit vector $\hat{\boldsymbol{h}} = [sin(\psi),\ cos(\psi),\ 0]^{T}$,

$$\boldsymbol{a} = \boldsymbol{u} \cdot \hat{\boldsymbol{h}}. \tag{18}$$

3) Drift Reduction:

As indicated by the kinetic model with linear acceleration input (Appendix 6.1), to calculate the displacement, acceleration measurement needs to be integrated first to obtain the velocity. Then, the velocity has to be integrated for the second time. Therefore, the noise in the acceleration measurements will be accumulated which result in huge drift in displacement estimation.

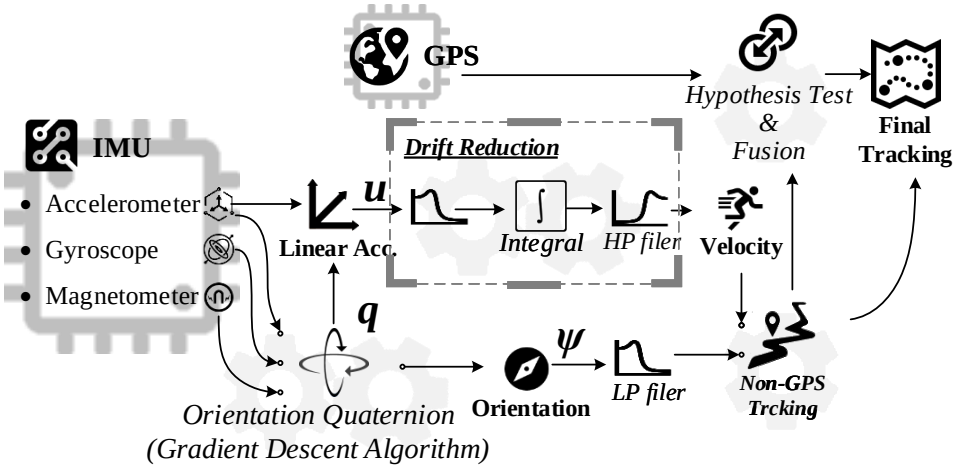

Figure 3. Sensor Data Processing Diagram

In the indoor mobile unit tracking, considering the limited space, we assume that the mobile object tends to stop, and there is *no strict-constant-speed* in the movement. Therefore, in our proposed UTMLS, the drift in the calculated velocity is eliminated by a high-pass filter (the "Drift Reduction" box in fig. 3).

Fig.3 illustrates the sensor data processing procedure in our system. The accelerometer, gyroscope, (in rigid body frame) and magnetometer measured signals are first processed by quaternion based gradient descent algorithm to produce the orientation (in the earth inertial frame). Next, as shown in the "Drift Reduction" box in fig. 3, the velocity is calculated by integrating the low-pass filtered linear acceleration, and a high-pass filter for eliminating the drift. Then, with the speed and orientation, the mobile unit dead-reckoning (non-GPS tracking) is achieved. The "Hypothesis Test & Fusion" block represents the proposed hypothesis test method for evaluating the GPS accuracy. It determines whether or not that the GPS readings should be integrated with non-GPS tracking.

3. PROTOTYPE IMPLEMENTATION

The proposed algorithm is implemented on the Samsung Galaxy S®6 Android phone. The onboard IMU motion sensors (including the acceleration sensor, gyroscope, and geomagnetic field sensor) are accessed through Android SensorManager. The GPS latitude/longitude is periodically obtained through Android LocationManager. In our experiments, motion sensor readings are refreshed every $\Delta t = 6$ milliseconds, latitude/longitude is updated once per second. The proposed scheme including the quaternion gradient descent algorithm, kalman filter, low-pass and high-pass filters are developed and evaluated by using the MathWorks® Matlab. Next, the Matlab code is converted into C/C++ code through MATLAB Coder. Then, the algorithm API library is built by using the Android ndk-build (native development kit) tool. Finally, C/C++ APIs are wrapped by Java Native Interface (JNI) so that they can be used in Java environment.

The software structure is illustrated in Fig. 4. The sensoring services, including the low-pass and high-pass filtering, are implemented as one Android Handler runnable object. And, the non-GPS tracking, hypothesis-test, Kalman filtering process are realized as a standalone Handler service. Besides, file I/O service is a standalone Handler thread.

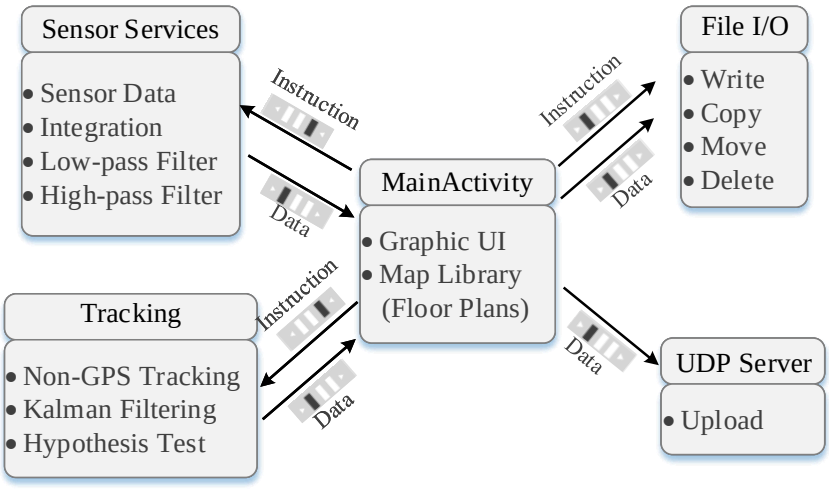

Figure 4. Software Diagram

UDP service (for uploading data to PC Matlab evaluation program) is realized by using the Android AsyncTask. Handler threads exchange information with MainActivity through Android MessageQueue.

4. EXPERIMENTAL RESULTS

In the Samsung Galaxy S®6, a 6-axis MotionTracking device, InvenSense® MPU-6500™, provides a 0.3mg noising accelerometer and a $\pm 5°/s$ zero-rate-output $0.1°/s$ noising gyroscope [25, 26].

For the evaluation of the proposed system, two experiments are conducted. First, an indoor experiment is first implemented to evaluate the non-GPS tracking accuracy. In the second experiment, an experimental path is chosen to traverse the building. The tracking error of the proposed hypothesis test based fusion method is compared with conventional Kalman filtering result.

The actual/reference path that the experimenter followed is shown in Appendix 6.2 Fig.9, Fig.10. The indoor experiment is conducted on the 3rd floor of engineering research building (ERL), Missouri University of Science & Technology. While, for the indoor-outdoor complex scenario, the experiment is implemented on the 1st floor inside, and sidewalk outside (near) the ERL building.

4.1. Non-GPS Tracking. In our indoor tracking experiment, twenty trials are conducted. At the same time, the tracking results by using the conventional non-drift-reduction method are recorded for comparison.

In Fig. 5, the tracking errors with and without the proposed drift reduction are compared. The x-axis of the figure represents the index of *evaluation positions* shown in Fig.9 (Appendix 6.2). For the purpose of comparison, tracking errors along the evaluation positions are fitted with second-order polynomial by using the linear regression. From Fig.5 we found that without drift reduction, the tracking error increases along with the moving distance (/time). In contrast, the error is maintained at a constant level when drift

reduction is applied. Therefore, the proposed drift reduction method effectively suppressed the accumulated error in the tracking.

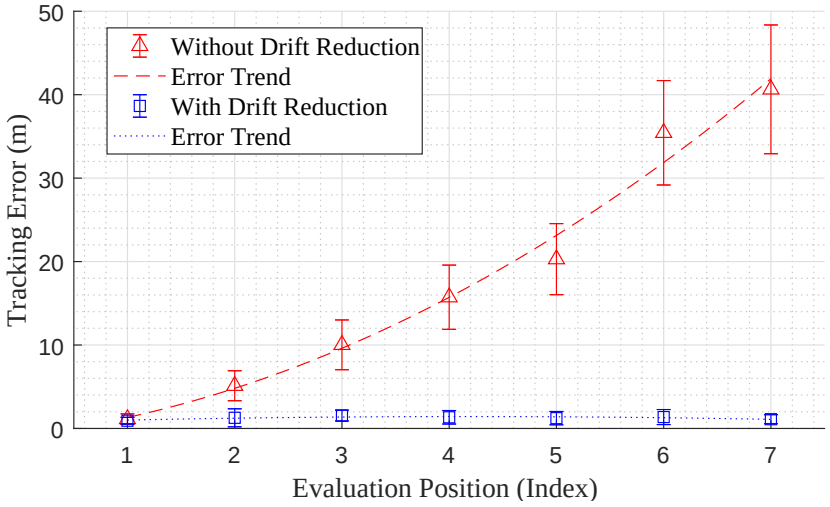

Figure 5. Indoor Tracking Error Comparison

Table 1. Tracking Error Comparison

Pos. Idx.[a]	**D.R.**[b] (m)		**w/o D.R**[c] (m)		**Imprv.**[d]
	err.	**std. dev.**	**err.**	**std. dev.**	
1	0.930	0.402	1.132	0.618	18%
2	1.277	1.079	5.120	1.796	75%
3	1.544	0.653	10.022	2.983	85%
4	1.339	0.809	15.728	3.850	91%
5	1.236	0.799	20.29	4.257	94%
6	1.366	0.903	35.434	6.257	96%
7	1.107	0.542	40.64	7.715	97%

[a] Position Index (Appendix 6.2 Fig.9)
[b] Drift Reduction
[c] Without Drift Reduction
[d] Improvement of **D.R.** over **w/o D.R.**

The tracking errors and error standard deviations at each evaluating position are shown in Table 1. On average, the error of the drift-reduction based tracking is 1.027 m. (Tracking results of the twenty trials are shown in Fig. 6 for reference.) While, without the proposed drift reduction, the averaged tracking error is accumulated with acceleration noise.

The proposed non-GPS tracking method effectively reduced the drift in the velocity estimation, hence the overall tracking accuracy is improved.

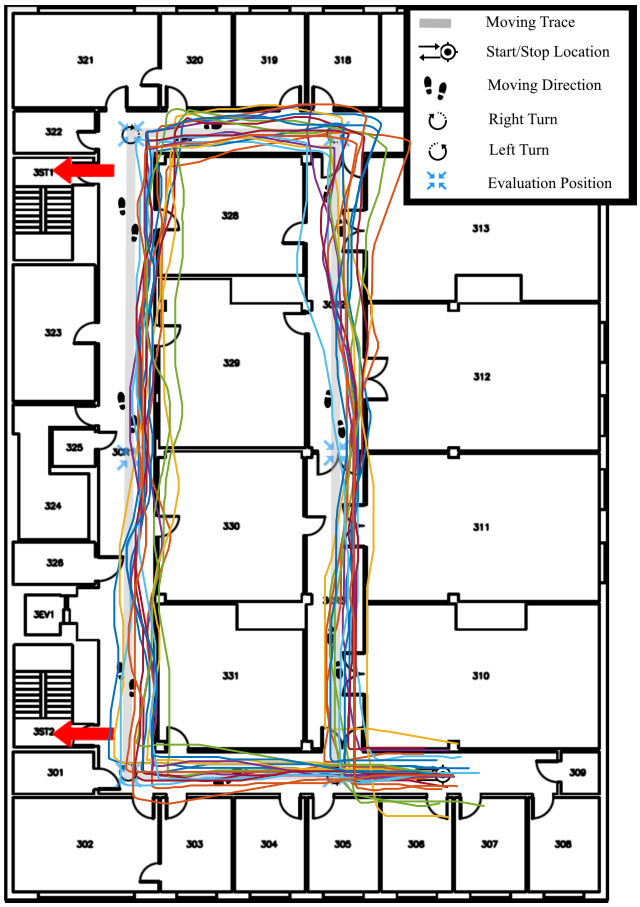

Figure 6. Proposed Non-GPS Tracking Results

4.2. UTMLS. The tracking error of the proposed UTMLS and conventional Kalman filtering results are compared in Fig.7. The tracking "Error Trend" in the figure are the linear regression result of fitting the error data with the second-order polynomial. The "Er-

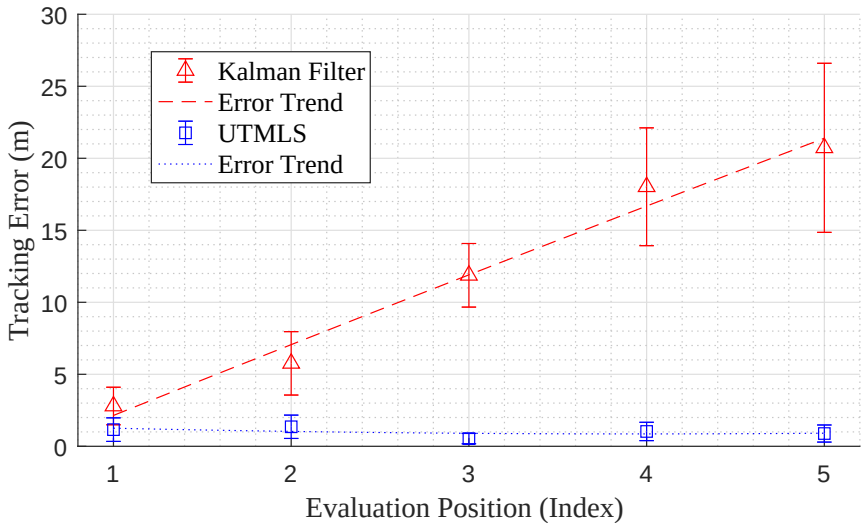

Figure 7. Tracking Error Comparison between UTMLS and Kalman Filtering

ror Trend" of the Kalman filtering based tracking shows an error divergence along with the evaluation positions (distance), whereas the UTMLS based one prevents the error deviation. This can be interpreted by Fig.8 which is one field trial instance in our experiment. As the tracked object is traveling into the building, since the GPS receiver makes use of the fading signal estimating the pseudo-range, erroneous position reports are provided. Therefore, in Fig.8, the "GPS Trace" diverges from the actual moving trajectory and "GPS error" gets large. Hence, the conventional Kalman filtering result is distorted by this GPS fault.

Table 2 shows the tracking error of the proposed UTMLS and Kalman Filtering results. In the table, the UTMLS has less error comparing to the conventional Kalman filtering result at each evaluating position (Appendix 6.2 Fig.10). This is due to the fact that, when the tracked object enters the building, the UTMLS effectively detects the GPS fault and switches the tracking mode. The erroneous GPS reports are prevented in the sensor fusion algorithm.

Table 2. Tracking Error in GPS Challenging/Fault Scenario

Pos. Idx.[a]	**UTMLS** (m)		**Kalman** (m)		**Imprv.**[b]
	err.	**std. dev.**	**err.**	**std. dev.**	
1	1.1582	0.81751	2.799	1.3034	59%
2	1.3558	0.8102	5.761	2.2013	76%
3	0.93447	0.35703	11.88	2.2081	92%
4	1.0309	0.63664	18.02	4.0904	94%
5	0.88671	0.59365	20.73	5.8701	96%

[a] Position Index (Appendix 6.2 Fig.10)
[b] Improvement of *UTMLS* over *Kalman Filtering*

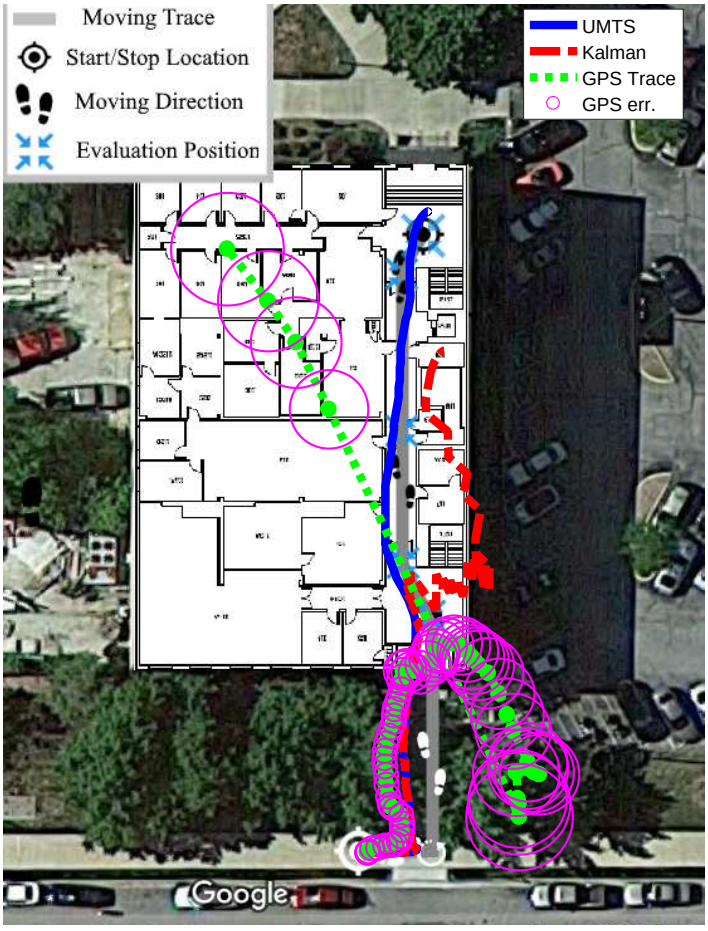

Figure 8. Comparison of UTMLS, Kalman Filtering, and GPS Fixed &Accuracy

5. CONCLUSION AND FUTURE WORKS

The proposed UTMLS system is successfully evaluated and validated by experiments with the prototype implementation. It achieves accurate mobile object tracking and smooth transitions in mixed GPS-friendly, GPS-challenging, and GPS-denied scenario. In Non-GPS indoor tracking mode, experimental results show that the proposed drift-reduction method effectively suppressed the accumulated error in consumer grade IMU and achieved overall $1m$ error accuracy. The proposed hypothesis test method effectively detected the GPS fault and triggered indoor/outdoor tracking mode switching. Overall, the UTMLS system maintains 1 m accuracy throughout the entire indoor-outdoor field trial, which is 92% more accurate than conventional Kalman filtering.

The future work should include developing a smarter context-aware fusion of the different location information. For example, to detect and correct when the matelic object is skewing the compass reading.

6. APPENDIX

6.1. Kinetic Model (Linear Acceleration Input). Let the state of the kinetic model encapsulate the displacement and velocity along the north east coordinates in the earth inertial frame,

$$\boldsymbol{x} = [x_1, v_1, x_2, v_2]^T. \tag{19}$$

where $[x_1, x_2]$ represents the displacements of the mobile unit along north and east directions, and $[v_1, v_2]$ is the speeds. And, the linear acceleration as the control input, i.e., $\boldsymbol{u} = [a_1, a_2]^T$.

The dynamic model matrices are,

$$\boldsymbol{A} = \begin{bmatrix} 0 & 1 & 0 & 0 \\ 0 & 0 & 0 & 0 \\ 0 & 0 & 0 & 1 \\ 0 & 0 & 0 & 0 \end{bmatrix}, \ \boldsymbol{B} = \begin{bmatrix} 0 & 0 \\ 1 & 0 \\ 0 & 0 \\ 0 & 1 \end{bmatrix},$$
$$\boldsymbol{F} = \begin{bmatrix} 1 & \Delta t & 0 & 0 \\ 0 & 1 & 0 & 0 \\ 0 & 0 & 1 & \Delta t \\ 0 & 0 & 0 & 1 \end{bmatrix}, \ \boldsymbol{G} = \begin{bmatrix} \frac{(\Delta t)^2}{2!} & 0 \\ \Delta t & 0 \\ 0 & \frac{(\Delta t)^2}{2!} \\ 0 & \Delta t \end{bmatrix}. \tag{20}$$

6.2. Moving Path in the Experiments. Fig. 9 and Fig. 10 show the paths along which the experiments are conducted.

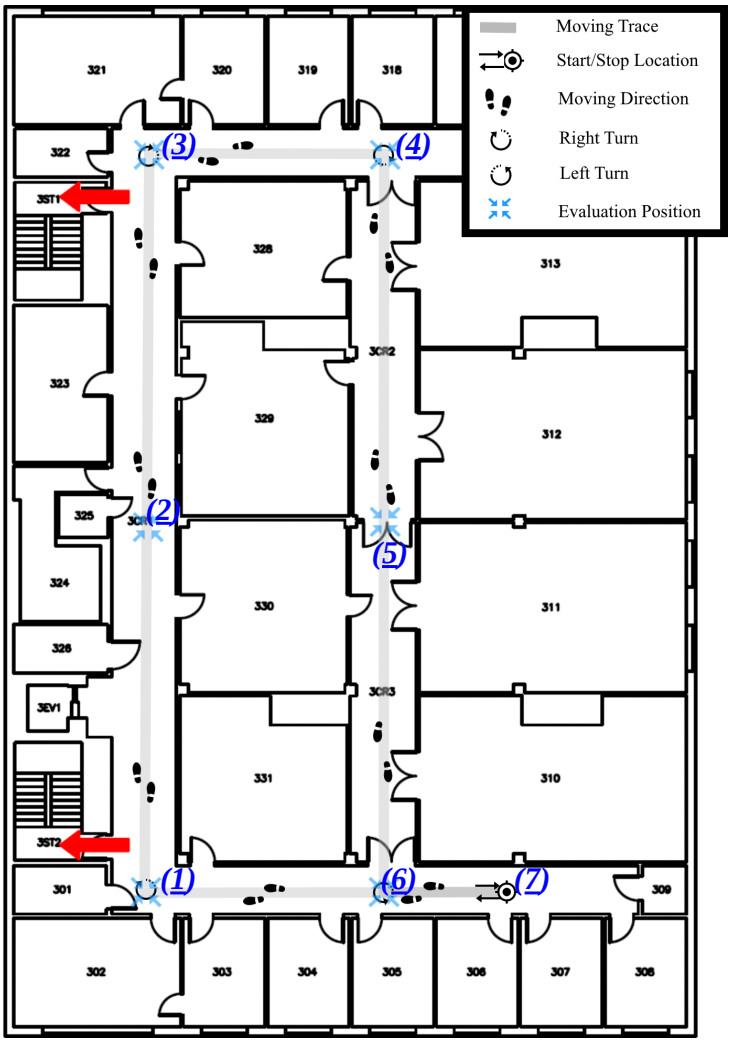

Note: ***(#)*** is the index of evaluating position

Figure 9. Indoor Moving Path

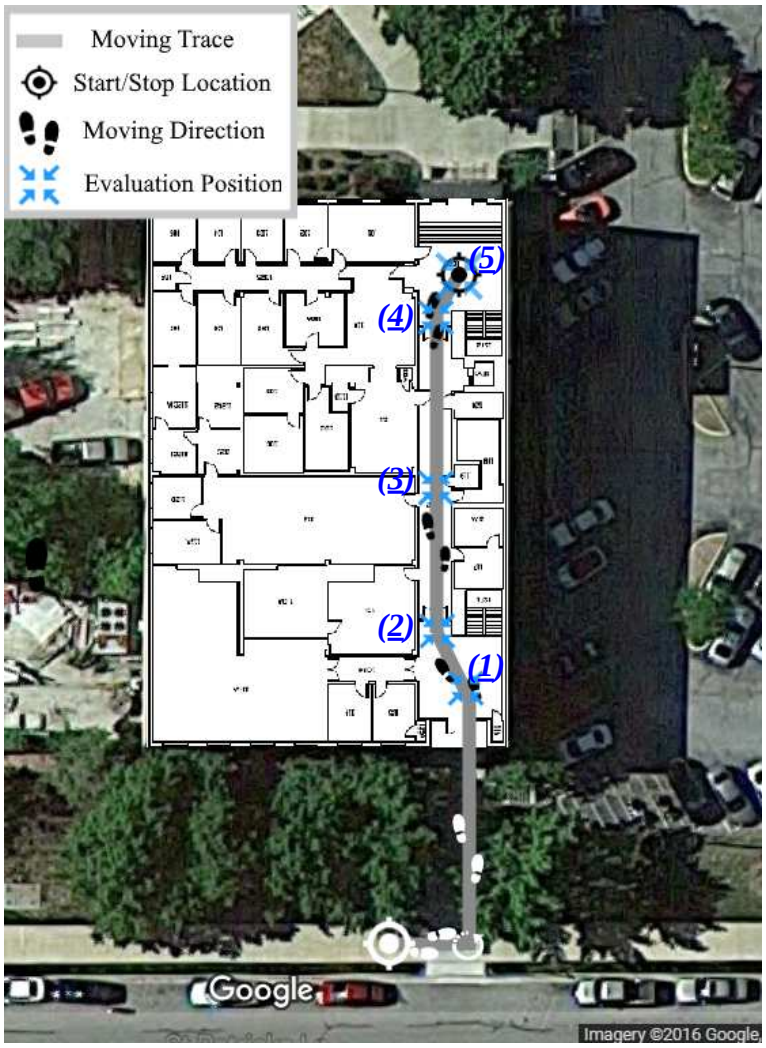

Note: ***(#)*** is the index of evaluating position

Figure 10. Outdoor Moving Path

Figure 11. Without Drift Reduction

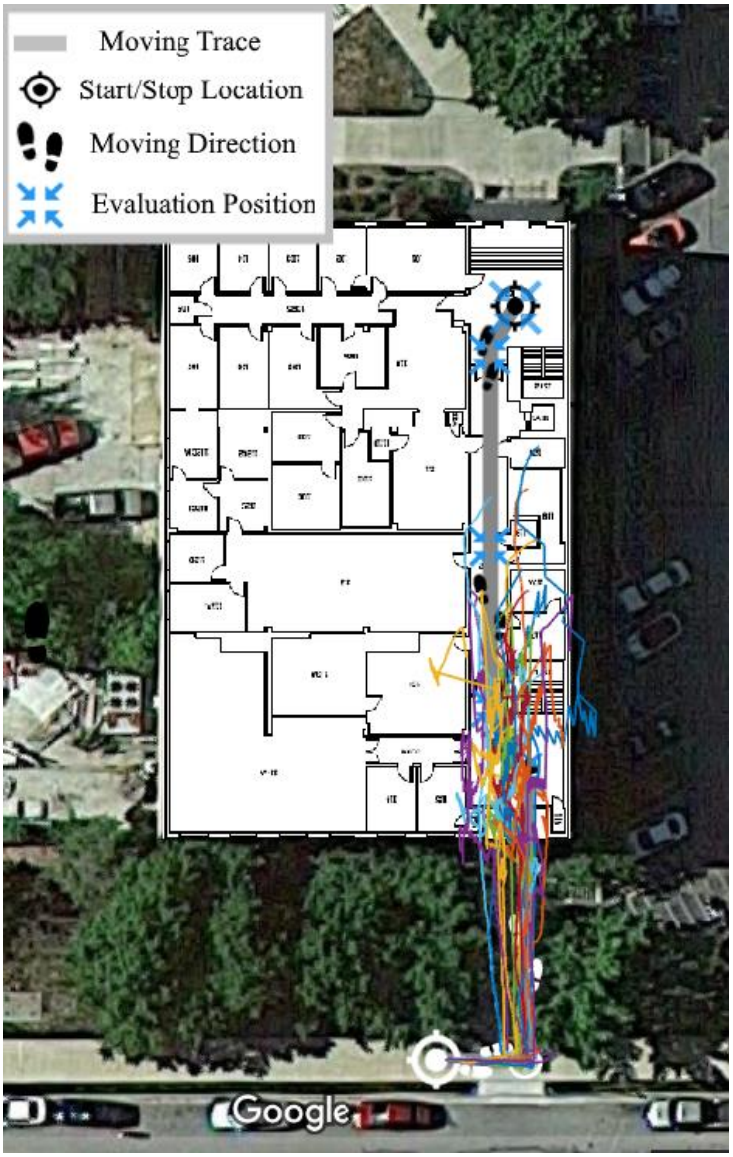

Figure 12. Kalman Filtering Results

REFERENCES

[1] Pratap Misra and Per Enge. *Global positioning system: signals, measurements, and performance*. Ganga-Jamuna Press, 2006. ISBN 978-0-9709544-1-1.

[2] B. Lubbers, S. Mildner, P. Oonincx, and A. Scheele. A study on the accuracy of GPS positioning during jamming. In *2015 International Association of Institutes of Navigation World Congress (IAIN)*, pages 1–6, October 2015. doi: 10.1109/IAIN.2015.7352258.

[3] M. L. Psiaki, T. E. Humphreys, and B. Stauffer. Attackers can spoof navigation signals without our knowledge. Here's how to fight back GPS lies. *IEEE Spectrum*, 53(8): 26–53, August 2016. ISSN 0018-9235. doi: 10.1109/MSPEC.2016.7524168.

[4] W. Yan, L. Wang, Y. Jin, and G. Shi. High accuracy Navigation System using GPS and INS system integration strategy. In *2016 IEEE International Conference on Cyber Technology in Automation, Control, and Intelligent Systems (CYBER)*, pages 365–369, June 2016. doi: 10.1109/CYBER.2016.7574851.

[5] M. Zhong, J. Guo, and Q. Cao. On Designing PMI Kalman Filter for INS/GPS Integrated Systems With Unknown Sensor Errors. *IEEE Sensors Journal*, 15(1): 535–544, January 2015. ISSN 1530-437X. doi: 10.1109/JSEN.2014.2334698.

[6] L. Bowen and Y. Danya. Calculation of vehicle real-time position overcoming the GPS positioning latency with MEMS INS. In *Proceedings of 2014 IEEE International Conference on Service Operations and Logistics, and Informatics*, pages 248–254, October 2014. doi: 10.1109/SOLI.2014.6960730.

[7] Aboelmagd Noureldin, Ahmed El-Shafie, and Mohamed Bayoumi. GPS/INS integration utilizing dynamic neural networks for vehicular navigation. *Information Fusion*, 12(1):48–57, January 2011. ISSN 1566-2535. doi: 10.1016/j.inffus.2010.01.003. URL https://www.sciencedirect.com/science/article/pii/S1566253510000175.

[8] Mohammed Olama, Charalambos Charalambous, Ioannis Papageorgiou, Seddik Djouadi, and Teja Kuruganti. *Position and Velocity Tracking in Cellular Networks Using the Kalman Filter.* INTECH Open Access Publisher, 2009. ISBN 978-953-307-000-1. OCLC: 884025728.

[9] John L. Crassidis. Sigma-point Kalman filtering for integrated GPS and inertial navigation. *IEEE Transactions on Aerospace and Electronic Systems*, 42(2):750–756, 2006. URL http://ieeexplore.ieee.org/abstract/document/1642588/.

[10] M. Alzantot and M. Youssef. UPTIME: Ubiquitous pedestrian tracking using mobile phones. In *2012 IEEE Wireless Communications and Networking Conference (WCNC)*, pages 3204–3209, April 2012. doi: 10.1109/WCNC.2012.6214359.

[11] Moustafa Youssef, Mohamed Amir Yosef, and Mohamed El-Derini. GAC: energy-efficient hybrid GPS-accelerometer-compass GSM localization. In *Global Telecommunications Conference (GLOBECOM 2010), 2010 IEEE*, pages 1–5. IEEE, 2010.

[12] Ionut Constandache, Romit Roy Choudhury, and Injong Rhee. Towards mobile phone localization without war-driving. In *Infocom, 2010 proceedings ieee*, pages 1–9. IEEE, 2010.

[13] I.T. Haque and C. Assi. Profiling-Based Indoor Localization Schemes. *IEEE Systems Journal*, 9(1):76–85, March 2015. ISSN 1932-8184. doi: 10.1109/JSYST.2013.2281257.

[14] Bang Wang, Shengliang Zhou, Wenyu Liu, and Yijun Mo. Indoor Localization Based on Curve Fitting and Location Search Using Received Signal Strength. *IEEE Transactions on Industrial Electronics*, 62(1):572–582, January 2015. ISSN 0278-0046. doi: 10.1109/TIE.2014.2327595.

[15] Heikki Laitinen, Jaakko Lahteenmaki, and Tero Nordstrom. Database correlation method for gsm location. In *Vehicular Technology Conference, 2001. VTC 2001 Spring. IEEE VTS 53rd*, volume 4, pages 2504–2508. IEEE, 2001.

[16] Ericsson Mobility Report. URL https://www.ericsson.com/res/docs/2016/ericsson-mobility-report-2016.pdf.

[17] Dan Simon. *Optimal State Estimation: Kalman, H Infinity, and Nonlinear Approaches*. Wiley-Interscience, 2006. ISBN 978-0-471-70858-2.

[18] Rudolph Emil Kalman. A new approach to linear filtering and prediction problems. *Journal of basic Engineering*, 82(1):35–45, 1960.

[19] T. W. Anderson, editor. *An Introduction to Multivariate Statistical Analysis*. Wiley, 1984.

[20] Lee J Bain and Max Engelhardt. *Introduction to probability and mathematical statistics*, volume 4. Duxbury Press Belmont, CA, 1992.

[21] Paul D. Ellis. *The Essential Guide to Effect Sizes: Statistical Power, Meta-Analysis, and the Interpretation of Research Results*. Cambridge University Press, July 2010. ISBN 978-0-521-14246-5. Google-Books-ID: 5obZnfK5pbsC.

[22] A. H. Mohamed and K. P. Schwarz. Adaptive Kalman Filtering for INS/GPS. *Journal of Geodesy*, 73(4):193–203, May 1999. ISSN 0949-7714, 1432-1394. doi: 10.1007/s001900050236. URL http://link.springer.com/article/10.1007/s001900050236.

[23] Jack B. Kuipers. *Quaternions and Rotation Sequences: A Primer with Applications to Orbits, Aerospace, and Virtual Reality*. Princeton University Press, 2002. ISBN 978-0-691-10298-6.

[24] Sebastian OH Madgwick, Andrew JL Harrison, and Ravi Vaidyanathan. Estimation of IMU and MARG orientation using a gradient descent algorithm. In *2011 IEEE International Conference on Rehabilitation Robotics*, pages 1–7. IEEE, 2011.

[25] MPU-6500 Product Specification Revision 1.1. URL http://www.glynstore.com/invensense-mpu-6500-6-axis-gyroscope-accelerometer-sensor-ic/.

[26] Inside the Samsung Galaxy S6 | Chipworks. URL https://www.chipworks.com/about-chipworks/overview/blog/inside-the-samsung-galaxy-s6.

II. BIAS AND CRB ANALYSIS OF LOS-BASED AND RSS-BASED RANGING METHODS

L. Wang and M. J. Zawodniok

Department of Electronic & Computer Engineering

Missouri University of Science and Technology

Rolla, Missouri 65409–0050

Tel: (409) 692-9235, (573) 341-4361

Email: lw3r6@mst.edu, mjzx9c@mst.edu

ABSTRACT

In this paper, bias and Cramer Rao Bound (CRB) analyses for both proposed line-of-sight (LoS) based and conventional received signal strength (RSS) based ranging methods are provided. A minimum bias of LoS-based ranging is derived, which is based on the asymptotic variance (AsV) of the estimator. Mean square error lower bound (MSEB), which is the summation of CRB and the square of minimum bias, is employed to compare with existing RSS-based methods. The existing RSS-based ranging methods are categorized, corresponding biases are analyzed. The multipath fading effect to the final range estimation has been model into the MSEB. The proposed LoS-based ranging method minimizes the effect of NLoS component (i.e. the multipath fading) in the received signal. The derived model was validated by simulation. Both the analytic model and simulation results show that the performance of the proposed LoS method is superior to that of the conventional RSS-based methods.

Keywords: Cramer-Rao Bound (CRB); Fading Channel; Line of Sight (LoS); Localization; Received Signal Strength (RSS); Ranging.

1. INTRODUCTION

Autonomous vehicles need reliable localization and navigation solution. Global navigation satellite systems (GNSS), as the most widely-used positioning technology, can provide accurate position estimation. However, it is limited by several conditions, such as the number of visible satellites, their relative position, their radio electric coverage [1]. Besides, it is also constrained by interference, and subjects to malicious jamming and spoofing. Therefore, a secondary solution is desired. The ideal one would be using the communication system. To avoid complexity and prevent dedicated hardware investment and costly process like TOA (time of arrival), TDOA (difference-of-arrival), and AoA (angle-of-arrival), it should rely on an existing standard, e.g. cellular network, and require little modification to the existing devices. Received signal strength indicator (RSSI), for example, is readily available in any RF devices. However, traditional RSSI based ranging methods suffer from low accuracy due to the fading. Moreover, a complete understanding of the accuracy limit of RSS-based ranging is missing. Hence, our work focuses on developing LoS-power-based ranging scheme, and deriving new theoretical limits for both LoS- and RSS-based methods.

The proposed LoS-based ranging scheme reduces the distance estimation error by distinguish LoS and NLoS components in the fading signal, while maintaining benefit of low hardware overhead over ToA, TDoA, and AoA. This method is suitable for channel with Ricean fading.

In this paper, the bias and Cramer-Rao Lower Bound (CRB [2, 3]) of the proposed range estimator is derived. For the purpose of comparison, the theoretical limit of conventional RSS based range estimation is also derived. To the best of the authors' knowledge, it is the first time that multipath fading effect is modeled into the RSS- and LoS-based range estimation error model. The analytical proof and simulation result show that the proposed LoS-ranging is able to suppress the multipath fading effect on the range estimation.

For the convenience of comparison, the existing RSS-based range estimators are classified into *MeanPower*, *MeanDist*, and *MeanStrength* in Section IV. The bias and CRB of these estimators are derived.

Assuming the presence of LoS signal component, our analyses (Bias and CRB modeling) are based on Ricean distribution of a fading channel. A complete analysis of range estimation for both strong signal (for example, greater than $0dBm$ (10^{-3}Watts)) and weak signal (e.g. less than $0dBm$ (10^{-3}Watts)) conditions has been established. Validated by simulation results, the similarity (Pearson Correlation Coefficient [4]) between our model and simulation results is above 90%. This paper also provides a performance comparison between RSS-based and LoS-based range estimation in the mean square error (MSE) sense. Analytical model and simulation results show that the LoS-based ranging is more accurate than RSS-based methods.

Existing works that benefit from LoS/NLoS estimation are mostly developed for ToA-based, e.g. [5, 6, 7, 8], or hybrid-based system (ToA/AoA/AoD) [9, 10]. To the best of the authors' knowledge, LoS signal power based ranging method is formulated and theoretically analyzed for the first time.

2. MOTIVATION

Received signal strength indicator provides measurements of the total power [11] present in a received signal. It is commonly used as an input to localization schemes [12, 13] (i.e., fingerprinting [14, 15, 16, 17], and path-loss [18]).

Widely accepted model of the signal amplitude received at mobile equipment (ME) over a local area is a composite distribution consisting of a fast fading (Rayleigh) and a slow fading (lognormal) [12, 19, 20]. The local average power (slow fading) is acquired by smoothing out the fast fading [12, 13, 21, 19, 22, 20]. The RSSI is the local average power and is indicated in *dBm* unit [11]. The smoothing operation renders the lognormal property of the local averaging power.

The conventional local average model (lognrmal) is not able to distinguish the NLoS component in the fading signal. The received signal is the original signal sent from transmitter after path-loss (LoS component) superimposed with several different copies of itself (NLoS component) from different paths (/directions) due to reflection, diffraction, and scattering. Hence, the magnitude of NLoS component in the fading signal depends on the environment. The local averaging of power converges to Normal distribution under the Central Limit Theorem (CLT). Thus, the RSSI (local averaging power) in conventional method has a lognormal distribution (see Appendix 9). The power of code/symbols will raise the mean level proportionally. As shown in Appendix 9, the average value of the received signal power contains an NLoS signal portion that is dependent on the environment. And this portion of the signal introduces bias to the range estimation. Both the RSSI-based range and position estimations have already been explored by Dr. Zanella and Bardella [21] and Dr. Li [22]. But NLoS effect has not been modeled.

The proposed LoS- and RSS-based ranging error models bring insight into how the multipath propagation affects range estimation, and enable elimination of bias and variance introduced by fading signal from the range estimation.

RSSI contains the power of transmitted payload (codes/symbols), fading channel which includes Line-of-Sight (LoS) and Non-Line-of-Sight (NLoS), and noise. Among all these factors, only the LoS power is a univariate function of the radial distance (range). Multi-path fading (NLoS components in the fading signal) is a time varying function of both range and environment. Hence, it introduces error to RSSI based ranging and localization. The fading signal power can be modeled as,

$$P_{RSS} = P_{LoS}(d) + P_{NLoS}\left(d, e\left([x, y], t\right)\right) + n_m. \tag{1}$$

in which, the LoS power $P_{LoS}(d)$ is a univariate function of the range from the receiver to the transmitter; the NLoS power, $P_{NLoS}(\cdot)$, is a time varying function of both the range distance and environment, $e(\cdot)$. The environmental effect, $e(\cdot)$, is a multivariate function of, but not limited to, geographical location of the mobile equipment ($[x, y]^T$) and time (t). n_m is the measurement noise which can be assume to be zero mean, white, and additive.

Generally, an empiric path-loss model based on Friis transmission equation [23] can be defined as,

$$P_r = (\kappa/d)^n. \tag{2}$$

where κ is a constant factor that depend on the antenna efficiency, gain, carrier signal wavelength, and transmission power. P_r is the received power. d is the range distance in meters, and n is a power factor. In free-space, n is equal to 2. In either urban or some suburban areas, n can be between 3 and 6. The distance is estimated from signal power measurement as,

$$d = f(\theta) = \kappa\, \theta^{-a}. \tag{3}$$

where $a = 1/n$. θ is a measured signal power. In ideal channel, θ is an estimator of the total power of received signal including LoS and NLoS components ($\hat{\Omega}$). In proposed method, we estimate the LoS component ($\hat{v}$) from channel measurement.

Conventional RSS measurement based empirical path-loss model has to overcome the multipath-fading by tuning parameters κ and a in (3)[18]. Time and effort consuming data-driven tuning of the parameters need to be carried out periodically to accommodate for the possible changes in the environment. Moreover, it averages time variation in fading thus reducing maximum accuracy.

In contrast, the LoS power varies monotonically with distance. It is consistent with path-loss model and is not affected by environmental conditions. Hence, more accurate ranging is possible with LoS-based method than RSS.

The remainder of this paper is organized as follows. In Section III, we discuss related works and effect of NLoS on the range estimation. Also, the RSS and LoS-based approaches are contrasted. In Section IV, the proposed scheme is introduced. In Section V, the bias and CRB of the proposed LoS-based ranging is analytically derived. In Section VI, conventional RSS-based ranging methods are classified. And bias and CRB based on Ricean distribution are derived. The performance comparison and simulation validations are given in Section VII. The paper is concluded in Section VIII.

3. RELATED WORKS

In this section, AoA, ToA, TDoA methods are introduced and compared with receive signal strength (RSS)-based technique. The effect of multipath fading on the range and localization accuracy is discussed. Performance of RSS-based methods in previous works is summarized and compared with our work.

The AoA method has been thoroughly investigated. High-resolution approaches, including MUSIC [24, 25] and ESPRIT [26] algorithms, can be applied to obtain AoA estimates. A directional antenna array with a minimum distance between elements is required. Various evaluations [24, 27] have revealed that the accuracy is proportional to the number of elements in both MUSIC and ESPRIT. Another popular localization method is based on ToA measurement. High localization accuracy requires a precise synchronization between transmitter (Tx) and receiver (Rx). This technique is commonly used in cellular networks because tight synchronization is ensured among base stations (BSs), for example, the CDMA standard [28]. In comparison, the time difference of arrival (TDoA) method relaxes the time synchronization requirement for mobile equipment [29, 30]. ToA employs coarse timing acquisition and fine acquisition to ensure high accuracy in a spread-spectrum communication system. The former is completed with either a sliding correlator or a matched filter. The latter is achieved with a delay-locked loop (DLL) [31, 32].

Overall, the AoA, ToA, and TDoA technologies require special hardware support. AoA requires an antenna array for high accuracy. ToA and TDoA require accurate synchronization, a correlator, and a DLL. The added cost may be prohibitive in many wireless applications. In contrast, RSSI is available in many off-the-shelf devices. Making software upgrade is sufficient to provide positioning services. However, the main challenge in RSS based ranging is low accuracy due to the presence of NLoS component in the fading signal. For the same positions, the RSS will vary due to the environmental fading. Hence, it is difficult to obtain accurate range estimates from one RSS measurement alone.

In order to eliminate the portions of power introduced by the transmitted symbols and NLoS component in the fading signal, we propose to decompose received signal into the LoS and NLoS components. The LoS signal component is extracted from fading channel, which is assumed to follow Ricean distribution random variable [33, 34, 35]. A typical mobile equipment (ME) estimates fading channel within its equalizer module during demodulation. The fading channel estimation implemented in ME is often based on pilots [36, 37, 38]. Such already available fading information is employed in the proposed approach to decompose the received signal strength and estimate LoS power.

The conventional models of RF channel were not tailored specifically for ranging and positioning applications. They were primarily established for either antenna pattern measurements [39] or planning and designing wireless networks [40]. Their purpose is to evaluate the signal coverage of a given terrain to ensure the communication quality and reliability. In contrast, the estimation of environmental effect and the mapping from signal strength to the range estimation are analyzed in this study. The range estimator's performance is also examined. Simulations were conducted to validate the analytical results.

The MSE of a point estimator of RSS-based ranging was derived in [41]. In contrast, CRB of all possible estimators of RSS-based ranging is derived in this paper. Also, biases of existing estimators are derived.

In [41], based on the point estimator's MSE, a "receiver error factor" (R-factor) was defined. Also, a threshold value of R-factor was used to eliminate those beacons under "NLoS-condition" [41] from positioning calculation thus improving the overall localization accuracy. In [18], a data-driven method uses offline generated path-loss model parameters to learn the stationary average effect of the environment on range estimation (acquiring calibration factors). In online stage, the range error was estimated based on the measured LoS-to-NLoS power ratio (K-ratio) and calibration factors (Radial Distance Error Indicator (RDEI)) which were acquired in offline stage. In contrast, the proposed LoS-based raging method eliminates the need for offline tuning. It effectively suppresses the multipath fading effect online through decomposing LoS and NLoS components in the received signal.

Another interesting research is radio tomographic imaging (RTI) [42, 43, 44], which was proposed by Dr. Patwari for device-free localization and tracking (DFT) [45, 46]. RTI makes use of the motion-transceiver link impact weights linearly connect "the drop in RSS" [47] and motion image voxel. The weights are determined by the shadow loss model [47, 48, 49]. Dr. Patwari's works model the shadow fading effect to the transceiver link, which is caused by the obstacle within or near the LoS link. The resolution of the RTI system depending on the voxel size of the area of interest, and the accuracy depends on the number and deploying shape of the transceiver nodes [47]. In contrast, our work makes use of the LoS link between beacon (transmitter) and the mobile device (receiver), eliminating fading effect caused by signal reflection, scattering, and diffraction from the environment. In our transmitter-receiver-ranging based localization system, no voxel size need to be predefined, and it does not require a relatively large number of nodes to be present.

In this paper, radio channel is modeled as a direct LoS (original) signal superimposed with several copies of itself (i.e., following Ricean distribution [19, 50, 51]). The MSE lower bound, i.e., the summation of CRB and minimum bias, is employed to compare the performance of LoS-based and RSS-based ranging methods because it take into account the NLoS effect on the range estimation.

4. THE PROPOSED LOS-BASED RANGING METHOD

4.1. Overview. The proposed LoS-based range estimation includes two steps: a LoS signal strength estimation based on fading signal and a transformation from LoS strength to distance.

A simplified baseband system with fading is shown in block diagram Fig. 3. Pilot symbols are inserted into the data sequence x_0 prior to modulation. After pulse shaping filter, the composite signal is transmitted over a channel characterized by time-vary frequency selective fading. Pilot symbols are placed in fixed position within a slot/burst. Assuming channel length is L, Ricean fading on each tap, i.e. $\mathbf{R} = [\mathbf{r}_1, \mathbf{r}_2, ...\mathbf{r}_L]$, contaminates the transmitted signal. At the receiver end, after the matched filter, the distorted signal pass through equalizer to reverse the distortion. Finally, data sequence is restored $\hat{x}_1$ after demodulation.

The output of the baseband signal in wireless communication system, s_1 in Fig. 3, is a composition of attenuated multiplicative fading signal on transmitted signal plus additive white Gaussian noise (AWGN). The probability density function (PDF) of the *fading signal envelope* (random variable R), $[\mathbf{r}_n]_i$ ($i = 1...N$, N is the number of samples per tap) in Fig. 3, when LoS signal component is presenting, is Ricean[33, 34, 35], and can be expressed as,

$$P_R(r) = \frac{2(K+1)r}{\Omega} e^{\left(-K - \frac{(K+1)r^2}{\Omega}\right)} \times I_0\left(2r\sqrt{\frac{K(K+1)}{\Omega}}\right). \tag{4}$$

where Ω represents the total power of LoS and NLoS (i.e. $v^2 + 2\sigma^2$), and K represents the Ricean factor (K-ratio). This factor is defined as the power ratio of LoS to NLoS ($K = v^2/2\sigma^2$). The $I_0(\cdot)$ represents the modified Bessel function of the first kind with order zero. The n^{th} moments of the Ricean distribution, μ_n [52],

$$\mu_n = \left(\frac{v^2}{2K}\right)^{n/2} 2^{n/2}\Gamma\left(1 + \frac{n}{2}\right) L_{n/2}(-K). \tag{5}$$

Our LoS signal component is calculated based on the estimated fading channel.

Time domain and frequency domain estimation methods for single carrier time-varying and frequency selective channel can be found in Dr. Xiao's [37, 38]. For CDMA system, time multiplexed pilot based methods can be found in [53, 54]. For OFDM system, pilot arrangement [55] and pilot assisted [56] methods can be found. These works focuses on estimating the combined effect of LoS and NLoS components for channel equalizations. Here, we focus on the range estimation based on LoS component alone.

As shown in Fig. 3, the fading channel estimation $\hat{\mathbf{R}}$ is provided by equalizer. The LoS component $\hat{v}$ is first decomposed from fading signal, based on estimated total power $\hat{\Omega}$ and Ricean K-ratio $\hat{K}$. Then, the LoS power is mapped to empirical path-loss model (3) to obtain the range estimation $\hat{d}_{LoS}$.

4.2. LoS Range Estimator. In general, the LoS component estimator can be expressed as,

$$\hat{v}^2 = f_{v^2}(\hat{\Omega}, \hat{K}) = \hat{\Omega}\frac{\hat{K}}{1+\hat{K}}. \tag{6}$$

where, $\hat{\Omega}$ is the estimator of the total power of fading signal, $\hat{K}$ is the LoS-to-NLoS K-ratio. We assume that the total power and K-ratio are estimated separately. Total power estimator is the second moment of Ricean fading, μ_2, which can be calculated based on fading signal power as,

$$\hat{\Omega} = \frac{1}{N}\sum_{i=1}^{N} r_i^2. \tag{7}$$

where N is the number of fading signal samples.

Based on Koay method [57]. The K estimator is obtained from $\hat{K} = \frac{1}{2}\epsilon^2$, where,

$$\epsilon = \sqrt{\xi(\epsilon)\left[1 + \frac{\mu_1^2}{\sigma_r^2}\right] - 2}. \tag{8}$$

where $\xi(\epsilon)$ is defined as correction factor [57], σ_r^2 is the variance of Ricean fading, $\sigma_r^2 = \mu_2 - \mu_1^2$. μ_1 and μ_2 are the first and second moments of the samples of fading signal.

To solve for ϵ, rearrange (8) to get,

$$g_k(\epsilon) = 1 - \frac{\xi(\epsilon)}{\epsilon^2 + 2} = \frac{\mu_1^2}{\mu_2}. \tag{9}$$

Thus, ϵ is obtained by solving $\epsilon = g_k^{-1}\left(\frac{\mu_1^2}{\mu_2}\right)$. The iterative solution is given by [57].

The final range is deduced from empirical path-loss model (a non-linear transformation) (3), with $\theta = \hat{v}^2$. Hence, $\hat{d}_{LoS} = f(\hat{v}^2) = \kappa(\hat{v}^2)^{-a}$.

5. ANALYSIS OF PROPOSED LOS-BASED RANGE ESTIMATOR

In this section, the CRB and the bias of a LoS-based range estimation is derived. Based on the derived fisher information matrix (FIM) of total power and K-ratio estimation from Ricean fading signal, the CRB of the LoS-based ranging is first proved in Lemma 1. Next, the asymptotic variance (AsV) of LoS component estimator is proved in Lemma 2, which is the fundamental source that introducing the bias of LoS-based ranging. In Lemma 3, we provide the bias.

5.1. CRB of LoS-based Range Estimation.

Lemma 1. *The CRB of the LoS-based range estimation ($\hat{d}_{LoS}$):*

$$CRB(\hat{d}_{LoS}) = \begin{cases} (a\kappa)^2(\hat{v}^2)^{-2(a+1)} CRB(\hat{v}^2), & v^2 \geq \sigma_{LoS} \\ \left\{ \left[\boldsymbol{J}^{-1}(\Omega)\right]_{1,1} CRB\left(\frac{K}{1+K}\right) \right\}^{a^2}, & v^2 < \sigma_{LoS}. \end{cases} \tag{10}$$

where $\boldsymbol{J}(\Omega)$ is the FIM, $\left[\boldsymbol{J}(\Omega)^{-1}\right]_{1,1}$ is given by (14). The CRB of the LoS-to-Total Power ratio ($K/(1+K)$) is given by (16). $CRB(\hat{v}^2)$ is the CRB of the LoS signal power estimation under strong signal condition, which is given by (17). $\sigma_{LoS} = 15dBm$ ($0.0316Watts$).

Proof. The Fisher Information Matrix (FIM, [58][59]) of the parameter vector $[\Omega, K]^T$ of PDF (4) can be found as,

$$\begin{aligned}
[\mathbf{J}(\Omega)]_{1,1} &= \int_0^\infty \left(\frac{\partial \ln P_R(r)}{\partial \Omega}\right)^2 P_R(r)dr \\
[\mathbf{J}(\Omega)]_{1,2} &= \int_0^\infty \frac{\partial \ln P_R(r)}{\partial \Omega}\frac{\partial \ln P_R(r)}{\partial K} P_R(r)dr \\
[\mathbf{J}(\Omega)]_{2,1} &= [\mathbf{J}(\Omega)]_{1,2} \\
[\mathbf{J}(\Omega)]_{1,1} &= \int_0^\infty \left(\frac{\partial \ln P_R(r)}{\partial K}\right)^2 P_R(r)dr.
\end{aligned} \tag{11}$$

where,

$$\frac{\partial \ln P_R(r)}{\partial \Omega} = -\frac{K}{1+K} - \frac{r^2}{\Omega}\frac{I_1\left(2r\sqrt{\frac{K(K+1)}{\Omega}}\right)}{I_0\left(2r\sqrt{\frac{K(K+1)}{\Omega}}\right)}\frac{2K+1}{\Omega K(K+1)}r. \tag{12}$$

$$\frac{\partial \ln P_R(r)}{\partial K} = \frac{(K+1)r^2}{\Omega^2} - \frac{1}{\Omega}\frac{I_1\left(2r\sqrt{\frac{K(K+1)}{\Omega}}\right)}{I_0\left(2r\sqrt{\frac{K(K+1)}{\Omega}}\right)}\sqrt{\frac{K(K+1)}{\Omega^3}}r. \tag{13}$$

By applying matrix inverse,

$$[\mathbf{J}(\Omega)^{-1}]_{1,1} = \frac{[\mathbf{J}(\Omega)]_{2,2}}{[\mathbf{J}(\Omega)]_{1,1}[\mathbf{J}(\Omega)]_{2,2} - [\mathbf{J}(\Omega)]_{1,2}^2}. \tag{14}$$

$$[\mathbf{J}(\Omega)^{-1}]_{2,2} = \frac{[\mathbf{J}(\Omega)]_{1,1}}{[\mathbf{J}(\Omega)]_{1,1}[\mathbf{J}(\Omega)]_{2,2} - [\mathbf{J}(\Omega)]_{1,2}^2}. \tag{15}$$

When signal is strong (the power of LoS component in the signal is greater than σ_{LoS}),

The CRB of the LoS-to-Total power ratio, $\zeta = f_\zeta(K) = K/(1+K)$, can be derived as, $\left[\frac{\partial f_\zeta}{\partial K}\right]^2 [\mathbf{J}^{-1}]_{2,2}$, that is,

$$CRB(\hat{\zeta}) = \frac{(1+K)^{-4}[\mathbf{J}]_{1,1}}{[\mathbf{J}_1(\Omega)]_{1,1}[\mathbf{J}]_{2,2} - [\mathbf{J}]_{1,2}^2}. \tag{16}$$

Assuming $\hat{\Omega}$ and $\hat{\zeta}$ are estimated separately, The CRB of LoS signal power estimation can be directly derived as $CRB(\hat{v}^2) = \left[\frac{\partial f_{v^2}}{\partial \boldsymbol{\theta}}\right] \boldsymbol{M}^{-1} \left[\frac{\partial f_{v^2}^T}{\partial \boldsymbol{\theta}}\right]$, where $\boldsymbol{M}$ is the FIM of distribution 4 with respect to (w.r.t.) the parameter $\boldsymbol{\theta} = [\hat{\Omega}, \hat{\zeta}]^T$, $\mathbf{M}^{-1} = \begin{bmatrix} [\mathbf{J}^{-1}]_{1,1} & 0 \\ 0 & CRB\left(\hat{\zeta}\right) \end{bmatrix}$.

That is,

$$CRB(\hat{v}^2) = \zeta^2[\mathbf{J}_1^{-1}]_{1,1} + \Omega^2 \times CRB(\zeta). \tag{17}$$

Thus, the CRB of LoS-based range estimation in strong signal condition is $CRB(\hat{d}_{LoS}) = \left[\frac{\partial f_{\text{P-to-R}}(\hat{v}^2)}{\partial \hat{v}^2}\right]^2 CRB(\hat{v}^2)$, which is the first expression in (10).

When signal is weak (the power of LoS component in the signal is less than σ_{LoS}), it is noted that there is a singularity around zero in the nonlinear transformation (3). For smaller power values ($< -10dBm$), directly applying (3) will lead to a higher analytic value than practical results (A bias of analytical model to the actual value). To preserve the linearity in the derivation, logarithm scale of (3) is considered,

$$\ln(\hat{d}) = \ln f(\theta) = \ln\kappa - a\ln(\theta). \tag{18}$$

here, $\theta = \hat{v}^2$ in (3). To begin with, we need to find the CRB of the logarithmized LoS power, (6), which is expressed as,

$$\ln(\hat{v}^2) = \ln f_{v^2}(\hat{\Omega}, \hat{\zeta}) = \ln(\hat{\Omega}) + \ln(\hat{\zeta}). \tag{19}$$

Assume $\hat{\Omega}$ and $\hat{\zeta}$ are estimated independently, we construct $\ln\mathbf{M}^{-1}$, $\ln\mathbf{M}$ is the FIM w.r.t. vector $\boldsymbol{\theta} = [\hat{\Omega}, \hat{\zeta}]^T$, and take logarithm on the diagonal elements.

$$\ln\mathbf{M}^{-1} = \begin{bmatrix} \ln[\mathbf{J}_1^{-1}(\Omega)]_{1,1} & 0 \\ 0 & \ln CRB(\hat{\zeta}) \end{bmatrix}. \tag{20}$$

The CRB of the logarithm LoS power is therefore obtained by $CRB(\ln\hat{v}^2) = \left[\frac{\partial \ln f_{v^2}}{\partial \boldsymbol{\theta}}\right] \ln\mathbf{M}^{-1} \left[\frac{\partial \ln f_{v^2}^T}{\partial \boldsymbol{\theta}}\right]$, which is,

$$CRB(\ln\hat{v}^2) = \ln[\mathbf{J}_1^{-1}(\Omega)]_{1,1} + \ln CRB\left(\frac{K}{1+K}\right). \tag{21}$$

Hence, the CRB of the logarithmized LoS-based range estimation is $CRB(\ln\hat{d}_{LoS}) = \left[\frac{\partial \ln f(\hat{v}^2)}{\partial \ln\hat{v}^2}\right]^2 CRB(\ln\hat{v}^2)$ (Note, $\theta = \hat{v}^2$ in (18)). Then, convert back to linearity, $CRB(\hat{d}_{LoS}) = exp\left(a^2\left\{\ln[\mathbf{J}_1^{-1}]_{1,1} + \ln CRB(\hat{\zeta})\right\}\right)$, which is the second expression in (10). □

5.2. The Bias of LoS-based Range Estimation. The nonlinear transformation(3) will introduce a bias to range estimates ($\hat{d}_{LoS}$). And the bias is depending on the magnitude of variance of the LoS power estimation.

In this section, the minimum variance of the LoS component estimation is first derived, next, the bias of LoS-based range estimation is obtained.

Here, we derive the AsV of the first and second moments based LoS component estimator. The AsV reveals the variance of an estimator as the sample size is tending to large [60]. Existing Ricean distribution parameter estimation methods can be found in [61, 62, 63, 64]. It was proved by Dr. Tepedelenlioglu, Dr. Abdi, and Dr. Giannakis in [39] that a K-ratio estimator that based on first and second moments of Ricean distribution ($\hat{K}_{1,2}$) is of the lowest asymptotic variance (AsV) among method of moment (MoM) K estimators.

Lemma 2. *The AsV of the fading channel LoS component estimator, based on the MOM, is*

$$AsV(\hat{v}^2) = \frac{4\mu_1^2\left(\mu_2 - \mu_1^2\right)}{\left[g'(K)\right]^2(1+K)^4} + \frac{4\mu_1(\mu_3 - \mu_1\mu_2)}{(1+K)^2 g'(K)}\left(\frac{g'(K)(1+K)K - \frac{\mu_1^2}{\mu_2}}{g'(K)(1+K)^2}\right) + (\mu_4 - \mu_2^2)\left(\frac{g'(K)(1+K)K - \frac{\mu_1^2}{\mu_2}}{g'(K)(1+K)^2}\right)^2. \tag{22}$$

where the nth moments(μ_n) are given by(5), and

$$g'(K) = \frac{2(K+1)L_{1/2}(-K)L'_{1/2}(-K) - L^2_{1/2}(-K)}{4(K+1)^2}\pi. \tag{23}$$

$$L'_{1/2}(-K) = \frac{1}{2}e^{-K/2}\left[\left(1 - \frac{K}{2}\right)I_0\left(\frac{K}{2}\right) + 3I_1\left(\frac{K}{2}\right) + \frac{K}{2}I_2\left(\frac{K}{2}\right)\right]. \tag{24}$$

Proof. First and second moments based LoS power estimator can be expressed as,

$$\hat{v}^2 = \phi(\mu_1, \mu_2) = \mu_2 \frac{g^{-1}\left(\frac{\mu_1^2}{\mu_2}\right)}{1 + g^{-1}\left(\frac{\mu_1^2}{\mu_2}\right)}. \tag{25}$$

in which μ_1 and μ_2 are the first and second moments of the samples of received signal amplitude, $g(\cdot)$ is the function that used for finding K-ratio from moments,

$$g(K) = \frac{\pi L^2_{1/2}(-K)}{4(K+1)} = \frac{\mu_1^2}{\mu_2}. \tag{26}$$

The AsV of a consistent estimate is given by [60], $AsV(\phi(\boldsymbol{\mu})) = \mathbf{G}(\phi(\boldsymbol{\mu}))\mathbf{C}(\boldsymbol{\mu})\mathbf{G}(\phi(\boldsymbol{\mu}))^T$, in which $\phi(\boldsymbol{\mu})$ is the function of parameter $\boldsymbol{\mu}$, (26); $\mathbf{G}(\phi(\cdot))$ represents Jacobian of the function $\phi(\boldsymbol{\mu})$; $\mathbf{C}(\boldsymbol{\mu})$ is the covariance matrix of the parameter vector $\boldsymbol{\mu} = [\mu_1, \mu_2]^T$.

Following standard result for the derivative of an inverse function, we get $\frac{\partial\phi}{\partial\boldsymbol{\mu}} = \left[\frac{2\mu_1}{(1+K)^2 g\prime(K)}, \frac{g\prime(K)(1+K)K - \frac{\mu_1^2}{\mu_2}}{g\prime(K)(1+K)^2}\right]^T$.

And the covariance matrix of statistics $\hat{\mu}_1 = \frac{1}{N}\sum_{i=1}^{N} r_i$, $\hat{\mu}_2 = \frac{1}{N}\sum_{i=1}^{N} r_i^2$ can be formed by moments as $\mathbf{C} = \begin{bmatrix} \mu_2 - \mu_1^2 & \mu_3 - \mu_1\mu_2 \\ \mu_3 - \mu_1\mu_2 & \mu_4 - \mu_2^2 \end{bmatrix}$. The AsV of the LoS com-ponent estimator $AsV(\hat{v}^2) = \left[\frac{\partial \phi}{\partial \mu}\right]^T \mathbf{C} \left[\frac{\partial \phi}{\partial \mu}\right]$, which is expressed in (22). □

It is worth noting that, the Koay method-based K esti-mator $\hat{K}_{\text{koay}}$ ([57]) is, es-sentially, a first and second moment-based estimator. The AsV map of Koay-based LoS estimator ($AsV(\hat{v}^2_{\text{koay}})$) over K-ratio and LoS power are identical to that of the first and second moment-based ($AsV(\hat{v}^2)$), which is given in Appendix **??**.

Lemma 3. *The bias of the LoS-based range estimator is*

$$B(\hat{d}_{LoS}) = \begin{cases} \frac{\kappa a(a+1)\left(\hat{v}^2\right)^{-(a+2)}}{2} AsV(\hat{v}^2), & v^2 \geq \sigma_{LoS} \\ 0, & v^2 < \sigma_{LoS} \end{cases}. \tag{27}$$

where $AsV(\hat{v}^2)$ is given in (22). $\sigma_{LoS} = 15dBm$ (0.0316Watts)

Proof. The mean and the variance of distance estimation $\hat{d}$ derived from r by (3) can be calculated as [4]

$$E[f(\theta)] \doteq f(\mu) + (1/2) f''(\mu) Var(\theta). \tag{28}$$

$$Var[f(\theta)] \doteq [f'(\mu)]^2 Var(\theta). \tag{29}$$

where $\mu = E[\theta]$.

When signal is strong (the power of LoS component in the signal is greater than σ_{LoS}), The expectation of distance estimates based on (28) can be expressed as

$$E[\hat{d}_{LoS}] = \kappa (v^2)^{-a} + \frac{\kappa a(a+1)}{2} (v^2)^{-(a+2)} AsV(\hat{v}^2). \tag{30}$$

Hence, the bias of range estimate is $B(\hat{d}_{LoS}) = E[\hat{d}_{LoS} - d]$, which lead to the first expression in (27).

When signal is weak (the power of LoS component in the signal is greater than σ_{LoS}), considering that there is a singularity around zero in (3), and (28)(29) has discarded the high order terms, to preserve the linearity in the derivation, the logarithmized equation, (18), is considered. We logarithmized the expectation (28) as,

$$E[\ln\hat{d}_{LoS}] = \ln f(v^2) + \frac{1}{2}\frac{\partial^2 \ln f(v^2)}{\partial \left(\ln v^2\right)^2} AsV(\ln v^2). \tag{31}$$

Back to linear scale,

$$E[\hat{d}_{LoS}] = exp\left\{E[\ln\hat{d}_{LoS}]\right\} = f(v^2)exp\left\{\frac{1}{2}\frac{\partial^2 \ln f(v^2)}{\partial(\ln v^2)^2}\ln AsV(v^2)\right\}. \tag{32}$$

Thus, the bias is $B(\hat{d}_{LoS}) = E[\hat{d}_{LoS}] - d$,

$$B(\hat{d}_{LoS}) = f(v^2)\left[exp\left\{\frac{1}{2}\frac{\partial^2 \ln f(v^2)}{\partial((ln)v^2)^2}\ln AsV(v^2)\right\} - 1\right]. \tag{33}$$

Noted that $\frac{\partial^2 \ln f(v^2)}{\partial(\ln v^2)^2} = 0$. Thus, $B(\hat{d}_{LoS}) = 0$, which is the second expression in (27). □

6. THEORETICAL LIMIT OF RSS-RANGING FOR COMPARISON

For the purpose of comparison, we derive the CRB and bias of RSS-based range estimation. The existing RSS-based range estimators are categorized into one of the three classes:

1. *Received Signal Power Average-based Distance Estimation (MeanPower):*

   An average of the received signal power is performed. The average value is put to the nonlinear transformation (3) so that range estimation can be achieved. Corresponding model and analysis can be found in [13, 21].

2. *Received Signal Strength-based Distance Average Estimation (MeanDist):*

Each received signal strength instance is converted to range estimates based on (3). The range instances are averaged to form an expectation value. Corresponding model and analysis can be found in [41].

3. *Received Signal Strength Average-based Distance Estimation (MeanStrength):*

   An average of the received signal amplitude (square root of the power) is performed. Range estimation is achieved when the mean amplitude value is put to the nonlinear transformation function (3). Corresponding model and analysis can be found in [12, 19].

Considering that the transmitting payload (code/symbols) is randomized by scrambler before transmitting (and recovered by descrambler at receiver) [65], the payload can be seen as a noise with constant power. For sake of simplicity, we assume the power of payload is negligible in RSSI.

In the following subsections, the bias of *MeanPower*, *MeanDist*, and *MeanStrength* are proved in Lemma 4 $\sim$ 6 respectively. The CRB and MSEB of RSS-based ranging are proved in Lemma 7.

6.1. MeanPower's Bias. The *MeanPower* is a transformation from the averaged signal power (R^2) to range:

$$\hat{d}_{MeanPower} = \kappa \left(\frac{1}{N} \sum_{i=1}^{N} r_i^2 \right)^{-a}. \tag{34}$$

where N is the number of samples, κ is the path-loss constant.

Lemma 4. *The MeanPower bias is given as,*

$$B_{MeanPower} = d \sum_{k=1}^{\infty} \binom{a+k-1}{a-1} (-K)^{-k}. \tag{35}$$

where K is the power ratio of LoS-to-NLoS ($K > 1$), d is the actual range.

Proof. The received signal power is a combination of LoS and NLoS ($\Omega = v^2 + 2\sigma^2$), where v^2 and $2\sigma^2$ represent the LoS and NLoS power respectively. Thus, the range is solved by (3), $d_{RSS} = \kappa\Omega^{-a} = \kappa(v^2 + 2\sigma^2)^{-a}$, which can be rearranged as $d_{RSS} = \kappa(v^2)^{-a}\left[1 + \sum_{k=1}^{\infty}\binom{a+k-1}{a-1}\left(\frac{2\sigma^2}{v^2}\right)^k\right]$. The path-loss parameters are found under ideal conditions. By the definition of K-ratio, we get (35). □

6.2. MeanDist's Bias. The *MeanDist* is an average of range estimates from received signal strength,

$$\hat{d}_{MeanDist} = \frac{1}{N}\sum_{i=1}^{N}\left(\kappa r_i^{-2a}\right). \tag{36}$$

Lemma 5. *The MeanDist is an average of range estimates from received signal strength,*

$$B_{MeanDist} = \frac{\kappa}{\left[\sigma\sqrt{\frac{\pi}{2}}M\left(-\frac{1}{2},1,-K\right)\right]^{2a}}\left\{1 + a(2a+1) \times \frac{2\sigma^2 + v^2 - \frac{\pi}{2}\sigma^2 M^2\left(-\frac{1}{2},1,-K\right)}{\left[\sigma\sqrt{\frac{\pi}{2}}M\left(-\frac{1}{2},1,-K\right)\right]^2}\right\} - d. \tag{37}$$

where $M(\cdot)$ is the confluent hypergeometric function of the first kind.

Proof. The expectation and variance of the received signal amplitude (R) are,

$$\mu = \sigma\sqrt{\frac{\pi}{2}}M\left(-\frac{1}{2},1,-K\right). \tag{38}$$

$$Var[R] = 2\sigma^2 + v^2 - \frac{\pi}{2}\sigma^2 M^2\left(-\frac{1}{2},1,-K\right). \tag{39}$$

Take (38)(39) into (28), we get the expectation of the range estimates

$$E[d_{RSS}] = \frac{\kappa}{\left[\sigma\sqrt{\frac{\pi}{2}}M\left(-\frac{1}{2},1,-K\right)\right]^{2a}}\left\{1 + a(2a+1)\frac{2\sigma^2 + v^2 - \frac{\pi}{2}\sigma^2 M^2\left(-\frac{1}{2},1,-K\right)}{\left[\sigma\sqrt{\frac{\pi}{2}}M\left(-\frac{1}{2},1,-K\right)\right]^2}\right\}. \tag{40}$$

Thus, the bias of radial distance estimate is $B_{est} = E[d_{RSS}] - d$, we get (37). □

Remark 2. *Under strong LoS conditions ($K \to \infty$), the bias of MeanDist is given as,*

$$B_{RSS|LoS} = \frac{a(2a+1)}{v^2} d. \tag{41}$$

Proof. It is noted in [41] that under strong LoS conditions,

$$\begin{aligned} &\lim_{K\to\infty} M^2\left(-\frac{1}{2}, 1, -\frac{v^2}{2\sigma^2}\right) = \frac{2v^2}{\pi\sigma^2} \\ &\lim_{K\to\infty} \left[1 + K - \frac{\pi}{4} M^2\left(-\frac{1}{2}, 1, -K\right)\right] = 1. \end{aligned} \tag{42}$$

The expectation of range estimate (40) can be simplified as,

$$E[d_{RSS}] = \frac{\kappa}{v^{2a}} \left[1 + \frac{a(2a+1)}{v^2}\right]. \tag{43}$$

When $K \to \infty$, $2\sigma^2/v^2 = 0$. Equation (41) is obtained when (3) ($\theta = \Omega$) is substituted into (43). □

6.3. MeanStrength's Bias. The *MeanStrength* is a transformation of the averaged received signal amplitudes,

$$\hat{d}_{MeanStrength} = \kappa \left(\frac{1}{N}\sum_{i=1}^{N} r_i\right)^{-2a}. \tag{44}$$

Lemma 6. *The MeanStrength's bias is given as,*

$$B_{MeanStrength} = \frac{\kappa}{\left[\sigma\sqrt{\frac{\pi}{2}} M\left(-\frac{1}{2}, 1, -K\right)\right]^{2a}} - d. \tag{45}$$

Proof. The proof is in the same manner as Lemma 5, and is omitted here. □

It is obvious that as the LoS signal component's power is stronger, the variation in the estimation will be smaller, and accordingly, the bias in the range estimation is smaller. A comparison of the analytical biases between the three types of estimators is given in Fig. 1. (The simulation results are shown in Fig. 10, Fig. 11, and Fig. 5.) In this figure, *MeanPower*'s bias is the largest. *MeanDist*'s bias is the smallest.

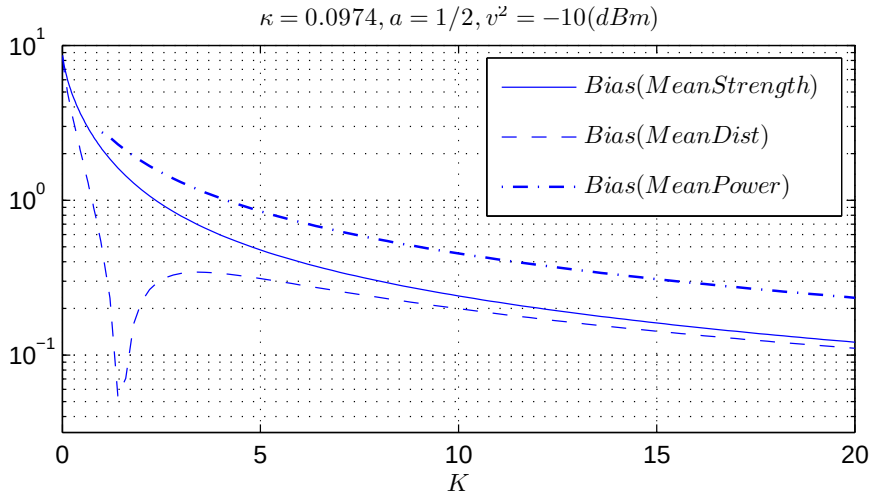

Figure 1. Bias Comparison of RSS-based Estimators

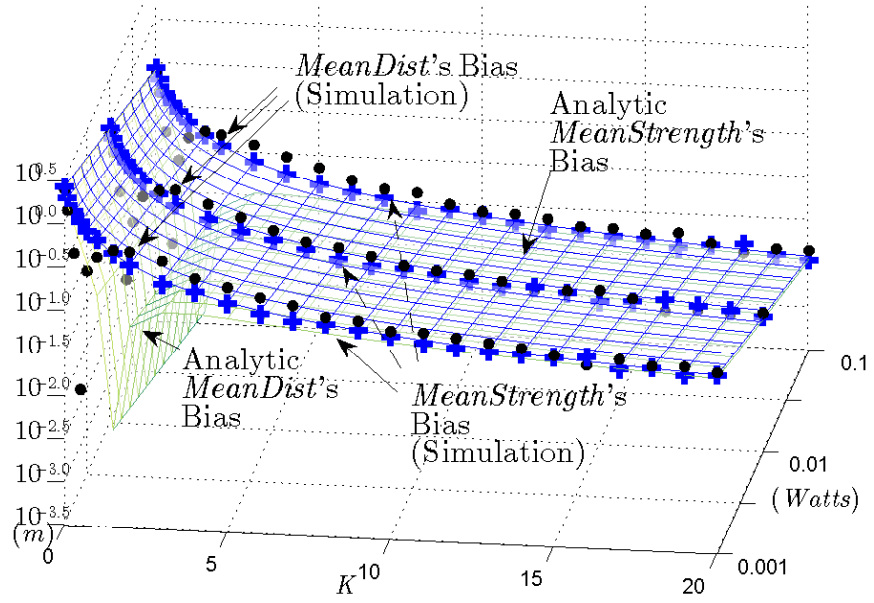

Figure 2. Analytical and Simulation Biases Comparison between *MeanStrength* and *MeanDist*

The MeanStrength is examined throughout the remainder of this paper for following reasons. First, as illustrated in Fig. 2 (also see Fig. 11 Fig. 5.), the averaged bias values of the *MeanDist* estimates from the collected simulation results are higher than what its analytical model indicated. This is due to the effect of the linearization of transformation from power estimation to distance estimation. And when K-ratio value is greater than 1, the averaged bias values of *MeanDist* estimates are higher than that of the *MeanStrength*'s. Thus, in practice, the bias of *MeanStrength* is the smallest among the three types of estimators. Second, in *MeanDist*, before the average operation (to obtain expectation value), a non-linear transformation is performed for each samples. Hence, *MeanDist* will allocate more computational resources than others.

6.4. CRB and MSE Bound of RSS-based Ranging. The mean square error lower bound (MSEB) of the RSS-based range estimators is defined as the summation of the CRB of the estimation and the square of the minimum bias.

The RSS-based range estimation is obtained by (3) ($\hat{\theta} = \hat{\Omega}$): $\hat{d}_{RSS} = f(\hat{\Omega}) = \kappa\hat{\Omega}^{-a}$.

Lemma 7. *The MSEB of RSS-based range estimation ($\hat{d}_{RSS}$),*

$$MSEB(\hat{d}_{RSS}) = \begin{cases} (a\kappa)^2\Omega^{-2(a+1)}\left[\boldsymbol{J}(\Omega)^{-1}\right]_{1,1} + B^2(\hat{d}_{RSS}), & v^2 \geq \sigma_{RSS} \\ \left[\boldsymbol{J}(\Omega)^{-1}\right]_{1,1}^{a^2} + B^2(\hat{d}_{RSS}), & v^2 < \sigma_{RSS} \end{cases}. \tag{46}$$

where $\boldsymbol{J}(\Omega)$ is Fisher information matrix(FIM), $\left[\boldsymbol{J}(\Omega)^{-1}\right]_{1,1}$ is given by (14), $\sigma_{RSS} = 30dBm$ ($0Watts$).

Proof. We calculated the mean square error bound of range estimator as $MSEB = CRB + Bias^2$. The bias of estimators (B_{est}) has been discussed in previous sections ((35)(37)(45)).

When signal is strong (the power of LoS component in the signal is greater than σ_{RSS}), the CRB of RSS-based range estimation can be obtained as $CRB(\hat{d}_{RSS}) = \left[\frac{\partial f(\Omega)}{\partial \Omega}\right]^2 [\mathbf{J}(\Omega)^{-1}]_{1,1}$, which lead to

$$CRB(\hat{d}_{RSS}) = \frac{(a\kappa)^2 \Omega^{-2(a+1)} [\mathbf{J}]_{2,2}}{[\mathbf{J}]_{1,1}[\mathbf{J}]_{2,2} - [\mathbf{J}]_{1,2}^2}. \tag{47}$$

which is in the first expression in (46).

When signal is weak (the power of LoS component in the signal is less than σ_{RSS}), to preserve the linearity in the derivation, as in the proof of lemma 1, logarithm scale (18) is considered, here, $\theta = \hat{\Omega}$.

Since the total power is estimated from collected signal samples first, then, is transformed into range value in *MeanStrength* (44), the CRB of the range estimation based on total received signal power is $CRB(\ln \hat{d}_{RSS}) = \left[\frac{\partial \ln f(\hat{\Omega})}{\partial \ln \hat{\Omega}}\right]^2 \ln\left(\left[\mathbf{J}(\Omega)^{-1}\right]_{1,1}\right)$. That is,

$$CRB(\ln \hat{d}_{RSS}) = a^2 \ln\left(\left[\mathbf{J}(\Omega)^{-1}\right]_{1,1}\right). \tag{48}$$

Back to the linear scale, $CRB(\hat{d}_{RSS}) = exp\left\{a^2 \ln\left(\left[\mathbf{J}(\Omega)^{-1}\right]_{1,1}\right)\right\}$, we get,

$$CRB(\hat{d}_{RSS}) = \left\{\left(\left[\mathbf{J}(\Omega)^{-1}\right]_{1,1}\right)\right\}^{a^2}. \tag{49}$$

which is in the second expression in (46). □

7. SIMULATION VALIDATION AND PERFORMANCE COMPARISON

In this section, analytic models are validated through simulation results. The performance of the proposed LoS-based and existing RSS-based ranging is compared.

The block diagram of the simulation is shown in Fig. 3. Pilot-resident frames are modulated and transmitted through a frequency-selective Ricean fading channel. Sum-of-sinusoids simulator provides fading signal on each tap. Fading signal (***R***) is estimated by "fading channel estimator" module. LoS signal component and range are estimated by "LoS component estimator" and "Range estimation" module, respectively, in which the proposed LoS range estimator, introduced in Section III B, is applied.

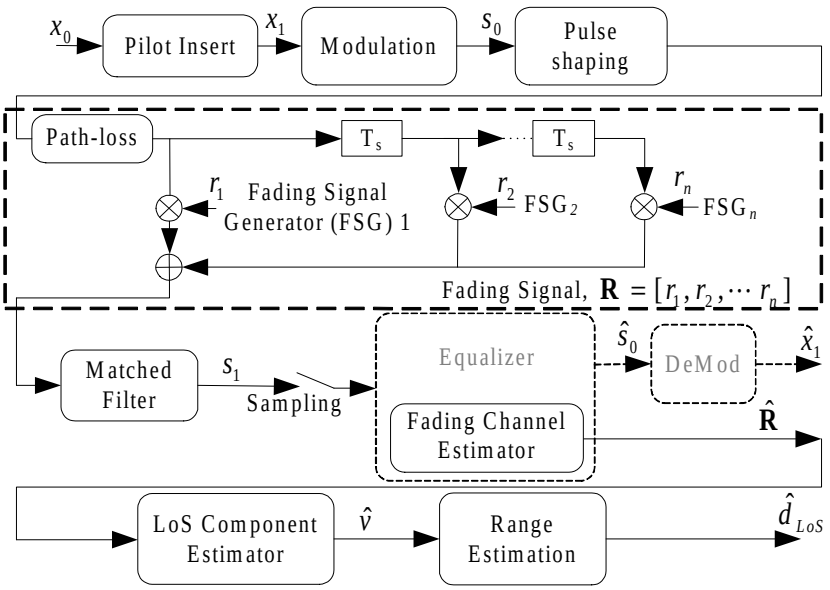

Figure 3. Simulation Block Diagram

Without a loss in either generality or accuracy, the sum-of-sinusoids simulator, which was proposed in [35], is applied to generate fading signal. The following parameters were used for setting the simulator: Doppler frequency of $100Hz$, a number of fading paths ≥ 20, and a random generated angle of arrival.

Taking GSM network as an example, assuming carrier frequency of $900MHz$, and symbol rate of $270kbps$ [66], the Doppler $100Hz$-corresponding vehicle velocity is $75mph$ $(33m/s)$.

It is worth noting that, for lower Doppler frequency, to ensure the same estimation accuracy, a larger sample size (longer sample period) is desired.

The empirical path-loss parameters is set to be $a = 1/2$ and $\kappa = 0.0974$. The magnitudes of the received signal and corresponding range distance are plotted in Fig. 4 for reference. The parameters of empirical path-loss model are assumed to be found based on signal's LoS component power measurements.

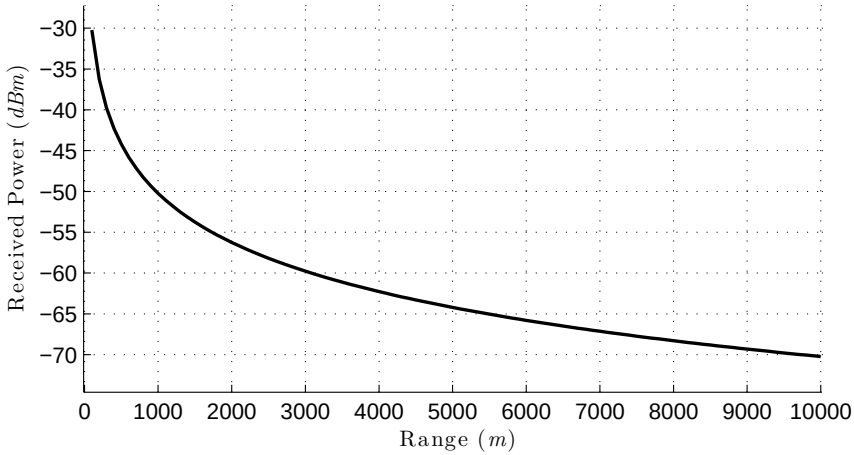

Figure 4. Range v.s. Signal Power

In the following subsections, the derived bias for each of the classified RSS-ranging method is validated and compared in Subsection A. Next, the derived mean square error models for LoS- and RSS-ranging are validated in Subsection B. In Subsection C and D, the RMSE and 90% percentile of LoS- and RSS- ranging are compared and analyzed. The accuracy improvement by applying the proposed LoS-ranging is concluded in Subsection D.

7.1. Bias of RSS-based Range Estimation. In this subsection, analytic biases of RSS-based range estimations are validated by collected simulation results. Three LoS power cases are examined: $-40dBm$, $-50dBm$, and $-60dBm$. For MeanPower and MeanStrength methods, the biases of simulation results coincide with analytic models (which can be found in Appendix C, Fig. 10 and Fig. 11).

The analytic model of the MeanDist's bias was slightly different from that recorded in the experimental results (Fig. 5). This difference occurred as a result of linearization of a nonlinear transformation within the estimation process, where the high order terms were omitted from the estimation ((28)(29)).

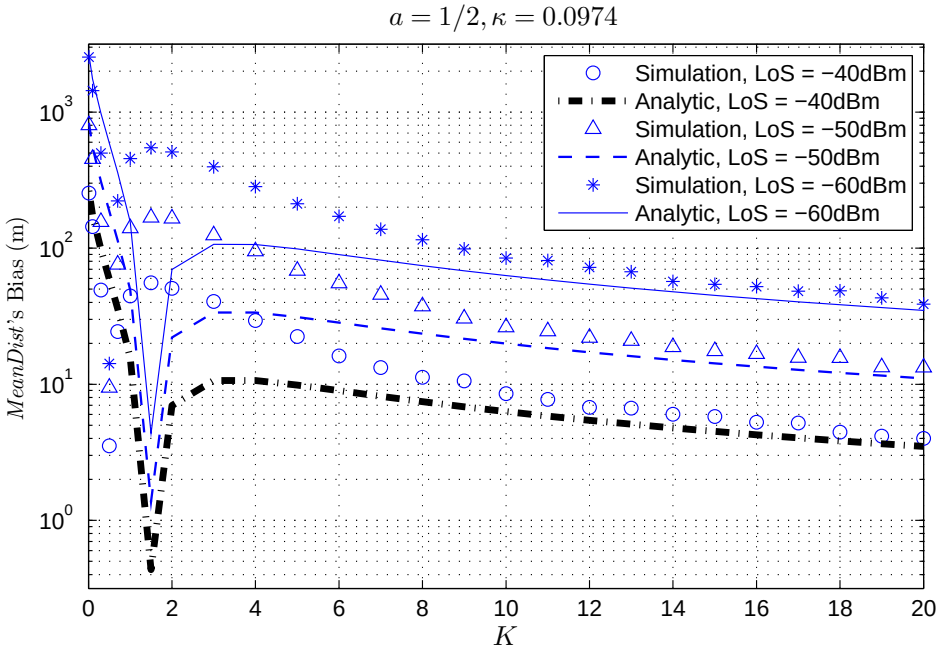

Figure 5. MeanDist's Bias

As indicated in Fig. 2, the corresponding bias values of the *MeanDist* estimation are higher than analytic bias model. And when K-ratio value is greater than 1, the bias of collected *MeanDist* estimation results are higher than that of the *MeanStrength*'s. So the bias of *MeanStrength* is the smallest among the three types of estimators. Hence, *MeanStrength* is used in the rest of the simulation for the performance comparison between the proposed LoS-based method and RSS-based methods.

7.2. Range Estimate's MSE. To validate the MSEB model of LoS- and RSS-based ranging methods, the collected simulation results of RSS-based range estimates (*MeanStrength*) and LoS-based estimates are compared.

In FCC regulation [67], the maximum transmit power in the industrial, scientific and medical (ISM) band is 4Watts. For the purpose of integrity, the model validation and MSE comparison were realized in two signal power ranges:

Strong: $4Watts \sim 1Watts$

Weak: $-10dBm \sim -80dBm(1e-11Watts)$

The MSEs of collected simulation results have been illustrated in logarithm scale in Fig. 6 Fig. 7. Overall, both simulation results and analytical model shows that, the error of range estimation increases as the signal power decreases. The error of RSS-based range estimates increases as NLoS signal component increases. While, the effect of NLoS component to the LoS-based range estimates is less than RSS-based method.

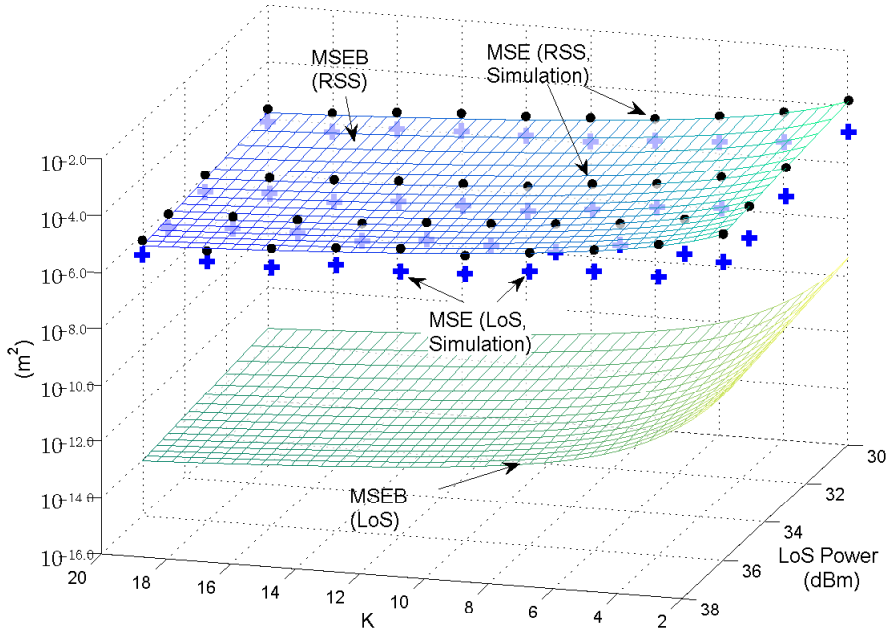

Figure 6. Logarithm Scale MSE Model and Simulation Results (Strong Signal level)

Fig. 6 and Fig. 7 show that the MSE of *MeanStrength* attained the analytical MSEB. The MSE of the collected LoS-based range estimates underneath the MSEB of the RSS'. Both the RSS-based and the LoS-based range estimation's MSE increase as the received

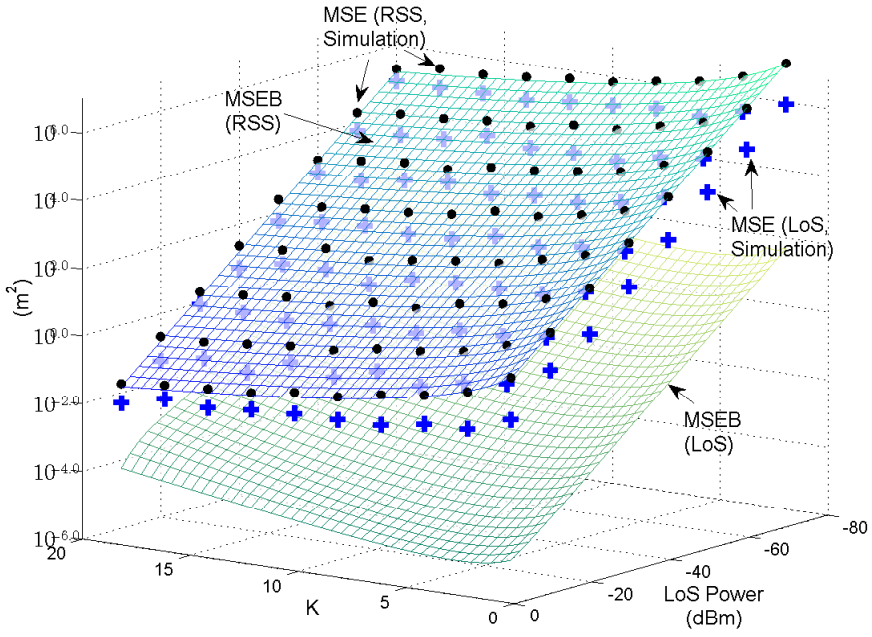

Figure 7. Logarithm Scale MSE Model and Simulation Results (Weak Signal level)

signal's LoS power decreases. The comparison between the simulation results and the analytical MSEB of LoS-based range estimation shows that more efficient LoS-based range estimator, getting close to the accuracy bound, is still possible.

The similarities of the MSE model and simulation results are measured by the depth of linear dependency (Pearson Correlation Coefficient [4]). They are summarized in Table 1.

Overall, the similarities in different cases are above 90%.

Table 1. The Depth of Linear Dependencies of Collected Simulation Results and Error Bound Model (in Logrithm Scale)

Signal Power Range	**Ranging Method**	**Simularity (%)**
Strong	RSS-based	99.49
Strong	LoS-based	91.82
Weak	RSS-based	99.96
Weak	LoS-based	95.33

7.3. RMSE Comparison. To outline the performance of the RSS-based and the proposed LoS-based method, the root mean square error (RMSE) values of simulation results are first compared.

In Table 2, the K-ratio is set to be 1 (LoS power component in the fading signal is equal to NLoS component). On average, the proposed LoS-based method reduce the RMSE of ranging by 80%.

Table 2. RMSE Comparison under Weak Signal Power ($K = 1$) (Path-loss parameters: $a = 1/2$, $\kappa = 0.0974$)

LoS Power Range (dBm)	**Actual Range (ref.) (m)**	**RMSE of RSS (m)**	**RMSE of LoS (m)**	**Acc. Imprv.*** **(%)**
−10	9.74	2.14	0.345	83.88
−20	30.8	6.782	1.095	83.85
−30	97.4	21.448	3.742	82.55
−40	308	67.823	10.955	83.85
−50	974	214.476	34.641	83.85
−60	3080	678.233	109.545	83.85
−70	9740	2144.76	346.41	83.85

* $(RMSE_{RSS} - RMSE_{LoS})/RMSE_{RSS}$

In Table 3, we compare the RMSE when K-ratio is 10. The accuracy improvement, on average, is about 55% to 60%.

Table 3. RMSE Comparison under Weak Signal Power ($K = 10$) (Path-loss parameters: $a = 1/2$, $\kappa = 0.0974$)

LoS Power Range (dBm)	**Actual Range (ref.) (m)**	**RMSE of RSS (m)**	**RMSE of LoS (m)**	**Acc. Imprv. (%)**
−10	9.74	0.2526	0.1161	54.05
−20	30.8	0.8953	0.4141	53.75
−30	97.4	2.4114	1.0557	56.22
−40	308	8.3960	4.0053	52.29
−50	974	30.8504	13.246	57.07
−60	3080	83.7717	35.669	57.42
−70	9740	271.674	104.924	61.38

Overall, by examining $K = 1 \sim 20$, and *Strong* $\sim$ *Weak* conditions, the RMSE has been improved by 56.7% when LoS-based ranging is applied.

7.4. Ranging Error CDF Comparison. In this subsection, we compare the 90% percentile of the ranging error by applying RSS and proposed LoS methods.

Fig. 8 and Fig. 9 show the 90% percentile for K-ratio equals to 2 and 10. The LoS component in the received signal power is equal to $-60dBm$, i.e. under weak signal condition. The RSS-ranging results in a slow growing curve (dot lines in Fig. 8 and Fig. 9) since the NLoS portion within the fading signal introduced large error. NLoS effect have been suppressed in LoS-ranging. Hence, it performs better – the result indicates that all errors are concentrated around the same and small value. A large difference between RSS and LoS-ranging indicates a higher accuracy of LoS-ranging.

Overall, the averaged 90%-percentile has been improved by 66.7%, when LoS ranging is applied. Moreover, both the simulation results and analytical model show that the performance of LoS-based methods is superior to RSS-based methods.

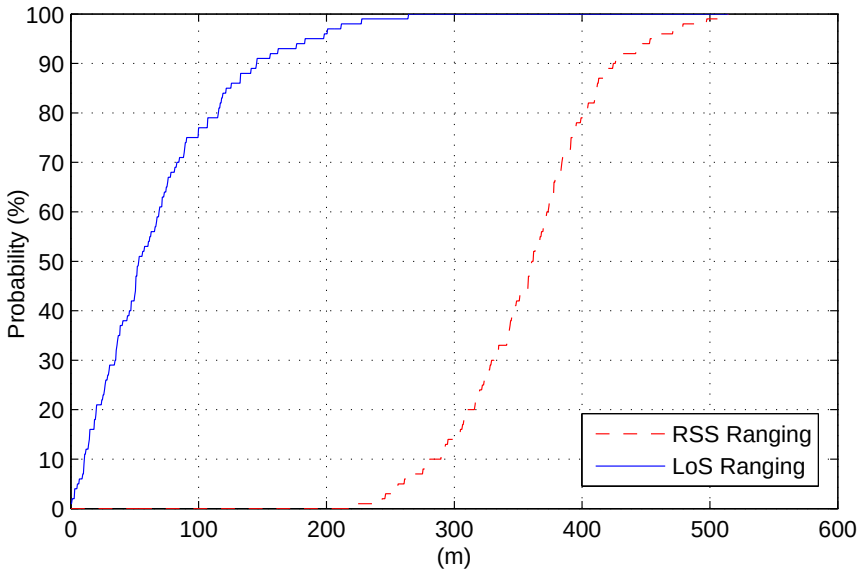

Figure 8. Ranging Error cumulative distribution function (CDF)
(K=2, Signal Power = -60dBm)

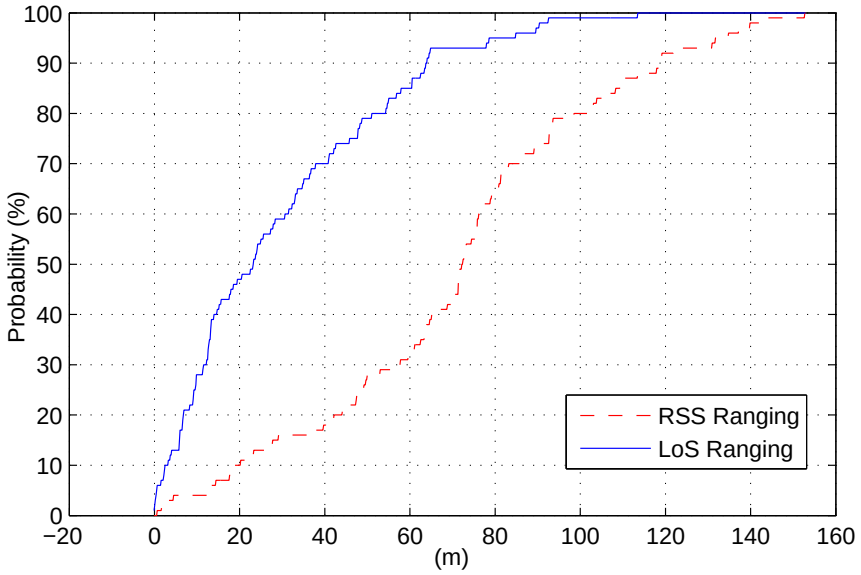

Figure 9. Ranging Error CDF
(K=10, Signal Power = -60dBm)

8. CONCLUSION

The MSE of simulation results validates our analytic model. The similarity is above 90%. Our analytical model effectively modeled the error behavior of RSS and LoS-based range estimation under both strong signal (i.e. greater than 1 Watts) and weak signal (i.e.

$10^{-3}Watts$(i.e. $-10dBm$) $\sim 10^{-10}Watts$ (i.e. $-70dBm$)) conditions. The simulation results along with the analytic model indicate that the performance of the proposed LoS-based ranging method is superior to that of the conventional RSS-based methods. On average, the proposed LoS-based range estimator improves the MSE by 55% and 90%-percentile accuracy by 66% when compared with the RSS-ranging method. In our future work, a more efficient LoS-based range estimator that can approach the CRB is to be designed, experiment is to be conducted, the relationship between the Doppler frequency, sampling rate, sample size, and ranging accuracy is to be studied.

9. APPENDIX

Lemma 8. *The distribution of the local average power (in Watts)* $\bar{P} = \sum_{i=1}^{N} P_i$ *converges in distribution to lognormal, with expectation*

$$E[\bar{P}] = [\gamma\sigma^2(2+v^2)]^{\frac{10}{ln10}} exp\left(\frac{1+v^2}{(2+v^2)^2}\frac{100-10Nln10}{N(ln10)^2}\right). \tag{50}$$

And variance,

$$\begin{aligned} Var[\bar{P}] = [\gamma\sigma^2(2+v^2)]^{\frac{20}{ln10}} \left[exp\left(\frac{100(1+v^2)}{N(ln10)^2(2+v^2)^2}\right) - 1\right] \\ \times exp\left(\frac{2(1+v^2)}{(2+v^2)^2}\frac{100-10Nln10}{N(ln10)^2}\right). \end{aligned} \tag{51}$$

where $\gamma = (1mW)^{-1}$, $2\sigma^2$ *and* v^2 *represent the NLoS and the LoS power respectively, and* N *is the number of samples.*

Proof. The received signal's envelope, random variable R, follows Ricean distribution ($R \sim Rice(v^2, \sigma^2)$). Therefore, $\left(\frac{R}{\sigma}\right)^2 \sim noncentral\chi_2^2(v^2)$ with parameter v^2 (LoS power) and degree of freedom of 2. Thus, the expectation and the variance of random variable R^2 are $E[R^2] = \sigma^2(2+v^2)$ and $\text{Var}[R^2] = 4\sigma^4(1+v^2)$, respectively.

Consider the power expressed in a logarithm scale (in dBm), $P_l = 10\log_{10}(\gamma R^2)$, with $\gamma = (1mW)^{-1}$. The expectation and variance, following (28)(29), are

$$E[P_l] \doteq 10\log_{10}[\gamma\sigma^2(2+v^2)] - \frac{10}{\ln 10}\frac{1+v^2}{(2+v^2)^2}. \tag{52}$$

$$\mathrm{Var}[P_l] \doteq \frac{100}{(\ln 10)^2}\frac{1+v^2}{(2+v^2)^2}. \tag{53}$$

By Central Limit Theorem (CLT), $\sqrt{N}\left(\frac{1}{N}\sum_{i=1}^{N} P_{li} - E[P_l]\right) \xrightarrow{d} \mathcal{N}(0, \sigma^2_{P_l})$

Thus, the averaged power $\bar{P}_l = \frac{1}{N}\sum_{i=1}^{N} P_{li}$,

$$\bar{P}_l \xrightarrow{d} \mathcal{N}(\mu_{\bar{P}_l}, \sigma^2_{\bar{P}_l}). \tag{54}$$

where $\mu_{\bar{P}_l} = E[P_l]$, and $\sigma^2_{\bar{P}_l} = \frac{100(1+v^2)}{N(\ln 10)^2(2+v^2)^2}$.

The expectation and the variance of $\bar{P}$ are $E[\bar{P}] = exp\left(\mu_{\bar{P}_l} + \frac{1}{2}\sigma^2_{\bar{P}_l}\right)$ and $\mathrm{Var}[\bar{P}] = (exp(\sigma^2_{\bar{P}_l}) - 1)(E[\bar{P}_l])^2$, respectively. □

Lemma 8 reveals that the NLoS power was calculated into the local average power (50). So conventional range estimates from RSS-based path-loss model were distorted by NLoS fading from environment. This was the reason that Okumura-Hata model has different formula for different environment configurations (i.e., urban, suburban, open area).

Lemma 9. *The AsV of the fading channel LoS component estimator, based on the Koay K estimator, is*

$$\begin{aligned} AsV(\hat{v}^2_{Koay}) = {} & (\mu_2 - \mu_1^2)\frac{4\mu_1^2\epsilon^2}{[g'_k(\epsilon)]^2\left[1+\frac{1}{2}\epsilon^2\right]^4} \\ & + 2(\mu_3 - \mu_1\mu_2)\frac{\mu_1\epsilon^3(1+\epsilon^2)g'_k(\epsilon) - \frac{\mu_1^2}{2\mu_2}\epsilon^2}{[g'_k(\epsilon)]^2\left[1+\frac{1}{2}\epsilon^2\right]^4} \\ & + (\mu_4 - \mu_2^2)\frac{\left[\frac{1}{2}\epsilon^2(1+\frac{1}{2}\epsilon^2)g'_k(\epsilon) - \frac{\mu_1^2}{\mu_2}\epsilon\right]^2}{[g'_k(\epsilon)]^2\left[1+\frac{1}{2}\epsilon^2\right]^4}. \end{aligned} \tag{55}$$

where $\epsilon = \frac{v}{\sigma} = \sqrt{2K}$,

$$g_k'(\epsilon) = \frac{2\epsilon\xi(\epsilon) - \xi'(\epsilon)(\epsilon^2+2)}{(\epsilon^2+2)^2} \tag{56}$$

The derivative of the correction factor is

$$\begin{aligned}\xi'(\epsilon) = 2\epsilon + \frac{\pi}{8}e^{-\frac{\epsilon^2}{2}}\left[(2+\epsilon^2)I_0\left(\frac{\epsilon^2}{4}\right) + \epsilon^2 I_1\left(\frac{\epsilon^2}{4}\right)\right] \\ \times\left[\left(\frac{1}{2}\epsilon^3 - 2\epsilon\right)I_0\left(\frac{\epsilon^2}{4}\right) - 6\epsilon I_1\left(\frac{\epsilon^2}{4}\right) - \frac{1}{2}\epsilon^3 I_2\left(\frac{\epsilon^2}{4}\right)\right].\end{aligned} \tag{57}$$

Proof. Let $\boldsymbol{\mu} = [\mu_1, \mu_2]^T$. The Koay method LoS component estimation can be expressed with respect to μ_2 and ϵ as,

$$\hat{v}_{koay}^2 = \phi_k(\mu_1, \mu_2) = \mu_2 \frac{\epsilon^2}{2+\epsilon^2}. \tag{58}$$

Following the standard result for the derivative of an inverse function, we get,

$$\frac{\partial \phi_k}{\partial \boldsymbol{\mu}} = \left[\frac{2\mu_1\epsilon}{g_k'(\epsilon)\left[1+\frac{1}{2}\epsilon^2\right]^2}, \frac{\frac{1}{2}\epsilon^2(1+\frac{1}{2}\epsilon^2)g_k'(\epsilon) - \frac{\mu_1^2}{\mu_2}\epsilon}{g_k'(\epsilon)\left[1+\frac{1}{2}\epsilon^2\right]^2}\right]^T. \tag{59}$$

The AsV of the LoS component estimator is $AsV = \left[\frac{\partial\phi_k}{\partial\boldsymbol{\mu}}\right]^T \boldsymbol{C}\left[\frac{\partial\phi_k}{\partial\boldsymbol{\mu}}\right]$ ($\mathbf{C} = \begin{bmatrix} \mu_2 - \mu_1^2 & \mu_3 - \mu_1\mu_2 \\ \mu_3 - \mu_1\mu_2 & \mu_4 - \mu_2^2 \end{bmatrix}$), which is expressed by(55). □

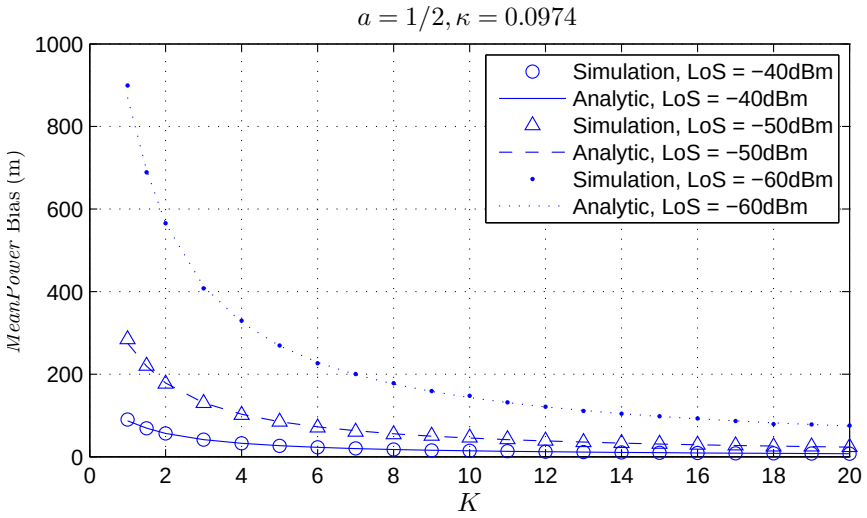

Figure 10. MeanPower's Bias

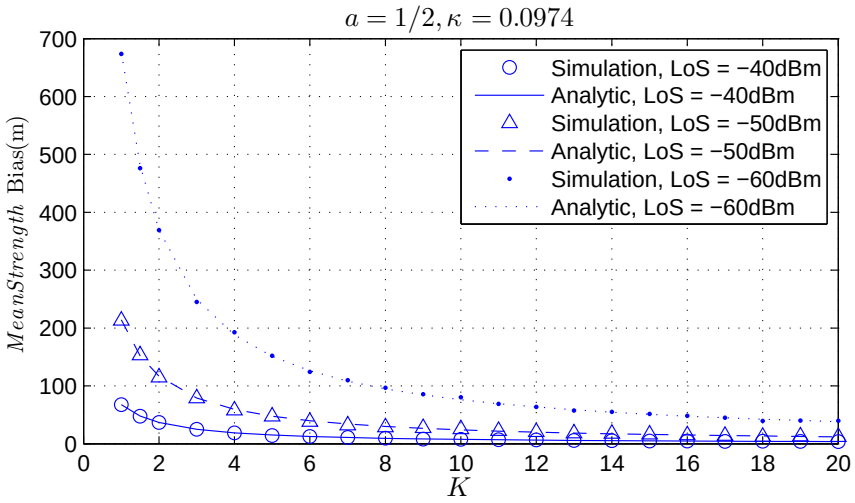

Figure 11. MeanStrength's Bias

REFERENCES

[1] Pratap Misra and Per Enge. *Global positioning system: signals, measurements, and performance*. Ganga-Jamuna Press, 2006. ISBN 978-0-9709544-1-1.

[2] S.M. Kay. *Fundamentals of Statistical Signal Processing: Estimation theory*. Fundamentals of Statistical Signal Processing. Prentice-Hall PTR, 1993. ISBN 9780133457117. URL http://books.google.com/books?id=aFwESQAACAAJ.

[3] C Radhakrishna Rao. Information and the accuracy attainable in the estimation of statistical parameters. In *Breakthroughs in statistics*, pages 235–247. Springer, 1992.

[4] Lee J Bain and Max Engelhardt. *Introduction to probability and mathematical statistics*, volume 4. Duxbury Press Belmont, CA, 1992.

[5] Yiu-Tong Chan, Wing-Yue Tsui, Hing-Cheung So, and Pak-Chung Ching. Time-of-arrival based localization under NLOS conditions. *IEEE Transactions on Vehicular Technology*, 55(1):17–24, January 2006. ISSN 0018-9545. doi: 10.1109/TVT.2005.861207.

[6] F. Benedetto, G. Giunta, A. Toscano, and L. Vegni. Dynamic los/nlos statistical discrimination of wireless mobile channels. In *Vehicular Technology Conference, 2007. VTC2007-Spring. IEEE 65th*, pages 3071–3075, April 2007. doi: 10.1109/VETECS.2007.629.

[7] S. Marano, W.M. Gifford, H. Wymeersch, and M.Z. Win. NLOS identification and mitigation for localization based on UWB experimental data. *IEEE Journal on Selected Areas in Communications*, 28(7):1026–1035, September 2010. ISSN 0733-8716. doi: 10.1109/JSAC.2010.100907.

[8] B.Y. Shikur and T. Weber. Robust cooperative localization in mixed LOS and NLOS environments using TOA. In *2014 11th Workshop on Positioning, Navigation and Communication (WPNC)*, pages 1–6, March 2014. doi: 10.1109/WPNC.2014.6843291.

[9] P. Stefanut, D.P. Gaillot, A. Nasr, M. Lienard, and P. Degauque. A localization technique for LOS and NLOS scenario. In *Wireless Technology Conference (EuWIT), 2010 European*, pages 121–124, September 2010.

[10] K. Papakonstantinou and D. Slock. Cramer-Rao bounds for hybrid localization methods in LoS and NLoS environments. In *2010 IEEE 21st International Symposium on Personal, Indoor and Mobile Radio Communications Workshops (PIMRC Workshops)*, pages 213–217, September 2010. doi: 10.1109/PIMRCW.2010.5670364.

[11] Martin Sauter. *From GSM to LTE: an introduction to mobile networks and mobile broadband*. John Wiley & Sons, 2010.

[12] William CY Lee. Estimate of local average power of a mobile radio signal. *Vehicular Technology, IEEE Transactions on*, 34(1):22–27, 1985.

[13] Mark D Austin and GL Stüber. Velocity adaptive handoff algorithms for microcellular systems. *IEEE Transactions on Vehicular Technology*, 43(3):549–561, 1994.

[14] Veljo Otsason, Alex Varshavsky, Anthony LaMarca, and Eyal De Lara. Accurate gsm indoor localization. In *UbiComp 2005: Ubiquitous Computing*, pages 141–158. Springer, 2005.

[15] Heikki Laitinen, Jaakko Lahteenmaki, and Tero Nordstrom. Database correlation method for gsm location. In *Vehicular Technology Conference, 2001. VTC 2001 Spring. IEEE VTS 53rd*, volume 4, pages 2504–2508. IEEE, 2001.

[16] I.T. Haque and C. Assi. Profiling-Based Indoor Localization Schemes. *IEEE Systems Journal*, 9(1):76–85, March 2015. ISSN 1932-8184. doi: 10.1109/JSYST.2013.2281257.

[17] Bang Wang, Shengliang Zhou, Wenyu Liu, and Yijun Mo. Indoor Localization Based on Curve Fitting and Location Search Using Received Signal Strength. *IEEE Transactions on Industrial Electronics*, 62(1):572–582, January 2015. ISSN 0278-0046. doi: 10.1109/TIE.2014.2327595.

[18] Lei Wang and Maciej Zawodniok. Rssi-based localization in cellular networks. In *Local Computer Networks Workshops (LCN Workshops), 2012 IEEE 37th Conference on*, pages 820–826. IEEE, 2012.

[19] William C Lee. *Mobile communications engineering*. McGraw-Hill Professional, 1982.

[20] Thomas N Rubinstein. The standard deviations of the local means of land mobile radio signals in flat suburban terrain. In *Vehicular Technology Conference, 1986. 36th IEEE*, volume 36, pages 52–56. IEEE, 1986.

[21] Andrea Zanella and Andrea Bardella. Rss-based ranging by multichannel rss averaging. *Wireless Communications Letters, IEEE*, 3(1):10–13, 2014.

[22] Xinrong Li. Rss-based location estimation with unknown pathloss model. *Wireless Communications, IEEE Transactions on*, 5(12):3626–3633, 2006.

[23] Harald T Friis. A note on a simple transmission formula. *proc. IRE*, 34(5):254–256, 1946.

[24] Ralph O Schmidt. Multiple emitter location and signal parameter estimation. *Antennas and Propagation, IEEE Transactions on*, 34(3):276–280, 1986.

[25] Richard Klukas and Michel Fattouche. Line-of-sight angle of arrival estimation in the outdoor multipath environment. *Vehicular Technology, IEEE Transactions on*, 47(1): 342–351, 1998.

[26] Richard Roy and Thomas Kailath. Esprit-estimation of signal parameters via rotational invariance techniques. *Acoustics, Speech and Signal Processing, IEEE Transactions on*, 37(7):984–995, 1989.

[27] Moustafa M Abdalla, Mostafa B Abuitbel, and Mohamed A Hassan. Performance evaluation of direction of arrival estimation using music and esprit algorithms for mobile communication systems. In *Wireless and Mobile Networking Conference (WMNC), 2013 6th Joint IFIP*, pages 1–7. IEEE, 2013.

[28] Telecommunications Industry Association et al. The cdma2000 itu-r rtt candidate submission,", 1998.

[29] Ismail Guvenc and Chia-Chin Chong. A survey on toa based wireless localization and nlos mitigation techniques. *Communications Surveys & Tutorials, IEEE*, 11(3): 107–124, 2009.

[30] Ali H Sayed, Alireza Tarighat, and Nima Khajehnouri. Network-based wireless location: challenges faced in developing techniques for accurate wireless location information. *Signal Processing Magazine, IEEE*, 22(4):24–40, 2005.

[31] James J Caffery and Gordon L Stuber. Overview of radiolocation in cdma cellular systems. *Communications Magazine, IEEE*, 36(4):38–45, 1998.

[32] James Caffery and Gordon L Stuber. Subscriber location in cdma cellular networks. *Vehicular Technology, IEEE Transactions on*, 47(2):406–416, 1998.

[33] Sklar Bernard. Digital communications fundamentals and applications. *Chap15, Prentice-Hall International, inc*, 2001.

[34] Matthias Patzold. *Mobile fading channels*. John Wiley & Sons, Inc., 2003.

[35] Chengshan Xiao, Yahong Rosa Zheng, and Norman C Beaulieu. Novel sum-of-sinusoids simulation models for rayleigh and rician fading channels. *Wireless Communications, IEEE Transactions on*, 5(12):3667–3679, 2006.

[36] James K Cavers. An analysis of pilot symbol assisted modulation for rayleigh fading channels [mobile radio]. *Vehicular Technology, IEEE Transactions on*, 40(4):686–693, 1991.

[37] Chengshan Xiao and Jan C Olivier. Nonselective fading channel estimation with nonuniformly spaced pilot symbols. *International Journal of Wireless Information Networks*, 7(3):177–185, 2000.

[38] Jingxian Wu, Chengshan Xiao, and Jan C Olivier. Time-varying and frequency-selective channel estimation with unequally spaced pilot symbols. *International Journal of Wireless Information Networks*, 11(2):93–104, 2004.

[39] Cihan Tepedelenlioglu, Ali Abdi, and Georgios B Giannakis. The ricean k factor: estimation and performance analysis. *Wireless Communications, IEEE Transactions on*, 2(4):799–810, 2003.

[40] S. Saunders and A. Aragón-Zavala. *Antennas and Propagation for Wireless Communication Systems: 2nd Edition*. John Wiley & Sons, 2007. ISBN 9780470848791. URL http://books.google.com/books?id=D1WF5Z1Yz7YC.

[41] Mohammed Rana Basheer and Sarangapani Jagannathan. R-factor: A new parameter to enhance location accuracy in rssi based real-time location systems. In *Sensor, Mesh and Ad Hoc Communications and Networks, 2009. SECON'09. 6th Annual IEEE Communications Society Conference on*, pages 1–9. IEEE, 2009.

[42] J. Wilson and N. Patwari. Radio Tomographic Imaging with Wireless Networks. *IEEE Transactions on Mobile Computing*, 9(5):621–632, May 2010. ISSN 1536-1233. doi: 10.1109/TMC.2009.174.

[43] Yang Zhao and N. Patwari. Robust Estimators for Variance-Based Device-Free Localization and Tracking. *IEEE Transactions on Mobile Computing*, 14(10):2116–2129, October 2015. ISSN 1536-1233. doi: 10.1109/TMC.2014.2385710.

[44] M. Bocca, O. Kaltiokallio, N. Patwari, and S. Venkatasubramanian. Multiple Target Tracking with RF Sensor Networks. *IEEE Transactions on Mobile Computing*, 13(8): 1787–1800, August 2014. ISSN 1536-1233. doi: 10.1109/TMC.2013.92.

[45] K. Woyach, D. Puccinelli, and M. Haenggi. Sensorless Sensing in Wireless Networks: Implementation and Measurements. In *2006 4th International Symposium on Modeling and Optimization in Mobile, Ad Hoc and Wireless Networks*, pages 1–8, April 2006. doi: 10.1109/WIOPT.2006.1666495.

[46] Dian Zhang, Jian Ma, Quanbin Chen, and L.M. Ni. An RF-Based System for Tracking Transceiver-Free Objects. In *Fifth Annual IEEE International Conference on Pervasive Computing and Communications, 2007. PerCom '07*, pages 135–144, March 2007. doi: 10.1109/PERCOM.2007.8.

[47] R.K. Martin, A. Folkerts, and T. Heinl. Accuracy vs. Resolution in Radio Tomography. *IEEE Transactions on Signal Processing*, 62(10):2480–2491, May 2014. ISSN 1053-587X. doi: 10.1109/TSP.2014.2311969.

[48] N. Patwari and P. Agrawal. Effects of Correlated Shadowing: Connectivity, Localization, and RF Tomography. In *International Conference on Information Processing in Sensor Networks, 2008. IPSN '08*, pages 82–93, April 2008. doi: 10.1109/IPSN.2008.7.

[49] P. Agrawal and N. Patwari. Correlated link shadow fading in multi-hop wireless networks. *IEEE Transactions on Wireless Communications*, 8(8):4024–4036, August 2009. ISSN 1536-1276. doi: 10.1109/TWC.2009.071293.

[50] William C Jakes and Donald C Cox. *Microwave mobile communications*. Wiley-IEEE Press, 1994.

[51] Raymond Steele, H Ahmadi, and A Krishna. Mobile radio communications. In *IEEE Proceedings*, volume 82, pages 1468–1468. [New York, NY]: Institute of Electrical and Electronics Engineers,[1963-, 1994.

[52] Gordon L Stüber. *Principles of mobile communication*. Springer Science & Business Media, 2011.

[53] K.A. Qaraqe and S. Roe. Channel estimation algorithms for third generation w-cdma communication systems. In *Vehicular Technology Conference, 2001. VTC 2001 Spring. IEEE VTS 53rd*, volume 4, pages 2675–2679 vol.4, 2001. doi: 10.1109/VETECS.2001.944086.

[54] Abdelmonaem Lakhzouri. *Channel Estimation and Mobile Phone Positioning in CDMA Based Wireless Communication Systems*. June 2005. ISBN 952-15-1368-3. URL http://dspace.cc.tut.fi/dpub/handle/123456789/73.

[55] S. Coleri, M. Ergen, A. Puri, and A. Bahai. Channel estimation techniques based on pilot arrangement in OFDM systems. *IEEE Transactions on Broadcasting*, 48(3): 223–229, September 2002. ISSN 0018-9316. doi: 10.1109/TBC.2002.804034.

[56] Zijian Tang, R.C. Cannizzaro, G. Leus, and P. Banelli. Pilot-Assisted Time-Varying Channel Estimation for OFDM Systems. *IEEE Transactions on Signal Processing*, 55 (5):2226–2238, May 2007. ISSN 1053-587X. doi: 10.1109/TSP.2007.893198.

[57] Cheng Guan Koay and Peter J Basser. Analytically exact correction scheme for signal extraction from noisy magnitude mr signals. *Journal of Magnetic Resonance*, 179(2): 317–322, 2006.

[58] V Papathanasiou. Some characteristic properties of the fisher information matrix via cacoullos-type inequalities. *Journal of Multivariate analysis*, 44(2):256–265, 1993.

[59] Ram Zamir. A proof of the fisher information inequality via a data processing argument. *Information Theory, IEEE Transactions on*, 44(3):1246–1250, 1998.

[60] Boaz Porat. *Digital processing of random signals: theory and methods*. Prentice-Hall, Inc., 1994.

[61] Jan Sijbers, Arnold Jan den Dekker, Paul Scheunders, and Dirk Van Dyck. Maximum-likelihood estimation of rician distribution parameters. *IEEE Trans. Med. Imaging*, 17(3):357–361, 1998.

[62] Thomas L Marzetta. Em algorithm for estimating the parameters of a multivariate complex rician density for polarimetric sar. In *Acoustics, Speech, and Signal Processing, 1995. ICASSP-95., 1995 International Conference on*, volume 5, pages 3651–3654. IEEE, 1995.

[63] Larry J Greenstein, David G Michelson, and Vinko Erceg. Moment-method estimation of the ricean k-factor. *Communications Letters, IEEE*, 3(6):175–176, 1999.

[64] Ali Abdi, Cihan Tepedelenlioglu, Mostafa Kaveh, and Georgios Giannakis. On the estimation of the k parameter for the rice fading distribution. *Communications Letters, IEEE*, 5(3):92–94, 2001.

[65] Michael Rice. *Digital Communications: A Discrete-time Approach*. Prentice Hall, 2009. ISBN 978-0-13-030497-1.

[66] 3gpp specification: 45.004. URL http://www.3gpp.org/DynaReport.

[67] Fcc rules for wireless equipment operating in the ism bands, 2015. URL http://www.afar.net/tutorials/fcc-rules.

III. NEW THEORETICAL LIMIT ANALYSIS OF LOS AND RSS BASED POSITIONING METHODS FOR RICEAN FADING CHANNEL IN RF SYSTEMS

L. Wang and M. J. Zawodniok

Department of Electronic & Computer Engineering

Missouri University of Science and Technology

Rolla, Missouri 65409–0050

Tel: (409) 692-9235, (573) 341-4361

Email: lw3r6@mst.edu, mjzx9c@mst.edu

ABSTRACT

In this paper, bias and CRB analysis for both proposed line-of-sight (LoS) and conventional radio-signal-strength (RSS) based positioning methods are derived. In contrast to the conventional lognormal based analysis, the derived error models take into account the environmental multipath fading effect. The proposed LoS-based scheme improves positioning accuracy by eliminating the effect of non-range dependent portion of powers from received signal. It suppresses non-line-of-sight (NLoS) disturbance to the positioning result through estimating the LoS component from fading signal. Hence, it is robust to environmental fading disturbance. The derived error models are validated by simulation. Both analytical model and simulation results show that the accuracy and robustness of the proposed LoS-based positioning is superior to that of the conventional RSS-based methods. The derived theoretical limits would guide the integration of power-based positioning systems into future autonomous vehicles and interconnected vehicular applications.

Keywords: Cramer-Rao Bound (CRB); Fading Channel; Line of Sight (LoS); Localization; Received Signal Strength (RSS).

1. INTRODUCTION

Reliable position estimation is required for autonomous vehicle navigation. Global navigation satellite systems (GNSS) are the most widely-used positioning technology. However, GNSS often provide insufficient accuracy and reliability, depending on the number of visible satellites, the relative position and radio electric coverage of the satellites.[1] Additionally, interference and malicious jamming or spoofing can lead to GNSS failure. Therefore, a secondary solution is required for robust navigation system that works in both indoor and outdoor scenario.

The ideal augmenting solution would use the existing communication systems, for example, cellular network, wireless local area network (WLAN), wireless sensor network (WSN), and radio-frequency identification (RFID). Furthermore, little modification to the existing devices is preferred to minimize complexity and avoid cost of dedicated hardware. Radio signal strength indicator (RSSI), for example, is readily available in any RF devices. However, traditional RSSI based positioning methods suffer from low accuracy and are vulnerable to environmental fading. Moreover, the expected accuracy is not well understood. Hence, our work focuses on developing LoS-based positioning scheme, and deriving new error models for both LoS- and RSS-based methods.

In this paper, we derive the mean square error bounds (MSEBs) in forms of Cramer-Rao Lower Bound (CRB), and bias for both the proposed LoS- and conventional RSS-based positioning. Assuming the presence of LoS signal component, the envelope of channel fading follows Ricean distribution. The proposed error model brings insight into how the multipath propagation affects positioning results. To the best of the authors' knowledge, this is the first time that multipath fading effect is explicitly accounted for in the signal power based positioning analysis. Validated by numerical results, the proposed error model is capable of predicting LoS- and RSS-based positioning error, which can aid in assessing expected performance and planning the deployment of reference position (RP, i.e. beacons, access points, anchor nodes, cell towers etc.)

The proposed LoS-based positioning scheme reduces the position estimation error by estimating only range dependent LoS signal component from received signal. The portions of power that introduced by the transmitted symbols and inter symbol interference (ISI) are eliminated by fading channel estimation; and environmental non-line-of-sight (NLoS) fading signal power is suppressed by LoS component estimation. Hence, more accurate positioning is possible. Typical mobile equipment (ME) in the existing standards estimates channel fading within its equalizer during demodulation. Thus, by tapping into the fading signal, the proposed LoS-based positioning maintains benefit of low hardware overhead over time of arrival(ToA), difference-of-arrival(TDoA), and angle-of-arrival(AoA).

This paper also provides a performance comparison of existing power based linear and nonlinear multilateration schemes. The linear schemes includes least square (CLS) [2], constrained weighted least square (CWLS)[3]. Nonlinear schemes includes nonlinear least square (NLS)[4], and maximum-likelihood based nonlinear positioning (ML) [5]. Analytical model and simulation results show that the LoS-based positioning is more accurate and robust than RSS-based methods.

2. MOTIVATION

The main challenge in RSS based positioning is low accuracy due to the presence of multipath fading. In multipath environment, due to the signal reflection, diffraction, and scattering from objects that surround the transmitter (Tx) and receiver (Rx), the transmitted signal traverse multiple paths before reaching the Rx. As a result, the received signal is the transmitted signal that traverses along direct LoS propagation path superimposed with several copies of it from different NLoS paths. Besides, due to different lengths of NLoS paths, the signal (/symbol) transmitted at a particular time instance arrives at the Rx over a spread of time. This will result in intersymbol-interference (ISI) in wireless communication system. Thus, the environment dependent NLoS signal component injects temporal and spatial variation to the total power measurement.

The RSSI provides total power measurement in the received signal [6], which can be modeled as the summation of LoS, NLoS, symbol, and ISI power,

$$P_{RSSI} = P_{LoS}(d) + P_{NLoS}(d, env(\mathbf{x}, t)) + P_S + P_{ISI}. \quad (1)$$

where the LoS power, $P_{LOS}(\cdot)$, is a univariate function of the actual radial distance (range) between transmitter and receiver, d. The NLoS power, $P_{NLoS}(\cdot)$, is a time varying function of the distance (d) and the environment ($env(\cdot)$). The environmental effect is mainly caused by multipath fading. And, it is a multivariate function of, but not limited to, geographical location of the ME ($\mathbf{x}$), and time (t). P_S is the symbol power. P_{ISI} contains what is introduced by ISI, i.e. symbol overlapping at given sampling time instance in a frequency-selective fading channel. Consequently, the current RSS based range estimation has a significant error due to the variation of the NLoS components in the fading signal.

In the proposed LoS-based method, through fading channel estimation, fading signals on different taps are decoupled. The power due to the ISI (overlapping at symbol spaced time instances) is eliminated. The LoS component extracted from fading signal, ($P_{v^2}(d)$), varies monotonically with distance (path-loss) and is not affected by multipath propagation. Hence, more accurate ranging and positioning results are possible.

The remainder of this paper is organized as follows. Related works are introduced in Section 3. In Section 4, the proposed LoS-based positioning is presented. Corresponding bias and CRB are derived in Section 5. For the purpose of comparison, Ricean fading channel based bias and CRB analysis for conventional RSS-based positioning are also derived. In Section 6, the proposed error models are validated by simulation. The accuracy improvement of the proposed LoS-positioning is shown. The positioning performance by using nonlinear NLS and ML methods are evaluated. The entire paper is concluded in Section 6.

3. RELATED WORKS

Signal power based positioning approaches poses minimum hardware requirements on the RF system. RSSI is available in many off-the-shelf devices. Making software upgrade is sufficient. In contrast, the AoA [7, 8, 9], ToA [10, 11], and TDoA [12, 13, 14] technologies require special hardware support. AoA requires directional antenna array; and its accuracy is proportional to the number of elements [15, 16]. ToA require accurate synchronization which is achieved with delay-locked loop (DLL) [10]. TDoA relaxes the synchronization requirement by employing either a sliding correlator or a matched filter [13]. The added cost may be prohibitive in many wireless applications.

Fingerprinting methods [17, 18, 19] address the fading effect by establishing RSSI fingerprint map in offline phase. The position estimation is obtained by matching the online RSSI reading with the prestored fingerprint database. Fingerprinting methods minimize the NLoS signal induced spatial and temporal variance at the cost of onerous periodic fingerprint map calibration. In addition, the grid size used for calibration and number of RPs per grid determine the localization accuracy [20]. In contrast, the proposed LoS-based positioning method eliminate fading effect by discrimination of LoS and NLoS components in the received signal. It requires no cumbersome map building, maintenance, and calibration; and is robust to environmental changing.

To account for the fading effect, mean square error in fading channel range estimation (R-factor) was proposed in [21] as the quality metric for localization. Localization accuracy was improved by identify a subset of RPs that were less affected by multipath fading. The downside is that there has to be a great number of RPs for evaluation; and the position was still estimated based on total power of received signal which contains environment dependent NLoS component. To mitigate fading effect, an offline generated localization error calibration factor, RDEI, was proposed in [22] to correct online estimation. In

contrast, the proposed LoS-based positioning method eliminates the need for offline tuning. It effectively suppresses the multipath fading effect through decoupling LoS components from fading signal.

Widely accepted model of the signal amplitude received at ME over a local area is a composite distribution consisting of a fast fading (Rayleigh) and a slow fading (lognormal)[23, 24, 25]. The local average power (slow fading) is acquired by smoothing out the fast fading [23, 26, 27, 24, 25, 28]. The RSSI is the local average power and is indicated in dBm unit [6]. Under the Central Limit Theorem (CLT), the smoothing operation renders the lognormal property of the local averaging power. Conventional lognormal based CRB analysis for RSS-based positioning can be found in [29, 27]. However, as shown in [30], the average value of the received signal power contains the environment dependent NLoS component. It is difficult to distinguish LoS and NLoS singal component based on lognomral model. In contrast, the theoretical analysis in this paper are based on Ricean fading model [24, 31, 32]. The derived error model for LoS-based and RSS-based positioning is able to decouple the NLoS effect from localization results.

4. THE PROPOSED LOS-BASED POSITIONING

4.1. Overview. The proposed LoS-based positioning system is shown as a block diagram in Fig. 1. At least three geographically separated RPs that broadcast message are required in the system. Depending on communication technologies, the format of frames/slots may be specifically designed for convenience of channel estimation. As an example and without loss of generality, here, we assume the broadcast message contains pilots. The fading signal is interpolated over the entire frame from the pilot message.

The received signal, r_i, contains the power of LoS and NLoS signal components (P_{LoS} and P_{NLoS}), symbol power (P_S), and the power introduced by ISI (P_{ISI}). Through channel estimation (Section 4.3), P_S and P_{ISI} are eliminated. Via LoS component estimation

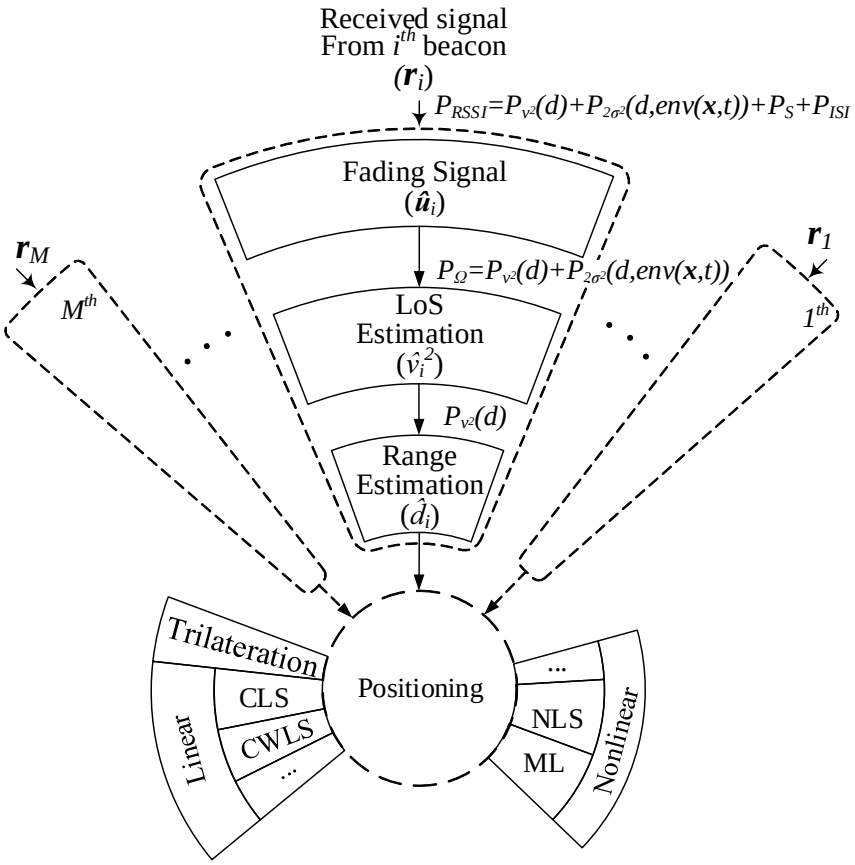

Figure 1. Proposed LoS-based Positioning System

(Section 4.4), the environment dependent NLoS signal component, $P_{2\sigma^2}$, is eliminated. Hence, only the portion of power that is univariate function of range, $P_{LoS5}(d)$, is left for range estimation.

Finally, positioning block converts all range estimates into location estimates. The transformation function between range and position could be either linear (Trilateration, CLS, CWLS [2][3]) or nonlinear (NLS, ML [4][5][29]) depending on the computational and accuracy requirement of the specific application.

4.2. System Model. Based on empiric path-loss model [33], the range estimation is obtained as [30],

$$\hat{d} = f(\theta) = \kappa\theta^{-\frac{1}{n}} \tag{2}$$

where κ is a constant factor that depend on the antenna efficiency, gain, carrier signal wavelength, and transmission power. n is a power factor. In free-space, n is equal to 2. In either urban or some suburban areas, n can be between 3 and 6. θ is the signal power measurement.

For ranging-based positioning system, the target position is determined by a function of range, $\mathbf{d} = [d_1, d_2, \cdots, d_M]^T$, and reference locations, $\mathbf{x}_{ref} = [\mathbf{x}_1, \mathbf{x}_2, \cdots, \mathbf{x}_M]$ with $\mathbf{x} = [x_i, y_i]^T$ (M is the number of references), as,

$$\mathbf{x} = \boldsymbol{G}(\mathbf{d}; \mathbf{x}_{ref}) + \mathbf{e}_G. \tag{3}$$

where $\boldsymbol{G}$ represents the $M \times 1$ inverse $\boldsymbol{g}$ function vector; the $i$the element $[\boldsymbol{G}]_i = g^{-1}(\mathbf{x}, \mathbf{x}_i)$, where,

$$d_i = g(\mathbf{x}; \mathbf{x}_i) = \sqrt{(x - x_i)^2 + (y - y_i)^2}. \tag{4}$$

The techniques to model and realize the nonlinear function $\boldsymbol{G}$ include CLS, CWLS, NLS, ML, etc.

The LoS-based positioning system can be modeled as,

$$\hat{\mathbf{x}} = \boldsymbol{G}(\boldsymbol{f}(\boldsymbol{\theta}), \mathbf{x}_{ref}) \mid_{[\boldsymbol{\theta}]_i = \hat{v_i^2}} + \mathbf{e} \tag{5}$$

where $\boldsymbol{\theta}$ is the power measurement vector, $\boldsymbol{f}$ is the path-loss function vector, $[\boldsymbol{f}]_i = f(\theta_i)$. $\hat{v_i^2}$ represents LoS power estimation. The error term, $\mathbf{e}$, including the variance and bias of the power-based positioning which will be derived in Section 5.

4.3. Channel Estimation. In multipath fading channel, because of the signal reflection, refraction, and atmospheric conditions, the transmitted signal reaches the receiver through multiple paths. These paths are of different lengths. Hence, the symbol spaced signal that sampled on given time instance is a composite of the channeled correct symbol

and multiple channeled preceding symbols. This environment dependent ISI will distort the total power measurement. Therefore, the RSS-based positioning accuracy is fluctuating and sensitive to the environment.

To decouple the power of symbol and ISI from received signal power, fading signal estimation is required, in which LoS signal component is embedded.

4.3.1. Received Signal. The symbol spaced samples of fading channel output at time instance k is given by [34],

$$r(k) = \sum_{j=0}^{L_{ch}-1} h(j,k)b(k-j) + n(k). \tag{6}$$

where L_{ch} is the memory length of the discrete-time channel impulse response (CIR) (i.e. the number of taps), $b(k)$ is the kth symbol value for PSK, or a general QAM modulation, and CIR $h(j,k)$ is the jth tap channel fading, $n(k)$ is AWGN.

Assuming $h(j,t)$ has power Ω, the autocorrelation function of the jth tap fading signal $h(j,t)$ is

$$R_h(\tau) = \Omega\tilde{R}_h(\tau). \tag{7}$$

where $\tilde{R}_h(\tau)$ is the unit power equivalent.

Assume pilot symbols are inserted into the data sequence prior to pulse shaping, and the composite signal is transmitted over a channel characterized by frequency selective fading and additive noise. Pilot symbols are placed in fixed position within a slot/burst. The number of pilots per slot is L_P. Each slot contains L_s symbols. The pilot position within

one slot is $(k_1, k_2, \cdots, k_{Lp})$. Equation (6) can be written in matrix form as [35], (8).

$$\underbrace{\begin{bmatrix} r(k+L_{ch}-1) \\ r(k+L_{ch}) \\ \vdots \\ r(k+2L_{ch}-2) \end{bmatrix}}_{:=\mathbf{r}(k)} = \underbrace{\begin{bmatrix} b(k+L_{ch}-1) & \cdots & b(k+1) & b(k) \\ b(k+L_{ch}) & \ddots & b(k+2) & b(k+1) \\ \vdots & \ddots & \ddots & \vdots \\ b(k+2L_{ch}-1) & \cdots & b(k+L_{ch}) & b(k+L_{ch}-1) \end{bmatrix}}_{:=\mathbf{B}(k)} \underbrace{\begin{bmatrix} h(1,k) \\ h(2,k) \\ \vdots \\ h(L_{ch},k) \end{bmatrix}}_{:=\mathbf{h}(k)} + \underbrace{\begin{bmatrix} n(k+L_{ch}-1) \\ n(k+L_{ch}) \\ \vdots \\ n(k+2L_{ch}-2) \end{bmatrix}}_{:=\mathbf{n}(k)}. \tag{8}$$

where $\mathbf{h}(k)$ $(L_{ch} \times 1)$ is the channel impulse response vector at time instant k. $\mathbf{B}(k)$ is the $L_{ch} \times L_{ch}$ matrix which is made up of consecutive $(2L_{ch} - 1)$ pilot symbols $[b(k), b(k + 1), \cdots, b(k + 2k - 2)]$, and $\mathbf{n}$ $(L_{ch} \times 1)$ is the noise vector.

4.3.2. Fading Signal Estimation. Based on leased square criterion, fading signal on pilots is estimated as [35],

$$\hat{\mathbf{h}}(k) = \mathbf{B}^{\dagger}(k)\mathbf{r}(k). \tag{9}$$

where the dagger denotes pseudo-inverse.

It has been proved in [36] that the interpolation matrix is constant when estimate fading over an entire slot from fading at pilot symbol locations. [36] provided a statistical method to acquire interpolation matrix. It requires to generate a certain amount of fading samples for offline training. [34] interpolates the kth fader from pilot-position fading samples in flat fading channel. In this section we expand [34], to interpolate fading samples of entire slot from fader on pilot-position for frequency-selective fading channel.

The fading estimate of altogether L_{ch} taps can be denoted as a $L_{ch} \times L_P$ matrix $\hat{\mathbf{H}} = [\hat{\mathbf{h}}(1), \cdots, \hat{\mathbf{h}}(k), \cdots \hat{\mathbf{h}}(L_P)]$. Corresponding symbol spaced signal samples is $\mathbf{R} = [\mathbf{r}(1), \cdots, \mathbf{r}(k), \cdots, \mathbf{r}(L_P)]$.

Define column vector $\hat{\mathbf{u}}$ ($L_P \times 1$) as the transpose of each row of $\hat{\mathbf{H}}$ (i.e. $\hat{\mathbf{u}}(j) \coloneqq [\hat{\mathbf{H}}(j,:)]^T$, $1 \leq j \leq L_{ch}$. $\hat{\mathbf{u}}(j)$ represents the fading signal on jth tap at time instance k ($k = 1, k = 2, \cdots, k = L_P$). Define $\mathbf{a}(j)$ as the transpose of each row of $\mathbf{R}$ (i.e. $\mathbf{a}(j) = [\mathbf{R}(j,:)]^T$).

Thus, the elements of $\mathbf{a}(j)$ is the fading signal on jth tap kth pilot position,

$$[\mathbf{a}(j)]_k = r(j,k). \tag{10}$$

The elements of $\hat{\mathbf{u}}(j)$, $\hat{u}(j,k) = r(j,k)/b(k)$. In vector form,

$$\hat{\mathbf{u}}(j) = \mathbf{a}(j)./\mathbf{b}. \tag{11}$$

where ./ denotes element-wise division, $\mathbf{b}$ represents a vector of pilot symbols.

To interpolate entire fading of jth tap,

$$\tilde{\mathbf{u}}(j) = \mathbf{I}(j)\hat{\mathbf{u}}. \tag{12}$$

where $\tilde{\mathbf{u}}(j)$ is the interpolated fading signals on entire slot, ($L_s \times 1$); $\hat{\mathbf{u}}(j)$ is fading estimation on pilot positions, ($L_P \times 1$); $\mathbf{I}(j)$ is the interpolation matrix for jth tap, ($L_s \times L_P$). $\mathbf{I}(j)$ is determined by (51) (see Appendix 8.1).

The entire slot fading estimation has two advantages:

- Expand the sample size of fading signal to improve the LoS component estimation accuracy.
- Generally, pilots are not evenly distributed within frame, entire slot fading estimation provides an opportunity to acquire channel fading in fixed sample rate, which is required by LoS estimation.

4.4. Power Estimation. In mobile fading channel, the probability density function (PDF) of the envelope of the channel fading is a random variable R ($R = |\mathbf{u}(j,i)|$) which follows Ricean distribution [37], and can be expressed as,

$$P_R(r) = \frac{2(K+1)r}{\Omega} e^{\left(-K-\frac{(K+1)r^2}{\Omega}\right)} I_0\left(2r\sqrt{\frac{K(K+1)}{\Omega}}\right) \tag{13}$$

where Ω represents the total power of LoS and NLoS (i.e. $v^2 + 2\sigma^2$), and K represents the Ricean factor (K-ratio). This factor is defined as the power ratio of LoS to NLoS ($K = v^2/2\sigma^2$). The $I_0(\cdot)$ represents the modified Bessel function of the first kind with order zero. The n^{th} moments of the Ricean distribution, μ_n [38],

$$\mu_n = \left(\frac{v^2}{2K}\right)^{n/2} 2^{n/2}\Gamma\left(1+\frac{n}{2}\right) L_{n/2}(-K). \tag{14}$$

where, $L_q(\cdot)$ is laguerre polynomials [39].

The LoS component estimator can be expressed as [30],

$$\hat{v^2} = \hat{\Omega}\frac{\hat{K}}{1+\hat{K}}. \tag{15}$$

where, $\hat{\Omega}$ is the estimator of the total power of fading signal, $\hat{K}$ is the LoS-to-NLoS K-ratio. We assume that the total power and K-ratio are estimated independently. Total power estimator is the second moment of Ricean fading, μ_2, which can be calculated based on fading signal power,

$$\hat{\Omega} = \frac{1}{N}\sum_{i=1}^{N} r_i^2. \tag{16}$$

where N is the number of fading signal samples.

The K estimator is obtained based on Koay method [40],

$$\hat{K} = \frac{1}{2}\epsilon^2. \tag{17}$$

where $\epsilon = \sqrt{\xi(\epsilon)\left[1 + \frac{\mu_1^2}{\sigma_r^2}\right] - 2}$, $\xi(\epsilon)$, σ_r^2 is the variance of fading signal envelope, $\sigma_r^2 = \mu_2 - \mu_1^2$. μ_1 and μ_2 are the first and second moments of the samples of fading signal. An iterative solution for ϵ is given in [40].

5. ERROR MODEL

In this Section, the mean square error bound (MSEB) of the power-based position estimation, $\hat{\mathbf{x}}$, is derived. The power estimation from M RPs, $\boldsymbol{\theta} = [\theta_1, \theta_2, \cdots, \theta_M]^T$, can be expressed as a function of position $\hat{\mathbf{x}}$,

$$\boldsymbol{\theta} = \boldsymbol{z}(\hat{\mathbf{x}}) + \mathbf{e}_\theta. \tag{18}$$

where function $\boldsymbol{z}(\cdot)$ encapsulates the path-loss and circle functions as,

$$\boldsymbol{z}(\hat{\mathbf{x}}) = \boldsymbol{F}\left(\boldsymbol{g}\left(\hat{\mathbf{x}}, \mathbf{x}_{ref}\right)\right). \tag{19}$$

in which, $\boldsymbol{F}$ is a $M \times 1$ function vector; the ith element is the inverse of function (2), i.e. $\theta_i = [\boldsymbol{F}]_i = f^{-1}(d_i)$. And $g_i = [\boldsymbol{g}]_i$ is given by (4).

Due to the nonlinearity of function $\boldsymbol{z}(\cdot)$, the MSEB contains two parts, variance and bias [41],

$$E\left((\hat{\mathbf{x}} - \mathbf{x})^2\right) \geq CRB(\hat{\mathbf{x}}) + Bias^2(\hat{\mathbf{x}}) \tag{20}$$

In the following subsections, the MSEB for LoS-based and conventional RSS-based position estimation are derived respectively.

5.1. Theoretical Limit and Error Model of the LoS-based Positioning. Assume that the parameters of empirical path-loss model (κ_i, n_i, $i = 1, 2, \cdots, M$) are known.

Lemma 1 presents the derived CRB limit of positioning error for LoS-based estimation. Lemma 2 gives the bias of the estimation.

Lemma 10. *The CRB of LoS-based position estimation on* $\boldsymbol{x} = [x, y]^T$*, given reference positions* $\boldsymbol{x}_i = [x_i, y_i]^T$*,* $1 \le i \le M$*, is* $\boldsymbol{J}_v(\boldsymbol{x})^{-1}$*,*

$$
\begin{aligned}
[\boldsymbol{J}_v(\boldsymbol{x})]_{1,1} =& 4\sum_{i=1}^{M} \frac{\kappa_i^{2n_i} n_i^2 d_i^{-2(n_i+2)}(x-x_i)^2}{AsV\left(\hat{v_i^2}\right)} \\
&+2\sum_{i=1}^{M} \frac{c^{-2}\zeta_{v,i}^2 \kappa_i^{4n_i} n_i^2 d_i^{-4(n_i+1)}(x-x_i)^2}{AsV\left(\hat{v_i^2}\right)}
\end{aligned}
$$

$$
\begin{aligned}
[\boldsymbol{J}_v(\boldsymbol{x})]_{2,2} =& 4\sum_{i=1}^{M} \frac{\kappa_i^{2n_i} n_i^2 d_i^{-2(n_i+2)}(y-y_i)^2}{AsV\left(\hat{v_i^2}\right)} \\
&+2\sum_{i=1}^{M} \frac{c^{-2}\zeta_{v,i}^2 \kappa_i^{4n_i} n_i^2 d_i^{-4(n_i+1)}(y-y_i)^2}{AsV\left(\hat{v_i^2}\right)}
\end{aligned}
$$

$$
\begin{aligned}
[\boldsymbol{J}_v(\boldsymbol{x})]_{1,2} =& [\boldsymbol{J}_v(\boldsymbol{x})]_{2,1} = \\
& 4\sum_{i=1}^{M} \frac{\kappa_i^{2n_i} n_i^2 d_i^{-2(n_i+2)}(x-x_i)(y-y_i)}{AsV\left(\hat{v_i^2}\right)} \\
&+2\sum_{i=1}^{M} \frac{c^{-2}\zeta_{v,i}^2 \kappa_i^{4n_i} n_i^2 d_i^{-4(n_i+1)}(x-x_i)(y-y_i)}{AsV\left(\hat{v_i^2}\right)}.
\end{aligned} \tag{21}
$$

where, $\zeta_{v,i} = \zeta_v(K_i)$ *is given by (22),* $AsV\left(\hat{v_i^2}\right)$ *is given by [30], (23), c is the converge rate of the asymptotic variance [42], M represents number of beacons (/reference locations), and N is the sample size.*

$$
\begin{aligned}
\zeta_v(K) =& \frac{\frac{3\pi}{2}L_{1/2}(-K)L_{3/2}(-K) - \pi(1+K)L_{1/2}^2(-K)}{K^2(1+K)^4[\eta'(K)]^2}\left[\frac{K}{1+K} - \frac{\frac{\pi}{4}L_{1/2}^2(-K)}{(1+K)^3\eta'(K)}\right] \\
&+ \frac{(1+K)L_{1/2}^2(-K) - \frac{\pi^2}{16}L_{1/2}^4(-K)}{K^2(1+K)^4[\eta'(K)]^2} \\
&+ \frac{1+2K}{K^3}\left[\frac{K}{1+K} - \frac{\frac{\pi}{4}L_{1/2}^2(-K)}{(1+K)^3\eta'(K)}\right]^2.
\end{aligned} \tag{22}
$$

$$
\begin{aligned}
AsV\left(\hat{v^2}\right) =& \frac{4\mu_1^2\left(\mu_2-\mu_1^2\right)}{\left[\eta'(K)\right]^2(1+K)^4} \\
&+ \frac{4\mu_1(\mu_3-\mu_1\mu_2)}{(1+K)^2\eta'(K)}\left(\frac{\eta'(K)(1+K)K-\frac{\mu_1^2}{\mu_2}}{\eta'(K)(1+K)^2}\right) \\
&+ (\mu_4-\mu_2^2)\left(\frac{\eta'(K)(1+K)K-\frac{\mu_1^2}{\mu_2}}{\eta'(K)(1+K)^2}\right)^2 .
\end{aligned} \tag{23}
$$

$$
c = \sqrt{N}. \tag{24}
$$

$$
\eta(K) = \frac{\pi L_{1/2}^2(-K)}{4(K+1)} = \frac{\mu_1^2}{\mu_2}. \tag{25}
$$

where K is LoS-to-NLoS ratio, and $L_{1/2}(\cdot)$ represents Laguerre polynomial.

Proof. Assumes that the LoS signal component estimation from each reference location is independent. By central limit theory (CLT),

$$
\mathbf{e}_\theta \mid_{\theta=\hat{v^2}} \sim \mathcal{N}(\mathbf{0}, \mathbf{\Sigma}_v) \tag{26}
$$

where $\mathbf{\Sigma}_v = diag\left(AsV\left(\hat{v_1^2}\right), AsV\left(\hat{v_2^2}\right), \cdots, AsV\left(\hat{v_M^2}\right)\right)$, and the ith element of $\boldsymbol{z}$,

$$
[\boldsymbol{z}]_i = \kappa_i^{n_i}\left[g_i(\hat{\mathbf{x}})\right]^{-n_i} \tag{27}
$$

in which, $g_i(\hat{\mathbf{x}})$ is given by (4).

It has been shown in [30], the asymptotic variance (AsV) of the LoS component in fading signal is (23). AsV reveals the variance of an estimator as the sample size is tending to large [43].

By rearranging (23), we get,

$$
AsV(\hat{v_i^2}) = \zeta_{v,i}(v_i^2)^2 \tag{28}
$$

where v_i^2 is the actual LoS power.

By taking the path-loss model (2) into (28),

$$[\mathbf{\Sigma}_v]_{ii} = AsV(\hat{v_i^2}) = \zeta_{v,i}\kappa_i^{2n_i}(d_i^2)^{n_i} \tag{29}$$

The general Gaussian fisher information matrix (FIM) [41],

$$[\mathbf{J}_v(\mathbf{x})]_{kl}=\left[\frac{\partial \mathbf{z}}{\partial \mathbf{x}}\right]^T \mathbf{\Sigma}_v^{-1}\left[\frac{\partial \mathbf{z}}{\partial \mathbf{x}}\right]+\frac{1}{2}Tr\left[\mathbf{\Sigma}_v^{-1}\frac{\partial \mathbf{\Sigma}_v}{\partial [\mathbf{x}]_k}\mathbf{\Sigma}_v^{-1}\frac{\partial \mathbf{\Sigma}_v}{\partial [\mathbf{x}]_l}\right]. \tag{30}$$

where, the subscripts of $[\cdot]_{kl}$ denotes the kth (row) lth (column) element in the matrix, $Tr[\cdot]$ is the trace operator, and,

$$\frac{[\partial \mathbf{z}]_i}{\partial \mathbf{x}} = -2\kappa_i^{n_i} n_i d_i^{-(n_i+2)}\left[(x-x_i),(y-y_i)\right]. \tag{31}$$

$$\left[\frac{\partial \mathbf{\Sigma}_v}{\partial \mathbf{x}}\right]_{i,i} = -2\zeta_{v,i}\kappa_i^{2n_i} n_i d_i^{-2(n_i+1)}[(x-x_i),(y-y_i)]. \tag{32}$$

□

The bias in the range-based positioning is derived in Lemma 2. The bias of the positioning is caused by the variance in the power estimation and the nonlinear transformation from power measurement to range estimation.

Lemma 11. *The bias of LoS based position estimation* $\hat{\boldsymbol{x}} = [\hat{x}, \hat{y}]^T$ *at* $\boldsymbol{x} = [x, y]^T$*, given reference positions* $\boldsymbol{x}_i = [x_i, y_i]^T$*, is*

$$Bias_{\boldsymbol{x}}^{LoS}(\hat{\boldsymbol{x}})=\frac{1}{\sum_{i=1}^M\left(\frac{\partial g_i}{\partial x}\right)^2\sum_{i=1}^M\left(\frac{\partial g_i}{\partial y}\right)^2-\left(\sum_{i=1}^M\frac{\partial g_i}{\partial x}\frac{\partial g_i}{\partial y}\right)^2}\begin{bmatrix}\frac{1}{2}\sum_{j=1}^M f''(v_j^2)AsV(\hat{v_j^2})\left(\frac{\partial g_j}{\partial x}\sum_{i=1}^M\left(\frac{\partial g_i}{\partial y}\right)^2-\frac{\partial g_j}{\partial y}\sum_{i=1}^M\left(\frac{\partial g_i}{\partial x}\frac{\partial g_i}{\partial y}\right)\right)\\ \frac{1}{2}\sum_{j=1}^M f''(v_j^2)AsV(\hat{v_j^2})\left(\frac{\partial g_j}{\partial y}\sum_{i=1}^M\left(\frac{\partial g_i}{\partial x}\right)^2-\frac{\partial g_j}{\partial x}\sum_{i=1}^M\left(\frac{\partial g_i}{\partial x}\frac{\partial g_i}{\partial y}\right)\right)\end{bmatrix}. \tag{33}$$

in which, $g_i = g(\boldsymbol{x};\boldsymbol{x}_i)$ *is function (4), and* $f(\cdot)$ *is the path-loss model (2).*

Proof. The expectation of distance estimation $\hat{d}$ derived from LoS estimation can expressed as [44],

$E[f(\hat{v^2})] \doteq f(\mu)|_{\mu=v^2} + \frac{1}{2} f''(\mu) AsV(\hat{v^2})\Big|_{\mu=v^2}$,

$$\hat{d_i}(\mathbf{x}) = d_i(\mathbf{x}) + \frac{1}{2} f''(v_i^2) AsV(\hat{v_i^2}) \tag{35}$$

And, the Taylor expansion of the inverse-circle function (4) in terms of $\hat{\mathbf{x}}$,

$$d_i(\hat{\mathbf{x}}) = d_i(\mathbf{x}) + \left[\mathbf{D}_{\boldsymbol{g}}(\mathbf{x})\right]_i (\hat{\mathbf{x}} - \mathbf{x}) \tag{36}$$

in which, $\mathbf{D}_{\boldsymbol{g}}$ represents Jacobian matrix of function $\boldsymbol{g}$, i.e. $\mathbf{D}_{\boldsymbol{g}} = \frac{\partial}{\partial \mathbf{x}} \boldsymbol{g}$.

Let $E\left[\hat{d_i}(\mathbf{x})\right] = E\left[d(\hat{\mathbf{x}})\right]$, we have, $\left[\mathbf{D}_{\boldsymbol{g}}(\mathbf{x})\right]_i (\hat{\mathbf{x}} - \mathbf{x}) = \frac{1}{2} f''(v_i^2) AsV(\hat{v_i^2})$. Therefore, the bias,

$$E(\hat{\mathbf{x}} - \mathbf{x}) = \mathbf{D}_{\boldsymbol{g}}^{\dagger} \mathbf{s}_v. \tag{37}$$

where

$$\mathbf{s}_v = \frac{1}{2} \left[f''(v_1^2) AsV(\hat{v_1^2}), f''(v_2^2) AsV(\hat{v_2^2}), \cdots, f''(v_M^2) AsV(\hat{v_M^2}) \right]^T. \tag{38}$$

which lead to (33). □

Definition 1. *The power-based position estimation error is modeled as the square root of the summation of the squared positioning bias and the trace of CRB.*

Here, the error model of the LoS-based positioning is,

$$E_{LoS} = \sqrt{trace\left[\mathbf{J}_v^{-1}(\mathbf{x})\right] + \left[Bias_{\mathbf{x}}^{LoS}(\mathbf{x})\right]_x^2 + \left[Bias_{\mathbf{x}}^{LoS}(\mathbf{x})\right]_y^2} \tag{39}$$

5.2. Theoretical Limit and Error Model of the RSS-based Positioning. For the purpose of comparison, Ricean fading model based CRB and bias analysis are presented in this section. Because the conventional lognormal analysis is not able to distinguish fading effect from localization results.

Considering that the transmitting payload (code/symbols) is randomized by scrambler before transmitting (and recovered by descrambler at receiver) [45], the payload is assumed to be a noise with constant power in conventional RSS-based methods. Here, we assume, in the conventional RSS-based methods, the power of payload is negligible.

The total power estimator based on the envelope of fading signal is the 2nd moment of Ricean distributed random variable,

$$E[\hat{\Omega}] = \mu_2 = 2\sigma^2 + v^2 \tag{40}$$

When $\hat{\Omega}$ is used for position estimation, the presence of NLoS signal power will inject bias. In this section, we show the CRB and the bias of RSS based positioning, in Lemma 3 and 4 respectively. Also, the error model of RSS-based positioning is given at the end of this section.

Lemma 12. *The CRB of RSS based position estimation $\hat{\boldsymbol{x}}$ at $\boldsymbol{x}$, given reference positions $\boldsymbol{x}_i$, $1 \le i \le M$, is $\boldsymbol{J}_\Omega(\boldsymbol{x})^{-1}$, where*

$$\begin{aligned}[\boldsymbol{J}_\Omega(\boldsymbol{x})]_{1,1} =& 4\sum_{i=1}^{M} \frac{\kappa_i^{2n_i} n_i^2 d_i^{-2(n_i+2)}(x-x_i)^2}{AsV(\hat{\Omega}_i)} \\ &+2\sum_{i=1}^{M} \frac{c^{-2}\zeta_{\Omega,i}^2 \kappa_i^{4n_i} n_i^2 d_i^{-4(n_i+1)}(x-x_i)^2}{AsV(\hat{\Omega}_i)}\end{aligned}$$

$$\begin{aligned}[\boldsymbol{J}_\Omega(\boldsymbol{x})]_{2,2} =& 4\sum_{i=1}^{M} \frac{\kappa_i^{2n_i} n_i^2 d_i^{-2(n_i+2)}(y-y_i)^2}{AsV(\hat{\Omega}_i)} \\ &+2\sum_{i=1}^{M} \frac{c^{-2}\zeta_{\Omega,i}^2 \kappa_i^{4n_i} n_i^2 d_i^{-4(n_i+1)}(y-y_i)^2}{AsV(\hat{\Omega}_i)}\end{aligned}$$

$$[\boldsymbol{J}_{\Omega}(\boldsymbol{x})]_{1,2} = [\boldsymbol{J}_{\Omega}(\boldsymbol{x})]_{2,1} = 4\sum_{i=1}^{M} \frac{\kappa_i^{2n_i} n_i^2 d_i^{-2(n_i+2)}(x-x_i)(y-y_i)}{AsV(\hat{\Omega}_i)} + 2\sum_{i=1}^{M} \frac{c^{-2}\zeta_{\Omega,i}^2 \kappa_i^{4n_i} n_i^2 d_i^{-4(n_i+1)}(x-x_i)(y-y_i)}{AsV(\hat{\Omega}_i)}. \tag{41}$$

where, $\zeta_{\Omega,i} = \zeta_{\Omega}(K_i)$*,*

$$\zeta_{\Omega}(K) = (1+2K)K^{-2} \tag{42}$$

where K is the LoS-to-NLoS ratio.

Proof. The variance of total power estimation based on fading signal envelopes can be found by moments as,

$$Var\left(\hat{\Omega}\right) = \mu_4 - \mu_2^2 \tag{43}$$

where μ_4 and μ_2 are the 4th and 2nd moment (9).

Assume independent power estimation from each reference position, by CLT,

$$\mathbf{e}_{\theta}\mid_{\theta=\hat{\Omega}} \sim \mathcal{N}(\mathbf{0}, \boldsymbol{\Sigma}_{\Omega}) \tag{44}$$

where $\boldsymbol{\Sigma}_{\Omega} = diag\left(Var(\hat{\Omega}_1), Var(\hat{\Omega}_2), \cdots, Var(\hat{\Omega}_M)\right)$.

Given LoS-to-NLoS ratio $K = v^2/2\sigma^2$, by rearranging (43), we get $Var(\hat{\Omega}) = \zeta_{\Omega,i}(\Omega_i)$. Taking $\theta = \Omega$ into (2), the variance of power estimation can be expressed as,

$$Var(\hat{\Omega}) = \zeta_{\Omega,i}\kappa_i^{2n_i}\left(d_i^2\right)^{n_i}. \tag{45}$$

where $\zeta_{\Omega,i}$ is given by (42).

The rest of the proof are in the same manner as Lemma 1, and is omitted here. □

Lemma 13. *The bias of RSS based position estimation* $\hat{\boldsymbol{x}} = [\hat{x}, \hat{y}]^T$ *at* $\boldsymbol{x} = [x, y]^T$*, given reference positions* $\boldsymbol{x}_i = [x_i, y_i]^T$*, is,*

$$Bias_{\boldsymbol{x}}^{RSS}(\hat{\boldsymbol{x}}) = \frac{1}{\sum_{i=1}^{M}\left(\frac{\partial g_i}{\partial x}\right)^2 \sum_{i=1}^{M}\left(\frac{\partial g_i}{\partial y}\right)^2 - \left(\sum_{i=1}^{M}\frac{\partial g_i}{\partial x}\frac{\partial g_i}{\partial y}\right)^2} \begin{bmatrix} \sum_{j=1}^{M}\left\{g_j\left[(1+K_j^{-1})^{-1/n_j}-1\right]+\frac{1}{2N}f''(\Omega_j)AsV(\hat{\Omega}_j)\right\}\left(\frac{\partial g_j}{\partial x}\sum_{i=1}^{M}\left(\frac{\partial g_i}{\partial y}\right)^2 - \frac{\partial g_j}{\partial y}\sum_{i=1}^{M}\left(\frac{\partial g_i}{\partial x}\frac{\partial g_i}{\partial y}\right)\right) \\ \sum_{j=1}^{M}\left\{g_j\left[(1+K_j^{-1})^{-1/n_j}-1\right]+\frac{1}{2N}f''(\Omega_j)AsV(\hat{\Omega}_j)\right\}\left(\frac{\partial g_j}{\partial y}\sum_{i=1}^{M}\left(\frac{\partial g_i}{\partial x}\right)^2 - \frac{\partial g_j}{\partial x}\sum_{i=1}^{M}\left(\frac{\partial g_i}{\partial x}\frac{\partial g_i}{\partial y}\right)\right) \end{bmatrix} \tag{46}$$

in which, $g_i = g(\boldsymbol{x}; \boldsymbol{x}_i)$ *is function (4), and* $f(\cdot)$ *is the path-loss model (2).*

Proof. Take the total power, $\Omega = v^2 + 2\sigma^2$, into (2), and rearrange,

$$f(\Omega) = \kappa\left[v^2\left(1 + K^{-1}\right)\right]^{-1/n} \tag{47}$$

Take (47) into the expectation [44] $E[f(\hat{\Omega})] \doteq f(\mu)\mid_{\mu=\Omega} + \frac{1}{2}f''(\mu)AsV(\hat{\Omega})\mid_{\mu=\Omega}$,

$$\hat{d}(\mathbf{x}) = d(\mathbf{x})(1 + K^{-1})^{-1/n} + \frac{1}{2}f''(\Omega)AsV(\hat{\Omega}). \tag{48}$$

Thus,

$$\mathbf{s}_{\Omega} = \begin{bmatrix} d_1(\mathbf{x})\left[(1 + K_1^{-1})^{-\frac{1}{n_1}}\right] + \frac{1}{2}f''(\Omega_1)AsV(\hat{\Omega}_1) \\ d_2(\mathbf{x})\left[(1 + K_2^{-1})^{-\frac{1}{n_2}}\right] + \frac{1}{2}f''(\Omega_2)AsV(\hat{\Omega}_2) \\ \vdots \\ d_M(\mathbf{x})\left[(1 + K_M^{-1})^{-\frac{1}{n_M}}\right] + \frac{1}{2}f''(\Omega_M)AsV(\hat{\Omega}_M) \end{bmatrix} \tag{49}$$

The rest of the proof are in the same manner as Lemma 2, and is omitted here. □

Based on Definition 1, the error model of the RSS-based positioning is,

$$E_{RSS} = \sqrt{trace\left[\mathbf{J}_{\Omega}^{-1}(\mathbf{x})\right] + \left[Bias_{\mathbf{x}}^{RSS}(\mathbf{x})\right]_x^2 + \left[Bias_{\mathbf{x}}^{RSS}(\mathbf{x})\right]_y^2} \tag{50}$$

6. SIMULATION RESULTS

In this section, analytic error models are validated by simulation. Agreement between simulation and error model are compared using similarity score (Pearson Correlation Coefficient [44][46]). Next, nonlinear least square and maximum likelihood positioning results are compared with the error models. Corresponding accuracy improvements and computational cost are discussed. Finally, the performance comparison of LoS and RSS-based positioning is given.

The derived theory holds independently of underlying wireless technology and corresponding communication ranges. Overall, the maximum distance to reference points (i.e. the cell towers, access points, fixed sensors, anchor nodes, beacons, etc.) varies from several meters to tens of kilometers [47][48]. For example, the communication range for the passive RFID is between $1 \sim 200m$, for Zigbee is between $10 \sim 100m$, for the Bluetooth Low Energy (BLE) is between $1 \sim 50m$, for GSM is less than $35km$, and for CDMA is less than $50km$. Additionally, the range varies with transmission power, for example, in pico and femto cells [49, 50, 51], it is $10m$ to $2km$.

In this work, we validate the derived CRB and the proposed error model using a representative simulation area, $500m \times 520m$. For smaller or larger area, corresponding theoretical limit can be obtained from our model. Other simulation results confirm the conclusion (For example, simulation results for an $6.7km \times 6.9km$ area is attached in the Appendix 8.2), though are omitted here due to limited space.

In the representative $500m \times 520m$ *simulation area*, the RPs are placed as follows:

- The center of the area is the origin of coordinates.
- Reference positions are evenly distributed around the center with radius of $250m$.

Fig. 2 shows an example of simulation area with three RPs. The RPs form a regular triangle. The distance from the center to each reference is $250m$. The magnitude of the received signal power at $450m$ is $-80dBm$. The magnitudes of the received signal power and corresponding ranges are plotted in Fig. 3 for reference.

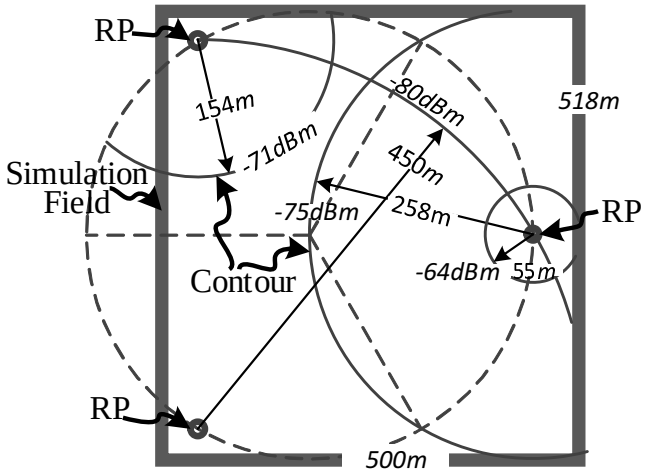

Figure 2. Simulation Field

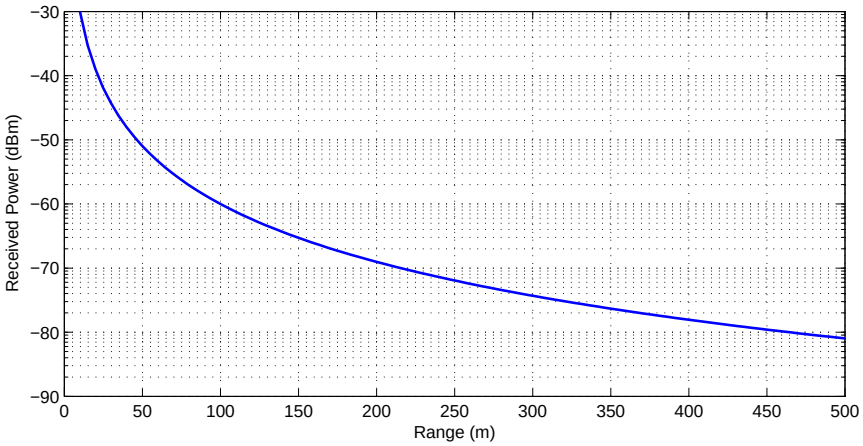

Figure 3. Path-loss

We simulate the signal propagation in multipath fading channel. The path-loss parameters is set to $n = 3$ and $\kappa = 20dbm$ [52, 53, 54, 55, 56]. The Ricean fading is generated based on the sum-of-sinusoids simulator proposed in [57]. The parameters used for generating the fading are: Doppler frequency of $300Hz$, symbol duration of 4.115×10^{-5}

seconds, a number of fading paths ≥ 20, and the angle of arrival was generate randomly within $[-\pi, \pi)$. The number of samples of the fading signal at each location is 3×10^4. The received signal RSS and LoS component estimates are used to calculate ranges and positions.

Five localization algorithms are employed: trilateration, constrained least square (CLS), weighted constrained least square (WCLS), nonlinear least square (NLS), and maximum likelihood (ML). The grid size in our simulation is equal to $36m \times 38m$. Altogether 190 positions are simulated. The average error at each point is calculated over 100 runs with random fading. Positioning error of each method is compared with our *analytical error model* ($\mathbf{E_{LoS}}$ and $\mathbf{E_{RSS}}$).

It is worth noting that the presented results do not depend on specific implementation of fading channel estimation. For example, the results apply equally to either time multiplexed pilot based methods [58][59] in CDMA, or pilot arrangement [60] and pilot assisted [61] methods in OFDM. Hence, we focus on the positioning results and validation of positioning error model alone.

6.1. Model Validation. In this section, we validate the proposed positioning error models for both RSS and LoS based schemes.

6.1.1. RSS Model. Fig. 4 shows representative RSS-based positioning results, for K-ratio equals to 10 and 100. The reference positions, $RP_1 \sim RP_3$, are indicated. For lower K-ratio, the fading increases thus resulting in large NLoS component. In turn, the RSS ranging is skewed by the NLoS-induced bias (42). Consequently, the localization accuracy decreases with K-ratio.

The average errors comparison and similarity between linear methods and analytic model are summarized in Table 1 (see Table 9 for larger area). Overall, the averaged similarity score is about +0.85. It indicates a high similarity between simulation and our error model [46], thus validating the proposed error model. Furthermore, it is shown by both simulation and analytic model that the average localization error of 5-RP (Pentagon)

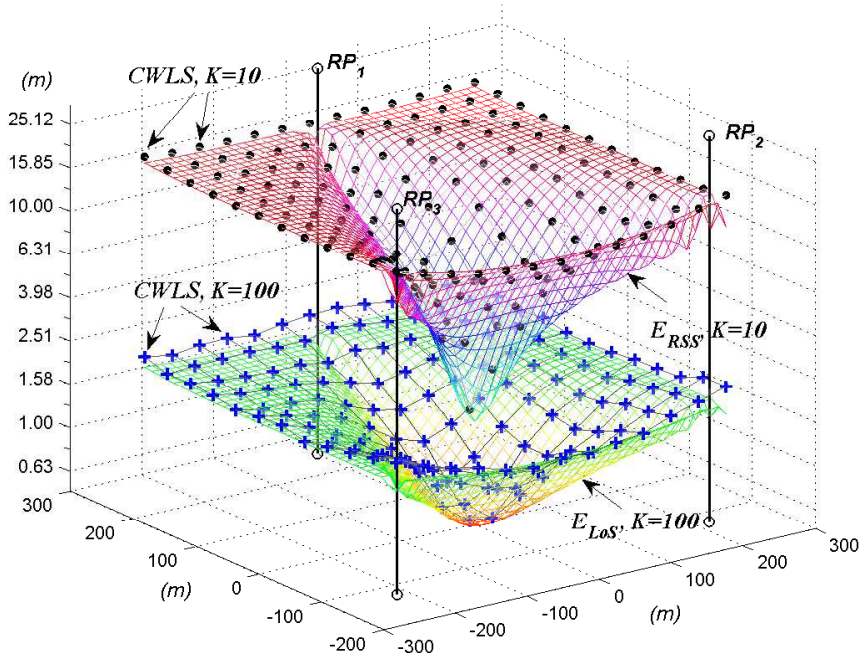

Figure 4. Positioning error comparison.
(Beacon-geometry: Triangle; K-ratio: 10 and 100; RSS)

is higher than 3-RP (Triangle), i.e., *the localization error* increases with the number of reference positions. It is in contrast to a general belief that higher diversity improves accuracy. This is caused by the high range estimation bias (46) for each reference point that accumulates in RSS-based positioning method, thus increasing localization error.

Table 1. The Similarity between
Simulation Results and Error Model (RSS)

RP Geometry	**K-ratio**	**Avg. Err. (Simulation) (m)**	**Avg. E_{RSS} (Analytic) (m)**	**Simularity**
Pentagon (5 RPs)	100	1.123	1.044	+0.838
	50	1.969	1.987	+0.886
	10	7.903	9.091	+0.937
Triangle (3 RPs)	100	1.138	1.025	+0.803
	50	1.947	1.795	+0.809
	10	7.338	7.450	+0.804

6.1.2. LoS Model. Fig. 5 shows representative LoS-based positioning result for K equals to 10 and 100. The positioning errors in simulations is slightly larger than the analytical error model, E_{LoS}. That is in agreement with the theoretical result since CRB gives the best possible accuracy that can be obtained.

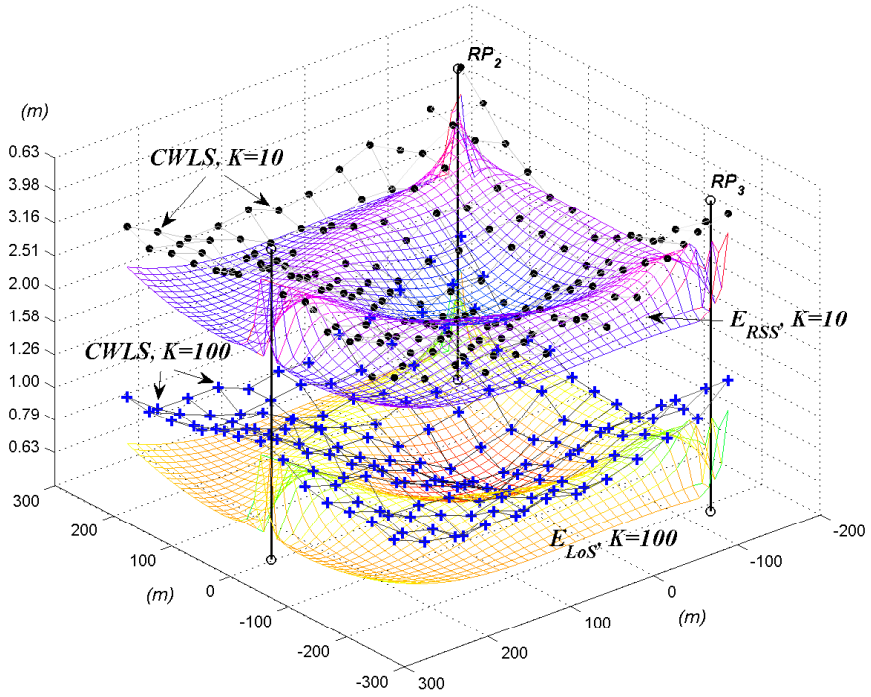

Figure 5. Positioning Error Comparison
(Beacon-geometry: Triangle; K-ratio: 10 and 100; LoS)

The average errors comparison and similarity between linear methods and analytic model are summarized in Table 2 (see Table 8 for larger area). The overall average similarity score is about +0.85, which indicates a high similarity between the simulation and our proposed error model for LoS-based positioning.

In contrast to RSS-based method, both simulation and analytical results of LoS-based positioning show *an increase in accuracy* with number of reference positions (from triangle to pentagon). This is due to the fact that the bias in range estimate is suppressed by LoS scheme. Hence, LoS scheme is able to take the advantage of this diversity.

Table 2. The Similarity between
Simulation Results and Error Model (LoS)

RP Geometry	**K-ratio**	**Avg. Err. (Simulation) (m)**	**Avg. E_{LoS} (Analytic) (m)**	**Simularity**
Pentagon (5-RP)	100	0.579	0.381	+0.772
	50	0.808	0.561	+0.753
	10	1.752	1.316	+0.795
Triangle (3-RP)	100	0.720	0.637	+0.947
	50	1.001	0.939	+0.904
	10	2.257	2.199	+0.937

6.2. Nonlinear Positioning Algorithms. In this section, the accuracy comparison between linear and nonlinear methods and corresponding computational cost are presented.

The averaged localization error of linear (CLS and CWLS) and nonlinear (NLS and ML) algorithms are shown in Table 3 (LoS) and Table 4 (RSS) (Table 11 and 10 for large area). The average positioning accuracy by using the nonlinear algorithms is improved by 37% in RSS-based positioning, and 10% in LoS-based positioning.

Table 3. Accuracy Improvement, Nonlinear/Linear (LoS)

RP Geometry	**K-ratio**	**Avg. Err. of Linear (m)**	**Avg. Err. of Nonlinear (m)**	**Impv. Nonliear/Linear**
Pentagon	100	0.618	0.540	13%
	50	0.881	0.735	17%
	10	1.984	1.519	23%
Triangle	100	0.731	0.702	4%
	50	1.006	0.974	3%
	10	2.267	2.187	4%

The nonlinear algorithms are iterative with varying number of iterations. The calculations are stopped when the change in position estimation between consecutive iterations is smaller than a predefined threshold. In our simulation, the threshold for both LoS and

Table 4. Accuracy Improvement, Nonlinear/Linear (RSS)

RP Geometry	**K-ratio**	**Avg. Err. of Linear (m)**	**Avg. Err. of Nonlinear (m)**	**Impv. Nonliear/Linear**
Pentagon	100	1.347	0.899	33%
	50	2.539	1.399	45%
	10	11.317	4.489	60%
Triangle	100	1.223	1.010	43%
	50	2.162	1.626	25%
	10	8.851	5.067	17%

Table 5. Accuracy Improvement and Computational Cost of Nonlinear Methods (LoS)

RP Geometry	**K-ratio**	**Avg. Num. Iteration**		δ^*_{nl}	**Avg.Err.** (m)		Δ^*_{nl}
		NLS	ML		NLS	ML	
Pentagon	100	12	18	1.48	0.559	0.522	6.7%
	50	19	26	1.32	0.757	0.714	5.7%
	10	47	56	1.18	1.545	1.493	3.4%
Triangle	100	10	14	1.35	0.701	0.703	-0.3%
	50	15	20	1.29	0.968	0.974	-0.6%
	10	34	46	1.36	2.147	2.187	-1.8%

RSS case is set to 1×10^{-4}. We quantify the computational cost as the number of iterations used to reach the iteration-threshold. The positioning error and computation for NLS and ML are included in Table 6 and Table 5 (Table 12 and Table 13 for larger area).

ML algorithm takes doubled iteration numbers than NLS across the RP geometry and K-ratio settings in both RSS- and LoS-base positioning. In addition, ML is more accurate than NLS by 24% in RSS-based positioning, while, renders no advantages in LoS-based case.

Table 6. Accuracy Improvement and Computational Cost of Nonlinear Methods (RSS)

RP Geometry	K-ratio	Avg. Num. Iteration		δ^*_{nl}	Avg.Err. (m)		Δ^*_{nl}
		NLS	ML		NLS	ML	
Pentagon	100	23	35	1.52	1.069	0.729	31.8%
	50	44	57	1.29	1.732	1.066	38.4%
	10	110	147	1.33	5.981	2.998	49.9%
Triangle	100	20	25	1.25	1.045	0.976	6.6%
	50	36	43	1.19	1.655	1.596	3.6%
	10	101	148	1.47	5.402	4.733	12.4%

* $\delta_{nl} = \frac{Num.of It.(ML)}{Num.of It.(NLS)}$, $\Delta_{nl} = \frac{err.(ML) - err.(NLS)}{err.(NLS)}$

To summarize,

- Nonlinear methods are effective in reducing the effect of ranging bias in positioning accuracy. Hence, they are beneficial in RSS-based approach. For LoS based positioning, the benefits of nonlinear scheme are smaller since the LoS ranging already suppresses the bias.

- For *RSS based schemes*, ML renders higher accuracy improvement than NLS at the cost of forty percent more iterations. For *LoS based schemes*, NLS reaches practically the same accuracy as ML, while only requiring half of the iterations that ML needed.

6.3. LoS-based Positioning vs. RSS-based Positioning. LoS- and RSS-based positioning errors are summarized in Table 7 (Table 14 for larger area). An example of positioning error map for CWLS based schemes is given in Fig. 6.

The fading increases the bias of RSS-based positioning resulting in low accuracy. The LoS-based positioning is able to suppressing the fading effect effectively. As shown in Table 7, across all the methods and reference position configurations, the accuracy of LoS-based positioning is superior over RSS-based. On average, the LoS-based positioning method improves the accuracy by 55%.

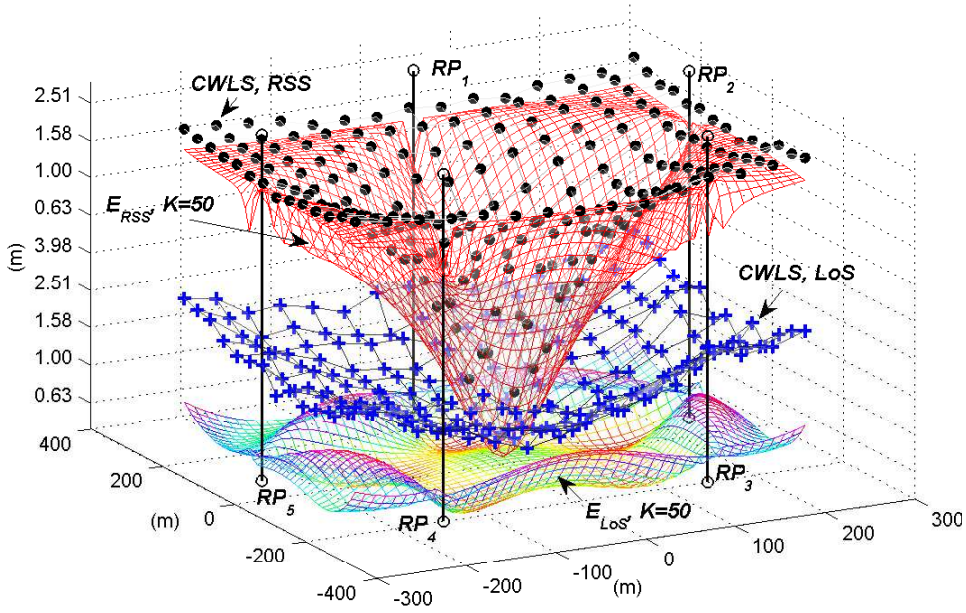

Figure 6. LoS-based v.s. RSS-based Positioning.
(Beacon-geometry: Pentagon, LoS/NLoS K-ratio: 50)

Table 7. Accuracy Improvement and Computational Cost of Nonlinear Methods (RSS)

RP Geometry	LoS /RSS	K ratio	CLS (m)	CWLS (m)	NLS (m)	ML (m)	Avg. LoS/RSS
Pentagon	LoS	100	0.651	0.586	0.559	0.522	48.4%
	RSS	100	1.406	1.287	1.069	0.729	
	LoS/RSS:		53.7%	54.5%	47.7%	28.5%	
	LoS	50	0.929	0.834	0.757	0.714	58.9%
	RSS	50	2.647	2.430	1.732	1.066	
	LoS/RSS:		64.9%	65.7%	56.3%	33.0%	
	LoS	10	2.092	1.876	1.545	1.493	77.8%
	RSS	10	11.860	10.773	5.981	2.998	
	LoS/RSS:		82.4%	82.6%	74.2%	50.2%	
Triangle	LoS	100	0.749	0.725	0.701	0.703	37.6%
	RSS	100	1.358	1.234	1.045	0.976	
	LoS/RSS:		44.9%	41.2%	32.9%	28.0%	
	LoS	50	1.044	1.012	0.968	0.974	45.1%
	RSS	50	1.845	2.190	1.655	1.596	
	LoS/RSS:		43.4%	53.8%	41.5%	39.0%	
	LoS	10	2.373	2.297	2.147	2.187	69.4%
	RSS	10	10.345	8.913	5.402	4.733	
	LoS/RSS:		77.1%	74.2%	60.3%	53.8%	

7. CONCLUSION

In this paper, we derived the theoretical limit of accuracy in terms of CRB and bias in presence of Ricean fading, for power based localization. The simulation results validate our analytical model. The similarity between our model and simulation results is above +80%. Overall, LoS-based positioning method provides higher accuracy than RSS-based method by 55%. In RSS-based positioning system, it is preferred to use only three reference positions. In contrast, increasing the number of RPs in LoS-based positioning system will help improve the accuracy. Nonlinear algorithms are more effective in reducing positioning error in RSS-based method. The tradeoff in applying nonlinear methods is that, for *RSS based schemes*, ML can improve positioning accuracy significantly at the cost of doubling the number of iterations over NLS. For *LoS based schemes*, there is practically no benefit of using ML algorithm when compared to NLS. Overall, the proposed LoS-based positioning obtains under meter accuracy in outdoor and middle sized localization area.

8. APPENDIX

8.1. Interpolation Matrix for Freqeuncy-Selective Fading Channel.

Lemma 14. *The interpolation matrix ($L_s \times L_P$) of the jth tap is*

$$\boldsymbol{I}(j) = \boldsymbol{C}(j) \left[\boldsymbol{R}^{\dagger}(j)\right]^{h}. \tag{51}$$

in which, $\boldsymbol{C}(j)$ is a $L_s \times L_P$ matrix, for jth tap, with elements,

$$[\boldsymbol{C}(j)]_{i,k} = \tilde{R}_h\left((\epsilon(k) - i)\, T_s\right). \tag{52}$$

and $\boldsymbol{R}(j)$ is the $L_P \times L_P$ autocorrelation matrix for the jth tap,

$$[\boldsymbol{R}(j)]_{k,i} = \tilde{R}_h\left((\epsilon(k) - i)\, T_s\right) + \frac{N_o \delta(i,k)}{L_{ch}\, |\boldsymbol{b}|^2\, \Omega}. \tag{53}$$

in which, $\delta(i,k)$ is Kronecker delta. $\tilde{R}_h$ is the unit power equivalent autocorrelation function (7); $\epsilon(\cdot)$ is a function convert symbol index in pilot-symbol sequence into the position/index within entire slot; N_o is the Gaussian noise power density in both real and imaginary component.

Proof. The jth tap fading at position i is interpolated by vector $\mathbf{I}(i,j)$ as,

$$\tilde{\mathbf{u}}(j,i) = \mathbf{I}(j,i)\hat{\mathbf{u}}(j). \tag{54}$$

in which, $\mathbf{I}(j,i)$ is the $1 \times L_P$ vector (the ith row) within $\mathbf{I}(j)$.

Thus, the interpolation error of the jth tap fader at position i is given by

$$\mathbf{e}(j,i) = \mathbf{u}(j,i) - \tilde{\mathbf{u}}(j,i). \tag{55}$$

where $\mathbf{u}(j,i)$ is the actual fading value of jth tap on ith position. And, the interpolated fading signal on position i is $\tilde{\mathbf{u}}(j,i) = [\tilde{\mathbf{u}}(j)]_i$.

The square error of interpolation,

$$\sigma_e^2(i,j) = \sigma_u^2 - 2Re\left[\sigma_{uv}^2(i,j)\right] + \sigma_v^2(i,j). \tag{56}$$

where the covariance, $\sigma_{uv}^2(j,i) = \frac{1}{2}E\left[\mathbf{u}(j,i)\tilde{\mathbf{u}}^h(j,i)\right] = \frac{1}{2}E\left[\mathbf{u}(j,i)\mathbf{a}^h(j)\right]\mathbf{I}^h(j,i)./\mathbf{b}^*$,

$$\sigma_{uv}^2(j,i) = \mathbf{C}(j,i)\mathbf{I}^h(j,i). \tag{57}$$

in which $\mathbf{C}(j,i)$ is the $1 \times L_P$ vector (the ith row) in $\mathbf{C}(j)$ (52).

And the variance, $\sigma_v^2 = \frac{1}{2}E\left[\tilde{\mathbf{u}}(j,i)\tilde{\mathbf{u}}^h(j,i)\right], = \frac{1}{2}E\left[\mathbf{I}(j,i)\mathbf{a}(j)\mathbf{a}^h(j)\mathbf{I}^h(j,i)\right]./|\mathbf{b}|^2$

$$\sigma_v^2(j,i) = \mathbf{I}(j,i)\mathbf{R}(j)\mathbf{I}^h(j,i). \tag{58}$$

Let $\boldsymbol{\sigma}(j) = \left[\sigma_e^2(j,1), \sigma_e^2(j,2), \cdots, \sigma_e^2(j,L_s)\right]^T$. The optimal interpolation matrix that minimized the square error (56) can be found from $\frac{\partial \boldsymbol{\sigma}(j)}{\partial \mathbf{I}(j)}$, which lead to,

$$\mathbf{I}^h(j) = \mathbf{R}^{\dagger}(j)\mathbf{C}^h(j).$$

which is equivalent to (51). □

8.2. Numerical Experimental Result for Large Area.

For Larger area, following settings are adopted:

- Area size: $\boldsymbol{6.7km \times 6.9km}$
- Reference positions are evenly distributed around the center with radius of $3.5km$.
- The path loss parameters are: $n = 2$ and $\kappa = 12.83dbm$. The magnitude of the received signal power at $3.5km$ is $-75dBm$

Table 8. The Similarity between
Simulation Results and Error Model (LoS)

RP Geometry	**K-ratio**	**Avg. Err. (Simulation) (m)**	**Avg. E_{LoS} (Analytic) (m)**	**Simularity**
Pentagon	100	12.92	8.52	+0.76
	50	81.29	12.08	+0.75
	10	41.30	27.68	+0.73
Triangle	100	14.98	14.26	+0.87
	50	21.15	20.21	+0.85
	10	47.75	46.24	+0.83

Table 9. The Similarity between
Simulation Results and Error Model (RSS)

RP Geometry	**K-ratio**	**Avg. Err. (Simulation) (m)**	**Avg. E_{RSS} (Analytic) (m)**	**Simularity**
Pentagon	100	28.16	20.7	+0.93
	50	52.82	40.09	+0.95
	10	232.4	187.4	+0.95
Triangle	100	25.19	18.16	+0.71
	50	44.71	32.96	+0.75
	10	181.8	149	+0.79

Table 10. Accuracy Improvement, Nonlinear/Linear (LoS)

RP Geometry	**K-ratio**	**Avg. Err. of Linear (m)**	**Avg. Err. of Nonlinear (m)**	**Impv. Nonliear/Linear**
Pentagon	100	12.915	9.1675	29.02%
	50	18.285	12.915	29.37%
	10	34.32	29.01	15.47%
Triangle	100	15.08	13.9	7.82%
	50	21.245	19.59	7.79%
	10	48.11	43.645	9.28%

Table 11. Accuracy Improvement, Nonlinear/Linear (RSS)

RP Geometry	**K-ratio**	**Avg. Err. of Linear** (m)	**Avg. Err. of Nonlinear** (m)	**Impv. Nonliear/Linear**
Pentagon	100	28.16	13.77	51.10%
	50	52.815	23.325	55.84%
	10	232.35	84.69	63.55%
Triangle	100	26.695	16.5	38.19%
	50	47.965	29.235	39.05%
	10	197.25	141.5	28.26%

Table 12. Accuracy Improvement and Computational Cost of Nonlinear Methods (RSS)

RP Geometry	**K-ratio**	δ^*_{nl}	**Avg. Err.** (m)		Δ^*_{nl}
			NLS	ML	
Pentagon	100	1.58	16.27	11.27	30.7%
	50	1.70	28.69	17.96	37.4%
	10	2.08	111.0	58.38	47.4%
Triangle	100	1.83	18.52	14.48	21.8%
	50	1.94	30.55	27.92	8.6%
	10	2.27	101.6	87.0	14.4%

Table 13. Accuracy Improvement and Computational Cost of Nonlinear Methods (LoS)

RP Geometry	**K-ratio**	δ^*_{nl}	**Avg. Err.** (m)		Δ^*_{nl}
			NLS	ML	
Pentagon	100	1.44	9.353	8.982	4.0%
	50	1.53	13.19	12.64	4.2%
	10	1.74	29.64	28.38	4.3%
Triangle	100	1.75	13.73	14.07	-2.5%
	50	1.83	19.37	19.81	-2.3%
	10	2.03	43.41	43.88	-1.1%

* $\delta_{nl} = \frac{Num.of It.(ML)}{Num.of It.(NLS)}$, $\Delta_{nl} = \frac{err.(ML) - err.(NLS)}{err.(NLS)}$

Table 14. Accuracy Improvement and Computational Cost of Nonlinear Methods (RSS)

RP Geometry	LoS /RSS	K ratio	CLS (m)	CWLS (m)	NLS (m)	ML (m)	Avg. LoS/RSS
Pentagon	**LoS**	100	13.62	12.21	9.353	8.982	44.1%
	RSS	100	29.42	26.90	16.27	11.27	
	LoS/RSS:		53.7%	54.6%	45.0%	22.9%	
	LoS	50	19.28	17.29	13.19	12.64	54.3%
	RSS	50	55.12	50.51	28.69	17.96	
	LoS/RSS:		65.0%	65.8%	55.4%	30.9%	
	LoS	10	43.59	39.0	29.64	28.38	72.4%
	RSS	10	244.7	220.0	111.0	58.38	
	LoS/RSS:		82.2%	82.3%	73.5%	51.5%	
Triangle	**LoS**	100	15.31	14.85	13.73	14.07	34.0%
	RSS	100	28.00	25.39	18.52	14.48	
	LoS/RSS:		45.3%	41.5%	27.0%	22.8%	
	LoS	50	21.64	20.96	19.37	19.81	44.7%
	RSS	50	50.72	45.21	30.55	27.92	
	LoS/RSS:		57.3%	53.6%	37.5%	30.0%	
	LoS	10	48.91	47.31	43.41	43.88	65.5%
	RSS	10	213.1	181.4	101.6	87.0	
	LoS/RSS:		77.0%	73.9%	57.6%	50.4%	

REFERENCES

[1] Pratap Misra and Per Enge. *Global positioning system: signals, measurements, and performance*. Ganga-Jamuna Press, 2006. ISBN 978-0-9709544-1-1.

[2] A.J. Fenwick. Algorithms for position fixing using pulse arrival times. *Radar, Sonar and Navigation, IEE Proceedings* -, 146(4):208–212, August 1999. ISSN 1350-2395. doi: 10.1049/ip-rsn:19990538.

[3] Ka Wai Cheung, Hing-Cheung So, W-K Ma, and Yiu-Tong Chan. A constrained least squares approach to mobile positioning: algorithms and optimality. *EURASIP journal on applied signal processing*, 2006:150–150, 2006.

[4] C. Mensing and S. Plass. Positioning Algorithms for Cellular Networks Using TDOA. In *2006 IEEE International Conference on Acoustics, Speech and Signal Processing, 2006. ICASSP 2006 Proceedings*, volume 4, pages IV–IV, May 2006. doi: 10.1109/ICASSP.2006.1661018.

[5] J.C. Chen, R.E. Hudson, and K. Yao. Maximum-likelihood source localization and unknown sensor location estimation for wideband signals in the near-field. *IEEE Transactions on Signal Processing*, 50(8):1843–1854, August 2002. ISSN 1053-587X. doi: 10.1109/TSP.2002.800420.

[6] Martin Sauter. *From GSM to LTE: an introduction to mobile networks and mobile broadband*. John Wiley & Sons, 2010.

[7] Richard Klukas and Michel Fattouche. Line-of-sight angle of arrival estimation in the outdoor multipath environment. *Vehicular Technology, IEEE Transactions on*, 47(1): 342–351, 1998.

[8] S. Sakagami, S. Aoyama, K. Kuboi, S. Shirota, and Akira Akeyama. Vehicle position estimates by multibeam antennas in multipath environments. *IEEE Transactions on Vehicular Technology*, 41(1):63–68, February 1992. ISSN 0018-9545. doi: 10.1109/25.120146.

[9] V. Thotla, M. J. Zawodniok, S. Jagannathan, M. T. A. Ghasr, and S. Agarwal. Detection and Localization of Multiple R/C Electronic Devices Using Array Detectors. *IEEE Transactions on Instrumentation and Measurement*, 64(1):241–251, January 2015. ISSN 0018-9456. doi: 10.1109/TIM.2014.2331432.

[10] James Caffery and Gordon L Stuber. Subscriber location in cdma cellular networks. *Vehicular Technology, IEEE Transactions on*, 47(2):406–416, 1998.

[11] H. Shen, Z. Ding, S. Dasgupta, and C. Zhao. Multiple Source Localization in Wireless Sensor Networks Based on Time of Arrival Measurement. *IEEE Transactions on Signal Processing*, 62(8):1938–1949, April 2014. ISSN 1053-587X. doi: 10.1109/TSP.2014.2304433.

[12] Ismail Guvenc and Chia-Chin Chong. A survey on toa based wireless localization and nlos mitigation techniques. *Communications Surveys & Tutorials, IEEE*, 11(3):107–124, 2009.

[13] Ali H Sayed, Alireza Tarighat, and Nima Khajehnouri. Network-based wireless location: challenges faced in developing techniques for accurate wireless location information. *Signal Processing Magazine, IEEE*, 22(4):24–40, 2005.

[14] IEEE Draft Amendment Standard for Local and Metropolitan Area Networks - Part 16: Air Interface for Broadband Wireless Access Systems - Advanced Air Interface. *IEEE P802.16m/D9, October 2010*, pages 1–1156, October 2010.

[15] Ralph O Schmidt. Multiple emitter location and signal parameter estimation. *Antennas and Propagation, IEEE Transactions on*, 34(3):276–280, 1986.

[16] Moustafa M Abdalla, Mostafa B Abuitbel, and Mohamed A Hassan. Performance evaluation of direction of arrival estimation using music and esprit algorithms for mobile communication systems. In *Wireless and Mobile Networking Conference (WMNC), 2013 6th Joint IFIP*, pages 1–7. IEEE, 2013.

[17] I.T. Haque and C. Assi. Profiling-Based Indoor Localization Schemes. *IEEE Systems Journal*, 9(1):76–85, March 2015. ISSN 1932-8184. doi: 10.1109/JSYST.2013.2281257.

[18] Bang Wang, Shengliang Zhou, Wenyu Liu, and Yijun Mo. Indoor Localization Based on Curve Fitting and Location Search Using Received Signal Strength. *IEEE Transactions on Industrial Electronics*, 62(1):572–582, January 2015. ISSN 0278-0046. doi: 10.1109/TIE.2014.2327595.

[19] Q. Luo, Y. Peng, J. Li, and X. Peng. RSSI-Based Localization Through Uncertain Data Mapping for Wireless Sensor Networks. *IEEE Sensors Journal*, 16(9):3155–3162, May 2016. ISSN 1530-437X. doi: 10.1109/JSEN.2016.2524532.

[20] Paramvir Bahl and Venkata N. Padmanabhan. RADAR: An in-building RF-based user location and tracking system. In *INFOCOM 2000. Nineteenth Annual Joint Conference of the IEEE Computer and Communications Societies. Proceedings. IEEE*, volume 2, pages 775–784. Ieee, 2000.

[21] Mohammed Rana Basheer and Sarangapani Jagannathan. R-factor: A new parameter to enhance location accuracy in rssi based real-time location systems. In *Sensor, Mesh and Ad Hoc Communications and Networks, 2009. SECON'09. 6th Annual IEEE Communications Society Conference on*, pages 1–9. IEEE, 2009.

[22] Lei Wang and Maciej Zawodniok. Rssi-based localization in cellular networks. In *Local Computer Networks Workshops (LCN Workshops), 2012 IEEE 37th Conference on*, pages 820–826. IEEE, 2012.

[23] William CY Lee. Estimate of local average power of a mobile radio signal. *Vehicular Technology, IEEE Transactions on*, 34(1):22–27, 1985.

[24] William C. Y. Lee. *Mobile Communications Engineering: Theory and Applications*. McGraw-Hill, Inc., New York, NY, USA, 1997. ISBN 1-59061-135-7.

[25] Thomas N Rubinstein. The standard deviations of the local means of land mobile radio signals in flat suburban terrain. In *Vehicular Technology Conference, 1986. 36th IEEE*, volume 36, pages 52–56. IEEE, 1986.

[26] Mark D Austin and GL Stüber. Velocity adaptive handoff algorithms for microcellular systems. *IEEE Transactions on Vehicular Technology*, 43(3):549–561, 1994.

[27] Xinrong Li. Rss-based location estimation with unknown pathloss model. *Wireless Communications, IEEE Transactions on*, 5(12):3626–3633, 2006.

[28] Andrea Zanella and Andrea Bardella. Rss-based ranging by multichannel rss averaging. *Wireless Communications Letters, IEEE*, 3(1):10–13, 2014.

[29] Reza Zekavat and R Michael Buehrer. *Handbook of position location: Theory, practice and advances*, volume 27. John Wiley & Sons, 2011.

[30] L. Wang and M. Zawodniok. Bias and CRB Analysis of LoS-based and RSS-based Ranging Methods. *IEEE Transactions on Vehicular Technology*, PP(99):1–1, 2016. ISSN 0018-9545. doi: 10.1109/TVT.2016.2518166.

[31] William C Jakes and Donald C Cox. *Microwave mobile communications*. Wiley-IEEE Press, 1994.

[32] Raymond Steele, H Ahmadi, and A Krishna. Mobile radio communications. In *IEEE Proceedings*, volume 82, pages 1468–1468. [New York, NY]: Institute of Electrical and Electronics Engineers,[1963-, 1994.

[33] Harald T Friis. A note on a simple transmission formula. *proc. IRE*, 34(5):254–256, 1946.

[34] James K Cavers. An analysis of pilot symbol assisted modulation for rayleigh fading channels [mobile radio]. *Vehicular Technology, IEEE Transactions on*, 40(4):686–693, 1991.

[35] Jingxian Wu, Chengshan Xiao, and Jan C Olivier. Time-varying and frequency-selective channel estimation with unequally spaced pilot symbols. *International Journal of Wireless Information Networks*, 11(2):93–104, 2004.

[36] Chengshan Xiao and Jan C Olivier. Nonselective fading channel estimation with nonuniformly spaced pilot symbols. *International Journal of Wireless Information Networks*, 7(3):177–185, 2000.

[37] Matthias Patzold. *Mobile fading channels*. John Wiley & Sons, Inc., 2003.

[38] Gordon L Stüber. *Principles of mobile communication*. Springer Science & Business Media, 2011.

[39] Wolfram Koepf. Identities for families of orthogonal polynomials and special functions. *INTEGRAL TRANSFORMS AND SPECIAL FUNCTIONS*, 5:69–102, 1995.

[40] Cheng Guan Koay and Peter J Basser. Analytically exact correction scheme for signal extraction from noisy magnitude mr signals. *Journal of Magnetic Resonance*, 179(2): 317–322, 2006.

[41] S.M. Kay. *Fundamentals of Statistical Signal Processing: Estimation theory*. Fundamentals of Statistical Signal Processing. Prentice-Hall PTR, 1993. ISBN 9780133457117. URL http://books.google.com/books?id=aFwESQAACAAJ.

[42] Cihan Tepedelenlioglu, Ali Abdi, and Georgios B Giannakis. The ricean k factor: estimation and performance analysis. *Wireless Communications, IEEE Transactions on*, 2(4):799–810, 2003.

[43] Boaz Porat. *Digital processing of random signals: theory and methods*. Prentice-Hall, Inc., 1994.

[44] Lee J Bain and Max Engelhardt. *Introduction to probability and mathematical statistics*, volume 4. Duxbury Press Belmont, CA, 1992.

[45] Michael Rice. *Digital Communications: A Discrete-time Approach*. Prentice Hall, 2009. ISBN 978-0-13-030497-1.

[46] Robert G. Malgady and David E. Krebs. Understanding correlation coefficients and regression. *Physical therapy*, 66(1):110–120, 1986. URL http://ptjournal.apta.org/content/66/1/110.short.

[47] Vijay Garg. *Wireless Communications & Networking*. Morgan Kaufmann, July 2010. ISBN 978-0-08-054907-1.

[48] Andrea Goldsmith. *Wireless Communications*. Cambridge University Press, August 2005. ISBN 978-1-139-44584-9.

[49] Gordon L. Stüber. *Principles of Mobile Communication*. Springer Science & Business Media, March 2013. ISBN 978-1-4757-6268-6.

[50] A.J. Goldsmith and L.J. Greenstein. A measurement-based model for predicting coverage areas of urban microcells. *IEEE Journal on Selected Areas in Communications*, 11(7):1013–1023, September 1993. ISSN 0733-8716. doi: 10.1109/49.233214.

[51] Jerry D. Gibson. *Mobile Communications Handbook, Third Edition*. CRC Press, August 2012. ISBN 978-1-4398-1723-0.

[52] Daniel B. Faria and others. Modeling signal attenuation in ieee 802.11 wireless lans-vol. 1. *Computer Science Department, Stanford University*, 1, 2005. URL http://gregorio.stanford.edu/kiwi/files/faria-TR-KP06-0118.pdf.

[53] Lorne C. Liechty. Path loss measurements and model analysis of a 2.4 GHz wireless network in an outdoor environment. In *Georgia Institute of Technology*, 2007.

[54] S. Tiraspolsky, A. Rubtsov, A. Maltsev, and A. Davydov. Mobile WiMAX - Deployment Scenarios Performance Analysis. In *3rd International Symposium on Wireless Communication Systems, 2006. ISWCS '06*, pages 353–357, September 2006. doi: 10.1109/ISWCS.2006.4362318.

[55] Mardeni. R and T. Siva Priya. Optimised COST-231 Hata Models for WiMAX Path Loss Prediction in Suburban and Open Urban Environments. *Modern Applied Science*, 4(9), August 2010. ISSN 1913-1852, 1913-1844. doi: 10.5539/mas.v4n9p75. URL http://www.ccsenet.org/journal/index.php/mas/article/view/6462.

[56] M. Alshami, T. Arslan, J. Thompson, and A.T. Erdogan. Frequency analysis of path loss models on WIMAX. In *Computer Science and Electronic Engineering Conference (CEEC), 2011 3rd*, pages 1–6, July 2011. doi: 10.1109/CEEC.2011.5995815.

[57] Chengshan Xiao, Yahong Rosa Zheng, and Norman C Beaulieu. Novel sum-of-sinusoids simulation models for rayleigh and rician fading channels. *Wireless Communications, IEEE Transactions on*, 5(12):3667–3679, 2006.

[58] K.A. Qaraqe and S. Roe. Channel estimation algorithms for third generation w-cdma communication systems. In *Vehicular Technology Conference, 2001. VTC 2001 Spring. IEEE VTS 53rd*, volume 4, pages 2675–2679 vol.4, 2001. doi: 10.1109/VETECS.2001.944086.

[59] Abdelmonaem Lakhzouri. *Channel Estimation and Mobile Phone Positioning in CDMA Based Wireless Communication Systems*. June 2005. ISBN 952-15-1368-3. URL http://dspace.cc.tut.fi/dpub/handle/123456789/73.

[60] S. Coleri, M. Ergen, A. Puri, and A. Bahai. Channel estimation techniques based on pilot arrangement in OFDM systems. *IEEE Transactions on Broadcasting*, 48(3): 223–229, September 2002. ISSN 0018-9316. doi: 10.1109/TBC.2002.804034.

[61] Zijian Tang, R.C. Cannizzaro, G. Leus, and P. Banelli. Pilot-Assisted Time-Varying Channel Estimation for OFDM Systems. *IEEE Transactions on Signal Processing*, 55 (5):2226–2238, May 2007. ISSN 1053-587X. doi: 10.1109/TSP.2007.893198.

IV. ARPAP: A NOVEL ANTENNA RADIATION PATTERN AWARE POWER BASED POSITIONING IN RF SYSTEM

L. Wang and M. J. Zawodniok

Department of Electronic & Computer Engineering

Missouri University of Science and Technology

Rolla, Missouri 65409–0050

Tel: (409) 692-9235, (573) 341-4361

Email: lw3r6@mst.edu, mjzx9c@mst.edu

ABSTRACT

Traditional power-based localization methods suffer from low accuracy in the practical application environment. The main challenges are the antenna directivity and fading effect. Conventional methods assume omnidirectional antenna directivity such that the solution is the intersections of multiple circle-shape contours. This strong assumption results in significant localization error in practical non-isotropic antenna applications. In this article, a novel antenna radiation-pattern-aware power-based positioning (ARPAP) scheme is proposed. It reduces the antenna directivity effect by including the antenna pattern into the localization system model. It reduces the bias error that introduced by power measurement through estimating the line-of-sight (LOS) component in received signal strength (RSS). Moreover, the error mode for the proposed ARPAP system, along with the theoretical limit, Cramer-Rao Bound (CRB), and bias of the proposed positioning system are derived. The Pearson correlation coefficient between the proposed error model and simulation result shows a high similarity score. The proposed positioning scheme and analytic error model are instantiated for the cellular network. Both analytical model and simulation results demonstrate the superiority of the proposed method over traditional methods.

Keywords: Positioning; Received Signal Strength Indicator; Line of Sight; Ranging; Antenna Radiation Pattern.

1. INTRODUCTION

Many areas of applications, such as the autonomous vehicle, security, healthcare, robotics, geographical routing, etc., require reliable and accurate location estimation. The global navigation satellite systems (GNSS) is widely used due to its ability to provide accurate positioning service. However, its accuracy relies on the number of visible satellites, the relative position, radio electric coverage of the satellites [1]. Moreover, it suffers from the temporary decrease in accuracy and disruption due to jamming and spoof [2, 3, 4, 5]. Hence a secondary backup mechanism is needed. The ideal cost-effective one would be reusing the existing wireless network infrastructures, for example, the cellular network, WiFi access points, and wireless sensor network (WSN).

Existing radio-frequency (RF) based localization schemes using signal strength has the advantage of cost-efficiency but for its low accuracy. A variety of positioning techniques have been proposed for wireless networks, such as angle-of-arrival (AOA)[6, 7, 8], time-of-arrival (TOA)[9, 10], time-difference-of-arrival (TDoA)[11, 12, 13], and received signal strength (RSS) [14, 15, 16]. AoA requires directional antenna array; and its accuracy is proportional to the number of elements [17][18]. ToA requires high-precision timing and synchronization components. TDoA relaxes the synchronization requirement by employing either a sliding correlator or a matched filter [12]. The added cost may be prohibitive in many wireless applications. The availability of the Received Signal Strength Indicator (RSSI) in most of the commercial off-the-shelf radio transceivers has promoted the design of several RSSI-based techniques, [19, 20, 21, 22, 23].

However, RSS-based methods suffer from low accuracy. There are two primary reasons - antenna directivity and fading. First, traditional methods, [24, 25, 21, 22, 23, 26, 27], find the intersection of circular contours around the *reference position*s (RP) with

estimated radius. This reduces the computational complexity and overload but introduces error due to the antenna directivity. In realistic application environments, antenna directivity changes the power radiation pattern of the RP. As a result, power based range estimation accuracy varies with arrival angle. Antenna radiation pattern depends on antenna geometry configuration (shape and dimension), dielectric material, combination (antenna array), and signal wavelength. Thus, the over-relaxed assumption in conventional methods results in large ranging and positioning error.

Second, multipath fading has a distinct impact on the fluctuation of the RF signal power measurements, hence introduces bias and variance in the range and position estimation. In the multipath environment, due to the signal reflection, diffraction, and scattering from objects that surround the transmitter (Tx) and receiver (Rx), the transmitted signal traverse multiple paths before reaching the Rx. As a result, the received signal is the transmitted signal that traverses along direct LOS propagation path superimposed with several copies of it from different NLoS paths. The effect of NLoS components on the received signal can be either constructive or destructive to the original (LOS) signal. Hence, the power measurement can be either weakened or strengthened by the environment. As a result, the range and position estimation are distorted by the environment.

In this paper, we propose antenna radiation-pattern-aware power-based positioning (ARPAP) method to address these two issues. *ARPAP takes into account the antenna directivity. The derived analytical error model and simulations show that the proposed scheme with LOS component estimation effectively improves the power based positioning accuracy. An instantiation of the entire scheme for the cellular network, as an example, is provided.*

In ARPAP, the antenna radiation patterns of both Tx and Rx have been modeled into the RF signal propagation and attenuation path loss. The position estimation is obtained by fitting the intersection of several non-circular power contours (of non-isotropic antennas) based on Taylor series expansion. Simulation results show that ARPAP elimi-

nated the antenna directivity introduced bias in traditional lateration methods. Also, power measurement noise injected positioning error is reduced. To address the multipath fading effect, LOS component estimation is performed before the range estimation. Since RSSI provides measurements of the total power [28] present in a received signal, it is sensitive to environmental fading. In our previous study [27][29], LOS based ranging and positioning have been shown to be robust. Thus, by LOS estimation ARPAP eliminates NLoS signal power.

Additionally, we derived ARPAP error model. The model is based on the theoretical analysis of the ARPAP system mean square error bound (MSEB) in Ricean fading channel. The MSEB is in the forms of Cramer-Rao Lower Bound (CRB), and bias for both LOS- and RSS-based lateration. The proposed error model bring insight into how the multipath propagation effects the positioning results and enable the elimination of bias and variance introduced by fading signal from the position estimation. The derived error model will help system designers to determine whether the ARPAP achievable performance meets their application requirement.

Moreover, the proposed scheme is instantiated for the cellular network. The derived error models are validated by simulation result. The Pearson correlation coefficient [30][31] between our error model and simulation results show a high similarity score.

The remainder of this paper is organized as follows. In Section II, the motivation of our work is present. In Section III, related works are introduced. Section IV presents the positioning system model and the proposed localization method. The corresponding correlation matrix is derived. In Section V, theoretical limit and error model of the proposed positioning system is derived. Section VI instantiates the proposed scheme and error model in the cellular network. In Section VII, we validated the proposed method and error model by simulation results. The positioning error of the proposed method is compared with

both constrained weighted least square (CWLS) and Gaussian-Newton method. Also, the accuracy comparison of RSS and LOS signal power based positioning is given. The paper is concluded in Section VIII.

2. MOTIVATION

In this section, we present the rationale why antenna directivity has to be taken into account. Let's consider a three-dimensional render of the antenna pattern. Fig 1 shows the pattern and spatial placement of reference position (RP) and mobile transceiver (MT). One RP is placed at $[X_{RP}, Y_{RP}]^T$, and an MT is at $[X_{MT}, Y_{MT}]^T$. Under traditional lateration methods isotropic antenna assumption, the radio waves from both RP and MT are emitted equally in all directions. Therefore, the radiation patterns are assumed spherical. As a result, the power contour is a circle. However, in realistic non-isotropic antenna scenario, the power contours are not circular centering at the RP and MT location. Fig. 1 shows a cellular 3-sector antenna on RP as an example. The half power beam width is 70^o. And the MT antenna is a dipole. The antenna gain between RP and MT is not only determined

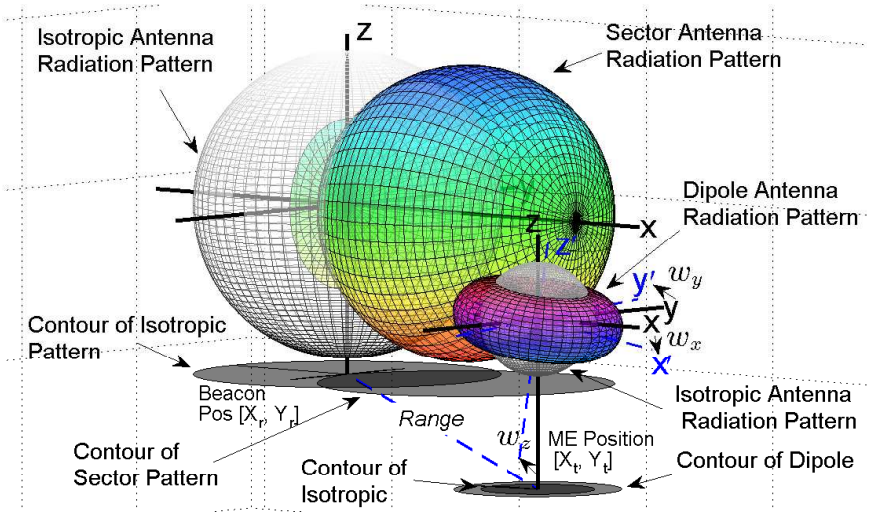

Figure 1. Isotropic antenna and sector & dipole antenna radiation pattern

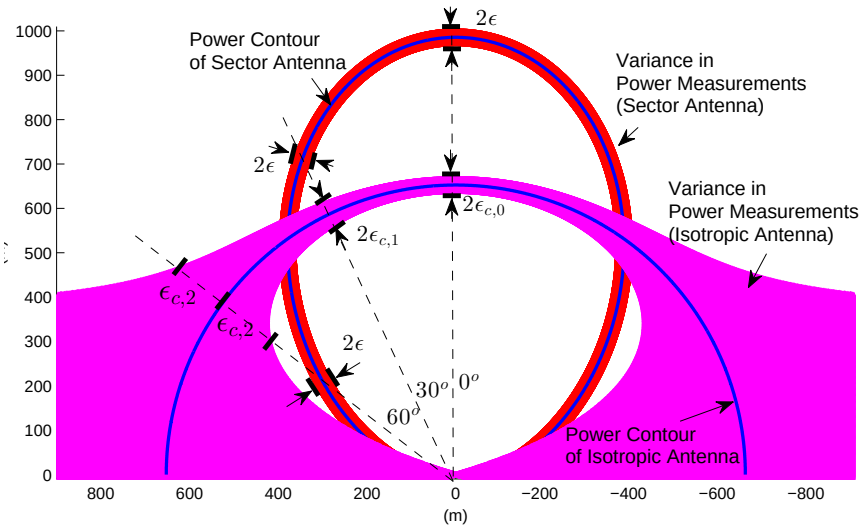

Figure 2. Uncertainty in power measurements on 2D plane

by the relative directions between them respectively but also the orientation of the MT. (see Appendix A1 for orientation) Thus, the power contour is not a circle anymore. Non-circular power contour means that given the same amount of measured power, the distance between RP and MT varies with azimuth and elevation angles between each other. Since it is difficult to observe the intersection and errors in the 3D graph, for simplicity and without loss of generality, Fig. 2 compares the sector antenna power contour (which looks like an oval) with the isotropic antenna in the 2D plane.

The noise in the power measurements will be magnified when traditional lateration methods are applied in the non-isotropic antenna scenario. Suppose we measure the received power along the contour, assuming that the measurement has a constant standard deviation (ε), since conventional lateration methods intrinsically convert non-circular contour into circular, the variance of measurements after the conversion will be magnified directionally. In Fig. 2, three representative directions are selected, 0°, 30°, and 60°. On each direction, the standard deviation of the power measurements are $\varepsilon_{c,0^\circ} = \varepsilon$, $\varepsilon_{c,30^\circ} > \varepsilon_{c,0^\circ}$, and $\varepsilon_{c,60^\circ} > \varepsilon_{c,30^\circ}$. It is worth note that the magnification effect is proportional to the inverse of the antenna directivity factor. (For detail, see remark 3)

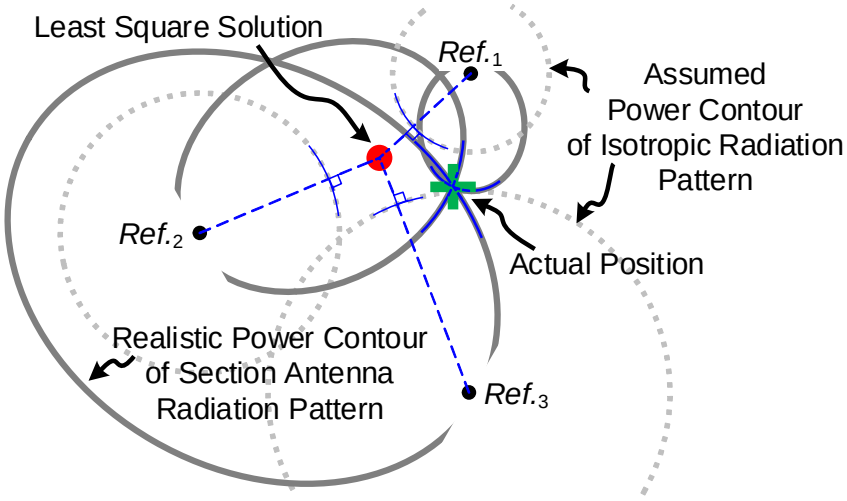

Figure 3. Power contour and intersection under different antenna radiation pattern

Furthermore, as indicated in Fig. 3, the actual position of MT in the non-isotropic antenna system is the intersection of several non-circular power contour (the solid curve). Conventional range-based positioning aims at finding the location that minimizes the ranges(radius) of multiple RP circular contour (the dashed circle). Consequently, the estimated position will diverge from the actual position.

3. RELATED WORKS

Existing studies of power based techniques, e.g. [32, 33, 34, 23], employ either extra hardware or offline profiling to account for the antenna directivity and fading effect.

Recently, DoA assistance, i.e. the joint RSS/DoA-based localization scheme, is proposed to address the antenna radiation pattern in cognitive network. In [32], Dr. Janis propose to take the estimated DoA (from SLS DoA/RSS algorithm [35]) into Stansfield estimator [36] to obtain position estimation. In [37], the DoA of the primary user (PU) is assume to be estimated by MUSIC[17] or ESPRIT[38], and RSS measurements are used to estimate the range from conventional pathloss model [39][40]. Dr. Jun Wang analyzed the theoretical limit (CRB) of the joint RSS/DoA-based localization methods in [37]. Slow

fading (Lognormal) model is used in his analysis. These DoA assisted methods require switched beam antenna system (a circular array) mounted on each cognitive radio (CR) to perform the DoA estimation. [32] shows that 10 is a good performance/complexity trade-off of the number of sectors on each CR. In contrast, our proposed method makes use of only the power estimation. Special hardware (antenna array) in the DoA module is eliminated.

Lateration and fingerprinting are two main RSS-based indoor localization techniques. Fingerprinting methods [41][33][34][42] address the fading effect by establishing RSSI fingerprint map in offline phase. The position estimation is obtained by matching the online RSSI reading with the pre-stored fingerprint database. The function mapping from location to the RSS measurement (or database) is created by frequent offline calibration measurement. The position estimation is obtained by minimizing a cost function between online observed RSS and database. However, the offline calibration stage is cumbersome. And the calibration resolution determines the online estimation accuracy. Moreover, fingerprinting methods are vulnerable to environmental change of the area of interesting. Therefore, the offline training has to be carried out periodically. In contrast, our proposed method requires no offline training and adapts to environmental changes.

In the existing lateration methods (e.g. [25][23][26][29][21]), contour of the received signal strength is assumed to be equal around a beacon in a fixed radial distance (range). Different varieties of multilateration algorithms have been proposed to perform position estimate based on circle contour, for example, constrained least square (CLS) [43], constrained weighted least square (CWLS)[24], nonlinear least square (NLS)[44], and maximum-likelihood based nonlinear positioning (ML)[45]. Since the antenna radiation pattern is missing in the model of the power based positioning system, there is a bias in the position estimation. As indicated in our simulation results, the missing of the antenna radiation pattern in the conventional multilateration model results in huge positioning errors.

Recently, Dr. Martin introduces a circular range-minimization scheme which is based on Gauss-Newton method. It finds position by minimizing the error between range measurements and the RSSI model. In [46], transceiver antenna pattern is modeled as "Antenna Error" term in RSSI model and is assumed to be unique for both transmitter and receiver in wireless sensor network. In contrast, the individual effect of the transmitter and receiver antenna radiation pattern is modeled into our proposed empirical spatial-pathloss. The position in the proposed scheme is obtained through Taylor expansion [47] of it. The circular range-minimizing scheme employs Gauss-Newton method which suits for optimization of the deterministic cost function. In contrast, the proposed method is fit for position estimation based on noised measurements. Our simulation results indicate 40% accuracy improvement of the proposed method over circular range-minimizing method.

4. POSITIONING SYSTEM MODEL AND SOLUTION

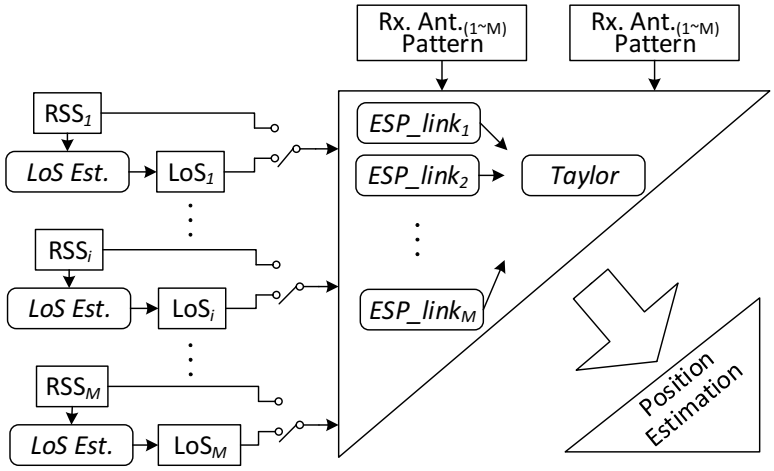

Figure 4. Overview of the Proposed Positioning Solution

4.1. Overview. The proposed ARPAP system estimates the MT position by minimizing the difference between the signal measurements and the proposed empirical spatial path loss model (ESP). The proposed ESP model extends the classic *one-slobe path loss*

propagation model [48][39] into three-dimension. The advanced ESP model describes not only how the signal attenuates with distance but also how it attenuated in space (azimuth and elevation).

It is worth noting that depending on the application requirement, i.e., the computational complexity and readiness of the hardware, ARPAP system can take either RSS measurements or LOS estimates as the input source. RSS indication is made readily available from all common wireless transceivers. LOS component within the RSS is determined from the fading signal which comes from receiver equalizer during the demodulation. RSS-ARPAP system eliminates the antenna directivity introduced bias error. LOS-ARPAP can not only eliminate bias error but also reduce environmental fading effect at large.

This Section is organized as follows. An antenna radiation-pattern-aware path loss model, named empirical spatial-path loss (ESP) model, is proposed in Section 4.2. Then, the antenna radiation-pattern-aware positioning (ARPAP) system model is present in Section 4.3. The solution to the system is derived in Section 4.4. Corresponding covariance matrix for both RSS- and LOS- ARPAP solution is derived in Section 4.5.

4.2. The Proposed Empirical Spatial Pathloss (ESP) Model. Antenna is a spatial power radiation filter that determines the distribution of transmitted power in space. Antenna directivity can be expressed as [40],

$$D(\varphi, \alpha) = \frac{4\pi B_0}{P_{rad}} F(\varphi, \alpha). \tag{1}$$

where spatial function, $F(\varphi, \alpha)$, represents the space (φ, α) dependent function, such that the radiation intensity (Watts/Unite Solid Angle) is $U = B_0 F(\varphi, \alpha)$. And, B_0 is a power related constant. φ is the azimuth angle, α is the elevation angle [40] (See Appendix 7.2.2 for detail). The total radiation power (in Watts) is $P_{rad} = 4\pi B_0 \int_{-\pi}^{\pi} \int_{0}^{\pi} F(\varphi, \alpha) sin\alpha d\alpha d\varphi$.

The amount of power collected by the receiving antenna is the product of power density at the particular geographical location and the receiver antenna effective area [40]. In free-space, the received signal power can be expressed as,

$$P_r = e_t e_r P_t \frac{\lambda^2 B_{0,t} B_{0,r}}{P_{rad,t} P_{rad,r}} (PLF) \frac{F_t(\varphi_t, \alpha_t) F_r(\varphi_r, \alpha_r)}{d^2}. \tag{2}$$

where P_t is the total transmitted power, $e_{t(/r)}$ is the efficiency of the transmitting(/receiving) antenna, λ is the wavelength of the carrier frequency used for communication, $B_{0,t(/r)}$ is the radiation intensity related constants of transmitting (/receiving) antenna, $P_{rad,t(/r)}$ is the antenna radiation power of transmitter (/receiver), $F_{t(/r)}(\cdot)$ is the spatial function in radiation intensity of transmitter (/receiver). (PLF) represents the polarization loss factor, which is assume to be 1 for simplicity. d is the distance from the transmitter to the receiver,

$$d_k^2 = ||\mathbf{x} - \mathbf{x}_k|| + h^2. \tag{3}$$

where $\mathbf{x} = [x, y]^T$ represents the 2-dimensional (2D) coordinates of the MT, $\mathbf{x}_k = [x_k, y_k]^T$ represents the 2D coordinates of the k^{th} RP, $k = 1 \sim M$. M is the total number of RPs. And, h is the relative height between RP and MT.

Generalize (2), we have the empirical spatial-pathloss model defined as follow.

Definition 2. *An empirical path loss model multiplexed with the antenna directivity function is called empirical spatial path loss model, ESP,*

$$P_{ESP} = \kappa Q / d^n. \tag{4}$$

where, Q is the transmit-receive antenna directivity factor,

$$Q = F_t(\varphi_t, \alpha_t) F_r(\varphi_r, \alpha_r). \tag{5}$$

In (4), the exponential parameter, n, is an environmental dependent factor which varies between 2 to 6 (n is equal to 2 in free-space, and between 3 and 6 in either urban or some suburban areas). The scalar, κ, is a power and gain related factor. Analytically, $\kappa = e_t e_r P_t \frac{\lambda^2 B_{0,t} B_{0,r}}{P_{rad,t} P_{rad,r}} (PLF)$. Practically, κ is an empirical value and is obtained from experiments.

It is worth noting that, in traditional empirical path loss model, the antenna directivity is included into the scalar factor. The traditional scalar factor is found by the experimental results and is never accurate. It is subjected to the environment due to fading and antenna directivity. In contrast, ESP separates the antenna directivity from traditional scalar factor, and ARPAP addresses directivity effect on positioning. Moreover, by decomposing LOS from fading signal, the ESP model is more accurate and stable than the traditional empirical model.

Remark 3. *In non-isotropic antenna scenario, conventional lateration methods will magnify the power measurement noise.*

(For detail, see Appendix 9.1)

4.3. Positioning System Model. Based on the empirical spatial pathloss model, the received power from the k^{th} RP, $\mathbf{x}_k$, at actual location $\mathbf{x}$, can be expressed as,

$$\xi(\mathbf{x}, \mathbf{x}_k) = f(p_k). \tag{6}$$

where $f(\cdot) = \ln(\cdot)$. And,

$$\xi(\mathbf{x}, \mathbf{x}_k) = \ln \kappa + \gamma G_t(\mathbf{x}, \mathbf{x}_k) + \gamma G_r(\mathbf{x}, \mathbf{x}_k) - n \ln d(\mathbf{x}, \mathbf{x}_k). \tag{7}$$

$$G_t(\mathbf{x}, \mathbf{x}_k) = 10 log_{10} F_t \left(\varphi_t(\mathbf{x}, \mathbf{x}_k), \alpha_t(\mathbf{x}, \mathbf{x}_k)\right). \tag{8}$$

$$G_r(\mathbf{x}, \mathbf{x}_k) = 10 log_{10} F_r \left(\varphi_r(\mathbf{x}, \mathbf{x}_k), \alpha_r(\mathbf{x}, \mathbf{x}_k)\right). \tag{9}$$

$\gamma = \ln(10)/10$.

Thus, given M reference positions, let $\boldsymbol{\theta} = [\theta_1, \theta_2, \cdots, \theta_M]^T$ be the power estimation, $\theta_k = \tilde{p}_k$. The positioning system can be modeled as,

$$\hat{\mathbf{x}} = \boldsymbol{\Theta}\left(f(\boldsymbol{\theta}), \mathbf{x}_{ref}\right) + \mathbf{e}. \tag{10}$$

where $\mathbf{x}_{ref} = [\mathbf{x}_1, \mathbf{x}_2, \cdots, \mathbf{x}_M]$, $\boldsymbol{\Theta}$ represents a vector function of $\xi^{-1}(\tilde{p}_k, \mathbf{x}_k)$, i.e. $\boldsymbol{\Theta} = [\xi_1^{-1}, \xi_2^{-1}, \cdots .\xi_M^{-1}]^T$.

4.4. Position Estimation. The measurement of the received power from the k^{th} RP is,

$$\xi_k(\hat{\mathbf{x}}) = f(\theta_k) + e_k. \tag{11}$$

where e_k is the measurement error.

By Taylor expansion [47], keeping the first order terms,

$$\xi_k(x, y)\Big|_{\mathbf{x}=\mathbf{x}_0} + \left.\frac{\partial \xi_k}{\partial x}\right|_{\mathbf{x}=\mathbf{x}_0} \delta_x + \left.\frac{\partial \xi_k}{\partial y}\right|_{\mathbf{x}=\mathbf{x}_0} \delta_y \approx f(\theta_k) + e_k \tag{12}$$

where $\mathbf{x}_0 = [x_0, y_0]^T$ is the guess of the true position $\mathbf{x} = [x, y]^T$. And with the correction by $\boldsymbol{\delta} = [\delta_x, \delta_y]^T$, the position estimation is updated as,

$$\mathbf{x} = \mathbf{x}_0 + \boldsymbol{\delta}. \tag{13}$$

Hence, the positioning problem is to determine $\boldsymbol{\delta} = [\delta_x, \delta_y]^T$ through (12).

Providing measurements of recceived power from M RPs, we have,

$$\boldsymbol{\nabla}_{\xi}(\mathbf{x}_0)\boldsymbol{\delta} = \mathbf{z} - \mathbf{e}. \tag{14}$$

where, $\mathbf{z} = [f(\theta_1) - \xi_1, f(\theta_2) - \xi_2, \cdots f(\theta_M) - \xi_M]^T$, $\boldsymbol{\delta} = \begin{bmatrix} \delta_x & \delta_y \end{bmatrix}^T$, $\mathbf{e} = [e_1, e_2, \cdots e_M]^T$, and

$$\boldsymbol{\nabla}_{\boldsymbol{\xi}}(\mathbf{x}_0) = \begin{bmatrix} \frac{\partial \xi_1}{\partial x} & \frac{\partial \xi_1}{\partial x} & \cdots & \frac{\partial \xi_M}{\partial x} \\ \frac{\partial \xi_1}{\partial y} & \frac{\partial \xi_1}{\partial y} & \cdots & \frac{\partial \xi_M}{\partial y} \end{bmatrix}^T_{\mathbf{x}=\mathbf{x_0}}. \tag{15}$$

To minimize the square error of (14),

$$\boldsymbol{\delta} = \left[\boldsymbol{\nabla}_{\boldsymbol{\xi}}(\boldsymbol{x}_0)^T \boldsymbol{\Sigma}^{-1} \boldsymbol{\nabla}_{\boldsymbol{\xi}}(\boldsymbol{x}_0)\right]^{-1} \boldsymbol{\nabla}_{\boldsymbol{\xi}}(\boldsymbol{x}_0)^T \boldsymbol{\Sigma}^{-1} \boldsymbol{z} \tag{16}$$

where, $\boldsymbol{\Sigma}$ is the covariance matrix of measurements.

4.5. Covariance Matrix for Taylor Position Estimation. The covariance matrix, $\boldsymbol{\Sigma}$, used for RSS- and LoS- ARPAP is given by Lemma 15.

Lemma 15. *The covariance matrix for RSS-ARPAP is,*

$$\boldsymbol{\Sigma}_{RSS} = diag([\varepsilon_{\Omega,1}, \varepsilon_{\Omega,2}, \cdots, \varepsilon_{\Omega,M}]). \tag{17}$$

The covariance matrix for LoS based positioning is,

$$\boldsymbol{\Sigma}_{LoS} = diag([\varepsilon_{v,1}, \varepsilon_{v,2}, \cdots, \varepsilon_{v,M}]). \tag{18}$$

where, $\varepsilon_{v,k} = \varepsilon_v(K_k)$ $(k = 1 \sim M)$ which is given in (20), with $\eta(K) = \frac{\pi L^2_{1/2}(-K)}{4(K+1)}$, and $L_{1/2}(\cdot)$ represents Laguerre polynomial. And $\varepsilon_{\Omega,k} = \varepsilon_\Omega(K_k)$, with

$$\varepsilon_\Omega(K) = (1 + 2K)/(1 + K)^2. \tag{19}$$

$$\begin{aligned}\varepsilon_v(K) =& \frac{(1+K)L_{1/2}^2(-K) - \frac{\pi^2}{16}L_{1/2}^4(-K)}{K^2(1+K)^4[\eta'(K)]^2} \\ &+ \frac{\frac{3\pi}{2}L_{1/2}(-K)L_{3/2}(-K) - \pi L_{1/2}^2(-K)(1+K)}{K^2(1+K)^4[\eta'(K)]^2}\left[\frac{K}{1+K} - \frac{\frac{\pi}{4}L_{1/2}^2(-K)}{\eta'(K)(1+K)^3}\right] \\ &+ \frac{1+2K}{K^3}\left[\frac{K}{1+K} - \frac{\frac{\pi}{4}L_{1/2}^2(-K)}{\eta'(K)(1+K)^3}\right]^2\end{aligned} \tag{20}$$

Proof. In mobile fading channel, the probability density function (PDF) of the envelobe of the channel fading is a random variable R following Ricean distribution [49],

$$P_R(r) = \frac{2(K+1)r}{\Omega}e^{\left(-K-\frac{(K+1)r^2}{\Omega}\right)}I_0\left(2r\sqrt{\frac{K(K+1)}{\Omega}}\right). \tag{21}$$

where K represents the LoS-to-NLoS power ratio, i.e. $K = v^2/2\sigma^2$, and $I_0(\cdot)$ is the modified Bessel function of the first kind. The total power is,

$$\Omega = v^2 + 2\sigma^2. \tag{22}$$

In [27], it has been shown that the asymptotic variance of LoS component estimation and the total power estimation can be expressed in terms of K and v^2 as,

$$AsV(\hat{v}^2) = \varepsilon_v(K)v^4. \tag{23}$$

$$AsV(\hat{\Omega}) = c_1(K)v^4. \tag{24}$$

where, function $\varepsilon_v(K)$ is given by (22). And function $c_1(K)$,

$$c_1(K) = (1+2K)/K^2. \tag{25}$$

The variance of the logarithmized power measurement, $\ln(\theta)$, can be obtained as [30], $VAR(\ln\theta) = \left[f'_{\theta}(\mu_\theta)\right]^2\Big|_{\mu_\theta=E[\theta]} VAR(\theta)$, which is,

$$VAR(\ln\theta) = \mu_\theta{}^{-2} VAR(\theta). \tag{26}$$

Thus, it is straightforward that for RSS based positioning, the variance of the logarithmized RSS measurements is

$$VAR(\ln\hat{\Omega}) = \varepsilon_\Omega(K). \tag{27}$$

where $\varepsilon_\Omega(K) = c_1(K)\left(\frac{K}{1+K}\right)^2$, which is (19). And the variance of the logarithmized LoS measurements is

$$VAR(\ln\hat{v}^2) = \varepsilon_v(K). \tag{28}$$

Assume power measurements from different RPs are independent, we get the co-variance matrix for RSS based and LoS based positioning (17)(18). □

Remark 4. *In multipath fading channel, the variance of both LoS and RSS measurements depend only on the environment effects, i.e. the LoS-to-NLoS ratio K.*

5. ERROR MODEL AND THEORETICAL LIMITS

In this Section, the mean square error bound (MSEB) for the ARPAP positioning is derived. The power measurements from M RPs, $\boldsymbol{\theta} = [\theta_1, \theta_2, \cdots, \theta_M]^T$, can be expressed as a function of position $\hat{\mathbf{x}}$,

$$f(\boldsymbol{\theta}) = \boldsymbol{\xi}(\hat{\boldsymbol{x}}, \boldsymbol{x}_{ref}) + \mathbf{e}_\theta. \tag{29}$$

where $\boldsymbol{\xi}$ represents a vector function of $\xi_k(\hat{\mathbf{x}})$.

Due to the nonlinearity of function $\xi(\cdot)$, the MSEB contains two parts, variance and bias [50],

$$E\left((\hat{\mathbf{x}}-\mathbf{x})^2\right) \geq CRB(\hat{\mathbf{x}}) + Bias^2(\hat{\mathbf{x}}). \tag{30}$$

In the following subsections, the MSEB for LoS- and RSS-based position estimation are derived respectively.

5.1. Bias of the Positioning. The bias in the position estimation is caused by two factors: 1) Propagated power measurements variance in the nonlinear position estimation function. 2) The NLoS signal power from fading environment. lemma 16 provides a general model of power-based positioning bias that take into account these two factors. Lemma 17 and 18 provide the bias specifically for RSS-ARPAP and LOS-ARPAP.

Lemma 16. *The bias of ARPAP estimation is,*

$$E(\mathbf{x}-\hat{\boldsymbol{x}}) = \boldsymbol{\nabla}^{\dagger}_{\xi}(\mathbf{x}) \cdot \mathbf{s}. \tag{31}$$

where $\mathbf{x}$ *is the actual position,* $\hat{\mathbf{x}}$ *is the position estimation,* $\boldsymbol{\nabla}_{\boldsymbol{\xi}}(\mathbf{x})$ *is given in (15). And* $\mathbf{s}$*,*

$$[\mathbf{s}]_k = f(\mu_{\theta,k}) - \xi_k(\mathbf{x}) + \frac{1}{2}f''(\mu_{\theta,k})VAR(\theta). \tag{32}$$

with $\mu_{\theta,k} = E[\theta_k]$*,* $k = 1 \sim M$*.*

Proof. Expand the left side of (11) around $\hat{\mathbf{x}}$, and take expectation,

$$\xi(\mathbf{x}) = E\left[\xi(\hat{\mathbf{x}})\right] + \boldsymbol{\nabla}_{\boldsymbol{\xi}}(\hat{\mathbf{x}})E\left(\mathbf{x}-\hat{\mathbf{x}}\right). \tag{33}$$

Take the expectation of the right side of (11),

$$E\left[f(\theta)\right] = f(\mu_\theta) + \frac{1}{2}f''(\mu_\theta)VAR(\theta). \tag{34}$$

Let $\xi(\mathbf{x}) = E\left[f(\theta)\right]$, we get (31). □

Lemma 17 and 18 provide LOS-ARPAP and RSS-ARPAP analytic bias.

Lemma 17. *The bias of LoS- ARPAP is given by,*

$$Bias_{\mathbf{x}}^{LoS}(\hat{\mathbf{x}})=\frac{-1/2}{\sum_{i=1}^{M}\left(\frac{\partial\xi_i}{\partial x}\right)^2\sum_{i=1}^{M}\left(\frac{\partial\xi_i}{\partial y}\right)^2-\sum_{i=1}^{M}\left(\frac{\partial\xi_i\partial\xi_i}{\partial x\,\partial y}\right)^2\Big|_{\hat{\mathbf{x}}=\mathbf{x}}}\left[\begin{matrix}\sum_{j=1}^{M}v_j^{-4}AsV(\hat{v}_j^2)\left(\frac{\partial\xi_j}{\partial x}\sum_{i=1}^{M}\left(\frac{\partial\xi_i}{\partial y}\right)^2-\frac{\partial\xi_j}{\partial y}\sum_{i=1}^{M}\left(\frac{\partial\xi_i\partial\xi_i}{\partial x\,\partial y}\right)\right)\\ \sum_{j=1}^{M}v_j^{-4}AsV(\hat{v}_j^2)\left(\frac{\partial\xi_j}{\partial y}\sum_{i=1}^{M}\left(\frac{\partial\xi_i}{\partial x}\right)^2-\frac{\partial\xi_j}{\partial x}\sum_{i=1}^{M}\left(\frac{\partial\xi_i\partial\xi_i}{\partial x\,\partial y}\right)\right)\end{matrix}\right]\Bigg|_{\hat{\mathbf{x}}=\mathbf{x}} \tag{35}$$

Proof. By using the LoS component, $f(\mu_{\theta,k})\Big|_{\mu_{\theta,k}=E[\hat{v}_k^2]=v_k^2} = \xi_k(\mathbf{x})$, we get,

$$[\mathbf{s}]_{LoS,k} = -\frac{1}{2N}v_k^{-4}AsV(\hat{v}_k^2). \tag{36}$$

where N is the number of samples used for power estimation.

The asymptotic variance of LoS component estimation $AsV(\hat{v}^2)$ is given by (23).

Take (36) into (31), and after expanding, we get (36). □

Lemma 18. *The bias of RSS- ARPAP is given by (38).*

$$Bias_{\mathbf{x}}^{RSS}(\hat{\mathbf{x}})=\frac{1}{\sum_{i=1}^{M}\left(\frac{\partial\xi_i}{\partial x}\right)^2\sum_{i=1}^{M}\left(\frac{\partial\xi_i}{\partial y}\right)^2-\sum_{i=1}^{M}\left(\frac{\partial\xi_i\partial\xi_i}{\partial x\,\partial y}\right)^2\Big|_{\hat{\mathbf{x}}=\mathbf{x}}}\left[\begin{matrix}\sum_{j=1}^{M}\left\{ln(1+K^{-1})-\frac{1}{2}\Omega_j^{-2}Var(\hat{\Omega}_j)\right\}\left(\frac{\partial\xi_j}{\partial x}\sum_{i=1}^{M}\left(\frac{\partial\xi_i}{\partial y}\right)^2-\frac{\partial\xi_j}{\partial y}\sum_{i=1}^{M}\left(\frac{\partial\xi_i\partial\xi_i}{\partial x\,\partial y}\right)\right)\\ \sum_{j=1}^{M}\left\{ln(1+K^{-1})-\frac{1}{2}\Omega_j^{-2}Var(\hat{\Omega}_j)\right\}\left(\frac{\partial\xi_j}{\partial y}\sum_{i=1}^{M}\left(\frac{\partial\xi_i}{\partial x}\right)^2-\frac{\partial\xi_j}{\partial x}\sum_{i=1}^{M}\left(\frac{\partial\xi_i\partial\xi_i}{\partial x\,\partial y}\right)\right)\end{matrix}\right]\Bigg|_{\hat{\mathbf{x}}=\mathbf{x}} \tag{38}$$

Proof. By using the RSS components, $f(\mu_{\theta,k})\Big|_{\mu_{\theta,k}=E[\hat{\Omega}_k]=\Omega_k} = \ln v_k^2 + \ln(1+K_k^{-1}) = \xi_k(\mathbf{x}) + \ln(1+K_k^{-1})$ in (32). Therefore,

$$[\mathbf{s}]_{RSS,k} = \ln(1+K_k^{-1}) - \frac{1}{2N}\Omega_k^{-2}VAR(\hat{\Omega}_k). \tag{39}$$

The variance of the RSS measurement can be obtained from moments of Rice distribution, and is given by (24).

Take (39) into (31), and after expanding, we get (37). □

5.2. CRB of the Positioning. A general CRB for ARPAP system is derived in lemma 19. The CRB for the RSS and LOS specific methods are given in Remark 5. The CRB quantifies the minimum variance of an ideal estimator can achieve.

Lemma 19. *The CRB of ARPAP system is* $\mathbf{I^{-1}}$ *where,*

$$\begin{aligned}
[\mathbf{I}]_{1,1} &= \sum_{i=1}^{M} \varsigma_{x,i}^2 \varepsilon_{\theta,i}^{-1} \\
[\mathbf{I}]_{2,2} &= \sum_{i=1}^{M} \varsigma_{y,i}^2 \varepsilon_{\theta,i}^{-1} \\
[\mathbf{I}]_{1,2} &= [\mathbf{I}]_{2,1} = \sum_{i=1}^{M} \varsigma_{x,i} \varsigma_{y,i} \varepsilon_{\theta,i}^{-1}
\end{aligned} . \tag{40}$$

where,

$$\begin{aligned}
\varsigma_{x,i} &= \gamma \left(\tfrac{\partial}{\partial x} G_t + \tfrac{\partial}{\partial x} G_r \right) - nd^{-2}(x - x_i) \\
\varsigma_{y,i} &= \gamma \left(\tfrac{\partial}{\partial y} G_t + \tfrac{\partial}{\partial y} G_r \right) - nd^{-2}(y - y_i)
\end{aligned} \tag{41}$$

And N is the number of samples used for power estimation, $\varepsilon_{\theta,i}$ *represents the environmental dependent term in power measurement variance, i.e.* ε_Ω *(*$\theta = \Omega$*)* ε_v *(*$\theta = v$*) in(25)(26).*

Proof. Assume independent power estimation from each reference position, the power measurements asymptotically follows normal distribution, by central limit theory,

$$\mathbf{e}_\theta \xrightarrow{N} \mathcal{N}(\mathbf{0}, \mathbf{\Sigma}) \tag{42}$$

where, $\mathbf{\Sigma}$ is the covariance matrix.

Follow the Fisher Information Matrix for general Gaussian [50],

$$[\boldsymbol{I}]_{k,l} = \left[\left[\frac{\partial \boldsymbol{\xi}}{\partial \boldsymbol{x}} \right]^T \mathbf{\Sigma}^{-1} \left[\frac{\partial \boldsymbol{\xi}}{\partial \boldsymbol{x}} \right] \right]_{k,l} + \frac{1}{2} Tr \left[\mathbf{\Sigma}^{-1} \frac{\partial \mathbf{\Sigma}}{\partial [\boldsymbol{x}]_k} \mathbf{\Sigma}^{-1} \frac{\partial \mathbf{\Sigma}}{\partial [\boldsymbol{x}]_l} \right] \tag{43}$$

and $\varsigma_{x,i} = \left[\frac{\partial \boldsymbol{\xi}}{\partial x} \right]_i$, $\varsigma_{y,i} = \left[\frac{\partial \boldsymbol{\xi}}{\partial y} \right]_i$.

We get (40). □

Remark 5. *The CRB of RSS- and LoS- ARPAP positioning are,*

$$[\mathbf{I}]_{RSS}^{-\mathbf{1}} = \mathbf{I}^{-\mathbf{1}}\big|_{\theta=\hat{\Omega},\varepsilon_\theta=\varepsilon_\Omega} \tag{44}$$

$$[\mathbf{I}]_{LoS}^{-\mathbf{1}} = \mathbf{I}^{-\mathbf{1}}\big|_{\theta=\hat{\gamma}^2,\varepsilon_\theta=\varepsilon_v} \tag{45}$$

where ε_Ω and ε_v are given in (19) and (20), respectively.

5.3. Error Model. The power-based position estimation error is modeled as the square root of the summation of the squared positioning bias and the trace of CRB as,

$$E_p = \sqrt{Bias_{\mathbf{x}}^2 + Tr(\mathbf{I}^{-\mathbf{1}})}. \tag{46}$$

where $Bias_{\mathbf{x}}^{LoS}$, $Bias_{\mathbf{x}}^{RSS}$, $[\mathbf{I}]_{LoS}^{-\mathbf{1}}$, and $[\mathbf{I}]_{RSS}^{-\mathbf{1}}$ are given in (35), (38), (45), and (44), respectively.

6. APPLICATION EXAMPLE INSTANTIATION FOR CELLULAR NETWORK

The proposed method is applicable to many different systems include indoor and outdoor power based localizations for ZigBee, WiFi, the cellular network, White Space TV, Super WiFi [51], etc. As an example, in this Section, error model and CRB for ARPAP in the cellular network are instantiated. A general power radiation pattern model of base station antenna is used. And assume MT use dipole antenna.

6.1. Base Station Antenna Radiation Pattern and Available Localization Area. In [52], 3-sector (and 6-sector) base station (BS) antenna pattern is given as,

$$G_t(\varphi,\alpha) = -min\left[12\left(\frac{\varphi}{\varphi_{3dB}}\right)^2, G_m\right]. \tag{47}$$

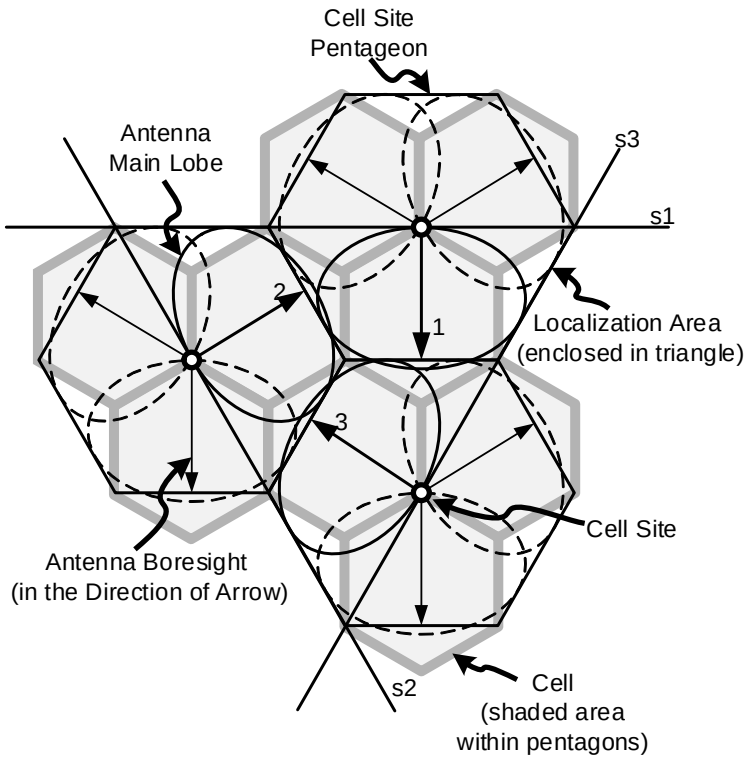

Figure 5. Localization Area

where $-180° \leq \varphi \leq 180°$. The maximum gain $G_m = 20dB$ in 3-sector BS antenna, and $G_m = 23dB$ in 6-sector BS antenna. The half power beam width, $\varphi_{3dB} = 70°$ in 3-sector BS antenna, and $\varphi_{3dB} = 30°$ in 6-sector BS antenna.

A general method to restore the three dimension antenna pattern can be found in [53]. An example of restored 3-D antenna pattern and received signal power map can be found in Appendix 9.3. Since it has not been defined but the antenna pattern on azimuth plane in [52], without loss of generality, we assume the antenna gain on elevation plane of the interested angle range is one, i.e. $G_t(\alpha_t) = 1$, $90° < \alpha_t < 180°$.

In the cellular network, the power radiated in side lobes is desired to be suppressed. We assume main lobe is in the range of $-90° \leq \varphi \leq 90°$, and all side lobes are in $-180° \leq \varphi \leq -90°$ and $90° \leq \varphi \leq 180°$. Thus, we define the main lobe covered area as

the *localization area*, which is indicated in Fig. 5 (the enclosed area by triangle $[s_1, s_2, s_3]$). When 3-sector antenna is mounted on the BS, one cell site covers three cell. The boresights of the three-antenna point to $\varphi_{o,1} = -90°$, $\varphi_{o,1} = 30°$, and $\varphi_{o,1} = 150°$, respectively.

The BS antenna radiation pattern can be modeled as,

$$G_t(\varphi_t, \alpha_t) = -12\left(\frac{\varphi_t - \varphi_o}{\varphi_{3dB}}\right)^2 + G_m. \tag{48}$$

where $-90° \leq \varphi_t - \varphi_o \leq 90°$, φ_o is the antenna boresight direction.

Lemma 25 provides the first derivative of the BS antenna directivity which is required for calculating the Jacobean matrix $\nabla_\xi(15)$, positioning bias (35)(38), and theoretical limits (44)(45).

Lemma 20. *The first derivative of the sector antenna spatial function of the kth beacon is*

$$\left\{\begin{array}{l} \frac{\partial}{\partial x}G_{t,k} = \frac{4320}{\pi\varphi_{3db,k}}\left(\frac{\varphi_{t,k}-\varphi_{o,k}}{\varphi_{3db,k}}\right)d_k^{-2}(y - y_k) \\ \frac{\partial}{\partial y}G_{t,k} = \frac{4320}{\pi\varphi_{3db,k}}\left(\frac{\varphi_{t,k}-\varphi_{o,k}}{\varphi_{3db,k}}\right)d_k^{-2}(x - x_k) \end{array}\right| _{\varphi_t = atan2d\left(\frac{y-y_k}{x-x_k}\right)} \tag{49}$$

where the location of the MT is $[x, y]^T$*, the location of the kth RP (the BS) is* $[x_k, y_k]^T$*, function* $atan2d(\cdot)$ *represents Four-quadrant inverse tangent in degrees, and* $d_k = \sqrt{(x - x_k)^2 + (y - y_k)^2}$.

Proof. The RP antenna azimuth angle, φ_t can be found by $\varphi_t = \text{atan2d}\left(\frac{y-y_k}{x-x_k}\right)$. The first derivative of the four-quadrant inverse function is,

$$\left\{\begin{array}{l} \frac{\partial}{\partial x}atan2d\left(\frac{y-y_k}{x-x_k}\right) = -\frac{y-y_k}{d_k^2} \\ \frac{\partial}{\partial y}atan2d\left(\frac{y-y_k}{x-x_k}\right) = -\frac{x-x_k}{d_k^2} \end{array}\right. \tag{50}$$

The rest of the proof is straightforward and is omitted. □

6.2. Receiving Antenna Radiation Pattern. Without loss of generality, assuming the receiving antenna is dipole, for the sake of simplicity, consider the directivity spatial function of an infinitesimal dipole antenna,

$$F_r(\varphi_r, \alpha_r) = sin^2(\alpha_r) \tag{51}$$

Using Euler angles, $[\Omega_x, \Omega_y, \Omega_z]^T$, represents the orientation of the receiving antenna. (Appendix 9.2)

Lemma 21 provides the first derivative of the receiving antenna directivity which is required for calculating the Jacobean matrix $\nabla_{\xi}(15)$, positioning bias (35)(38), and theoretical limits (44)(45).

Lemma 21. *The first derivative of the dipole antenna spatial function with orientation* $[\Omega_x, \Omega_y, \Omega_z]^T$ *is,*

$$\begin{cases} \frac{\partial}{\partial x} G_{r,k} = \gamma^{-1} \Gamma_k \left[sin(\Omega_y) d_R^{-1} - {}^{M}h_k d_R^{-3} (x_k - x) \right] \\ \frac{\partial}{\partial y} G_{r,k} = \gamma^{-1} \Gamma_k \left[cos(\Omega_y) sin(\Omega_x) d_R^{-1} - {}^{M}h_k d_R^{-3} (y_k - y) \right] \end{cases} \tag{52}$$

where,

$$\Gamma_k = \frac{\tan^{-1}\left(\operatorname{atan}\left({}^{M}h_k / d_R\right)\right)}{\sqrt{1 - \left({}^{M}h_k / d_R\right)^2}}. \tag{53}$$

and,

$${}^{M}h_k = sin(\Omega_y)(x_k - x) + cos(\Omega_x) cos(\Omega_y) h + cos(\Omega_y) sin(\Omega_x)(y_k - y). \tag{54}$$

Proof. Given the location of the k^{th} RP and MT, set the origin at the MT location, the spherical coordinates of the RP is,

$$\begin{cases} r_k = \sqrt{\Delta_{x,k}^2 + \Delta_{y,k}^2 + h_k^2} \\ \varphi_{r,k} = \text{atan}\left(\Delta_{y,k}/\Delta_{x,k}\right) \\ \alpha_{r,k} = \text{acos}\left(\frac{h_k}{r_k}\right) \end{cases} \tag{55}$$

where the displacement in inertial frame ${}^{E}\boldsymbol{\Delta x} = [\Delta x, \Delta y, h]^T = [(x_k - x), (y_k - y), h]^T$. Thus, the orientation of MT in the inertial frame "E" relative to MT body frame "M" is,

$${}^{M}\boldsymbol{\Delta x} = {}^{M}_{E}\boldsymbol{R}\ {}^{E}\boldsymbol{\Delta x}. \tag{56}$$

where ${}^{M}_{E}\boldsymbol{R}$ is rotation matrix (Appendix 9.2).

Thus, after rotation, ${}^{M}h_k = [0, 0, 1]\ {}^{M}_{E}\boldsymbol{R}\ {}^{E}\boldsymbol{\Delta x}$, which is (50). And the elevation angle, ${}^{M}\alpha_r = acos({}^{M}h_k/r_k)$. Differentiating the receiving antenna spatial function G_r, (57), we get (52).

$$G_r = \gamma^{-1} ln F_r(\varphi_r, \alpha_r). \tag{57}$$

□

6.3. Error Model and CRB. The error model (46) and CRB (40) of the ARPAP in the cellular network is obtained by taking the first derivative of RP and MT antenna directivities (49)(52) into (35)(38)(41), which is straightforward and is omitted here due to the limited space.

7. SIMULATION RESULT

As an instance application, the proposed ARPAP method is evaluated in the cellular network. In this Section, analytic error models are first validated by simulation. Next, the proposed ARPAP method is compared with the Gauss-Newton method. Finally, the performance comparison between LOS- and RSS-ARPAP is given.

In this work, we validate the derived positioning error model and theoretical limit using a representative simulation area. For smaller or larger area, the corresponding theoretical limit can be obtained from our model. Other simulation results we obtained confirm the conclusion, though are omitted here due to limited space.

We choose a representative simulation area and placed the RP as follows:

- The center of the area is the origin of coordinates.
- RPs are evenly distributed around the center with radius of $3.5km$.

Fig. 6 shows the contour map within the simulation area. The contour lines indicate $-10dBm$, $-75dBm$, and $-80dBm$. The signal attenuation parameters are set to be $\kappa = -18.52dBm$ and $n = 2$. The power impinges on the receiving antenna along the BS antenna boresight is shown in Fig. 7 which indicates the signal attenuation.

In our simulation, Koay method [54] is used to estimate the LOS signal component in RSS. Without a loss in either generality or accuracy, the sum-of-sinusoids simulator, which was proposed in [55], is applied to generate the fading signal. The Doppler frequency is set to be $100Hz$. The number of fading paths is configured to be ≥ 20. And the angle of arrival is randomly generated. Taking GSM network as an example, assuming carrier frequency of $900MHz$, and the symbol rate of $270kbps$ [56], the vehicle velocity is $75mph$ ($33m/s$) which is corresponding to the $100Hz$ Doppler frequency. The sample size of the fading signal is $3e4$.

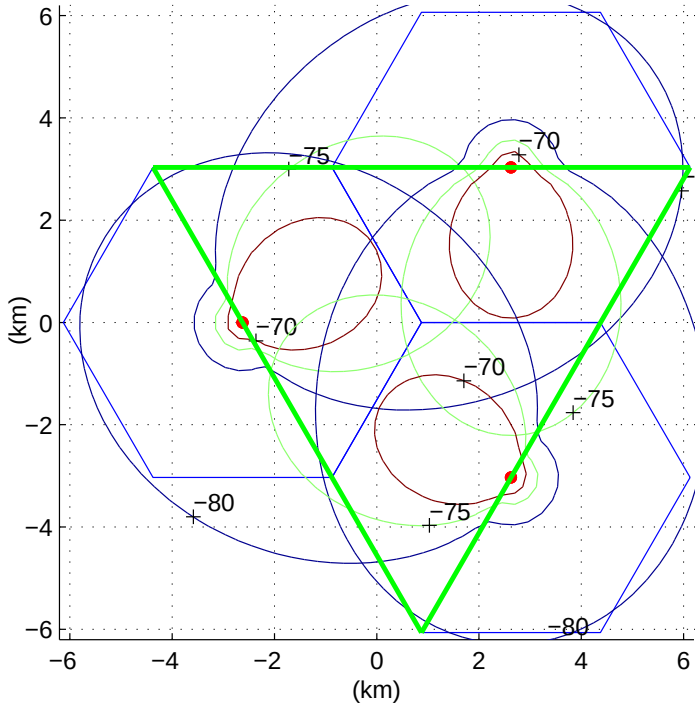

Figure 6. Simulation Area

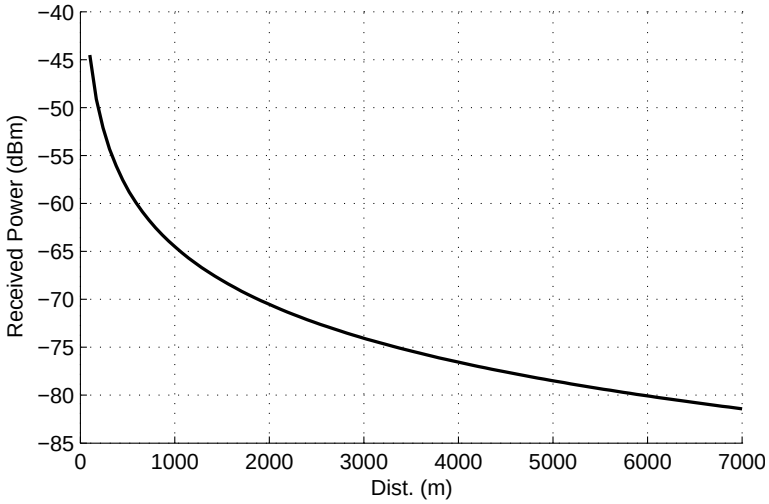

Figure 7. Path-loss Alone Bore-side Direction of Beacon Antenna

In the simulation, three environmental fading conditions, i.e. K-ratio equals to 10, 50 and 100, three receiving antenna attitude cases, i.e. Ω_y equals to 0°, 10°, and 30°, are compared. Other simulation results we obtained confirm the conclusion, though are omitted here due to limited space.

7.1. Comparison with the Lateration Methods. In this Section, we compare the proposed ARPAP results with 1) Lateration CWLS positioning results and 2) Gauss-Newton method [46].

1) Comparison with CWLS Positioning:

The CWLS method can be found in [24]. It obtains the solution by minimizing the squared ranging error.

Simulation results show an averaged bias error of several thousand meters when antenna radiation pattern is not isotropic. As an example, Fig. 8 shows a comparison of positioning error for $K = 100$ and $\Omega_y = 10°$.

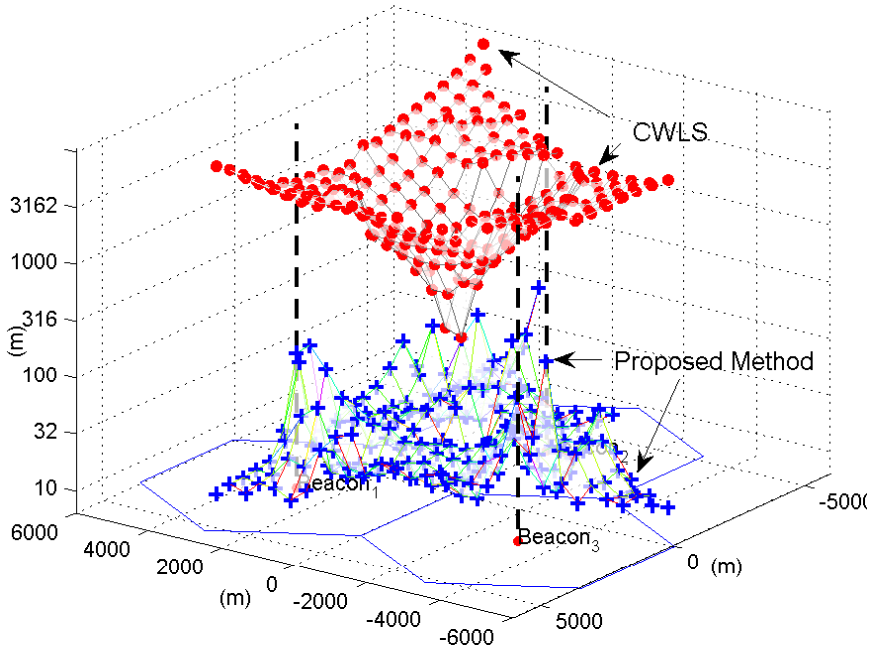

Figure 8. Positioning Error ($K = 100$, $\Omega_y = 10°$)

The averaged error of the CWLS method applied in the non-isotropic antenna scenario is as high as 3317meters for varying K (10, 50, 100) and Ω_y(0°, 10°,25°, 30°). In contrast, the averaged error of the proposed method is 27 meters in the $12Km \times 10Km$

area which is 99% improvement. The proposed ARPAP method effectively eliminates the positioning error due to the antenna directivity which has not been considered in conventional lateration system model.

2) Comparison with Gauss-Newton Method:

For completeness, the Gauss-Newton solution (GN) for the ARPAP (GN-ARPAP) is derived in Appendix D. Because the solution provided in [46] is specific for WSN.

Table 1 and Table 2 compare the averaged error (averaged over Ω_y° = 0°, 10°, 25°, 30°) of the proposed ARPAP and GN method. Overall, the proposed ARPAP is 40% more accurate than GN based approach. GN method finds MT position by minimizing the cost function which is the squared difference between path loss model and range measurement. Since it objects at optimizing deterministic function (cost function), GN method is sensitive to noise. On the contrary, the Taylor based method find the solution by expanding the ESP model and minimizing the measurement error. The Taylor-ARPAP is more suitable for the practical noising application.

Table 1. Comparison of Positioning Accuracy
(Based on RSS Measurements)

K-ratio	**P.M.**[1] **Avg. Err.**[2] (m)	**GN Avg. Err.**[2] (m)	**P.M/GN Imprv.**
100	32.37	56.14	42.34
50	56.79	89.25	36.37
10	230.02	307.22	25.13

In addition, Table 1 and Table 2 show that, positioning error increases with the NLoS signal components (i.e. the K-ratio decreases). Based on LOS estimation, the NLoS component is suppressed from fading signal, ARPAP can reduce positioning error caused by environment.

7.2. Error Model Validation. In this section, we validate the proposed ARPAP error model by simulation. Pearson correlation coefficient [30][31] is used to evaluate the similarity between the analytical model and simulation results.

Table 2. Comparison of Positioning Accuracy
(Based on LoS Measurements)

K-ratio	**P.M.**[1] **Avg. Err.**[2] (m)	**GN Avg. Err.**[2] (m)	**P.M/GN Imprv.** (%)
100	15.54	29.77	47.82
50	21.13	36.81	42.61
10	45.16	65.96	31.54

1. P.M.: Proposed Method
2. Avg. Err.: Averaged over Ω_y=0°, 10°, 25°, 30°.

Table 3 (RSS) and Table 4 (LOS) summarize the averaged error of the simulation results and the similarity scores. The overall average similarity score between simulation and analytical model for RSS- and LOS- ARPAP is +0.79 and +0.75 respectively. They indicate a high similarity [31], thus, validating the proposed error model.

Table 3. Similarity Between Error Model and Simulation (RSS)

K-ratio	**Avg. Err.**[1] **(Simulation)** (m)	**Avg. Err.** [1] **(Model)** (m)	**Similarity**
100	32.37	22.43	+0.79
50	56.79	44.52	+0.80
10	230.03	213.83	+0.76

Table 4. Similarity Between Error Model and Simulation (LoS)

K-ratio	**Avg. Err.**[1] **(Simulation)** (m)	**Avg. Err.** [1] **(Model)** (m)	**Similarity**
100	11.54	1.91	+0.84
50	12.33	1.93	+0.80
10	15.62	1.98	+0.81

1. Avg. Err.: Averaged over Ω_y=0°, 10°, 25°, 30°.

Fig. 9 and Fig. 10 show the representative RSS- and LOS- ARPAP results for K-ratio equals to 100 and Ω_y equals to 10°. The averaged positioning errors in the simulation are above the analytical model and vary in correspondence with the model prediction. The

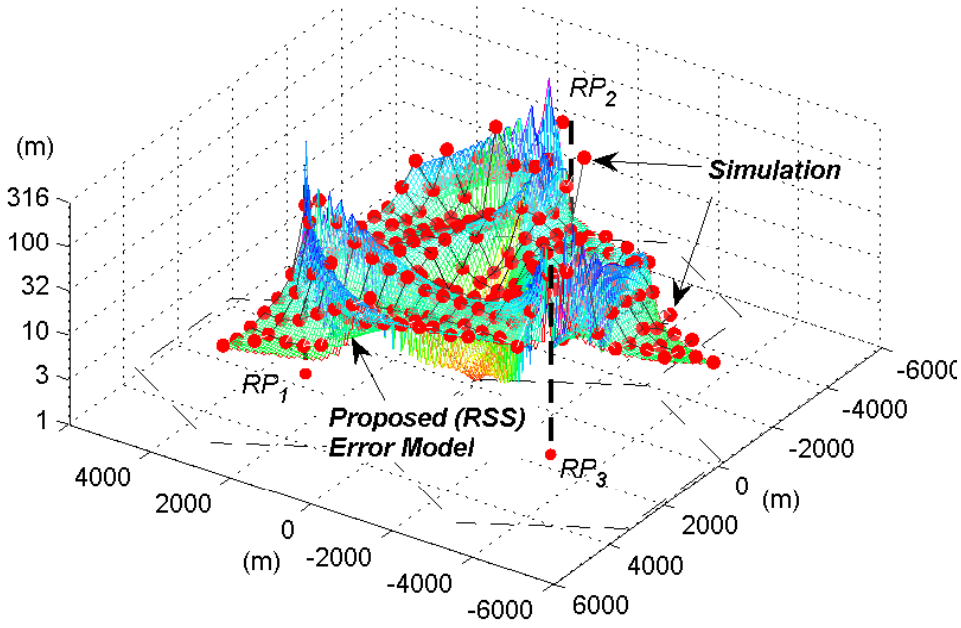

Figure 9. Validation, RSS, $K = 100$, $\Omega_y = 10°$

similarity score between simulation result and the model is +0.82% and +0.80 respectively. Due to the residuals in the LOS component estimation, in Fig. 10, the positioning error of simulation results is higher than what error model predicted. Since the analytical positioning error model is derived based on the analytic bias and CRB. The derived CRB provides a lower bound of positioning variance that the best power based positioning method can achieve.

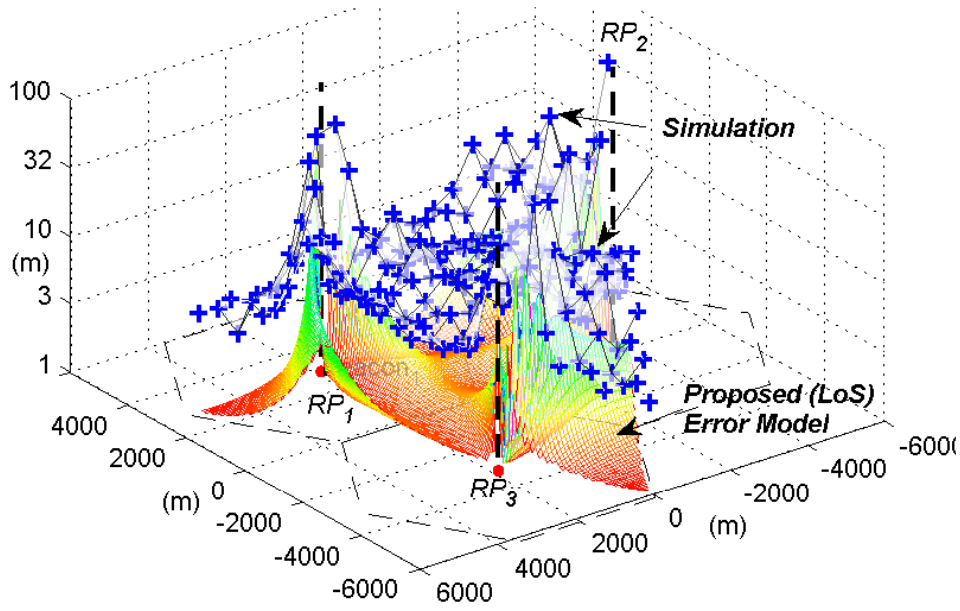

Figure 10. Validation, LoS, $K = 100$, $\Omega_y = 10°$

7.3. RSS-ARPAP vs. LoS-ARPAP. Table 5 summarizes the simulation results and error model prediction of RSS-ARPAP and LOS-ARPAP. The accuracy of LOS-ARPAP is superior to RSS one over all the conditions (environmental K-ratio and receiving antenna orientation). Fig. 11 shows a representative positioning error for K-ratio is equal to 50 and $\Omega_y = 10°$. The analytical model (the curved surface) and the simulation results of the LOS-ARPAP are below that of the RSS one. The LOS component estimation suppressed the environmental fading effect on the positioning result. On average, the LOS-based positioning method improves the accuracy by 65%.

Both simulation and analytic model indicate an increasing in the RSS- and the LOS-based positioning error with environmental fading (i.e. K-ratio decrease). Because NLoS components in the fading signal add uncertainty and bias to the power measurements [27]. However, by using the LOS component estimation, fading effect is suppressed. Hence accuracy is improved. The LOS-based method shows an efficiency increase in improving the accuracy with the environmental fading (i.e. from 53% to 80% as K from 100 to 10).

Table 5. Comparison of RSS- and LoS-based Positioning Accuracy

K-ratio	Mobile Ant. (Ω_y)	RSS		LoS		LoS/RSS Imprv.
		Err. Model (m)	Simulation (m)	Err. Model (m)	Simulation (m)	
100	0	21.99	25.86	1.91	11.54	55.4%
	10	21.98	26.70	1.93	12.33	53.8%
	25	22.79	34.81	1.96	15.62	55.1%
	30	22.94	42.11	1.96	22.66	46.2%
50	0	43.64	49.79	2.72	16.81	66.2%
	10	43.64	51.78	2.74	18.60	64.1%
	25	45.25	59.77	2.77	21.54	64.0%
	30	45.55	65.81	2.78	27.55	58.1%
10	0	209.6	214.67	6.21	41.10	80.9%
	10	209.6	222.22	6.28	39.71	82.1%
	25	217.33	238.67	6.36	45.76	80.8%
	30	218.8	244.45	6.37	54.07	77.9%

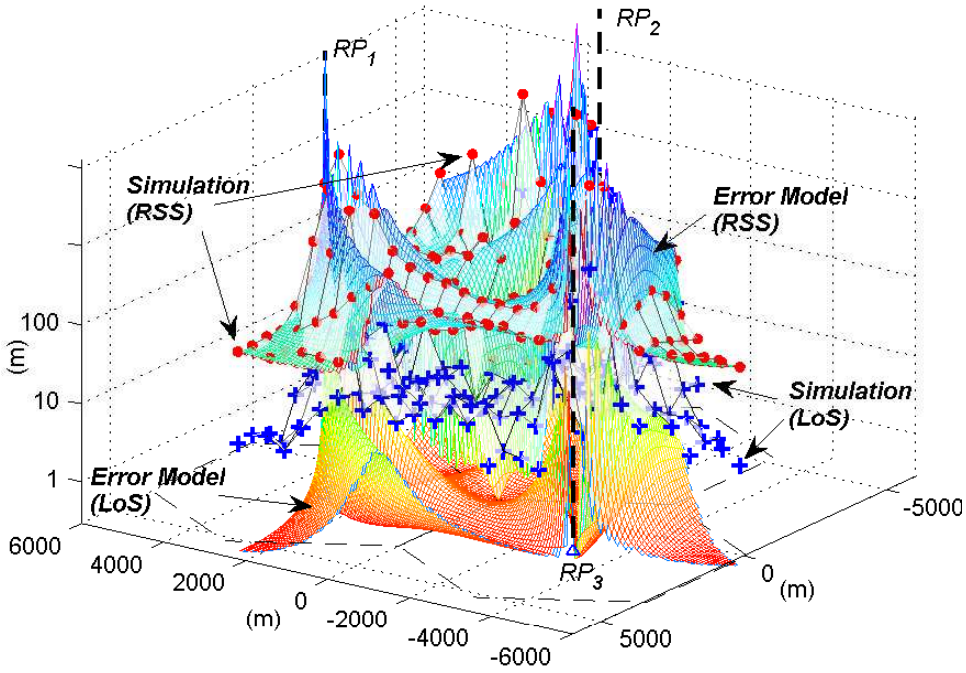

Figure 11. LoS vs. RSS power based positioning. $K = 50$, $\Omega_y = 10°$

Additionally, from Table 5 we find that, on each environmental case (each K-ratio), both of the positioning and error model predicted error increases with the changing of receiving antenna orientation (Ω_y diverges from 0°). Since the none of the dipole antenna

radiation pattern is in the direction of $\pm Z$-axis (body frame), as Ω_y diverges from 0°, the none heads down. The power measurement noise is magnified in the projected direction on the inertial azimuth plane.

8. CONCLUSION

The proposed ARPAP scheme provides a cost-effective augmenting solution to the GNSS. Simulation results show that ARPAP effectively eliminates the position estimation error due to the antenna directivity (overall accuracy improved by 98% comparing to conventional lateration method). And, it is robust for positioning application based on noised signal power measurement and is 40% improved accurate over Gaussian-Newton method. Simulation results validate the derived error model. The Pearson correlation coefficient shows a high similarity between the proposed error model and simulation results. The similarity score is +0.75 up on average. Furthermore, we show that by decomposing LoS and NLoS component in the fading signal, environment introduced positioning bias can be suppressed. On average, LOS-ARPAP is 65% more accurate than the positioning results based on RSS measurements.

ARPAP though accurate, cannot be used alone to replace GNSS. Hence, future work should include integration with other sensors, such as inertial measurement unit (IMU) and light detection and ranging (LiDAR).

9. APPENDIX

9.1. Antenna Directivity Effect on Power Measurement Variation. Conventional lateration methods applied in non-isotropic antenna scenario will magnify the power measurement noise directionally.

Let P_c denotes the conventional *empirical path loss model*, i.e., $P_c = \kappa/d^n$. Then, $P_{EPS} = QP_c$, where Q is the anteena factor (5). The power measurement $\tilde{p}$ with noise of standard deviation σ is,

$$\tilde{p} = p_{ESP} + \sigma. \tag{58}$$

Since P_c omit the antenna directivity Q, we have $Q^{-1}\tilde{p} = p_c + Q^{-1}\sigma$, where p_c represents the power measurement in conventional *empirical path loss model*.

Thus, the power measurements are factored by Q^{-1}, and the corresponding variance is factored by $Q^{-2}(Q \leq 1)$, i.e.,

$$p_c = Q^{-1}\tilde{p} + Q^{-1}\sigma. \tag{59}$$

Hence, to apply the traditional lateration methods in non-isotropic antenna scenario, the localization error in terms of bias and variance are both greater than for ARPAP.

9.2. Frame of Reference.

9.2.1. Orientation. A notation system of leading superscripts and subscripts in [57] is adopted to denote the relative frames of orientations. An arbitrary orientation of inertial frame "E" relative to MT body frame "M" can be achieved through a rotation of Euler angle set $[\Omega_z, \Omega_y, \Omega_x]^T$. The rotation matrix ${}^M_E\boldsymbol{R}$ defined by equation (60), describe the orientation of frame E relative to frame M.

$${}^M_E\boldsymbol{R} = \boldsymbol{R}_{\Omega_z}\boldsymbol{R}_{\Omega_y}\boldsymbol{R}_{\Omega_x}. \tag{60}$$

where, $\boldsymbol{R}_{\Omega_z} = \begin{bmatrix} cos\Omega_z & -sin\Omega_z & 0 \\ sin\Omega_z & cos\Omega_z & 0 \\ 0 & 0 & 1 \end{bmatrix}$, $\boldsymbol{R}_{\Omega_y} = \begin{bmatrix} cos\Omega_y & 0 & sin\Omega_y \\ 0 & 1 & 0 \\ -sin\Omega_y & 0 & cos\Omega_y \end{bmatrix}$,

$\boldsymbol{R}_{\Omega_x} = \begin{bmatrix} 1 & 0 & 0 \\ 0 & cos\Omega_x & -sin\Omega_x \\ 0 & sin\Omega_x & cos\Omega_x \end{bmatrix}$.

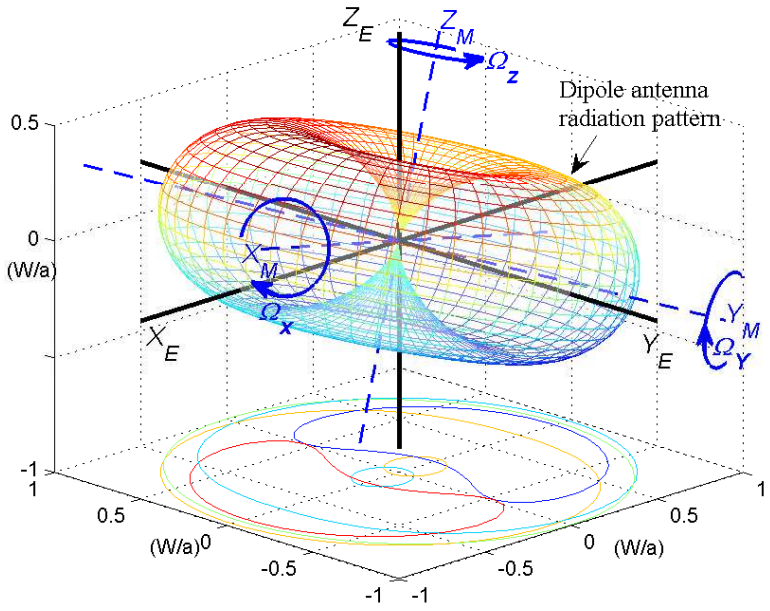

Figure 12. Orientation

9.2.2. Coordinate System for Antenna Analysis. Antenna radiation pattern represents the distribution of radiated energy from an antenna over a surface of constant radius centered upon the antenna. Fig. 13 shows the spherical coordinate system that is used for antenna analysis. Elevation plane angle α is the angle between the z-axis and the vector from the origin to the point (ranges from 0^o to 180^o). Azimuth plane angle φ is the angle between the x-axis and the projection of the point onto the x-y plane (ranges from 0^o to 360^o).

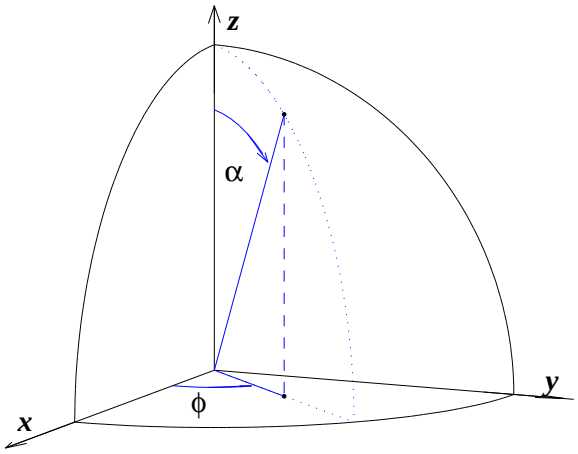

Figure 13. Coordinate System for Antenna Analysis

9.3. Antenna Directivity and Empirical Spatial-pathloss Example. The antenna directivity function ($F(\varphi, \alpha)$) can be found either by derivation from the electric current (e.g. half-wave dipole antenna [40]) or from antenna pattern specifications and manuals (e.g. [58, 59]). An example of a power map applying the proposed ESP model is given in this appendix.

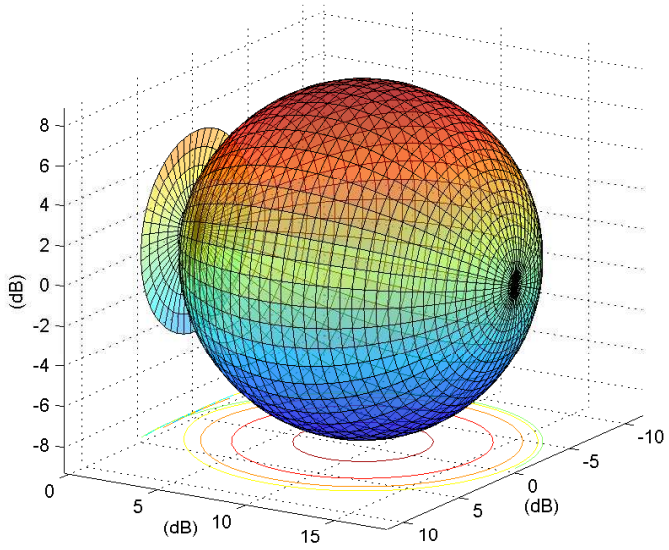

Figure 14. Restored Directivity of 3-Sector Antenna in cellular Network

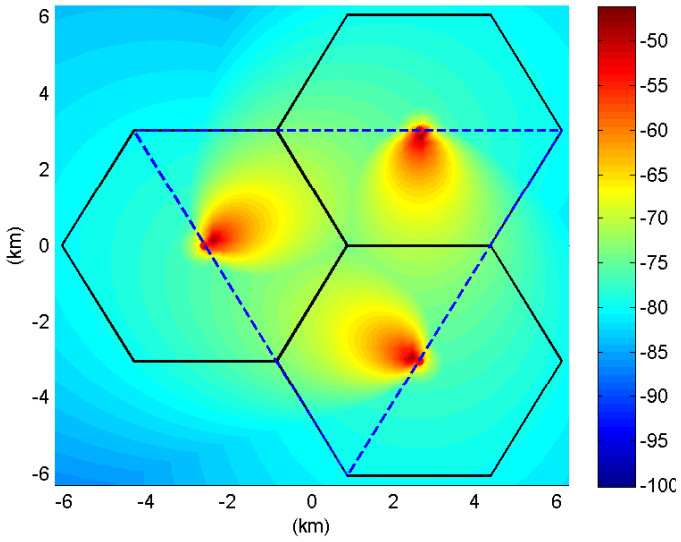

Figure 15. Spatial-Pathloss Power Map (dBm)

In this example, a 3-sector antenna with parameters specified in [52] (half power beam width $\varphi = 70°$, front back ratio (maximum attenuation) $FBR_h = 20dB$, maximum gain $G_m = 18dbi$) is restored as in Fig. 14. For simplicity , assume the vertical antenna gain in the space of interest is 1 [60].

Based on empirical spatial-pathloss model, a map of the signal power that impinge on the receiver antenna is shown in Fig 15. (Assume $\kappa = -18.52dBm$, antenna height is $10(m)$)

9.4. Gauss-Newton Position Estimation. The position can be found by minimizing a cost function,

$$f_{\text{cost}} = \sum_{k=1}^{M} \left\| d_k(\hat{\mathbf{x}}) - \tilde{d}_k \right\|. \tag{61}$$

where $d_k(\hat{\mathbf{x}}) = g(\hat{\mathbf{x}}, \mathbf{x}_k)$ is the range distance from $\hat{\mathbf{x}}$ to the k^{th} reference position, and $\tilde{d}_k$ is a function of power estimation θ_k.

$$\tilde{d}_k = \left(\kappa e^{\gamma G_t(\varphi_t, \alpha_t)} e^{\gamma G_r(\varphi_r, \alpha_r)} \theta_k^{-1} \right)^{1/n}. \tag{62}$$

In Gauss-Newton method, the noise is assumed to be negligible [46], the optimization method is recursively correcting the position guess as,

$$\hat{\mathbf{x}}^{(l+1)} = \hat{\mathbf{x}}^{(l)} - \left(\left[\mathbf{J}^{(l)} \right]^T \mathbf{J}^{(l)} \right)^{-1} \left[\mathbf{J}^{(l)} \right]^T \mathbf{D}_{\mathbf{d}}{}^{(l)}. \tag{63}$$

where superscript l represents the recursive index, $\boldsymbol{D}_d = \mathbf{d} - \tilde{\mathbf{d}}$ with $\mathbf{d} = [\mathbf{d_1}, \mathbf{d_2}, \cdots, \mathbf{d_M}]^{\mathbf{T}}$ and $\tilde{\mathbf{d}} = [\tilde{d}_1, \tilde{d}_2, \cdots, \tilde{d}_M]^T$, and

$$\mathbf{J} = \nabla \mathbf{d} - \nabla \tilde{\mathbf{d}}. \tag{64}$$

where $[\nabla \mathbf{d}]_i = \left[\frac{\partial}{\partial x} d_i, \frac{\partial}{\partial y} d_i \right]$ and $[\nabla \tilde{\mathbf{d}}]_i = \left[\frac{\partial}{\partial x} \tilde{d}_i, \frac{\partial}{\partial y} \tilde{d}_i \right]$, with

$$\begin{cases} \frac{\partial}{\partial x} d_{R,i} = \frac{x - x_i}{d_{R,i}} \\ \frac{\partial}{\partial y} d_{R,i} = \frac{y - y_i}{d_{R,i}} \end{cases}. \tag{65}$$

$$\begin{cases} \frac{\partial}{\partial x} \tilde{d}_{R,i} = \frac{\gamma}{n} \left[\frac{\partial}{\partial x} G_{t,i} + \frac{\partial}{\partial x} G_{r,i} \right] \\ \frac{\partial}{\partial y} \tilde{d}_{R,i} = \frac{\gamma}{n} \left[\frac{\partial}{\partial y} G_{t,i} + \frac{\partial}{\partial y} G_{r,i} \right] \end{cases}. \tag{66}$$

REFERENCES

[1] Pratap Misra and Per Enge. *Global positioning system: signals, measurements, and performance*. Ganga-Jamuna Press, 2006. ISBN 978-0-9709544-1-1.

[2] B. Lubbers, S. Mildner, P. Oonincx, and A. Scheele. A study on the accuracy of GPS positioning during jamming. In *2015 International Association of Institutes of Navigation World Congress (IAIN)*, pages 1–6, October 2015. doi: 10.1109/IAIN.2015.7352258.

[3] Q. Li, D. Xu, W. Wang, X. Wang, and Z. Han. Anti-jamming scheme for GPS receiver with vector tracking loop and blind beamformer. *Electronics Letters*, 50(19): 1386–1388, September 2014. ISSN 0013-5194. doi: 10.1049/el.2014.2274.

[4] M. L. Psiaki, T. E. Humphreys, and B. Stauffer. Attackers can spoof navigation signals without our knowledge. Here's how to fight back GPS lies. *IEEE Spectrum*, 53(8): 26–53, August 2016. ISSN 0018-9235. doi: 10.1109/MSPEC.2016.7524168.

[5] N. Carson, S. M. Martin, J. Starling, and D. M. Bevly. GPS spoofing detection and mitigation using Cooperative Adaptive Cruise Control system. In *2016 IEEE Intelligent Vehicles Symposium (IV)*, pages 1091–1096, June 2016. doi: 10.1109/IVS.2016.7535525.

[6] Richard Klukas and Michel Fattouche. Line-of-sight angle of arrival estimation in the outdoor multipath environment. *Vehicular Technology, IEEE Transactions on*, 47(1): 342–351, 1998.

[7] S. Sakagami, S. Aoyama, K. Kuboi, S. Shirota, and Akira Akeyama. Vehicle position estimates by multibeam antennas in multipath environments. *IEEE Transactions on Vehicular Technology*, 41(1):63–68, February 1992. ISSN 0018-9545. doi: 10.1109/25.120146.

[8] V. Thotla, M. J. Zawodniok, S. Jagannathan, M. T. A. Ghasr, and S. Agarwal. Detection and Localization of Multiple R/C Electronic Devices Using Array Detectors. *IEEE Transactions on Instrumentation and Measurement*, 64(1):241–251, January 2015. ISSN 0018-9456. doi: 10.1109/TIM.2014.2331432.

[9] James Caffery and Gordon L Stuber. Subscriber location in cdma cellular networks. *Vehicular Technology, IEEE Transactions on*, 47(2):406–416, 1998.

[10] H. Shen, Z. Ding, S. Dasgupta, and C. Zhao. Multiple Source Localization in Wireless Sensor Networks Based on Time of Arrival Measurement. *IEEE Transactions on Signal Processing*, 62(8):1938–1949, April 2014. ISSN 1053-587X. doi: 10.1109/TSP.2014.2304433.

[11] Ismail Guvenc and Chia-Chin Chong. A survey on toa based wireless localization and nlos mitigation techniques. *Communications Surveys & Tutorials, IEEE*, 11(3): 107–124, 2009.

[12] Ali H Sayed, Alireza Tarighat, and Nima Khajehnouri. Network-based wireless location: challenges faced in developing techniques for accurate wireless location information. *Signal Processing Magazine, IEEE*, 22(4):24–40, 2005.

[13] IEEE Draft Amendment Standard for Local and Metropolitan Area Networks - Part 16: Air Interface for Broadband Wireless Access Systems - Advanced Air Interface. *IEEE P802.16m/D9, October 2010*, pages 1–1156, October 2010.

[14] I.T. Haque and C. Assi. Profiling-Based Indoor Localization Schemes. *IEEE Systems Journal*, 9(1):76–85, March 2015. ISSN 1932-8184. doi: 10.1109/JSYST.2013.2281257.

[15] Kamin Whitehouse, Chris Karlof, and David Culler. A practical evaluation of radio signal strength for ranging-based localization. *ACM SIGMOBILE Mobile Computing and Communications Review*, 11(1):41–52, 2007. URL http://dl.acm.org/citation.cfm?id=1234829.

[16] J. Kang, D. Kim, and Y. Kim. RSS Self-calibration Protocol for WSN Localization. In *2007 2nd International Symposium on Wireless Pervasive Computing*, February 2007. doi: 10.1109/ISWPC.2007.342597.

[17] Ralph O Schmidt. Multiple emitter location and signal parameter estimation. *Antennas and Propagation, IEEE Transactions on*, 34(3):276–280, 1986.

[18] Moustafa M Abdalla, Mostafa B Abuitbel, and Mohamed A Hassan. Performance evaluation of direction of arrival estimation using music and esprit algorithms for mobile communication systems. In *Wireless and Mobile Networking Conference (WMNC), 2013 6th Joint IFIP*, pages 1–7. IEEE, 2013.

[19] M. Bocca, O. Kaltiokallio, N. Patwari, and S. Venkatasubramanian. Multiple Target Tracking with RF Sensor Networks. *IEEE Transactions on Mobile Computing*, 13(8): 1787–1800, August 2014. ISSN 1536-1233. doi: 10.1109/TMC.2013.92.

[20] Yang Zhao and N. Patwari. Robust Estimators for Variance-Based Device-Free Localization and Tracking. *IEEE Transactions on Mobile Computing*, 14(10):2116–2129, October 2015. ISSN 1536-1233. doi: 10.1109/TMC.2014.2385710.

[21] M.R. Gholami, R.M. Vaghefi, and E.G. Strom. RSS-Based Sensor Localization in the Presence of Unknown Channel Parameters. *IEEE Transactions on Signal Processing*, 61(15):3752–3759, August 2013. ISSN 1053-587X. doi: 10.1109/TSP.2013.2260330.

[22] Andrea Zanella and Andrea Bardella. Rss-based ranging by multichannel rss averaging. *Wireless Communications Letters, IEEE*, 3(1):10–13, 2014.

[23] A. Coluccia and F. Ricciato. RSS-Based Localization via Bayesian Ranging and Iterative Least Squares Positioning. *IEEE Communications Letters*, 18(5):873–876, May 2014. ISSN 1089-7798. doi: 10.1109/LCOMM.2014.040214.132781.

[24] Ka Wai Cheung, Hing-Cheung So, W-K Ma, and Yiu-Tong Chan. A constrained least squares approach to mobile positioning: algorithms and optimality. *EURASIP journal on applied signal processing*, 2006:150–150, 2006.

[25] Lei Wang and Maciej Zawodniok. Rssi-based localization in cellular networks. In *Local Computer Networks Workshops (LCN Workshops), 2012 IEEE 37th Conference on*, pages 820–826. IEEE, 2012.

[26] S. Tomic, M. Beko, and R. Dinis. RSS-Based Localization in Wireless Sensor Networks Using Convex Relaxation: Noncooperative and Cooperative Schemes. *IEEE Transactions on Vehicular Technology*, 64(5):2037–2050, May 2015. ISSN 0018-9545. doi: 10.1109/TVT.2014.2334397.

[27] L. Wang and M. Zawodniok. Bias and CRB Analysis of LoS-based and RSS-based Ranging Methods. *IEEE Transactions on Vehicular Technology*, PP(99):1–1, 2016. ISSN 0018-9545. doi: 10.1109/TVT.2016.2518166.

[28] Martin Sauter. *From GSM to LTE: an introduction to mobile networks and mobile broadband*. John Wiley & Sons, 2010.

[29] Lei Wang and Maciej J Zawodniok. New Theoretical Limit Analysis of LoS and RSS Based Positioning Methods for Ricean Fading Channel in RF Systems. *IEEE Transactions on Vehicular Technology*, page submitted on, April 2016. URL submittedonApril2016.

[30] Lee J Bain and Max Engelhardt. *Introduction to probability and mathematical statistics*, volume 4. Duxbury Press Belmont, CA, 1992.

[31] Robert G. Malgady and David E. Krebs. Understanding correlation coefficients and regression. *Physical therapy*, 66(1):110–120, 1986. URL http://ptjournal.apta.org/content/66/1/110.short.

[32] J. Werner, J. Wang, A. Hakkarainen, D. Cabric, and M. Valkama. Performance and Cramer-Rao Bounds for DoA/RSS Estimation and Transmitter Localization Using Sectorized Antennas. *IEEE Transactions on Vehicular Technology*, PP(99):1–1, 2015. ISSN 0018-9545. doi: 10.1109/TVT.2015.2445317.

[33] I.T. Haque and C. Assi. Profiling-Based Indoor Localization Schemes. *IEEE Systems Journal*, 9(1):76–85, March 2015. ISSN 1932-8184. doi: 10.1109/JSYST.2013.2281257.

[34] Bang Wang, Shengliang Zhou, Wenyu Liu, and Yijun Mo. Indoor Localization Based on Curve Fitting and Location Search Using Received Signal Strength. *IEEE Transactions on Industrial Electronics*, 62(1):572–582, January 2015. ISSN 0278-0046. doi: 10.1109/TIE.2014.2327595.

[35] J. Werner, Jun Wang, A. Hakkarainen, M. Valkama, and D. Cabric. Primary user DoA and RSS estimation in cognitive Radio networks using sectorized antennas. In *2013 8th International Conference on Cognitive Radio Oriented Wireless Networks (CROWNCOM)*, pages 43–48, July 2013. doi: 10.1109/CROWNCom.2013.6636792.

[36] R.G. Stansfield. Statistical theory of d.f. fixing. *Journal of the Institution of Electrical Engineers - Part IIIA: Radiocommunication*, 94(15):762–770, March 1947. doi: 10.1049/ji-3a-2.1947.0096.

[37] Jun Wang, Jianshu Chen, and Danijela Cabric. Cramer-Rao Bounds for Joint RSS/DoA-Based Primary-User Localization in Cognitive Radio Networks. *IEEE Transactions on Wireless Communications*, 12(3):1363–1375, March 2013. ISSN 1536-1276. doi: 10.1109/TWC.2013.012513.120966.

[38] Richard Roy and Thomas Kailath. Esprit-estimation of signal parameters via rotational invariance techniques. *Acoustics, Speech and Signal Processing, IEEE Transactions on*, 37(7):984–995, 1989.

[39] Harald T Friis. A note on a simple transmission formula. *proc. IRE*, 34(5):254–256, 1946.

[40] Constantine A. Balanis. *Antenna Theory: Analysis and Design*. John Wiley & Sons, December 2012. ISBN 978-1-118-58573-3.

[41] Veljo Otsason, Alex Varshavsky, Anthony LaMarca, and Eyal De Lara. Accurate gsm indoor localization. In *UbiComp 2005: Ubiquitous Computing*, pages 141–158. Springer, 2005.

[42] Heikki Laitinen, Jaakko Lahteenmaki, and Tero Nordstrom. Database correlation method for gsm location. In *Vehicular Technology Conference, 2001. VTC 2001 Spring. IEEE VTS 53rd*, volume 4, pages 2504–2508. IEEE, 2001.

[43] A.J. Fenwick. Algorithms for position fixing using pulse arrival times. *Radar, Sonar and Navigation, IEE Proceedings* -, 146(4):208–212, August 1999. ISSN 1350-2395. doi: 10.1049/ip-rsn:19990538.

[44] C. Mensing and S. Plass. Positioning Algorithms for Cellular Networks Using TDOA. In *2006 IEEE International Conference on Acoustics, Speech and Signal Processing, 2006. ICASSP 2006 Proceedings*, volume 4, pages IV–IV, May 2006. doi: 10.1109/ICASSP.2006.1661018.

[45] J.C. Chen, R.E. Hudson, and K. Yao. Maximum-likelihood source localization and unknown sensor location estimation for wideband signals in the near-field. *IEEE Transactions on Signal Processing*, 50(8):1843–1854, August 2002. ISSN 1053-587X. doi: 10.1109/TSP.2002.800420.

[46] M.K. Mwila, K. Djouani, and A. Kurien. An efficient approach to node localisation and tracking in wireless sensor networks. In *2014 IEEE Global Communications Conference (GLOBECOM)*, pages 492–497, December 2014. doi: 10.1109/GLOCOM.2014.7036856.

[47] W.H. Foy. Position-Location Solutions by Taylor-Series Estimation. *IEEE Transactions on Aerospace and Electronic Systems*, AES-12(2):187–194, March 1976. ISSN 0018-9251. doi: 10.1109/TAES.1976.308294.

[48] Andrea Goldsmith. *Wireless Communications*. Cambridge University Press, August 2005. ISBN 978-1-139-44584-9.

[49] Matthias Patzold. *Mobile fading channels*. John Wiley & Sons, Inc., 2003.

[50] S.M. Kay. *Fundamentals of Statistical Signal Processing: Estimation theory*. Fundamentals of Statistical Signal Processing. Prentice-Hall PTR, 1993. ISBN 9780133457117. URL http://books.google.com/books?id=aFwESQAACAAJ.

[51] Broadcast Bands. FEDERAL COMMUNICATIONS COMMISSION 47 CFR Parts 0 and 15. 2010. URL http://www.apwpt.org/downloads/unlicensed-operation-in-the-tv-broadcast12-06-.pdf.

[52] 3gpp specification: 25.996, . URL http://www.3gpp.org/DynaReport/25996.htm.

[53] F. Gunnarsson, M.N. Johansson, A. Furuskar, M. Lundevall, A. Simonsson, C. Tidestav, and M. Blomgren. Downtilted Base Station Antennas - A Simulation Model Proposal and Impact on HSPA and LTE Performance. In *Vehicular Technology Conference, 2008. VTC 2008-Fall. IEEE 68th*, pages 1–5, September 2008. doi: 10.1109/VETECF.2008.49.

[54] Cheng Guan Koay and Peter J Basser. Analytically exact correction scheme for signal extraction from noisy magnitude mr signals. *Journal of Magnetic Resonance*, 179(2): 317–322, 2006.

[55] Chengshan Xiao, Yahong Rosa Zheng, and Norman C Beaulieu. Novel sum-of-sinusoids simulation models for rayleigh and rician fading channels. *Wireless Communications, IEEE Transactions on*, 5(12):3667–3679, 2006.

[56] 3gpp specification: 45.004, . URL http://www.3gpp.org/DynaReport/45004.htm.

[57] John J. Craig. *Introduction to Robotics: Mechanics and Control*. Pearson, Upper Saddle River, N.J, 3 edition edition, August 2004. ISBN 978-0-201-54361-2.

[58] Ingo Lütkebohle. Connected Grid Antennas Installation Guide - Cisco. http://www.cisco.com/c/en/us/td/docs/routers/connectedgrid/antennas/\\installing/cg_antenna_install_guide.html, 2015. [Online; accessed 13-May-2015].

[59] Kathrein K 742 215. https://www.scribd.com/doc/153359687/Kathrein-K-742-215, 2015. [Online; accessed 7-Dec-2015].

[60] Z. D. Zaharis. Radiation pattern shaping of a mobile base station antenna array using a particle swarm optimization based technique. *Electrical Engineering*, 90(4):301–311, July 2007. ISSN 0948-7921, 1432-0487. doi: 10.1007/s00202-007-0078-y. URL http://link.springer.com/article/10.1007/s00202-007-0078-y.

V. ML ARPAP: THE MAXIMUM LIKELIHOOD BASED ANTENNA RADIATION-PATTERN-AWARE POWER-BASED POSITIONING IN RF SYSTEM

L. Wang and M. J. Zawodniok

Department of Electronic & Computer Engineering

Missouri University of Science and Technology

Rolla, Missouri 65409–0050

Tel: (409) 692-9235, (573) 341-4361

Email: lw3r6@mst.edu, mjzx9c@mst.edu

ABSTRACT

The antenna directivity and fading effect challenge conventional power-based localization methods. Maultilateration method assumes omnidirectional antenna radiation pattern such that circular power contours can be employed for position estimation. However, in the practical wireless communication systems, directional antennas are adopted. It results in noncircular power contours. Therefore, significant localization errors will be introduced when using the conventional multilateration. In this paper, a maximum likelihood estimation approach — ML ARPAP — is proposed for power-based positioning in the non-isotropic antenna employed system. A power contour circle fitting (PCCF) algorithm is proposed for obtaining the initial position guess for the ML ARPAP. Numerical results show that the proposed algorithm achieves accurate localization result, and effectively suppresses the error introduced by varying the orientation of a mobile device. Also, it is robust to environmental fading disturbance.

Keywords: Localization; Received Signal Strength; Line of Sight; Antenna Radiation Pattern.

1. INTRODUCTION

Locating people and objects has become a fundamental requirement in many practical applications, for example, the advanced driver assistance systems (ADAS), robotics, healthcare, security, geographical routing, etc. The most widely-used global navigation satellite systems (GNSS) could provide accurate position estimation given the presence of strong line-of-sight (LoS) satellite signal. However, satellites coverage and relative position, interference, and malicious jamming or spoofing can degrade its accuracy [1, 2, 3]. Therefore, a augmenting solution that can alleviate the GNSS deficiency is required. The ideal one would be using the existing wireless networks, such as the cellular network, WiFi access points, wireless sensor network (WSN).

Received signal strength (RSS) [4, 5, 6] is prefered due to its low complexity and hardware requirements. Other technologies include Time-of-arrival (TOA)[7, 8], time-difference-of-arrival (TDoA)[9, 10, 11], angle-of-arrival (AOA) [12, 13, 14], all of which require costly, dedicated infrastructure. Although, TOA-based systems require high-precision timing and synchronization components. TDoA-based systems relax the synchronization requirement while requiring either a sliding correlator or a matched filter [10]. AOA-based systems require antenna array; and its accuracy is proportional to the number of elements [15][16]. In contrast, Received Signal Strength Indicator (RSSI) is available in most of the commercial off-the-shelf radio transceivers [17, 18, 19, 20].

Lateration and fingerprinting are the two main RSS-based localization techniques. Fingerprinting methods require onerous offline pre-building and periodical fingerprint database calibration for minimizing environment introduced spatial and temporal variance. Besides, its accuracy is determined by the grid size used for calibration and the number of the *reference positions* (RPs) per grid [21].

Multilateration techniques, [22, 23, 24, 25], require minimum system maintenance; however, they suffer from low accuracy for two primary reasons: antenna directivity and multipath fading. First, they assume that the signal power emitted from RP is directional

independent such that *circular* contours (centered at corresponding RP) can be used for positioning. Though reduce the computational complexity and overload, they are sensitive to the radius distance estimation error. Moreover, in practical applications, antenna directivity changes the power radiation pattern from the RP. Thus, the over-relaxed assumption in conventional lateration methods results in a significant positioning error.

Multipath fading from the environment, as the second issue, also introduces bias and variance into the range and position estimation. In the practical multipath environment, the received signal is a superposition result of the original signal (Line-of-sight (LoS) component) and copies of it (No-LoS (NLoS) component) that are reflected, diffracted, and scattered from the environment. Hence, the power measurement can be either weakened or strengthened by the environment. As a result, the range and position estimation are distorted.

In this paper, a novel Maximum Likelihood based Antenna Radiation-Pattern-Aware Power-based positioning (ML ARPAP) method is proposed to address the antenna directivity and fading issue. In contrast to conventional lateration methods, ARPAP system takes account the antenna radiation pattern into the RF signal propagation and attenuation model. The position estimation is obtained by fitting the intersection of several non-circular power contours. Simulation results show that ML ARPAP reduced the antenna directivity introduced localization bias by using the conventional multilateration methods. And, power measurement noise-injected positioning error is further reduced by LOS component estimation.

Maximum likelihood (ML) estimator has the asymptotical efficiency. However, it suffers from initial condition sensitivity and convergence problems. For nonlinear problems, ML does not have a closed-form solution. Also, it requires an appropriate initial value guess. However, due to the high nonlinearity of the ARPAP system introduced by the antenna directivity, existing initial value searching procedures are not feasible.

Projections onto convex set (POCS) - based positioning algorithm in wireless sensor network was first proposed in [26] to solve the convex feasibility problem. In [27][28], the semidefinite programming (SDP) methods were proposed for reducing the complexity of POC based methods. A closed-form approximate solution to the ML equations namely approximate maximum likelihood (AML) algorithm was proposed in [29]. However, existing algorithms are based on the circular contour assumption where the positioning can be easily converted into SDP optimization problem (SDP optimization problem has standard solvers such as SeDuMi[30]). However, in realistic non-isotropic antenna scenario, the distance between Rx and Tx is direction-dependent - both Rx and Tx antenna directivity affect the distance estimation. Although [31] extended the circular-POC to hyperbolic for TDOA, existing POC-based methods are not feasible for the problem encountered in the ARPAP system, where the power contour is RX and Tx antenna radiation pattern (directivity) dependent.

Recently, particle swarm optimization (PSO)- based algorithm was proposed in [32]. However, the computational resource allocated by PSO is larger as the number of particles and area resolution used for searching. Especially, for a larger area, the computational cost would be very high.

In this paper, a power contour circle fit (PCCF) scheme is proposed for initializing the ML ARPAPE. Simulation results show that it effectively prevent nonlinear ML divergence in ARPAP system.

In [33], a gradient optimization (GO) algorithm is proposed. However, it is specifically for wireless sensor network. Besides, relaxed assumptions are made: no noise and unique Tx and Rx antenna directivity.

To the best of the author's knowledge, ARPAP system is the first generalized RF signal power-based localization scheme that takes into account antenna directivities for both transmitter and receiver. Existing methods, e.g. [22, 23, 24, 25], are based on circular power contour assumption and not feasible for the practical scenario that ARPAP can solve.

The rest of the paper is organized as follows. Section 2. presents our proposed ML ARPAPE system and MLE solution. In Section 3. the proposed PCCF algorithm is present. Section 4 instantiates the proposed scheme in the Cellular network. In Section 5., we validated the proposed method by simulation. The paper is concluded in Section 6.

2. THE ML ARPAPE

2.1. Overview. The proposed ML ARPAP system finds the mobile transceiver (MT) location by minimizing the weighted mean square error of power measurements and location (13). First, we propose the power contour circle fitting (PCCF) algorithm to find the initial condition (initial guess of position) to prevent the ML estimation from diverging. PCCF will be introduced in section 3. Next, ML-based accurate positioning is performed. Due to the nonlinearity of the ARPAP system, it is difficult to find the closed-form ML position estimator. Hence, an iterative Newton-Raphson solution, i.e., the Hessian matrix and gradient vector, is proposed in section 2.4.

Fig. 1 shows the overall framework of the system. The LoS component in the received signal is first estimated which helps reduce the environmental multipath fading injected positioning error. The orientation of the MT helps ARPAP system finding the receiver (Rx) and transmitter (Tx) antenna directivity in the direction of interest. The proposed PCCF scheme provides coarse position estimate which is used as the initial position guess for the ML based positioning.

It is worth noting that RSS indication is made readily available from all common wireless transceivers, while, the LOS component has to be estimated from the fading signal which comes from receiver equalizer during the demodulation. The proposed ML ARPAPE system can take either RSS or LOS estimates as the signal measurements depending on the application requirement, i.e., the computational complexity and readiness of the hardware. We derived the MLE for both: RSS and LoS in section 2.4.

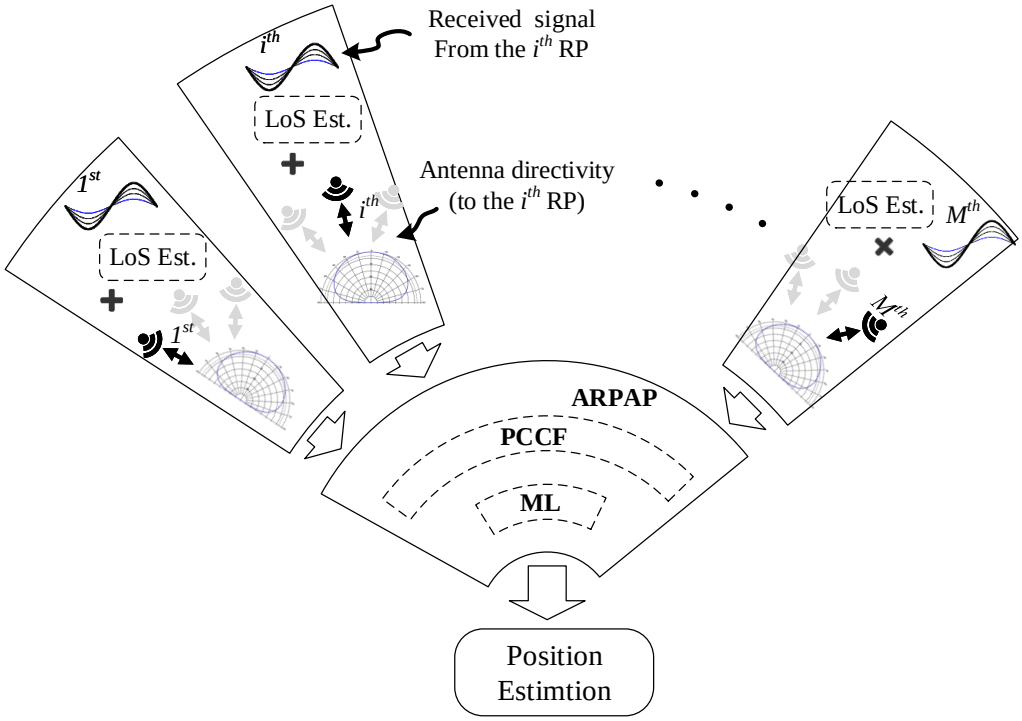

Figure 1. Overview of the proposed scheme

In this section, the ARPAP system model is first introduced. Next, maximum likelihood estimator for ARPAP (ML ARPAPE) is derived. Then, Newton-Raphson recursive solution for ML ARPAPE is derived. Finally, the covariance matrix for both RSS and LoS based positioning is provided.

2.2. ARPAP System Model. In non-isotropic antenna employed radio frequency (RF) system, the received signal power at MT from reference position (RP) is determined not only by the distance but also the antenna directivity. Given MT position $\mathbf{x} = [x, y]^T$, the received signal power can be modeled as,

$$P_r(\mathbf{x}) = \kappa F_t\left(\varphi_t(\mathbf{x}), \alpha_t(\mathbf{x})\right) F_r\left(\varphi_r(\mathbf{x}), \alpha_r(\mathbf{x})\right) / d^n(\mathbf{x}). \tag{1}$$

where, $F_{t(/r)}\left(\varphi_{t(/r)}, \alpha_{t(/r)}\right)$ is the space function in antenna directivity. $\varphi_{t(/r)}$ is the azimuth angle ($-\pi \sim \pi$), $\alpha_{t(/r)}$ is the elevation angle ($0 \sim \pi$) of transmitting (/receiving) antenna (See Appendix A2 for antenna analysis coordinate system). κ is the scale factor in Friis equation [34], which encapsulates the transmitting power, antenna gain, and losses. n is an exponential factor, which varies under different environmental conditions: in free-space, n is equal to 2, in either urban or some suburban areas, n can be between 3 and 6. Assume there are M RPs, each RP is placed at $\mathbf{x}_i = [x_i, y_i]^T$ ($i = 1 \sim M$), the distance from MT to the i^{th} RP is,

$$d(\mathbf{x}) = \sqrt{(x - x_i)^2 + (y - y_i)^2 + h_i^2}. \tag{2}$$

where, h_i represents the relative height.

Replace the receiving power in (1) with power estimation (θ), the ARPAP positioning system is modeled as,

$$\theta = \kappa e^{\gamma G_t(\varphi_t(\hat{\mathbf{x}}),\alpha_t(\hat{\mathbf{x}}))} e^{\gamma G_r(\varphi_r(\hat{\mathbf{x}}),\alpha_r(\hat{\mathbf{x}}))} d^{-n}(\hat{\mathbf{x}}) \tag{3}$$

where $\gamma = \ln(10)/10$, $G_{t/(r)}(\cdot)$ represents the transmitting (/receiving) antenna directivity function in logrithmic (decibel) unit, i.e. $10log_{10}F_{t(/r)}(\cdot) = G(\cdot)$. α is the elevation plane angle, φ represents the azimuth plane angle in spherical coordinates in antenna analysis [35] (see Appendix 7.2.2 for detail).

To reduce computational complexity, we consider the logarithmic version of (3),

$$\xi_i(\hat{\mathbf{x}}) = f(\theta_i) + e_i. \tag{4}$$

where e_k is the measurement error, and,

$$f(\theta) = \ln \theta. \tag{5}$$

$$\xi_k(\hat{\mathbf{x}}) = \ln \kappa + \gamma G_t(\varphi_t(\hat{\mathbf{x}}), \alpha_t(\hat{\mathbf{x}})) + \gamma G_r(\varphi_r(\hat{\mathbf{x}}), \alpha_r(\hat{\mathbf{x}})) - n \ln d. \tag{6}$$

and $\hat{\mathbf{x}} = [\hat{x}, \hat{y}]^T$ is the position estimation.

2.3. LoS Component Estimation. Here, we present the models of both the received signal amplitude and LoS component estimator that are used for deriving the ML ARPAP approach.

In mobile fading channel, the probability density function (PDF) of the envelobe of the channel fading, ρ, follows Ricean distribution [36], and can be expressed as,

$$P_\rho(\varrho) = \frac{2(K+1)\varrho}{\Omega} e^{\left(-K - \frac{(K+1)\varrho^2}{\Omega}\right)} I_0\left(2\varrho\sqrt{\frac{K(K+1)}{\Omega}}\right). \tag{7}$$

where Ω represents the total power, which includes the LoS component, v^2, and NLoS component, σ^2; K represents Ricean factor which is defined as the LoS-to-NLoS power ratio, i.e.$K = v^2/2\sigma^2$; $I_0(\cdot)$ is the modified Bessel function of the first kind.

$$\Omega = v^2 + 2\sigma^2. \tag{8}$$

The n^{th} moments of the Ricean distribution, μ_n [37],

$$\mu_n = \left(\frac{v^2}{2K}\right)^{n/2} 2^{n/2}\Gamma\left(1 + \frac{n}{2}\right) L_{n/2}(-K). \tag{9}$$

where, $L_q(\cdot)$ is laguerre polynomials [38].

The received signal strength indicator (RSSI) measures the total power received at RF client device [39], which is the second moment of Ricean fading, μ_2, which can be calculated as,

$$\hat{\Omega} = \frac{1}{N}\sum_{i=1}^{N} \varrho_i^2. \tag{10}$$

where N is the number of fading signal samples.

The LoS component estimator can be expressed as [40],

$$\widehat{v^2} = \hat{\Omega}\frac{\hat{K}}{1+\hat{K}}. \tag{11}$$

where, $\hat{K}$ is the LoS-to-NLoS K-ratio. We assume that the total power and K-ratio are estimated independently.

The K estimator can be obtained from Koay method [41],

$$\hat{K} = \frac{1}{2}\epsilon^2. \tag{12}$$

where $\epsilon = \sqrt{\xi(\epsilon)\left[1+\frac{\mu_1^2}{\sigma_\varrho^2}\right]-2}$, $\xi(\epsilon)$, σ_ϱ^2 is the variance of fading signal envelope, $\sigma_\varrho^2 = \mu_2 - \mu_1^2$. μ_1 and μ_2 are the first and second moments of the samples of fading signal. An iterative solution for ϵ is given in [41].

2.4. ML ARPAPE. In this section, a general MLE for Antenna Radiation-Pattern-Aware Positioning System is first given in Lemma 22. Next, the Newton-Raphson procedure (for solving for the estimator) and its Hessian matrix and gradient vector are derived in Lemma 23 and Lemma 24, respectively.

Lemma 22. *The MLE of the Antenna Radiation-Pattern-Aware Power-based Positioning System is,*

$$\hat{\mathbf{x}} = \arg\min_{\hat{\mathbf{x}}} \left(\mathbf{r}_\theta - \mathbf{t}_\theta\right)^T \mathbf{C}_\theta^{-1} \left(\mathbf{r}_\theta - \mathbf{t}_\theta\right). \tag{13}$$

where,

$$\mathbf{t}_\theta = \begin{bmatrix} \xi_1(\mathbf{x}) - \frac{1}{2}\mu_{\theta,1}^{-2} AsV(\theta_1) \\ \xi_2(\mathbf{x}) - \frac{1}{2}\mu_{\theta,2}^{-2} AsV(\theta_2) \\ \vdots \\ \xi_M(\mathbf{x}) - \frac{1}{2}\mu_{\theta,M}^{-2} AsV(\theta_M) \end{bmatrix}. \tag{14}$$

$$\begin{aligned} \mathbf{r}_\theta &= [ln\theta_1, ln\theta_2, \cdots, ln\theta_M]^T \\ \mathbf{C}_\theta &= diag\left(\mu_{\theta,1}^{-2} AsV(\theta_1), \mu_{\theta,2}^{-2} AsV(\theta_2), \cdots, \mu_{\theta,M}^{-2} AsV(\theta_M)\right) \end{aligned} \tag{15}$$

And, $AsV(\theta_k)(k = 1 \sim M)$ represents the asymptotic variance of power estimator θ_k, $\mu_{\theta,k} = E[\theta_k]$ is the expectation of the power estimator.

Proof. By Central Limit Theory, the power estimation asymptotically follows normal distribution as,

$$\ln\theta \xrightarrow{N} \mathcal{N}(\mu_{\ln\theta}, AsV(\ln\theta)). \tag{16}$$

Therefore, the expectation of $\ln\theta$ is [42] $\mu_{\ln\theta} = \ln\mu_\theta + (1/2)(\ln\mu_\theta)''_\theta AsV(\theta)$, i.e.,

$$\mu_{\ln\theta} = \ln\mu_\theta - \frac{1}{2}\mu_\theta^{-2} AsV(\theta). \tag{17}$$

and, the variation of $\ln\theta$ is $AsV(\ln\theta) = \left[(\ln\mu_\theta)'_\theta\right]^2 AsV(\theta)$, i.e.,

$$AsV(\ln\theta) = \mu_\theta^{-2} AsV(\theta). \tag{18}$$

where $(\cdot)'_\theta$ and $(\cdot)''_\theta$ represent the first and second derivative operation with respect to (w.r.t.) θ, respectively. Consider $\ln\mu_\theta = \xi(\mathbf{x})$, we have,

$$\ln\theta - \left(\xi(\mathbf{x}) - \frac{1}{2}\mu_\theta^{-2} AsV(\theta)\right) \xrightarrow{N} \mathcal{N}\left(0, \mu_\theta^{-2} AsV(\theta)\right). \tag{19}$$

Assume that the power measurements from the M beacon-MT paths are independent, the multivariate probability density function (PDF) of $\mathbf{r}_\theta$ is,

$$p(\mathbf{r}) = \frac{1}{(2\pi)^{M/2}|\mathbf{C}_\theta|^{1/2}} \exp\left\{-\frac{1}{2}(\mathbf{r}-\mathbf{t})^T \mathbf{C}_\theta^{-1}(\mathbf{r}-\mathbf{t})\right\}.$$

which is equivalent to,

$$\ln[p(\mathbf{r})] = \ln\left(\frac{1}{(2\pi)^{M/2}|\mathbf{C}_\theta|^{1/2}}\right) - \frac{1}{2}(\mathbf{r}-\mathbf{t})^T \mathbf{C}_\theta^{-1}(\mathbf{r}-\mathbf{t}). \tag{20}$$

Remark 6 will show that, for both RSS- and LoS-based positioning, $\mathbf{C}_\theta$ is independent of $\mathbf{x}$. Therefore, to find the maximum likelihood estimator is equivalent to minimize the second part of (20), i.e. (13). □

Lemma 23. *The Newton-Raphson iteration procedure [43, 44] to solve the MLE in (13) is,*

$$\hat{\mathbf{x}}^{(k+1)} = \hat{\mathbf{x}}^{(k)} - \mathbf{H}^{-1}(J_\theta(\hat{\mathbf{x}}^{(k)}))\nabla(J_\theta(\hat{\mathbf{x}}^{(k)})). \tag{21}$$

where $\mathbf{H}(J_\theta(\hat{\mathbf{x}}^{(k)}))$ *and* $\nabla(J_\theta(\hat{\mathbf{x}}^{(k)}))$ *are Hessian matrix and gradient vector computed at the* k^{th} *updating,*

$$\mathbf{H}(J_\theta(\mathbf{x})) = \frac{\partial^2 J_\theta(\mathbf{x})}{\partial \mathbf{x} \partial \mathbf{x}^T}. \tag{22}$$

$$\nabla(J_\theta(\mathbf{x})) = \begin{bmatrix} \frac{\partial J_\theta(\mathbf{x})}{\partial x} & \frac{\partial J_\theta(\mathbf{x})}{\partial y} \end{bmatrix}^T. \tag{23}$$

And, the cost function,

$$J_\theta(\mathbf{x}) = (\mathbf{r}_\theta - \mathbf{t}_\theta)^T \mathbf{C}_\theta^{-1} (\mathbf{r}_\theta - \mathbf{t}_\theta). \tag{24}$$

It is worth noting that the power estimator, θ, can be either the total received power (RSS, $\widehat{\Omega}$), or line-of-sight power component estimates (LoS, $\widehat{v^2}$).

Lemma 24. *The Hessian matrix and gradient vector in the Newton-Raphson procedure are given in (25) and (26), respectively.*

$$\begin{cases} [\mathbf{H}(J_\theta(\mathbf{x}))]_{1,1} = \frac{\partial^2}{\partial x^2} J_\theta(\mathbf{x}) = \sum_{i=1}^{M} \frac{2}{c_{\theta,i}} \left[\left(\frac{\partial}{\partial x} \xi_i(\mathbf{x}) \right)^2 - \left(r_{\theta,i} - \xi_i(\mathbf{x}) + \frac{1}{2} c_{\theta,i} \right) \frac{\partial^2}{\partial x^2} \xi_i(\mathbf{x}) \right] \\ [\mathbf{H}(J_\theta(\mathbf{x}))]_{2,2} = \frac{\partial^2}{\partial y^2} J_\theta(\mathbf{x}) = \sum_{i=1}^{M} \frac{2}{c_{\theta,i}} \left[\left(\frac{\partial}{\partial y} \xi_i(\mathbf{x}) \right)^2 - \left(r_{\theta,i} - \xi_i(\mathbf{x}) + \frac{1}{2} c_{\theta,i} \right) \frac{\partial^2}{\partial y^2} \xi_i(\mathbf{x}) \right] \\ [\mathbf{H}(J_\theta(\mathbf{x}))]_{1,2} = [\mathbf{H}(J_\theta(\mathbf{x}))]_{2,1} \\ = \frac{\partial^2}{\partial x \partial y} J_\theta(\mathbf{x}) = \sum_{i=1}^{M} \frac{2}{c_{\theta,i}} \left[\frac{\partial}{\partial x} \xi_i(\mathbf{x}) \frac{\partial}{\partial y} \xi_i(\mathbf{x}) - \left(r_{\theta,i} - \xi_i(\mathbf{x}) + \frac{1}{2} c_{\theta,i} \right) \frac{\partial^2}{\partial x \partial y} \xi_i(\mathbf{x}) \right] \end{cases}. \tag{25}$$

$$\begin{cases} \frac{\partial}{\partial x} J_\theta(\mathbf{x}) = -\sum_{i=1}^{M} \frac{2}{c_{\theta,i}} \left(r_{\theta,i} - \xi_i(\mathbf{x}) + \frac{1}{2} c_{\theta,i} \right) \frac{\partial}{\partial x} \xi_i(\mathbf{x}) \\ \frac{\partial}{\partial y} J_\theta(\mathbf{x}) = -\sum_{i=1}^{M} \frac{2}{c_{\theta,i}} \left(r_{\theta,i} - \xi_i(\mathbf{x}) + \frac{1}{2} c_{\theta,i} \right) \frac{\partial}{\partial y} \xi_i(\mathbf{x}) \end{cases}. \tag{26}$$

where

$$J_\theta(\mathbf{x}) = \sum_{i=1}^{M} \frac{\left(r_{\theta,i} - \xi_i(\mathbf{x}) + \frac{1}{2}c_{\theta,i}\right)^2}{c_{\theta,i}}. \tag{27}$$

For RSS-based localization,

$$c_{\theta,i}\Big|_{\theta=\widehat{\Omega}} = c_{\widehat{\Omega}}(K_i) = \frac{1+2K_i}{(1+K_i)^2}. \tag{28}$$

For LoS-based localization, $c_{\theta,i}\Big|_{\theta=\widehat{v^2}}$ *is given by,*

$$\begin{aligned} c_{\widehat{v^2}}(K) =& \frac{(1+K)L_{1/2}^2(-K) - \frac{\pi^2}{16}L_{1/2}^4(-K)}{K^2(1+K)^4[\eta'(K)]^2} \\ &+ \frac{\frac{3\pi}{2}L_{1/2}(-K)L_{3/2}(-K) - \pi L_{1/2}^2(-K)(1+K)}{K^2(1+K)^4[\eta'(K)]^2}\left[\frac{K}{1+K} - \frac{\frac{\pi}{4}L_{1/2}^2(-K)}{\eta'(K)(1+K)^3}\right]. \\ &+ \frac{1+2K}{K^3}\left[\frac{K}{1+K} - \frac{\frac{\pi}{4}L_{1/2}^2(-K)}{\eta'(K)(1+K)^3}\right]^2 \end{aligned} \tag{29}$$

with

$$\eta(K) = \frac{\pi L_{1/2}^2(-K)}{4(K+1)} \tag{29}$$

Proof. Here, we derive the Hessian matrix and gradient vector for both RSS-based and LoS-based localization.

RSS ***($\theta = \widehat{\Omega}$):***

In [40], it has been shown that the variance of the total power estimation can be expressed in terms of K and v^2 as,

$$VAR(\widehat{\Omega}) = \frac{1+2K}{K^2}v^4. \tag{30}$$

The expectation of $\ln\theta$, is $\mu_{ln\widehat{\Omega}} = \ln\Omega - \frac{1}{2}\Omega^{-2}AsV(\widehat{\Omega})$. Since the total power (8) can be expressed in terms of LoS signal power and K-ratio as $\Omega = v^2(1 + K^{-1})$, thus,

$$\mu_{ln\widehat{\Omega}} = \ln\Omega - (1/2)c_{\widehat{\Omega}}. \tag{31}$$

where $c_{\widehat{\Omega}}$ is given by (28).

Take (30)(31) into (14)(15), we get the cost function $J_\theta(\mathbf{x})\big|_{\theta=\widehat{\Omega}}$ in (27).

Take the first and second derivation of the cost function, we get Hessian matrix (25) and gradient vector (26), respectively.

LoS ***($\theta = \widehat{v^2}$):***

The asymptotic variance of the LoS component estimation can be expressed as [40],

$$AsV(\widehat{v^2}) = c_\theta|_{\theta=\widehat{v^2}}\, v^4. \tag{32}$$

where $c_{\widehat{v^2}}$ is given by (29).

The expectation of $\ln\theta$, (17), becomes,

$$\mu_{lnv^2} = \ln v^2 - (1/2)c_{\widehat{v^2}}. \tag{34}$$

Take (32)(34) into (14)(15), we get the cost function $J_\theta(\mathbf{x})\Big|_{\theta=\widehat{v^2}}$ in (27).

Take the first and second derivation of the cost function, we get Hessian matrix (25) and gradient vector (26), respectively. □

It is worth noting that by taking the expectation and variance of RSS estimator, (30)(31), into the covariance matrix (15), we get the covariance matrix of the positioning MLE, where the i^{th} element is,

$$\left[\mathbf{C}_{\widehat{\Omega}}\right]_{i,i} = c_{\widehat{\Omega}}(K_i). \tag{35}$$

And take (32)(34) into (15),

$$\left[\mathbf{C}_{\widehat{v^2}}\right]_{i,i} = c_{\widehat{v^2}}(K_i). \tag{36}$$

Notice that both $c_{\widehat{\Omega}}$ (28) and $c_{\widehat{v^2}}$ (29) are independent of MT location, we have following remark.

Remark 6. *The covariance matrix of the positioning MLE is independent of position.*

3. POWER CONTOUR CIRCLE FIT (PCCF)

Due to the nonlinearity of the ARPAP system, an initial position guess is required to prevent ARPAP positioning from diverging. In this section, we introduce the proposed power contour circle fitting (PCCF) algorithm.

3.1. Overview. In contrast to the assumption in conventional lateration methods, the shape of the power contour that is determined by the non-isotropic antenna directivity is not a circle that centered at the RP. In the proposed PCCF, power contours are fitted such that the origin and radius of the fitting circle are determined by circle fitting algorithm. Thus, a rough estimation of the MT location can be found by finding the intersection of multiple fitting circles where conventional multilateration methods are applicable. This fitting-multilateration procedure is repeated. At each iteration, the center and radius of the fitting circle are adjusted such that the guessing error around the estimated location is shrunk. And, as the position guess is getting closer and closer to the actual location, the segment of power contour that used for circle fitting is reduced so as to improve the accuracy. The flow chart of the algorithm is given in Fig. 2.

3.2. The CF Algorithm. For the convenience of reading, superscript $^{(k)}$ is used to represent the k^{th} iteration of the position guess.

We first define the power contour function. Then, the procedure to determine the contour based on the initial position guess and the orientation of MT is introduced. Next, the nonlinear contour function is sampled and fitted by a circle function. Following that, a

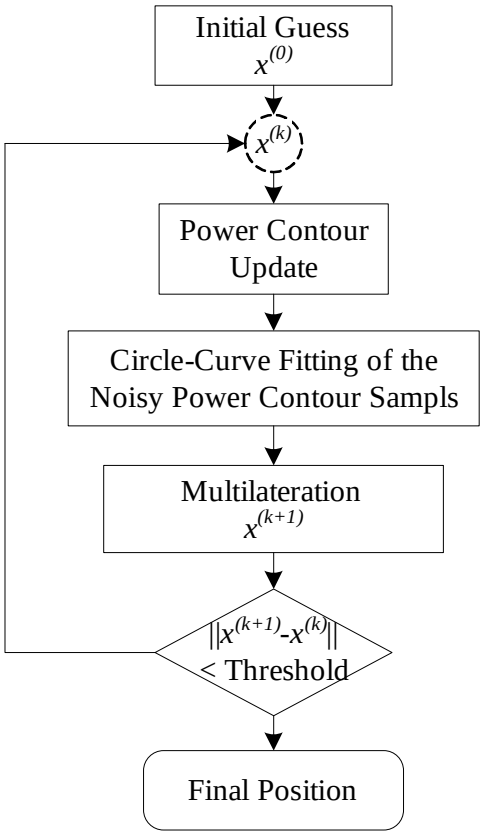

Figure 2. Overview of the CF Algorithm

rough position guess can be determined by multilateration method. By updating the initial position guess and repeating the procedure, more accurate position estimation can be found in a iterative fashion.

Definition 3. *A continuous position series, on which the received power level is a fixed given magnitude value (P_r) is termed power contour,*

$$\mathbf{x} = \left(P_r|_{\bar{p}}\right)^{-1}(\varphi_t, \alpha_t, \varphi_r, \alpha_r). \tag{37}$$

where, $\left(P_r|_{\bar{p}}\right)^{-1}$ represents the inverse of function (1), given power measurement $\bar{P}$.

As shown in Fig 3, $\boldsymbol{x}_0$ is the center of the localization area. The initial position can be chosen at $\boldsymbol{x}^{(0)} = \boldsymbol{x}_0$. The orientation (see Appendix 7.2.1 for detail) of the i^{th} RP relative to the MT inertial frame in antenna sphirical coordinates is $[\alpha_i^{00}, \varphi_i^{00}]$.

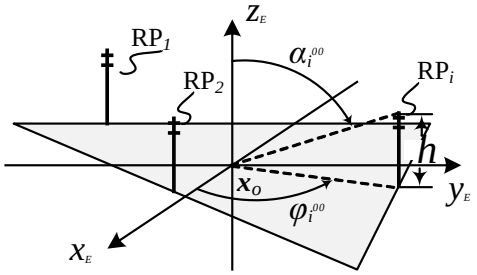

Figure 3. The orientation of the $i^{th}RP$ relative to $\boldsymbol{x}^{(0)} = \boldsymbol{x}_0$

Thus, the orientation of the i^{th} RP relative to MT body frame is $[\alpha_{r,i}^{(0)}, \varphi_{r,i}^{(0)}]^T = {}_E^M\boldsymbol{R}\left([\alpha_{r,i}^{00}, \varphi_{r,i}^{00}]^T\right)$, where ${}_E^M\boldsymbol{R}(\cdot)$ represents the rotation matrix (57).

$$[\alpha_{r,i}^{(k)}, \varphi_{r,i}^{(k)}]^T = {}_E^M\boldsymbol{R}\left([\alpha_{r,i}^{k0}, \varphi_{r,i}^{k0}]^T\right) \tag{38}$$

Suppose there are M reference positions, the MT antenna gain is $\boldsymbol{G}_r^{(0)} = \left[G_{r,i}\right]_{1\times M}$, where

$$G_{r,i} = G_r(\alpha_i^{(0)}, \varphi_i^{(0)}) \tag{39}$$

Then, the power contour at the k^{th} iteration,

$$P_{r,i}{}^{(k)}(\mathbf{x})\Big|_{\varphi_t} = \kappa e^{G_{t,i}^{(k)}(\varphi_t)} d_R(\mathbf{x}) A_i^{(k)}. \tag{40}$$

where,

$$A_i^{(k)} = e^{\gamma G_{r,i}^{(k)}}. \tag{41}$$

Sample the power contour (40) at L azimuth angles,

$$\mathbf{X}_i^{(k)} = \left(P_{r,i}^{(k)}\right)^{-1}(\boldsymbol{\varphi}^{(k)}). \tag{42}$$

where $\mathbf{X}_i^{(k)}$ is a $L \times 1$ vector, represents the set of position samples on the contour. $\boldsymbol{\varphi}^{(k)}$ is a $L \times 1$ vector that contains corresponding azimuth angle of the samples.

Next, each of the contour sample set, $\mathbf{X}_i^{(k)}$ ($i = 1 \sim M$), is fitted by circle function. The fitting algorithms can be found in [45, 46, 47, 48].

Fig. 4 depicts the two steps to determine a position guess. Let $\boldsymbol{\Theta}_i^{(k)}$ represents the contour-fitted circle function. Each circle fits a contour set $\boldsymbol{X}_i^{(k)}$. The $^{(k+1)}$ position guess is found by multilateration operation $\boldsymbol{T}(\cdot)$.

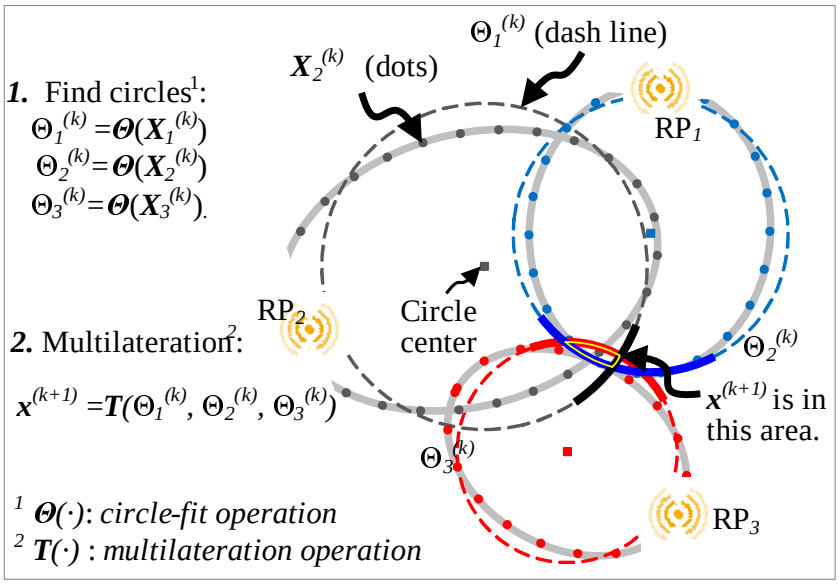

Figure 4. Get the 1^{st} position guess from contour samples

The k^{th} position guess, $\mathbf{x}^{(k)}$, is further taken as the initial guess for the $(k+1)^{th}$ iteration in the algorithm.

The PCCF algorithm is summarized in Fig 5. From the initial position guess, $\boldsymbol{x}^{(0)}$, and the orientation of the MT, $[\theta_1, \theta_2, \theta_3]^T$, the antenna directivity of the MT is determined by ${}_E^M\boldsymbol{R}$. Then, the receiving power contour is sampled on the RP antenna azimuth angle set, $\boldsymbol{\varphi}_i$. Next, circle functions that fit the contour sample set, $\boldsymbol{X}_i^{(k)}$, is found. Conventional

circular contour based multilateration method, $\boldsymbol{T}(\cdot)$, is applied to obtain a more accurate position guess, $\boldsymbol{x}^{(k+1)}$. Finally, the refined position guess can be used for repeating the procedure in an iterative fashion so as to reduce the position estimation error.

The threshold should be set to meet the minimum requirement of convergence for the subsequent method includes ML ARPAP and GO (presented in Section V). In Section V, the threshold value is set to be $1 \times 10^{-4}(m)$ for the positioning in a $24km^2$ area.

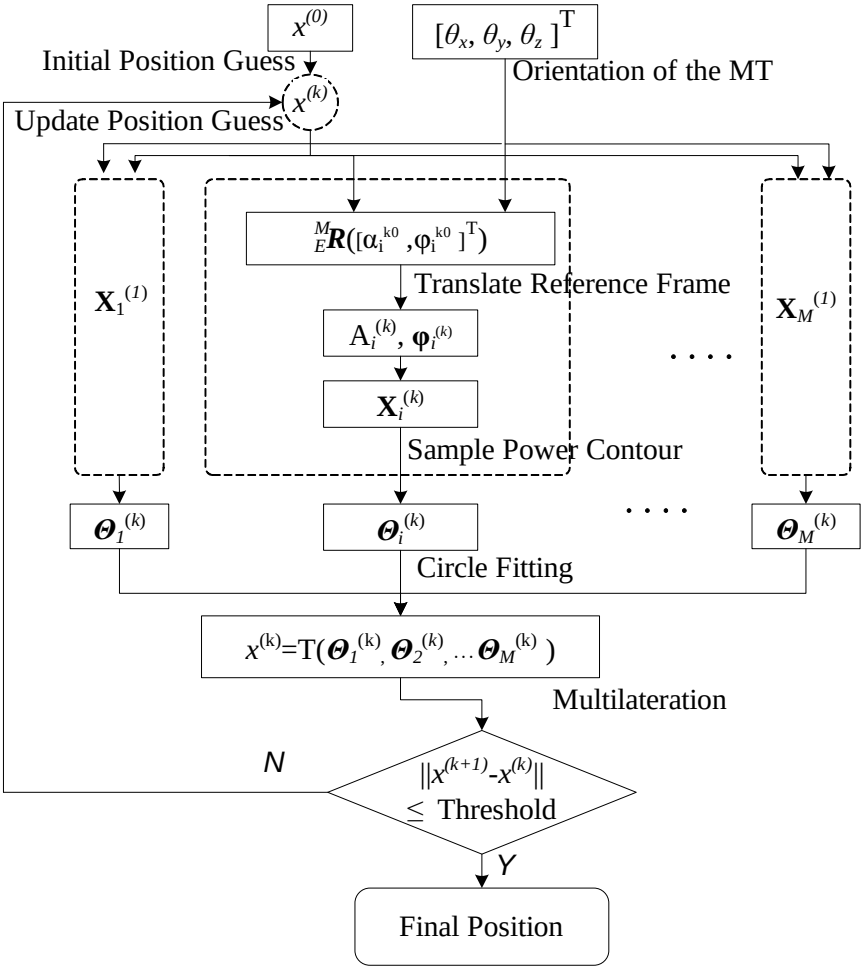

Figure 5. CF Algorithm

4. APPLICATION INSTANTIATION FOR CELLULAR NETWORK

The proposed method is applicable to many different systems include indoor and outdoor power based localizations for ZigBee, WiFi, cellular network, White Space TV, Super WiFi [49], etc. As an example, in this Section, a general power radiation pattern model of base station (BS) antenna is assumed. And a dipole antenna is assumed to be mounted on MT.

In this paper, the Cellular site antenna is assumed to be of three sectors. Since power radiated in side lobes is desired to be suppressed, we assume the main lobe is in the range of $-90° \leq \varphi \leq 90°$, all side lobes are in $-180° \leq \varphi \leq -90°$ and $90° \leq \varphi \leq 180°$. Thus, we define the 3-sector antenna boundaries [50] encapsulated area as the *localization area*, which is formed by the three main lobes of adjacent cell site antennas in Fig. 6. When 3-sector antenna is mounted on the BS, one cell site covers three cell. The boresights point to $\varphi_{o,1} = -90°$, $\varphi_{o,1} = 30°$, and $\varphi_{o,1} = 150°$, respectively.

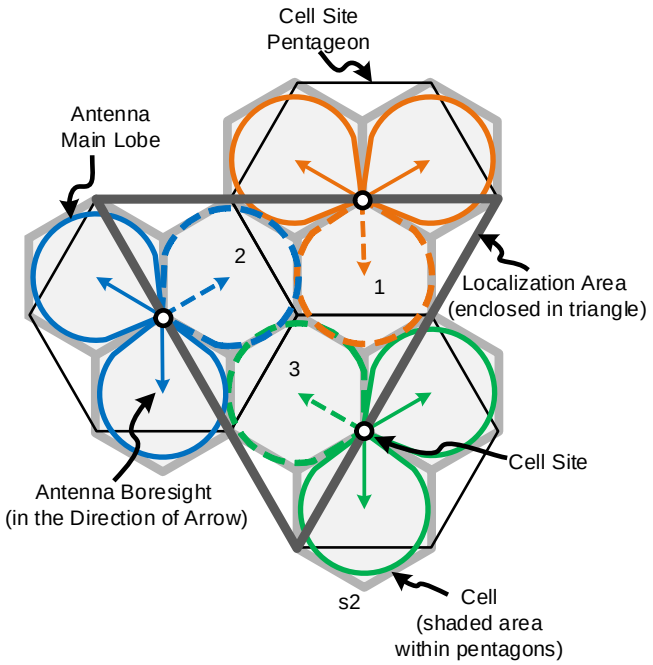

Figure 6. 3-sector antenna deployment and localization area

The antenna horizontal radiation pattern is specified by [50],

$$G_t(\varphi_t) = -12\left(\frac{\varphi_t - \varphi_o}{\varphi_{3dB}}\right)^2 + G_m. \tag{43}$$

where φ_o is the antenna boresight direction, $-90^\circ \leq \varphi_t - \varphi_o \leq 90^\circ$. In 3-sector antenna, the maximum gain $G_m = 20dB$, the half power beam width $\varphi_{3dB} = 70^\circ$. Without loss of generality, and for simplicity, the antenna gain in spherical elevation plane is assumed to be one, i.e., $G_t(\alpha_t) = 1$, $90^\circ < \alpha_t < 180^\circ$ [51]. To restore the antenna radiation pattern in three dimension [52],

$$G_t(\varphi_t, \alpha_t) = G_t(\varphi_t) + G_t(\alpha_t). \tag{44}$$

The first and second derivative of the sector antenna pattern can be found in Appendix 7.1.

Without loss of generality, assuming the receiving antenna (on MT) is dipole, the radiation pattern is [35],

$$G_r(\varphi_r, \alpha_r) = 2\gamma^{-1}\ln sin(\alpha_r) \tag{45}$$

where $\gamma = \ln(10)/10$.

The first and second derivative of the cellular network MT antenna is given in Appendix 7.1. The derivatives are used for calculating the Hessian matrix(22) and gradient vector (23) which is required by the Newton-Raphson solution (21) for the MLE (13) in cellular network.

5. SIMULATION RESULT

Simulations are conducted for evaluating the proposed ML ARPAP scheme in the cellular network. First, the scenario settings are discussed. Next, the localization accuracy of the ML ARPAP in different fading environments and attitude/orientation of MT is evaluated.

Then, the accuracy of ML ARPAP is compared with a gradient-descent optimization (GO) based method. Finally, the localization errors by using the LoS component and signal RSS are compared.

It is worth noting that, due to the nonlinearity of the ARPAP system, initial position guess using PCCF, is required for any accurate positioning scheme (ML ARPAP and GO) to prevent estimation from diverging.

5.1. Scenario Setting. It is worth noting that, the accuracy of a particular localization scheme dependents on the scenario setting, for example, the size of the evaluating area, the range and attenuation property of the signal used, the magnitude of noise in the environment. In this subsection, we introduce each of these factors considered in our simulation.

Fig. 7 depicts the cell tower position arrangement in the simulation. The size of the localization area in the simulation is $24.356km^2$ ($9.4mi^2$). The distance between each tower is $4.5km$ ($2.8mi$). The magnitude of the RF signal power at a particular location on the map is represented by color. The corresponding power level in *dBm* is indicated by the color bar beside the map.

Without a loss in either generality or accuracy, the *sum-of-sinusoids simulator* [53] is applied to generate the fading signal. The Doppler frequency is set to be $100Hz$. The number of NLoS paths is configured to be 20. The emitted power at the cell tower antenna is set to be $\boldsymbol{K} = -20.4576\ dBm$. Assuming the attenuation exponential factor in (3) is $n = 2$. The signal power range and attenuation along the base station (BS) antenna boresight is shown in Fig.8.

In the cellular network application, in contrast to the base station antenna, the orientation of the mobile equipment is nonstationary. ARPAP system is able to adapt to varied antenna pattern orientation, see Section IV Lemma. 7, 8. Therefore, in our

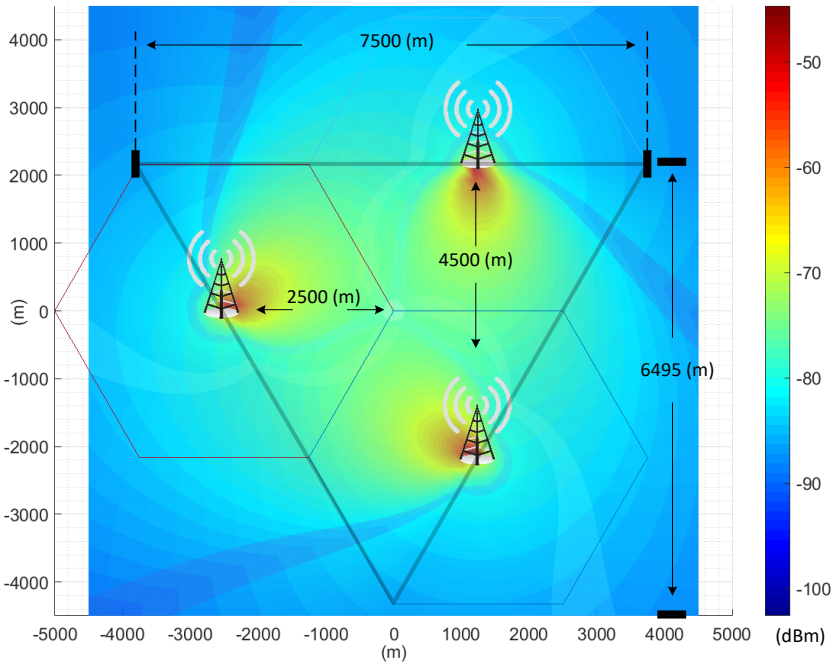

Figure 7. The Size of Simulation Area and the Map of Signal Power

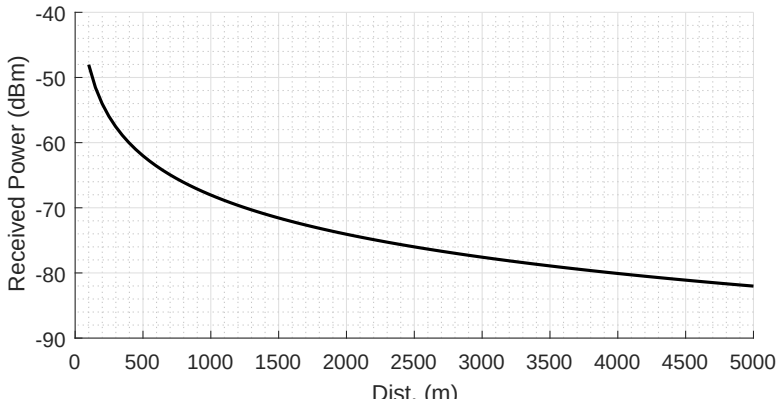

Figure 8. Signal Range and Attenuation

simulation, we varied the orientation of the MT. 0°, 20°, and 30° are added to the roll and pitch of the MT orientation, and corresponding localization errors are compared in Table 1 and 3.

5.2. Localization Error and Analysis. In our simulation, the simulated fading signal is processed with the LoS component estimation introduced in Section 2.3. Then, the proposed ARPAP PCCF scheme is used for producing the initial position guess for nonlinear positioning algorithm. The final position estimation is generated by the proposed ML ARPAP.

The gradient optimization scheme [33] is applied in our simulation for the purpose of comparison. Because the GO method was specifically introduced for wireless sensor network with relaxed assumptions, i.e. no noise, unique Tx and Rx antenna directivity. For the purpose of completeness, we derived the GO algorithm for the cellular network application, which can be found in Appendix 7.3. Moreover, due to the high nonlinearity of the ARPAP system, the proposed PCCF schemes has to be applied for finding the initial position guess for GO.

Table 1 summarizes the LoS-based localization errors of the proposed ARPAP CPCF, ML ARPAP, and the adapted GO scheme.

Table 1. Localization Error Comparison between Algorithms (LoS)

$\boldsymbol{\Delta_\theta}$[a] (°)	**K**[b]	**ML ARPAP (m)**	**PCCF**[c] **(m)**	**GO**[d] **(m)**	**Imprv.**[e] **(%)**
0	**100**	8.1361	36.166	14.345	43%
	50	11.828	48.328	18.782	37%
	10	27.952	131.83	37.006	24%
20	**100**	8.2399	29.941	24.513	66%
	50	11.475	52.814	29.972	62%
	10	27.492	142.19	52.837	48%
30	**100**	10.12	55.884	55.402	82%
	50	15.336	76.587	65.925	77%
	10	32.246	109.41	87.367	63%

[a] $\boldsymbol{\Delta_\theta}$: variation in degree added into the pitch and roll.
[b] **K**: the LoS-to-NLoS ratio in Rician fading model, (7). A larger value of K represents a strong LoS signal component comparing to the NLoS.
[c] **PCCF**: Provides initial position guesses for *both ML ARPAP and GO*.
[d] **GO**: Gradient optimization method.
[e] **Imprv.**: Accuracy improvement of ML ARPAP over the GO.

ML ARPAP offers more accurate position estimation than GO. This is due to the fact that ML ARPAP takes wireless fading channel into the positioning system model. Besides, ML ARPAP renders robustness to the orientation of the MT. As the $\mathbf{\Delta}_\theta$ increases, the accuracy improvement comparing to the GO is increased, since the antenna directivity is calculated based on the orientation of the MT.

The localization errors of PCCF and ML ARPAP over the simulation area is visualized in Fig.9. For the convenience of comparison, three-dimensional curves that fit for the scattered localization errors are plotted. The order of the curve fitting polynomial is 3. (i.e. $\sum_{k=0}^{3} \alpha_k x^i y^j$ with $i+j \leq k$; where α_k is the polynomial coefficients; x,y are the coordinates of the evaluating position.) The figure shows the localization errors when K-ratio is 10 and $\Delta_\theta = 0^o$. At each evaluation position, PCCF offers a rough position guess that enables the ML ARPAP to converge.

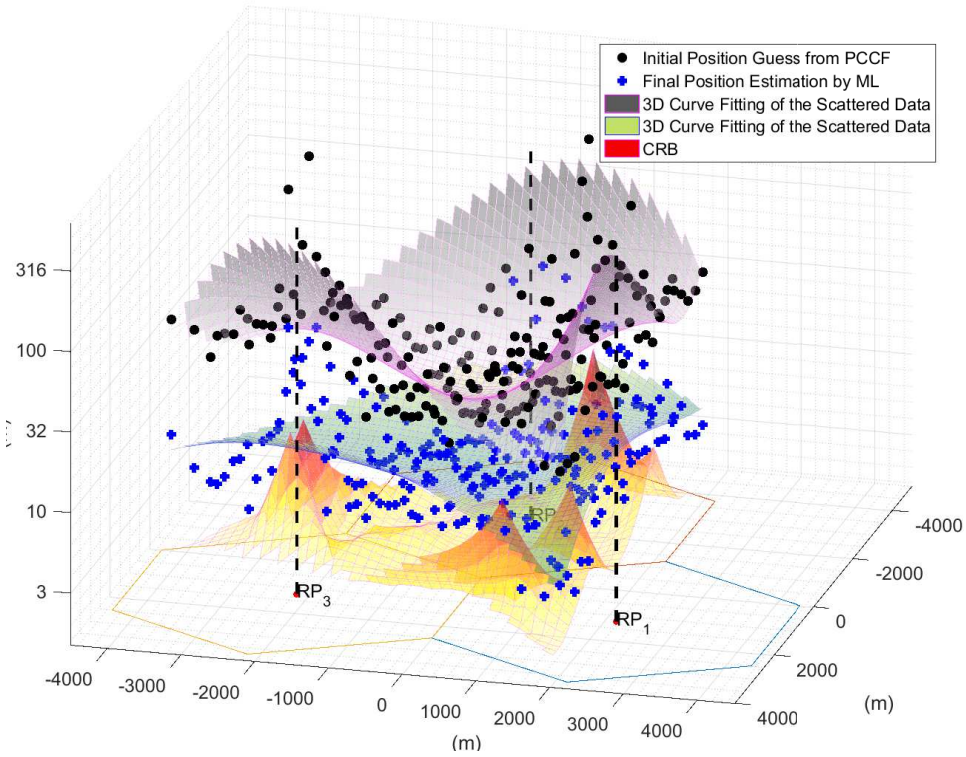

Figure 9. Comparison between PCCF Initial Guess and ML Estimation

The localization error for the case of RSS-based processing is provided in Appendix 7.4 Table 3.

The simulation is also conducted by varying the environmental noise — the LoS-to-NLoS K ratio. (A Higher value of K indicates stronger LoS signal component.) Table 2 compares the localization error between using the RSS and LoS estimation under different K-ratio.

Table 2. Localization Error Comparison between LoS and RSS

K	**ML ARPAP** Avg. Err. [a] (m)		**Imprv.**
	LoS	**RSS**	
100	8.83	21.17	58%
50	12.88	35.94	64%
10	29.23	154.5	81%

[a] Averaged over all $\mathbf{\Delta}_\theta$ cases in the simulation, i.e. 0°, 20°, and 30°.

Table 2 shows that the LoS based ML ARPAP is robust to the environmental fading disturbance comparing to the RSS-based one. Overall, the LoS-based localization accuracy is improved by about 68% over RSS. Besides, more accuracy improvement is achieved as NLoS fading is increased (as K-ratio value decreases from 100 to 10). Therefore, LoS component estimation in the ARPAP system effectively suppresses environmental disturbance.

6. CONCLUSION

The proposed ML ARPAP scheme is able to achieve good localization accuracy, i.e., 8 meters error in $24km^2$ area. The proposed PCCF algorithm ensures acceptable initial position guess for the convergence of ML and GO-based ARPAP positioning schemes. Simulation results show that the ML ARPAP is $50\%^+$ more accurate than gradient descent optimization based method for the cellular network scenario. The ML ARPAP is able

to suppress the localization error caused by variation in the orientation of the mobile transceiver. Moreover, LoS based ML ARPAP is robust to the environmental fading disturbance.

7. APPENDIX

7.1. First and Second Derivative of Antenna Radiation Pattern.

Lemma 25. *The first derivation of the kth RP sector antenna radiation pattern is*

$$\begin{cases} \frac{\partial}{\partial x} G_{t,k} = \frac{4320}{\pi \varphi_{3db,k}} \left(\frac{\varphi_{t,k} - \varphi_{o,k}}{\varphi_{3db,k}} \right) d_k^{-2} (y - y_k) \\ \frac{\partial}{\partial y} G_{t,k} = \frac{4320}{\pi \varphi_{3db,k}} \left(\frac{\varphi_{t,k} - \varphi_{o,k}}{\varphi_{3db,k}} \right) d_k^{-2} (x - x_k) \end{cases} . \tag{46}$$

where $\varphi_{t,k} = atan2d\left(\frac{y-y_k}{x-x_k}\right)$. $[x, y]^T$ *represents the location of the MT,* $[x_k, y_k]^T$ *is the kth RP location,* $atan2d(\cdot)$ *is the four-quadrant inverse tangent in degrees, and* $d_k = \sqrt{(x - x_k)^2 + (y - y_k)^2}$.

Lemma 26. *The second derivation of the kth RP sector antenna radiation pattern is*

$$\begin{cases} \frac{\partial^2}{\partial x^2} G_{t,k} = & \frac{-4320}{\pi \varphi_{3db,k}^2} d_k^{-4} \left\{ \frac{180}{\pi} (y - y_k)^2 + 2(\varphi_{t,k} - \varphi_0)(x - x_k)(y - y_k) \right\} \\ \frac{\partial^2}{\partial x^2} G_{t,k} = & \frac{-4320}{\pi \varphi_{3db,k}^2} d_k^{-4} \left\{ \frac{180}{\pi} (x - x_k)^2 - 2(\varphi_{t,k} - \varphi_0)(x - x_k)(y - y_k) \right\} \\ \frac{\partial^2}{\partial x \partial y} G_{t,k} = & \frac{4320}{\pi \varphi_{3db,k}^2} d_k^{-4} \left\{ \frac{180}{\pi} (x - x_k)(y - y_k) \right. \\ & \left. + (\varphi_{t,k} - \varphi_0) \left[(x - x_k)^2 - (y - y_k)^2 \right] \right\} \\ \frac{\partial^2}{\partial x \partial y} G_{t,k} = & \frac{\partial^2}{\partial y \partial x} G_{t,k} \end{cases} . \tag{47}$$

Lemma 27. *The first derivation of the MT antenna radiation pattern in the direction to the kth RP is,*

$$\begin{cases} \frac{\partial}{\partial x} G_{r,k} = \gamma^{-1} \Gamma_k \left[sin(w_y) d_k^{-1} - {}^{(M)}h_k d_k^{-3} (x_k - x) \right] \\ \frac{\partial}{\partial y} G_{r,k} = \gamma^{-1} \Gamma_k \left[cos(w_y) sin(w_x) d_k^{-1} - {}^{(M)}h_k d_k^{-3} (y_k - y) \right] \end{cases} \tag{48}$$

where $\Gamma_k = \frac{\Gamma_a}{\Gamma_b}$,

$$\begin{cases} \Gamma_a = tan^{-1} \left(atan \left(\frac{{}^{(M)}h_k}{d_k} \right) \right) \\ \Gamma_b = \sqrt{1 - \left(\frac{{}^{(M)}h_k}{d_k} \right)^2} \end{cases} . \tag{49}$$

and, ${}^{(M)}h$ *is the RP height in MT body frame.*

$$\begin{aligned} {}^{(M)}h_k = & sin(w_y)(x_k - x) \\ & + cos(w_x) cos(w_y) h + cos(w_y) sin(w_x)(y_k - y) \end{aligned} . \tag{50}$$

The Euler angle (w_x, w_y, w_z) *represents the orientation of the receiving antenna in Earth reference frame.*

Proof. The spherical coordinates of RP antenna relative to MT in earth frame ${}^{(E)}$ is,

$$\begin{cases} r_k = \sqrt{\Delta_{x,k}^2 + \Delta_{y,k}^2 + h_k^2} \\ \varphi_{r,k} = \text{atan} \left(\Delta_{y,k} / \Delta_{x,k} \right) \\ \alpha_{r,k} = \text{acos} \left(\frac{h_k}{r_k} \right) \end{cases} \tag{51}$$

where the displacement ${}^{(E)}\boldsymbol{\Delta x} = [\Delta x, \Delta y, h]^T = [(x_k - x), (y_k - y), h]^T$. The orientation of MT body frame ${}^{(M)}$ relative to the earth frame ${}^{(E)}$ can be represented by a rotation matrix $\boldsymbol{R}_E^M$. And the corresponding Euler angles $\boldsymbol{w} = [w_x, w_y, w_z]^T$. Hence, the displacement in MT body frame is ${}^{(M)}\boldsymbol{\Delta x} = \boldsymbol{R}_E^{M(E)} \boldsymbol{\Delta x}$. Thus, the height ${}^{(M)}h_k = [0, 0, 1] \boldsymbol{R}_E^M \boldsymbol{\Delta x}$, which is (50). And the elevation angle, ${}^{(M)}\alpha_r = acos \left({}^{(M)}h_k / r_k \right)$. Take the first derivation of the receiving antenna pattern G_r w.r.t. x and y, respectively, we get (48). □

Lemma 28. *The first derivation of the MT antenna radiation pattern in the direction to the kth RP is,*

$$\begin{cases} \frac{\partial^2}{\partial x^2} G_{r,k} = \frac{\partial}{\partial x}\Gamma\frac{\partial}{\partial x}\left(\frac{^{(M)}h_k}{d_k}\right) + \Gamma\frac{\partial^2}{\partial x^2}\left(\frac{^{(M)}h_k}{d_k}\right) \\ \frac{\partial^2}{\partial y^2} G_{r,k} = \frac{\partial}{\partial y}\Gamma\frac{\partial}{\partial y}\left(\frac{^{(M)}h_k}{d_k}\right) + \Gamma\frac{\partial^2}{\partial y^2}\left(\frac{^{(M)}h_k}{d_k}\right) \\ \frac{\partial^2}{\partial x\partial y} G_{r,k} = \frac{\partial^2}{\partial y\partial x} G_{r,k} = \frac{\partial}{\partial y}\Gamma\frac{\partial}{\partial x}\left(\frac{^{(M)}h_k}{d_k}\right) + \Gamma\frac{\partial^2}{\partial x\partial y}\left(\frac{^{(M)}h_k}{d_k}\right) \end{cases} \tag{52}$$

where,

$$\begin{cases} \frac{\partial}{\partial x}\Gamma = \left[\frac{\partial}{\partial x}\Gamma_a\Gamma_b - \frac{\partial}{\partial x}\Gamma_b\Gamma_a\right]/\Gamma_b^2 \\ \frac{\partial}{\partial y}\Gamma = \left[\frac{\partial}{\partial y}\Gamma_a\Gamma_b - \frac{\partial}{\partial y}\Gamma_b\Gamma_a\right]/\Gamma_b^2 \end{cases}. \tag{53}$$

$$\begin{cases} \frac{\partial}{\partial x}\left(\frac{^{(M)}h_k}{d_k}\right) = {}^{(M)}h_k d_k^{-3}(x_k - x) - sin(w_y)d_k \\ \frac{\partial}{\partial y}\left(\frac{^{(M)}h_k}{d_k}\right) = {}^{(M)}h_k d_k^{-3}(y_k - y) - cos(w_y)sin(w_y)d_k \end{cases}. \tag{54}$$

$$\begin{cases} \frac{\partial}{\partial x}\Gamma_a = \frac{tan^{-2}\left(acos\left(\frac{^{(M)}h_k}{d_k}\right)\right)sec^2\left(acos\left(\frac{^{(M)}h_k}{d_k}\right)\right)}{\sqrt{1-\left(\frac{^{(M)}h_k}{d_k}\right)^2}}\left[\frac{\partial}{\partial x}\left(\frac{^{(M)}h_k}{d_k}\right)\right] \\ \frac{\partial}{\partial y}\Gamma_b = -\left[1-\left(\frac{^{(M)}h_k}{d_k}\right)^2\right]^{-1/2}\left(\frac{^{(M)}h_k}{d_k}\right)\frac{\partial}{\partial x}\left(\frac{^{(M)}h_k}{d_k}\right) \end{cases}. \tag{55}$$

$$\begin{cases} \frac{\partial^2}{\partial x^2}\left(\frac{^{(M)}h_k}{d_k}\right) = & {}^{(M)}h_k 3d^{-5}(x_k - x)^2 - 2sin(w_y)d_k^{-3}(x_k - x) - {}^{(M)}h_k d_k^{-3} \\ \frac{\partial^2}{\partial y^2}\left(\frac{^{(M)}h_k}{d_k}\right) = & {}^{(M)}h_k 3d^{-5}(y_k - y)^2 - 2cos(w_y)sin(w_x)d_k^{-3}(y_k - y) - {}^{(M)}h_k d_k^{-3} \\ \frac{\partial^2}{\partial x\partial y}\left(\frac{^{(M)}h_k}{d_k}\right) = & \frac{\partial^2}{\partial y\partial x}\left(\frac{^{(M)}h_k}{d_k}\right) = \\ & {}^{(M)}h_k 3d^{-5}(x_k - x)(y_k - y) - sin(w_y)d_k^{-3}(y_k - y) \\ & -d_k^{-3}(x_k - x)cos(w_y)sin(w_x) \end{cases}. \tag{56}$$

7.2. Frame of Reference.

7.2.1. Orientation. A notation system of leading superscripts and subscripts in [54] is adopted to denote the relative frames of orientations. An arbitrary orientation of inertial frame "E" relative to MT body frame "M" can be achieved through a rotation of Euler angle set $[\theta_r, \theta_p, \theta_y]^T$. The rotation matrix ${}^{M}_{E}\boldsymbol{R}$ defined by equation (57), describe the orientation of frame E relative to frame M.

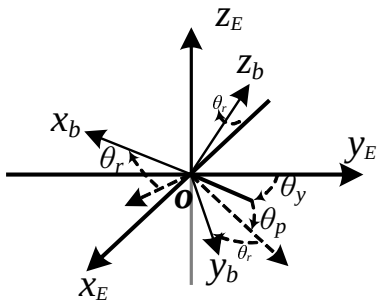

Figure 10. Orientation

$$ {}^{M}_{E}\boldsymbol{R} = \boldsymbol{R}_{\theta_y}\boldsymbol{R}_{\theta_r}\boldsymbol{R}_{\theta_p}. \tag{57} $$

where, $\boldsymbol{R}_{\theta_y} = \begin{bmatrix} cos\theta_y & -sin\theta_y & 0 \\ sin\theta_y & cos\theta_y & 0 \\ 0 & 0 & 1 \end{bmatrix}, \boldsymbol{R}_{\theta_r} = \begin{bmatrix} cos\theta_r & 0 & sin\theta_r \\ 0 & 1 & 0 \\ -sin\theta_r & 0 & cos\theta_r \end{bmatrix}, \boldsymbol{R}_{\theta_p} = \begin{bmatrix} 1 & 0 & 0 \\ 0 & cos\theta_p & -sin\theta_p \\ 0 & sin\theta_p & cos\theta_p \end{bmatrix}$

.

7.2.2. Coordinate System for Antenna Analysis. Antenna radiation pattern represents the distribution of radiated energy from an antenna over a surface of constant radius centered upon the antenna. Fig. 11 shows the spherical coordinate system that is used for antenna analysis. Elevation plane angle α is the angle between the z-axis and the vector from the origin to the point (ranges from 0^o to 180^o). Azimuth plane angle φ is the angle between the x-axis and the projection of the point onto the x-y plane (ranges from 0^o to 360^o).

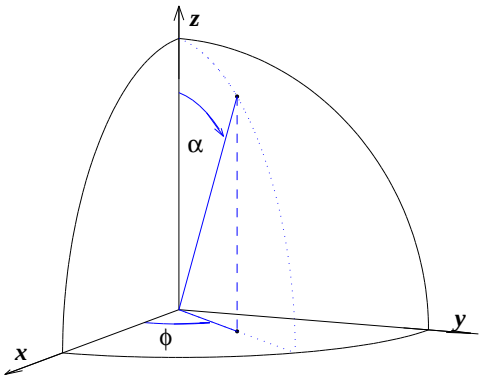

Figure 11. Coordinate System for Antenna Analysis

7.3. Gradient Optimization based Positioning. The position can be found by minimizing a cost function,

$$f_{\text{cost}} = \sum_{k=1}^{M} \left\| d_k(\hat{\mathbf{x}}) - \tilde{d}_k \right\|. \tag{58}$$

where $d_k(\hat{\mathbf{x}}) = g(\hat{\mathbf{x}}, \mathbf{x}_k)$ is the range distance from $\hat{\mathbf{x}}$ to the k^{th} reference position, and $\tilde{d}_k$ is a function of power estimation θ_k.

$$\tilde{d}_k = \left(\kappa e^{\gamma G_t(\varphi_t, \alpha_t)} e^{\gamma G_r(\varphi_r, \alpha_r)} \theta_k^{-1} \right)^{1/n}. \tag{59}$$

In [33], the noise is assumed to be negligible, the optimization method is recursively correcting the position guess as,

$$\hat{\mathbf{x}}^{(l+1)} = \hat{\mathbf{x}}^{(l)} - \left(\left[\mathbf{J}^{(l)} \right]^T \mathbf{J}^{(l)} \right)^{-1} \left[\mathbf{J}^{(l)} \right]^T \mathbf{D_d}^{(l)}. \tag{60}$$

where superscript l represents the recursive index, $\boldsymbol{D}_d = \mathbf{d} - \tilde{\mathbf{d}}$ with $\mathbf{d} = [\mathbf{d_1}, \mathbf{d_2}, \cdots, \mathbf{d_M}]^{\mathbf{T}}$ and $\tilde{\mathbf{d}} = [\tilde{d}_1, \tilde{d}_2, \cdots, \tilde{d}_M]^T$, and

$$\mathbf{J} = \nabla \mathbf{d} - \nabla \tilde{\mathbf{d}}. \tag{61}$$

where $[\nabla \mathbf{d}]_i = \left[\frac{\partial}{\partial x} d_i, \frac{\partial}{\partial y} d_i\right]$ and $[\nabla \tilde{\mathbf{d}}]_i = \left[\frac{\partial}{\partial x} \tilde{d}_i, \frac{\partial}{\partial y} \tilde{d}_i\right]$, with

$$\begin{cases} \frac{\partial}{\partial x} d_{R,i} = \frac{x - x_i}{d_{R,i}} \\ \frac{\partial}{\partial y} d_{R,i} = \frac{y - y_i}{d_{R,i}} \end{cases} . \tag{62}$$

$$\begin{cases} \frac{\partial}{\partial x} \tilde{d}_{R,i} = \frac{\gamma}{n} \left[\frac{\partial}{\partial x} G_{t,i} + \frac{\partial}{\partial x} G_{r,i}\right] \\ \frac{\partial}{\partial y} \tilde{d}_{R,i} = \frac{\gamma}{n} \left[\frac{\partial}{\partial y} G_{t,i} + \frac{\partial}{\partial y} G_{r,i}\right] \end{cases} . \tag{63}$$

7.4. RSS-based Localization Errors. The localization error by using the RSS estimation is shown in Table 3.

Table 3. Localization Error Comparison between Algorithms (RSS)

Δ_θ (°)	K	ML ARPAP (m)	PCCF (m)	GO (m)	Imprv. (%)
0	**100**	17.381	74.099	29.505	41%
	50	30.899	171.14	47.174	34%
	10	151.98	623.73	247.09	38%
20	**100**	26.36	125.87	47.359	44%
	50	42.967	189.38	73.607	42%
	10	157.33	608.44	220.25	29%
30	**100**	19.769	87.376	84.574	77%
	50	33.962	184.42	109.3	69%
	10	154.21	684.08	268.7	43%

REFERENCES

[1] Pratap Misra and Per Enge. *Global positioning system: signals, measurements, and performance*. Ganga-Jamuna Press, 2006. ISBN 978-0-9709544-1-1.

[2] B. Lubbers, S. Mildner, P. Oonincx, and A. Scheele. A study on the accuracy of GPS positioning during jamming. In *2015 International Association of Institutes of Navigation World Congress (IAIN)*, pages 1–6, October 2015. doi: 10.1109/IAIN.2015.7352258.

[3] M. L. Psiaki, T. E. Humphreys, and B. Stauffer. Attackers can spoof navigation signals without our knowledge. Here's how to fight back GPS lies. *IEEE Spectrum*, 53(8): 26–53, August 2016. ISSN 0018-9235. doi: 10.1109/MSPEC.2016.7524168.

[4] I.T. Haque and C. Assi. Profiling-Based Indoor Localization Schemes. *IEEE Systems Journal*, 9(1):76–85, March 2015. ISSN 1932-8184. doi: 10.1109/JSYST.2013.2281257.

[5] Kamin Whitehouse, Chris Karlof, and David Culler. A practical evaluation of radio signal strength for ranging-based localization. *ACM SIGMOBILE Mobile Computing and Communications Review*, 11(1):41–52, 2007. URL http://dl.acm.org/citation.cfm?id=1234829.

[6] J. Kang, D. Kim, and Y. Kim. RSS Self-calibration Protocol for WSN Localization. In *2007 2nd International Symposium on Wireless Pervasive Computing*, February 2007. doi: 10.1109/ISWPC.2007.342597.

[7] James Caffery and Gordon L Stuber. Subscriber location in cdma cellular networks. *Vehicular Technology, IEEE Transactions on*, 47(2):406–416, 1998.

[8] H. Shen, Z. Ding, S. Dasgupta, and C. Zhao. Multiple Source Localization in Wireless Sensor Networks Based on Time of Arrival Measurement. *IEEE Transactions on Signal Processing*, 62(8):1938–1949, April 2014. ISSN 1053-587X. doi: 10.1109/TSP.2014.2304433.

[9] Ismail Guvenc and Chia-Chin Chong. A survey on toa based wireless localization and nlos mitigation techniques. *Communications Surveys & Tutorials, IEEE*, 11(3): 107–124, 2009.

[10] Ali H Sayed, Alireza Tarighat, and Nima Khajehnouri. Network-based wireless location: challenges faced in developing techniques for accurate wireless location information. *Signal Processing Magazine, IEEE*, 22(4):24–40, 2005.

[11] IEEE Draft Amendment Standard for Local and Metropolitan Area Networks - Part 16: Air Interface for Broadband Wireless Access Systems - Advanced Air Interface. *IEEE P802.16m/D9, October 2010*, pages 1–1156, October 2010.

[12] Richard Klukas and Michel Fattouche. Line-of-sight angle of arrival estimation in the outdoor multipath environment. *Vehicular Technology, IEEE Transactions on*, 47(1): 342–351, 1998.

[13] S. Sakagami, S. Aoyama, K. Kuboi, S. Shirota, and Akira Akeyama. Vehicle position estimates by multibeam antennas in multipath environments. *IEEE Transactions on Vehicular Technology*, 41(1):63–68, February 1992. ISSN 0018-9545. doi: 10.1109/25.120146.

[14] V. Thotla, M. J. Zawodniok, S. Jagannathan, M. T. A. Ghasr, and S. Agarwal. Detection and Localization of Multiple R/C Electronic Devices Using Array Detectors. *IEEE Transactions on Instrumentation and Measurement*, 64(1):241–251, January 2015. ISSN 0018-9456. doi: 10.1109/TIM.2014.2331432.

[15] Ralph O Schmidt. Multiple emitter location and signal parameter estimation. *Antennas and Propagation, IEEE Transactions on*, 34(3):276–280, 1986.

[16] Moustafa M Abdalla, Mostafa B Abuitbel, and Mohamed A Hassan. Performance evaluation of direction of arrival estimation using music and esprit algorithms for mobile communication systems. In *Wireless and Mobile Networking Conference (WMNC), 2013 6th Joint IFIP*, pages 1–7. IEEE, 2013.

[17] M. Bocca, O. Kaltiokallio, N. Patwari, and S. Venkatasubramanian. Multiple Target Tracking with RF Sensor Networks. *IEEE Transactions on Mobile Computing*, 13(8): 1787–1800, August 2014. ISSN 1536-1233. doi: 10.1109/TMC.2013.92.

[18] Yang Zhao and N. Patwari. Robust Estimators for Variance-Based Device-Free Localization and Tracking. *IEEE Transactions on Mobile Computing*, 14(10):2116–2129, October 2015. ISSN 1536-1233. doi: 10.1109/TMC.2014.2385710.

[19] M.R. Gholami, R.M. Vaghefi, and E.G. Strom. RSS-Based Sensor Localization in the Presence of Unknown Channel Parameters. *IEEE Transactions on Signal Processing*, 61(15):3752–3759, August 2013. ISSN 1053-587X. doi: 10.1109/TSP.2013.2260330.

[20] Andrea Zanella and Andrea Bardella. Rss-based ranging by multichannel rss averaging. *Wireless Communications Letters, IEEE*, 3(1):10–13, 2014.

[21] Paramvir Bahl and Venkata N. Padmanabhan. RADAR: An in-building RF-based user location and tracking system. In *INFOCOM 2000. Nineteenth Annual Joint Conference of the IEEE Computer and Communications Societies. Proceedings. IEEE*, volume 2, pages 775–784. Ieee, 2000.

[22] A. Coluccia and F. Ricciato. RSS-Based Localization via Bayesian Ranging and Iterative Least Squares Positioning. *IEEE Communications Letters*, 18(5):873–876, May 2014. ISSN 1089-7798. doi: 10.1109/LCOMM.2014.040214.132781.

[23] Ka Wai Cheung, Hing-Cheung So, W-K Ma, and Yiu-Tong Chan. A constrained least squares approach to mobile positioning: algorithms and optimality. *EURASIP journal on applied signal processing*, 2006:150–150, 2006.

[24] Lei Wang and Maciej Zawodniok. Rssi-based localization in cellular networks. In *Local Computer Networks Workshops (LCN Workshops), 2012 IEEE 37th Conference on*, pages 820–826. IEEE, 2012.

[25] S. Tomic, M. Beko, and R. Dinis. RSS-Based Localization in Wireless Sensor Networks Using Convex Relaxation: Noncooperative and Cooperative Schemes. *IEEE Transactions on Vehicular Technology*, 64(5):2037–2050, May 2015. ISSN 0018-9545. doi: 10.1109/TVT.2014.2334397.

[26] A. O. Hero and D. Blatt. Sensor network source localization via projection onto convex sets (POCS). In *Proceedings. (ICASSP '05). IEEE International Conference on Acoustics, Speech, and Signal Processing, 2005.*, volume 3, pages iii/689–iii/692 Vol. 3, March 2005. doi: 10.1109/ICASSP.2005.1415803.

[27] Y.T. Chan, H.Y.C. Hang, and P.-C. Ching. Exact and Approximate Maximum Likelihood Localization Algorithms. *IEEE Transactions on Vehicular Technology*, 55(1): 10–16, January 2006. ISSN 0018-9545. doi: 10.1109/TVT.2005.861162. URL http://ieeexplore.ieee.org/document/1583909/.

[28] Reza Monir Vaghefi and R. Michael Buehrer. Asynchronous time-of-arrival-based source localization. In *ICASSP*, pages 4086–4090, 2013. URL http://www.buehrer.ece.vt.edu/papers/ICASSP.2013.6638427.pdf.

[29] Huagang Yu, Gaoming Huang, Jun Gao, and Xinhui Wu. Approximate Maximum Likelihood Algorithm for Moving Source Localization Using TDOA and FDOA Measurements. *Chinese Journal of Aeronautics*, 25(4):593–597, August 2012. ISSN 10009361. doi: 10.1016/S1000-9361(11)60423-8. URL http://linkinghub.elsevier.com/retrieve/pii/S1000936111604238.

[30] Jos F. Sturm. Using SeDuMi 1.02, a MATLAB toolbox for optimization over symmetric cones. *Optimization methods and software*, 11(1-4):625–653, 1999. URL http://www.tandfonline.com/doi/abs/10.1080/10556789908805766.

[31] M. Rydstrom, E. G. Strom, and A. Svensson. Robust Sensor Network Positioning Based on Projections onto Circular and Hyperbolic Convex Sets (POCS). In *2006 IEEE 7th Workshop on Signal Processing Advances in Wireless Communications*, pages 1–5, July 2006. doi: 10.1109/SPAWC.2006.346399.

[32] Stefania Monica and Gianluigi Ferrari. Maximum likelihood localization: When does it fail? *ICT Express*, 2(1):10–13, March 2016. ISSN 24059595. doi: 10.1016/j.icte.2016.02.004. URL http://linkinghub.elsevier.com/retrieve/pii/S2405959515300928.

[33] M.K. Mwila, K. Djouani, and A. Kurien. An efficient approach to node localisation and tracking in wireless sensor networks. In *2014 IEEE Global Communications Conference (GLOBECOM)*, pages 492–497, December 2014. doi: 10.1109/GLOCOM.2014.7036856.

[34] Harald T Friis. A note on a simple transmission formula. *proc. IRE*, 34(5):254–256, 1946.

[35] Constantine A. Balanis. *Antenna Theory: Analysis and Design*. John Wiley & Sons, December 2012. ISBN 978-1-118-58573-3.

[36] Matthias Patzold. *Mobile fading channels*. John Wiley & Sons, Inc., 2003.

[37] Gordon L Stüber. *Principles of mobile communication*. Springer Science & Business Media, 2011.

[38] Wolfram Koepf. Identities for families of orthogonal polynomials and special functions. *INTEGRAL TRANSFORMS AND SPECIAL FUNCTIONS*, 5:69–102, 1995.

[39] Martin Sauter. *From GSM to LTE: an introduction to mobile networks and mobile broadband*. John Wiley & Sons, 2010.

[40] L. Wang and M. Zawodniok. Bias and CRB Analysis of LoS-based and RSS-based Ranging Methods. *IEEE Transactions on Vehicular Technology*, PP(99):1–1, 2016. ISSN 0018-9545. doi: 10.1109/TVT.2016.2518166.

[41] Cheng Guan Koay and Peter J Basser. Analytically exact correction scheme for signal extraction from noisy magnitude mr signals. *Journal of Magnetic Resonance*, 179(2):317–322, 2006.

[42] Lee J Bain and Max Engelhardt. *Introduction to probability and mathematical statistics*, volume 4. Duxbury Press Belmont, CA, 1992.

[43] C. Mensing and S. Plass. Positioning Algorithms for Cellular Networks Using TDOA. In *2006 IEEE International Conference on Acoustics, Speech and Signal Processing, 2006. ICASSP 2006 Proceedings*, volume 4, pages IV–IV, May 2006. doi: 10.1109/ICASSP.2006.1661018.

[44] Victor S. Ryaben'kii and Semyon V. Tsynkov. *A Theoretical Introduction to Numerical Analysis*. CRC Press, November 2006. ISBN 978-1-58488-607-5.

[45] Wei Li, Jing Zhong, T.A. Gulliver, Bo Rong, Qingyang Hu, and Yi Qian. Fitting Noisy Data to a Circle: A Simple Iterative Maximum Likelihood Approach. In *2011 IEEE International Conference on Communications (ICC)*, pages 1–5, June 2011. doi: 10.1109/icc.2011.5963101.

[46] Zhenhua Ma, K.C. Ho, and Le Yang. Solutions and comparison of Maximum Likelihood and Full-Least-Squares estimations for circle fitting. In *IEEE International Conference on Acoustics, Speech and Signal Processing, 2009. ICASSP 2009*, pages 3257–3260, April 2009. doi: 10.1109/ICASSP.2009.4960319.

[47] Hu Juan-li, Deng Jia-bin, and Hu Chang. An Algorithm for Circle Curve Fitting Based on the Constrained Least Square Model Represented by Mosaic Observation Points. In *5th International Conference on Wireless Communications, Networking and Mobile Computing, 2009. WiCom '09*, pages 1–4, September 2009. doi: 10.1109/WICOM.2009.5302849.

[48] Gabriel Taubin. Estimation of planar curves, surfaces, and nonplanar space curves defined by implicit equations with applications to edge and range image segmentation. *IEEE Transactions on Pattern Analysis and Machine Intelligence*, 13(11):1115–1138, November 1991. ISSN 0162-8828. doi: 10.1109/34.103273.

[49] Broadcast Bands. FEDERAL COMMUNICATIONS COMMISSION 47 CFR Parts 0 and 15. 2010. URL http://www.apwpt.org/downloads/unlicensed-operation-in-the-tv-broadcast12-06-.pdf.

[50] 3gpp specification: 25.105. URL http://www.3gpp.org/DynaReport/25105.htm.

[51] Z. D. Zaharis. Radiation pattern shaping of a mobile base station antenna array using a particle swarm optimization based technique. *Electrical Engineering*, 90(4):301–311, July 2007. ISSN 0948-7921, 1432-0487. doi: 10.1007/s00202-007-0078-y. URL http://link.springer.com/article/10.1007/s00202-007-0078-y.

[52] F. Gunnarsson, M.N. Johansson, A. Furuskar, M. Lundevall, A. Simonsson, C. Tidestav, and M. Blomgren. Downtilted Base Station Antennas - A Simulation Model Proposal and Impact on HSPA and LTE Performance. In *Vehicular Technology Conference, 2008. VTC 2008-Fall. IEEE 68th*, pages 1–5, September 2008. doi: 10.1109/VETECF.2008.49.

[53] Chengshan Xiao, Yahong Rosa Zheng, and Norman C Beaulieu. Novel sum-of-sinusoids simulation models for rayleigh and rician fading channels. *Wireless Communications, IEEE Transactions on*, 5(12):3667–3679, 2006.

[54] John J. Craig. *Introduction to Robotics: Mechanics and Control*. Pearson, Upper Saddle River, N.J, 3 edition edition, August 2004. ISBN 978-0-201-54361-2.

SECTION

2. CONCLUSION AND FUTURE WORK

This dissertation developed a new, advanced power-based positioning system and a new theory for the error bound. The environmental fading effect, antenna radiation pattern and nonlinear nature of the localization system have been studied. The proposed LoS-based ranging and positioning is proven to be robust to environmental fading disturbance. The proposed ARPAP algorithm addressed the antenna directivity effect on positioning result. Theoretical limits and error models for the conventional multilateration in fading channel and the ARPAP system is derived. To detect the fault and evaluate the localization quality, we implemented a proposed UTMLS system with the consumer-grade inertial sensor. Experimental results show that it achieves the seamless transition between indoor and outdoor tracking modes while maintaining acceptable accuracy.

Future work may include finding a better LoS component estimator, reducing the computational complexity of the ARPAP positioning. In addition, future work could explore the LoS/RSS based heading estimation to reduce the requirement for magnetometer and gyroscope to calculate the antenna directivity.

BIBLIOGRAPHY

[1] Pratap Misra and Per Enge. *Global positioning system: signals, measurements, and performance*. Ganga-Jamuna Press, 2006. ISBN 978-0-9709544-1-1.

[2] B. Lubbers, S. Mildner, P. Oonincx, and A. Scheele. A study on the accuracy of GPS positioning during jamming. In *2015 International Association of Institutes of Navigation World Congress (IAIN)*, pages 1–6, October 2015. doi: 10.1109/IAIN.2015.7352258.

[3] M. L. Psiaki, T. E. Humphreys, and B. Stauffer. Attackers can spoof navigation signals without our knowledge. Here's how to fight back GPS lies. *IEEE Spectrum*, 53(8):26–53, August 2016. ISSN 0018-9235. doi: 10.1109/MSPEC.2016.7524168.

[4] William CY Lee. Estimate of local average power of a mobile radio signal. *Vehicular Technology, IEEE Transactions on*, 34(1):22–27, 1985.

[5] William C Lee. *Mobile communications engineering*. McGraw-Hill Professional, 1982.

[6] Thomas N Rubinstein. The standard deviations of the local means of land mobile radio signals in flat suburban terrain. In *Vehicular Technology Conference, 1986. 36th IEEE*, volume 36, pages 52–56. IEEE, 1986.

[7] Mark D Austin and GL Stüber. Velocity adaptive handoff algorithms for microcellular systems. *IEEE Transactions on Vehicular Technology*, 43(3):549–561, 1994.

[8] Andrea Zanella and Andrea Bardella. Rss-based ranging by multichannel rss averaging. *Wireless Communications Letters, IEEE*, 3(1):10–13, 2014.

[9] Xinrong Li. Rss-based location estimation with unknown pathloss model. *Wireless Communications, IEEE Transactions on*, 5(12):3626–3633, 2006.

[10] Martin Sauter. *From GSM to LTE: an introduction to mobile networks and mobile broadband*. John Wiley & Sons, 2010.

[11] Ka Wai Cheung, Hing-Cheung So, W-K Ma, and Yiu-Tong Chan. A constrained least squares approach to mobile positioning: algorithms and optimality. *EURASIP journal on applied signal processing*, 2006:150–150, 2006.

[12] Lei Wang and Maciej Zawodniok. Rssi-based localization in cellular networks. In *Local Computer Networks Workshops (LCN Workshops), 2012 IEEE 37th Conference on*, pages 820–826. IEEE, 2012.

[13] A. Coluccia and F. Ricciato. RSS-Based Localization via Bayesian Ranging and Iterative Least Squares Positioning. *IEEE Communications Letters*, 18(5):873–876, May 2014. ISSN 1089-7798. doi: 10.1109/LCOMM.2014.040214.132781.

[14] S. Tomic, M. Beko, and R. Dinis. RSS-Based Localization in Wireless Sensor Networks Using Convex Relaxation: Noncooperative and Cooperative Schemes. *IEEE Transactions on Vehicular Technology*, 64(5):2037–2050, May 2015. ISSN 0018-9545. doi: 10.1109/TVT.2014.2334397.

[15] L. Wang and M. Zawodniok. Bias and CRB Analysis of LoS-based and RSS-based Ranging Methods. *IEEE Transactions on Vehicular Technology*, PP(99):1–1, 2016. ISSN 0018-9545. doi: 10.1109/TVT.2016.2518166.

[16] Lei Wang and Maciej J Zawodniok. New Theoretical Limit Analysis of LoS and RSS Based Positioning Methods for Ricean Fading Channel in RF Systems. *IEEE Transactions on Vehicular Technology*, page submitted on, April 2016. URL submittedonApril2016.

[17] S.M. Kay. *Fundamentals of Statistical Signal Processing: Estimation theory*. Fundamentals of Statistical Signal Processing. Prentice-Hall PTR, 1993. ISBN 9780133457117. URL http://books.google.com/books?id=aFwESQAACAAJ.

[18] C Radhakrishna Rao. Information and the accuracy attainable in the estimation of statistical parameters. In *Breakthroughs in statistics*, pages 235–247. Springer, 1992.

[19] W. Yan, L. Wang, Y. Jin, and G. Shi. High accuracy Navigation System using GPS and INS system integration strategy. In *2016 IEEE International Conference on Cyber Technology in Automation, Control, and Intelligent Systems (CYBER)*, pages 365–369, June 2016. doi: 10.1109/CYBER.2016.7574851.

[20] M. Zhong, J. Guo, and Q. Cao. On Designing PMI Kalman Filter for INS/GPS Integrated Systems With Unknown Sensor Errors. *IEEE Sensors Journal*, 15(1): 535–544, January 2015. ISSN 1530-437X. doi: 10.1109/JSEN.2014.2334698.

[21] L. Bowen and Y. Danya. Calculation of vehicle real-time position overcoming the GPS positioning latency with MEMS INS. In *Proceedings of 2014 IEEE International Conference on Service Operations and Logistics, and Informatics*, pages 248–254, October 2014. doi: 10.1109/SOLI.2014.6960730.

[22] Aboelmagd Noureldin, Ahmed El-Shafie, and Mohamed Bayoumi. GPS/INS integration utilizing dynamic neural networks for vehicular navigation. *Information Fusion*, 12(1):48–57, January 2011. ISSN 1566-2535. doi: 10.1016/j.inffus.2010.01.003. URL https://www.sciencedirect.com/science/article/pii/S1566253510000175.

[23] Mohammed Olama, Charalambos Charalambous, Ioannis Papageorgiou, Seddik Djouadi, and Teja Kuruganti. *Position and Velocity Tracking in Cellular Networks Using the Kalman Filter*. INTECH Open Access Publisher, 2009. ISBN 978-953-307-000-1. OCLC: 884025728.

[24] John L. Crassidis. Sigma-point Kalman filtering for integrated GPS and inertial navigation. *IEEE Transactions on Aerospace and Electronic Systems*, 42(2):750–756, 2006. URL http://ieeexplore.ieee.org/abstract/document/1642588/.

[25] M. Alzantot and M. Youssef. UPTIME: Ubiquitous pedestrian tracking using mobile phones. In *2012 IEEE Wireless Communications and Networking Conference (WCNC)*, pages 3204–3209, April 2012. doi: 10.1109/WCNC.2012.6214359.

[26] Moustafa Youssef, Mohamed Amir Yosef, and Mohamed El-Derini. GAC: energy-efficient hybrid GPS-accelerometer-compass GSM localization. In *Global Telecommunications Conference (GLOBECOM 2010), 2010 IEEE*, pages 1–5. IEEE, 2010.

[27] Ionut Constandache, Romit Roy Choudhury, and Injong Rhee. Towards mobile phone localization without war-driving. In *Infocom, 2010 proceedings ieee*, pages 1–9. IEEE, 2010.

[28] I.T. Haque and C. Assi. Profiling-Based Indoor Localization Schemes. *IEEE Systems Journal*, 9(1):76–85, March 2015. ISSN 1932-8184. doi: 10.1109/JSYST.2013.2281257.

[29] Bang Wang, Shengliang Zhou, Wenyu Liu, and Yijun Mo. Indoor Localization Based on Curve Fitting and Location Search Using Received Signal Strength. *IEEE Transactions on Industrial Electronics*, 62(1):572–582, January 2015. ISSN 0278-0046. doi: 10.1109/TIE.2014.2327595.

[30] Heikki Laitinen, Jaakko Lahteenmaki, and Tero Nordstrom. Database correlation method for gsm location. In *Vehicular Technology Conference, 2001. VTC 2001 Spring. IEEE VTS 53rd*, volume 4, pages 2504–2508. IEEE, 2001.

[31] Ericsson Mobility Report. URL https://www.ericsson.com/res/docs/2016/ericsson-mobility-report-2016.pdf.

[32] Dan Simon. *Optimal State Estimation: Kalman, H Infinity, and Nonlinear Approaches*. Wiley-Interscience, 2006. ISBN 978-0-471-70858-2.

[33] Rudolph Emil Kalman. A new approach to linear filtering and prediction problems. *Journal of basic Engineering*, 82(1):35–45, 1960.

[34] T. W. Anderson, editor. *An Introduction to Multivariate Statistical Analysis*. Wiley, 1984.

[35] Lee J Bain and Max Engelhardt. *Introduction to probability and mathematical statistics*, volume 4. Duxbury Press Belmont, CA, 1992.

[36] Paul D. Ellis. *The Essential Guide to Effect Sizes: Statistical Power, Meta-Analysis, and the Interpretation of Research Results*. Cambridge University Press, July 2010. ISBN 978-0-521-14246-5. Google-Books-ID: 5obZnfK5pbsC.

[37] A. H. Mohamed and K. P. Schwarz. Adaptive Kalman Filtering for INS/GPS. *Journal of Geodesy*, 73(4):193–203, May 1999. ISSN 0949-7714, 1432-1394. doi: 10.1007/s001900050236. URL http://link.springer.com/article/10.1007/s001900050236.

[38] Jack B. Kuipers. *Quaternions and Rotation Sequences: A Primer with Applications to Orbits, Aerospace, and Virtual Reality*. Princeton University Press, 2002. ISBN 978-0-691-10298-6.

[39] Sebastian OH Madgwick, Andrew JL Harrison, and Ravi Vaidyanathan. Estimation of IMU and MARG orientation using a gradient descent algorithm. In *2011 IEEE International Conference on Rehabilitation Robotics*, pages 1–7. IEEE, 2011.

[40] MPU-6500 Product Specification Revision 1.1. URL http://www.glynstore.com/invensense-mpu-6500-6-axis-gyroscope-accelerometer-sensor-ic/.

[41] Inside the Samsung Galaxy S6 | Chipworks. URL https://www.chipworks.com/about-chipworks/overview/blog/inside-the-samsung-galaxy-s6.

[42] Yiu-Tong Chan, Wing-Yue Tsui, Hing-Cheung So, and Pak-Chung Ching. Time-of-arrival based localization under NLOS conditions. *IEEE Transactions on Vehicular Technology*, 55(1):17–24, January 2006. ISSN 0018-9545. doi: 10.1109/TVT.2005.861207.

[43] F. Benedetto, G. Giunta, A. Toscano, and L. Vegni. Dynamic los/nlos statistical discrimination of wireless mobile channels. In *Vehicular Technology Conference, 2007. VTC2007-Spring. IEEE 65th*, pages 3071–3075, April 2007. doi: 10.1109/VETECS.2007.629.

[44] S. Marano, W.M. Gifford, H. Wymeersch, and M.Z. Win. NLOS identification and mitigation for localization based on UWB experimental data. *IEEE Journal on Selected Areas in Communications*, 28(7):1026–1035, September 2010. ISSN 0733-8716. doi: 10.1109/JSAC.2010.100907.

[45] B.Y. Shikur and T. Weber. Robust cooperative localization in mixed LOS and NLOS environments using TOA. In *2014 11th Workshop on Positioning, Navigation and Communication (WPNC)*, pages 1–6, March 2014. doi: 10.1109/WPNC.2014.6843291.

[46] P. Stefanut, D.P. Gaillot, A. Nasr, M. Lienard, and P. Degauque. A localization technique for LOS and NLOS scenario. In *Wireless Technology Conference (EuWIT), 2010 European*, pages 121–124, September 2010.

[47] K. Papakonstantinou and D. Slock. Cramer-Rao bounds for hybrid localization methods in LoS and NLoS environments. In *2010 IEEE 21st International Symposium on Personal, Indoor and Mobile Radio Communications Workshops (PIMRC Workshops)*, pages 213–217, September 2010. doi: 10.1109/PIMRCW.2010.5670364.

[48] Veljo Otsason, Alex Varshavsky, Anthony LaMarca, and Eyal De Lara. Accurate gsm indoor localization. In *UbiComp 2005: Ubiquitous Computing*, pages 141–158. Springer, 2005.

[49] Harald T Friis. A note on a simple transmission formula. *proc. IRE*, 34(5):254–256, 1946.

[50] Ralph O Schmidt. Multiple emitter location and signal parameter estimation. *Antennas and Propagation, IEEE Transactions on*, 34(3):276–280, 1986.

[51] Richard Klukas and Michel Fattouche. Line-of-sight angle of arrival estimation in the outdoor multipath environment. *Vehicular Technology, IEEE Transactions on*, 47(1):342–351, 1998.

[52] Richard Roy and Thomas Kailath. Esprit-estimation of signal parameters via rotational invariance techniques. *Acoustics, Speech and Signal Processing, IEEE Transactions on*, 37(7):984–995, 1989.

[53] Moustafa M Abdalla, Mostafa B Abuitbel, and Mohamed A Hassan. Performance evaluation of direction of arrival estimation using music and esprit algorithms for mobile communication systems. In *Wireless and Mobile Networking Conference (WMNC), 2013 6th Joint IFIP*, pages 1–7. IEEE, 2013.

[54] Telecommunications Industry Association et al. The cdma2000 itu-r rtt candidate submission,", 1998.

[55] Ismail Guvenc and Chia-Chin Chong. A survey on toa based wireless localization and nlos mitigation techniques. *Communications Surveys & Tutorials, IEEE*, 11(3): 107–124, 2009.

[56] Ali H Sayed, Alireza Tarighat, and Nima Khajehnouri. Network-based wireless location: challenges faced in developing techniques for accurate wireless location information. *Signal Processing Magazine, IEEE*, 22(4):24–40, 2005.

[57] James J Caffery and Gordon L Stuber. Overview of radiolocation in cdma cellular systems. *Communications Magazine, IEEE*, 36(4):38–45, 1998.

[58] James Caffery and Gordon L Stuber. Subscriber location in cdma cellular networks. *Vehicular Technology, IEEE Transactions on*, 47(2):406–416, 1998.

[59] Sklar Bernard. Digital communications fundamentals and applications. *Chap15, Prentice-Hall International, inc*, 2001.

[60] Matthias Patzold. *Mobile fading channels*. John Wiley & Sons, Inc., 2003.

[61] Chengshan Xiao, Yahong Rosa Zheng, and Norman C Beaulieu. Novel sum-of-sinusoids simulation models for rayleigh and rician fading channels. *Wireless Communications, IEEE Transactions on*, 5(12):3667–3679, 2006.

[62] James K Cavers. An analysis of pilot symbol assisted modulation for rayleigh fading channels [mobile radio]. *Vehicular Technology, IEEE Transactions on*, 40(4):686–693, 1991.

[63] Chengshan Xiao and Jan C Olivier. Nonselective fading channel estimation with nonuniformly spaced pilot symbols. *International Journal of Wireless Information Networks*, 7(3):177–185, 2000.

[64] Jingxian Wu, Chengshan Xiao, and Jan C Olivier. Time-varying and frequency-selective channel estimation with unequally spaced pilot symbols. *International Journal of Wireless Information Networks*, 11(2):93–104, 2004.

[65] Cihan Tepedelenlioglu, Ali Abdi, and Georgios B Giannakis. The ricean k factor: estimation and performance analysis. *Wireless Communications, IEEE Transactions on*, 2(4):799–810, 2003.

[66] S. Saunders and A. Aragón-Zavala. *Antennas and Propagation for Wireless Communication Systems: 2nd Edition*. John Wiley & Sons, 2007. ISBN 9780470848791. URL http://books.google.com/books?id=D1WF5Z1Yz7YC.

[67] Mohammed Rana Basheer and Sarangapani Jagannathan. R-factor: A new parameter to enhance location accuracy in rssi based real-time location systems. In *Sensor, Mesh and Ad Hoc Communications and Networks, 2009. SECON'09. 6th Annual IEEE Communications Society Conference on*, pages 1–9. IEEE, 2009.

[68] J. Wilson and N. Patwari. Radio Tomographic Imaging with Wireless Networks. *IEEE Transactions on Mobile Computing*, 9(5):621–632, May 2010. ISSN 1536-1233. doi: 10.1109/TMC.2009.174.

[69] Yang Zhao and N. Patwari. Robust Estimators for Variance-Based Device-Free Localization and Tracking. *IEEE Transactions on Mobile Computing*, 14(10):2116–2129, October 2015. ISSN 1536-1233. doi: 10.1109/TMC.2014.2385710.

[70] M. Bocca, O. Kaltiokallio, N. Patwari, and S. Venkatasubramanian. Multiple Target Tracking with RF Sensor Networks. *IEEE Transactions on Mobile Computing*, 13 (8):1787–1800, August 2014. ISSN 1536-1233. doi: 10.1109/TMC.2013.92.

[71] K. Woyach, D. Puccinelli, and M. Haenggi. Sensorless Sensing in Wireless Networks: Implementation and Measurements. In *2006 4th International Symposium on Modeling and Optimization in Mobile, Ad Hoc and Wireless Networks*, pages 1–8, April 2006. doi: 10.1109/WIOPT.2006.1666495.

[72] Dian Zhang, Jian Ma, Quanbin Chen, and L.M. Ni. An RF-Based System for Tracking Transceiver-Free Objects. In *Fifth Annual IEEE International Conference on Pervasive Computing and Communications, 2007. PerCom '07*, pages 135–144, March 2007. doi: 10.1109/PERCOM.2007.8.

[73] R.K. Martin, A. Folkerts, and T. Heinl. Accuracy vs. Resolution in Radio Tomography. *IEEE Transactions on Signal Processing*, 62(10):2480–2491, May 2014. ISSN 1053-587X. doi: 10.1109/TSP.2014.2311969.

[74] N. Patwari and P. Agrawal. Effects of Correlated Shadowing: Connectivity, Localization, and RF Tomography. In *International Conference on Information Processing in Sensor Networks, 2008. IPSN '08*, pages 82–93, April 2008. doi: 10.1109/IPSN.2008.7.

[75] P. Agrawal and N. Patwari. Correlated link shadow fading in multi-hop wireless networks. *IEEE Transactions on Wireless Communications*, 8(8):4024–4036, August 2009. ISSN 1536-1276. doi: 10.1109/TWC.2009.071293.

[76] William C Jakes and Donald C Cox. *Microwave mobile communications*. Wiley-IEEE Press, 1994.

[77] Raymond Steele, H Ahmadi, and A Krishna. Mobile radio communications. In *IEEE Proceedings*, volume 82, pages 1468–1468. [New York, NY]: Institute of Electrical and Electronics Engineers,[1963-, 1994.

[78] Gordon L Stüber. *Principles of mobile communication*. Springer Science & Business Media, 2011.

[79] K.A. Qaraqe and S. Roe. Channel estimation algorithms for third generation w-cdma communication systems. In *Vehicular Technology Conference, 2001. VTC 2001 Spring. IEEE VTS 53rd*, volume 4, pages 2675–2679 vol.4, 2001. doi: 10.1109/VETECS.2001.944086.

[80] Abdelmonaem Lakhzouri. *Channel Estimation and Mobile Phone Positioning in CDMA Based Wireless Communication Systems*. June 2005. ISBN 952-15-1368-3. URL http://dspace.cc.tut.fi/dpub/handle/123456789/73.

[81] S. Coleri, M. Ergen, A. Puri, and A. Bahai. Channel estimation techniques based on pilot arrangement in OFDM systems. *IEEE Transactions on Broadcasting*, 48(3): 223–229, September 2002. ISSN 0018-9316. doi: 10.1109/TBC.2002.804034.

[82] Zijian Tang, R.C. Cannizzaro, G. Leus, and P. Banelli. Pilot-Assisted Time-Varying Channel Estimation for OFDM Systems. *IEEE Transactions on Signal Processing*, 55(5):2226–2238, May 2007. ISSN 1053-587X. doi: 10.1109/TSP.2007.893198.

[83] Cheng Guan Koay and Peter J Basser. Analytically exact correction scheme for signal extraction from noisy magnitude mr signals. *Journal of Magnetic Resonance*, 179 (2):317–322, 2006.

[84] V Papathanasiou. Some characteristic properties of the fisher information matrix via cacoullos-type inequalities. *Journal of Multivariate analysis*, 44(2):256–265, 1993.

[85] Ram Zamir. A proof of the fisher information inequality via a data processing argument. *Information Theory, IEEE Transactions on*, 44(3):1246–1250, 1998.

[86] Boaz Porat. *Digital processing of random signals: theory and methods*. Prentice-Hall, Inc., 1994.

[87] Jan Sijbers, Arnold Jan den Dekker, Paul Scheunders, and Dirk Van Dyck. Maximum-likelihood estimation of rician distribution parameters. *IEEE Trans. Med. Imaging*, 17(3):357–361, 1998.

[88] Thomas L Marzetta. Em algorithm for estimating the parameters of a multivariate complex rician density for polarimetric sar. In *Acoustics, Speech, and Signal Processing, 1995. ICASSP-95., 1995 International Conference on*, volume 5, pages 3651–3654. IEEE, 1995.

[89] Larry J Greenstein, David G Michelson, and Vinko Erceg. Moment-method estimation of the ricean k-factor. *Communications Letters, IEEE*, 3(6):175–176, 1999.

[90] Ali Abdi, Cihan Tepedelenlioglu, Mostafa Kaveh, and Georgios Giannakis. On the estimation of the k parameter for the rice fading distribution. *Communications Letters, IEEE*, 5(3):92–94, 2001.

[91] Michael Rice. *Digital Communications: A Discrete-time Approach*. Prentice Hall, 2009. ISBN 978-0-13-030497-1.

[92] 3gpp specification: 45.004, . URL http://www.3gpp.org/DynaReport.

[93] Fcc rules for wireless equipment operating in the ism bands, 2015. URL http://www.afar.net/tutorials/fcc-rules.

[94] A.J. Fenwick. Algorithms for position fixing using pulse arrival times. *Radar, Sonar and Navigation, IEE Proceedings* -, 146(4):208–212, August 1999. ISSN 1350-2395. doi: 10.1049/ip-rsn:19990538.

[95] C. Mensing and S. Plass. Positioning Algorithms for Cellular Networks Using TDOA. In *2006 IEEE International Conference on Acoustics, Speech and Signal Processing, 2006. ICASSP 2006 Proceedings*, volume 4, pages IV–IV, May 2006. doi: 10.1109/ICASSP.2006.1661018.

[96] J.C. Chen, R.E. Hudson, and K. Yao. Maximum-likelihood source localization and unknown sensor location estimation for wideband signals in the near-field. *IEEE Transactions on Signal Processing*, 50(8):1843–1854, August 2002. ISSN 1053-587X. doi: 10.1109/TSP.2002.800420.

[97] S. Sakagami, S. Aoyama, K. Kuboi, S. Shirota, and Akira Akeyama. Vehicle position estimates by multibeam antennas in multipath environments. *IEEE Transactions on Vehicular Technology*, 41(1):63–68, February 1992. ISSN 0018-9545. doi: 10.1109/25.120146.

[98] V. Thotla, M. J. Zawodniok, S. Jagannathan, M. T. A. Ghasr, and S. Agarwal. Detection and Localization of Multiple R/C Electronic Devices Using Array Detectors. *IEEE Transactions on Instrumentation and Measurement*, 64(1):241–251, January 2015. ISSN 0018-9456. doi: 10.1109/TIM.2014.2331432.

[99] H. Shen, Z. Ding, S. Dasgupta, and C. Zhao. Multiple Source Localization in Wireless Sensor Networks Based on Time of Arrival Measurement. *IEEE Transactions on Signal Processing*, 62(8):1938–1949, April 2014. ISSN 1053-587X. doi: 10.1109/TSP.2014.2304433.

[100] IEEE Draft Amendment Standard for Local and Metropolitan Area Networks - Part 16: Air Interface for Broadband Wireless Access Systems - Advanced Air Interface. *IEEE P802.16m/D9, October 2010*, pages 1–1156, October 2010.

[101] I.T. Haque and C. Assi. Profiling-Based Indoor Localization Schemes. *IEEE Systems Journal*, 9(1):76–85, March 2015. ISSN 1932-8184. doi: 10.1109/JSYST.2013.2281257.

[102] Bang Wang, Shengliang Zhou, Wenyu Liu, and Yijun Mo. Indoor Localization Based on Curve Fitting and Location Search Using Received Signal Strength. *IEEE Transactions on Industrial Electronics*, 62(1):572–582, January 2015. ISSN 0278-0046. doi: 10.1109/TIE.2014.2327595.

[103] Q. Luo, Y. Peng, J. Li, and X. Peng. RSSI-Based Localization Through Uncertain Data Mapping for Wireless Sensor Networks. *IEEE Sensors Journal*, 16(9):3155–3162, May 2016. ISSN 1530-437X. doi: 10.1109/JSEN.2016.2524532.

[104] Paramvir Bahl and Venkata N. Padmanabhan. RADAR: An in-building RF-based user location and tracking system. In *INFOCOM 2000. Nineteenth Annual Joint Conference of the IEEE Computer and Communications Societies. Proceedings. IEEE*, volume 2, pages 775–784. Ieee, 2000.

[105] William C. Y. Lee. *Mobile Communications Engineering: Theory and Applications*. McGraw-Hill, Inc., New York, NY, USA, 1997. ISBN 1-59061-135-7.

[106] Reza Zekavat and R Michael Buehrer. *Handbook of position location: Theory, practice and advances*, volume 27. John Wiley & Sons, 2011.

[107] Wolfram Koepf. Identities for families of orthogonal polynomials and special functions. *INTEGRAL TRANSFORMS AND SPECIAL FUNCTIONS*, 5:69–102, 1995.

[108] Robert G. Malgady and David E. Krebs. Understanding correlation coefficients and regression. *Physical therapy*, 66(1):110–120, 1986. URL http://ptjournal.apta.org/content/66/1/110.short.

[109] Vijay Garg. *Wireless Communications & Networking*. Morgan Kaufmann, July 2010. ISBN 978-0-08-054907-1.

[110] Andrea Goldsmith. *Wireless Communications*. Cambridge University Press, August 2005. ISBN 978-1-139-44584-9.

[111] Gordon L. Stüber. *Principles of Mobile Communication*. Springer Science & Business Media, March 2013. ISBN 978-1-4757-6268-6.

[112] A.J. Goldsmith and L.J. Greenstein. A measurement-based model for predicting coverage areas of urban microcells. *IEEE Journal on Selected Areas in Communications*, 11(7):1013–1023, September 1993. ISSN 0733-8716. doi: 10.1109/49.233214.

[113] Jerry D. Gibson. *Mobile Communications Handbook, Third Edition*. CRC Press, August 2012. ISBN 978-1-4398-1723-0.

[114] S. Tiraspolsky, A. Rubtsov, A. Maltsev, and A. Davydov. Mobile WiMAX - Deployment Scenarios Performance Analysis. In *3rd International Symposium on Wireless Communication Systems, 2006. ISWCS '06*, pages 353–357, September 2006. doi: 10.1109/ISWCS.2006.4362318.

[115] Mardeni. R and T. Siva Priya. Optimised COST-231 Hata Models for WiMAX Path Loss Prediction in Suburban and Open Urban Environments. *Modern Applied Science*, 4(9), August 2010. ISSN 1913-1852, 1913-1844. doi: 10.5539/mas.v4n9p75. URL http://www.ccsenet.org/journal/index.php/mas/article/view/6462.

[116] M. Alshami, T. Arslan, J. Thompson, and A.T. Erdogan. Frequency analysis of path loss models on WIMAX. In *Computer Science and Electronic Engineering Conference (CEEC), 2011 3rd*, pages 1–6, July 2011. doi: 10.1109/CEEC.2011.5995815.

[117] Q. Li, D. Xu, W. Wang, X. Wang, and Z. Han. Anti-jamming scheme for GPS receiver with vector tracking loop and blind beamformer. *Electronics Letters*, 50 (19):1386–1388, September 2014. ISSN 0013-5194. doi: 10.1049/el.2014.2274.

[118] N. Carson, S. M. Martin, J. Starling, and D. M. Bevly. GPS spoofing detection and mitigation using Cooperative Adaptive Cruise Control system. In *2016 IEEE Intelligent Vehicles Symposium (IV)*, pages 1091–1096, June 2016. doi: 10.1109/IVS.2016.7535525.

[119] Kamin Whitehouse, Chris Karlof, and David Culler. A practical evaluation of radio signal strength for ranging-based localization. *ACM SIGMOBILE Mobile Computing and Communications Review*, 11(1):41–52, 2007. URL http://dl.acm.org/citation.cfm?id=1234829.

[120] J. Kang, D. Kim, and Y. Kim. RSS Self-calibration Protocol for WSN Localization. In *2007 2nd International Symposium on Wireless Pervasive Computing*, February 2007. doi: 10.1109/ISWPC.2007.342597.

[121] Yang Zhao and N. Patwari. Robust Estimators for Variance-Based Device-Free Localization and Tracking. *IEEE Transactions on Mobile Computing*, 14(10):2116–2129, October 2015. ISSN 1536-1233. doi: 10.1109/TMC.2014.2385710.

[122] M.R. Gholami, R.M. Vaghefi, and E.G. Strom. RSS-Based Sensor Localization in the Presence of Unknown Channel Parameters. *IEEE Transactions on Signal Processing*, 61(15):3752–3759, August 2013. ISSN 1053-587X. doi: 10.1109/TSP.2013.2260330.

[123] J. Werner, J. Wang, A. Hakkarainen, D. Cabric, and M. Valkama. Performance and Cramer-Rao Bounds for DoA/RSS Estimation and Transmitter Localization Using Sectorized Antennas. *IEEE Transactions on Vehicular Technology*, PP(99):1–1, 2015. ISSN 0018-9545. doi: 10.1109/TVT.2015.2445317.

[124] J. Werner, Jun Wang, A. Hakkarainen, M. Valkama, and D. Cabric. Primary user DoA and RSS estimation in cognitive Radio networks using sectorized antennas. In *2013 8th International Conference on Cognitive Radio Oriented Wireless Networks (CROWNCOM)*, pages 43–48, July 2013. doi: 10.1109/CROWNCom.2013.6636792.

[125] R.G. Stansfield. Statistical theory of d.f. fixing. *Journal of the Institution of Electrical Engineers - Part IIIA: Radiocommunication*, 94(15):762–770, March 1947. doi: 10.1049/ji-3a-2.1947.0096.

[126] Jun Wang, Jianshu Chen, and Danijela Cabric. Cramer-Rao Bounds for Joint RSS/DoA-Based Primary-User Localization in Cognitive Radio Networks. *IEEE Transactions on Wireless Communications*, 12(3):1363–1375, March 2013. ISSN 1536-1276. doi: 10.1109/TWC.2013.012513.120966.

[127] Constantine A. Balanis. *Antenna Theory: Analysis and Design*. John Wiley & Sons, December 2012. ISBN 978-1-118-58573-3.

[128] M.K. Mwila, K. Djouani, and A. Kurien. An efficient approach to node localisation and tracking in wireless sensor networks. In *2014 IEEE Global Communications Conference (GLOBECOM)*, pages 492–497, December 2014. doi: 10.1109/GLOCOM.2014.7036856.

[129] W.H. Foy. Position-Location Solutions by Taylor-Series Estimation. *IEEE Transactions on Aerospace and Electronic Systems*, AES-12(2):187–194, March 1976. ISSN 0018-9251. doi: 10.1109/TAES.1976.308294.

[130] Broadcast Bands. FEDERAL COMMUNICATIONS COMMISSION 47 CFR Parts 0 and 15. 2010. URL http://www.apwpt.org/downloads/unlicensed-operation-in-the-tv-broadcast12-06-.pdf.

[131] 3gpp specification: 25.996, . URL http://www.3gpp.org/DynaReport/25996.htm.

[132] F. Gunnarsson, M.N. Johansson, A. Furuskar, M. Lundevall, A. Simonsson, C. Tidestav, and M. Blomgren. Downtilted Base Station Antennas - A Simulation Model Proposal and Impact on HSPA and LTE Performance. In *Vehicular Technology Conference, 2008. VTC 2008-Fall. IEEE 68th*, pages 1–5, September 2008. doi: 10.1109/VETECF.2008.49.

[133] 3gpp specification: 45.004, . URL http://www.3gpp.org/DynaReport/45004.htm.

[134] John J. Craig. *Introduction to Robotics: Mechanics and Control*. Pearson, Upper Saddle River, N.J, 3 edition edition, August 2004. ISBN 978-0-201-54361-2.

[135] Ingo Lütkebohle. Connected Grid Antennas Installation Guide - Cisco. http://www.cisco.com/c/en/us/td/docs/routers/connectedgrid/antennas/\\installing/cg_antenna_install_guide.html, 2015. [Online; accessed 13-May-2015].

[136] Z. D. Zaharis. Radiation pattern shaping of a mobile base station antenna array using a particle swarm optimization based technique. *Electrical Engineering*, 90(4):301–311, July 2007. ISSN 0948-7921, 1432-0487. doi: 10.1007/s00202-007-0078-y. URL http://link.springer.com/article/10.1007/s00202-007-0078-y.

[137] Victor S. Ryaben'kii and Semyon V. Tsynkov. *A Theoretical Introduction to Numerical Analysis*. CRC Press, November 2006. ISBN 978-1-58488-607-5.

[138] Wei Li, Jing Zhong, T.A. Gulliver, Bo Rong, Qingyang Hu, and Yi Qian. Fitting Noisy Data to a Circle: A Simple Iterative Maximum Likelihood Approach. In *2011 IEEE International Conference on Communications (ICC)*, pages 1–5, June 2011. doi: 10.1109/icc.2011.5963101.

[139] Zhenhua Ma, K.C. Ho, and Le Yang. Solutions and comparison of Maximum Likelihood and Full-Least-Squares estimations for circle fitting. In *IEEE International Conference on Acoustics, Speech and Signal Processing, 2009. ICASSP 2009*, pages 3257–3260, April 2009. doi: 10.1109/ICASSP.2009.4960319.

[140] Hu Juan-li, Deng Jia-bin, and Hu Chang. An Algorithm for Circle Curve Fitting Based on the Constrained Least Square Model Represented by Mosaic Observation Points. In *5th International Conference on Wireless Communications, Networking and Mobile Computing, 2009. WiCom '09*, pages 1–4, September 2009. doi: 10.1109/WICOM.2009.5302849.

[141] Gabriel Taubin. Estimation of planar curves, surfaces, and nonplanar space curves defined by implicit equations with applications to edge and range image segmentation. *IEEE Transactions on Pattern Analysis and Machine Intelligence*, 13(11):1115–1138, November 1991. ISSN 0162-8828. doi: 10.1109/34.103273.

[142] 3gpp specification: 25.105, . URL http://www.3gpp.org/DynaReport/25105.htm.

VITA

Lei Wang was born in Beijing, China. In 2002, he received his Bachelor Degree in Information Engineering from the Beijing University of Chemical Technology. Subsequently, he graduated with honor and obtained his Master Degree in Computer Technology in the same university in 2005. In May 2017, he received his Ph.D. in Computer Engineering from the Missouri University of Science and Technology, Rolla, Missouri, USA.